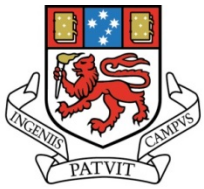


UNIVERSITY
OF TASMANIA

# Epigenetic mechanisms of arsenic-induced transformation in human keratinocytes

Katharine Jane Herbert

School of Health Sciences, Faculty of Health

Submitted in total fulfillment of the requirements of the degree of

Doctor of Philosophy

University of Tasmania

July, 2014

*Abstract*

Arsenic is an environmental toxin which increases skin cancer risk for exposed populations worldwide, however the biomolecular mechanism is yet to be fully elucidated. Genomewide epigenetic repatterning occurs with arsenic exposure – a process which is associated with altered gene expression and activity of epigenetic regulators. Whether this mechanism is a direct, or indirect, consequence of arsenic toxicity, and whether dysregulated maintenance of the epigenetic landscape drives arsenic-induced cancer, are questions which remain unanswered. SIRT1 is a lysine deacetylase with a well-characterised role in mediating cellular adaptation to metabolic stress; in part, by regulating activation of the tumour suppressor p53, and also by maintaining patterns of gene expression by regulating the activity of chromatin remodelling complexes. SIRT1 is overexpressed in numerous cancer subtypes, therefore the primary hypothesis guiding this thesis was that aberrant SIRT1 activity mediates the epigenetic events which initiate and promote arsenic-induced skin cancer. The overarching aim for this study was to characterise the response of SIRT1 and its targeting microRNA, miR-34a in cultured human keratinocytes when exposed to arsenic over an extended time frame.

For the first part of this investigation, wild-type (primary) and p53-mutated (HaCaT) keratinocytes were used as an *in vitro* model to determine the role of the p53/SIRT1/miR-34a axis during cell death signalling. Using a SIRT1 siRNA targeting pool, and with a targeted SIRT1:miR-34a binding site block, this study found that microRNA biogenesis and maturation is dysregulated in HaCaT keratinocytes, causing overexpression of microRNA regulatory targets. Consequently, inhibition of the miR-34a target, SIRT1, was effective in overcoming apoptotic resistance in the HaCaT cell line by restoring p53 transcriptional activation.

Second, the role of SIRT1 in arsenic-induced transformation of cultured keratinocytes was determined by exposing primary keratinocytes to 0.5 µM arsenite in culture medium for 10 weeks. By analysing these cells for changes in gene expression, chromatin condensation and DNA methylation, this investigation

determined that arsenic-induced acetylation of H4K16 in keratinocytes was associated with remodelling of the *pri-miR-34a* promoter and up-regulation of miR-34a expression, which was sustained by DNA hypomethylation with extended arsenic exposure. SIRT1 initially accumulated in arsenic-exposed cells, however this effect was transient, indicating that arsenic not only inhibits SIRT1 activity, but also down-regulates expression over time. Finally, although arsenic treated primary keratinocytes display epigenetic changes consistent with dysregulation of SIRT1 activity and expression, these cells were unable to escape senescence during sustained exposure to arsenic *in vitro*.

These data reveal that dysregulation of the p53/SIRT1/miR-34a axis contributes significantly to keratinocyte carcinogenesis by blocking efficient cell death signalling. Consequently, treatment of skin cancers may be enhanced by using SIRT1 inhibitors as an adjuvant to pro-apoptotic chemotherapy. Although skin cancer-inducing concentrations of arsenic altered epigenetic patterns of miR-34a gene regulation by interfering with SIRT1 activity and expression in cultured human keratinocytes, extended exposure was insufficient to induce transformation in the absence of a second hit such as those provided by characteristic UV-induced p53 mutations.

*Declaration of Originality*

I hereby declare that this submission is my own work and to the best of my knowledge it contains no materials previously published or written by another person, and contains no material which has been accepted for a degree or diploma by this University or any other institution, except by way of background information and where due acknowledgement is made in the text of the thesis. I also declare that the intellectual content of this thesis is the product of my own work, except to the extent that assistance from others in the project's design and conception or in style, presentation and linguistic expression is acknowledged.

Signed: _____ Date:_____

*Statement of Authority of Access*

This thesis may be made available for loan and limited copying in accordance with the *Copyright Act 1968.*

*Statement Regarding Published Work*

The publishers of the papers comprising Chapters 4 and 5 hold the copyright for that content, and access to the material should be sought from the respective journals. The remaining non published content of the thesis may be made available for loan and limited copying and communication in accordance with the Copyright Act 1968.

*Statement of Co-Authorship*

The following people and institutions contributed to the publication of work undertaken as part of this thesis:

*Katharine Herbert; School of Health Science; University of Tasmania* = Candidate

*Dr Anthony L Cook; University of Tasmania* = Author 1

*A/Prof Elizabeth T Snow; University of Tasmania* = Author 2

Manucript 1: Located in Chapter 4

Herbert, KJ, Cook, AL and Snow, ET (2014). "SIRT1 modulates miRNA processing defects in p53-mutated human keratinocytes." *Journal of Dermatological Science* 74(2): 142-149.

Candidate conducted the experimental procedures, was the primary author, designed and developed the experimental model and performed the analysis. Author 1 and Author 2 contributed to the experimental conceptualisation, its formalisation and methodological development. Each author assisted with refinement and presentation of the manuscript.

*Percentage estimate of the contribution made by each author:*

Candidate: 60%

Author 1: 20%

Author 2: 20%

Manuscript 2: Located in Chapter 5

Herbert, KJ, Cook, AL and Snow, ET (2014). "SIRT1 inhibition restores apoptotic sensitivity in p53-mutated human keratinocytes." *Toxicology and Applied Pharmacology* (available online: 12 April 2014)

Candidate conducted the experimental procedures, was the primary author, designed and developed the experimental model and performed the analysis. Author 1 and Author 2 contributed to the experimental conceptualisation, its formalisation and methodological development. Each author assisted with refinement and presentation of the manuscript.

*Percentage estimate of the contribution made by each author:*

Candidate: 60%

Author 1: 20%

Author 2: 20%

We the undersigned agree with the above stated “proportion of work undertaken” for each of the above published (or submitted) peer-reviewed manuscripts contributing to this thesis:

Signed: Candidate _____

Author 1 _____

Author 2 _____

*Acknowledgements*

My supervisors A/Prof Elizabeth Snow and Dr Anthony Cook, both of whom have spent the past 4 years patiently guiding and supporting my stumbling attempts at research.

Dr Adele Holloway and Paulynn Chin, who have provided their skill and knowledge to troubleshoot my epigenetics-related experiments.

Project Funding –

Cancer Council Tasmania Research Small Grants Scheme – T1 Project # 103154

Stipend – Tasmania Graduate Research Scholarship [186]

Conference Funding –

University of Tasmania Research Travel Award

NIH Young Scientist Travel Funding

Molecular and Environmental Pathology Society of Australasia Student Travel Awards

Other –

School of Health Science Technical staff

Limitless emotional support from Kiran and Susan

*Table of Contents*

## *List of Figures*

CHAPTER 1



CHAPTER 2

SUPPLEMENTARY MATERIAL

## *List of Tables*

*Commonly Used Abbreviations*

| | |
|---|---|
| Ac | Acetyl group |
| ADP | Adenosine diphosphate |
| Ago-2 | Argonaute-2 |
| APE/Ref1 | Apurinic endonuclease/redox-factor 1 |
| As(III) | Arsenite |
| As(V) | Arsenate |
| ATM | Ataxia-telangiecatesia-mutated protein |
| ATP | Adenosine triphosphate |
| ATR | ATM and Rad3-related protein |
| bp | Base pair |
| BCC | Basal cell carcinoma |
| BER | Base excision repair |
| BSA | Bovine serum albumin |
| CDC | Cell division cycle protein |
| CDK | Cyclin dependent kinase |
| cDNA | copy DNA |
| CBP | P300/CREB-binding protein |
| ChART-PCR | Chromatin accessibility real time PCR |
| ChIP | Chromatin immunoprecipitation |
| CK2 | Casein kinase 2 |
| CPT | Camptothecin |
| CTP | cAMP response element binding protein |
| DBC-1 | Deleted in breast cancer 1 |
| DGCR8/Pasha | DiGeorge syndrome critical region gene receptor alpha |
| DMEM | Dulbecco's Modified Eagle's Medium |
| DMSO | Dimethyl sulfoxide |
| DNA | Deoxyribonucleic acid |
| DNMT1 | DNA methyltransferase 1 |
| DNMT3a & b | DNA methyltransferases 3a & b |
| DYRK | Dual specificity regulated kinase |
| EDTA | Ethylenediaminetetraacetic acid |
| FOXO | Forkhead box class O transcription factor |
| FBS | Foetal bovine serum |
| $G_1$ | Growth phase 1 |
| GADD45α | Growth arrest and DNA damage-inducible protein 45-alpha |
| GST | Glutathione-S-transferase |
| H3, H4, H2A, H2B | Histones 3, 4, 2A & 2B |
| HBSS | Hank's balanced salt solution |

| | |
|---|---|
| HDAC | Histone deacetylase |
| HIC1 | Hypermethylated in cancer 1 |
| HKGS | Human Keratinocyte Growth Supplement |
| HRP | Horseradish peroxidase |
| IARC | International Agency for Research on Cancer |
| $IC_{50}$ | Inhibitory Concentration (50) |
| JNK | c-Jun N-terminal kinase |
| K | Lysine |
| KAC | Lysine acetyltransferase |
| KDAC | Lysine deacetylase |
| LDH | Lactate dehydrogenase |
| LNA | Locked nucleic acid |
| LSD1 | Lysine-specific demethylase 1 |
| M | Mitosis phase |
| MDM2 | Murine double minute protein |
| me | Methyl group |
| MGMT | O6-methylguanine DNA methyltransferase |
| miRNA | Micro RNA |
| MNase | Micrococcal nuclease |
| mRNA | Messenger ribonucleic acid |
| MTFR | Methylene tetrahydrofolate reductase |
| NAD | Nicotinamide adenine dinucleotide |
| NAMPT | Nicotinamide phosphoribosyltransferase |
| NBS1 | Nijmegen breakage syndrome 1 |
| NER | Nucleotide excision repair |
| NF-κB | Nuclear factor kappa beta |
| NHEK | Normal human epidermal keratinocytes |
| NMSC | Non-melanoma skin cancer |
| *O*AADPr | 2'-*O*-acetyl-adenosine diphosphoribose |
| PARP-1 | Poly(ADP-ribose) polymerase |
| PBS | Phosphate buffered saline |
| PCR | Polymerase chain reaction |
| PcG | Polycomb group |
| PI3K | Phosphoinositide 3 kinase |
| Rb | Retinoblastoma protein |
| RIPA | Radioimmunoprecipitation assay |
| RISC | RNA-induced silencing complex |
| RNA | Ribonucleic acid |
| RNAi | Ribonucleic acid interference |

| | |
|---|---|
| ROS | Reactive oxygen species |
| RT-PCR | Reverse transcriptase-polymerase chain reaction |
| SAM | *S*-adenosyl methionine |
| SCC | Squamous cell carcinoma |
| SD | Standard deviation |
| SDS-PAGE | Sodium dodecyl sulfate polyacrylamide gel electrophoresis |
| SIRT | Silent information regulator 2 |
| siRNA | Short interfering ribonucleic acid |
| SWI/SNF | Switch/sucrose nonfermentable nucleosome remodelling complex |
| TBST | Tris-buffered Tween-20 |
| TEMED | N,N,N',N'-Tetramethylethylene |
| TNFα | Tumour necrosis factor alpha |
| *TP53* | Tumour protein 53 |
| UTR | Untranslated region |
| UV | Ultra violet |
| VEGF | Vascular endothelial growth factor |
| WRN | Werner helicase |
| XPA | Xeroderma Pigmentosum Group A |
| XRCC1 | X-ray Repair Cross Complementing protein 1 |

# Chapter 1 -
# Overview of the Literature

## 1.1 CARCINOGENESIS

### 1.1.1 Skin Cancer in Australia

Cancer incidence in Australia almost doubled between the years 1991 and 2009, with the greatest contributors being cancers of the prostate, bowel, breast and melanoma of the skin. For all cancers combined, age-standardised mortality decreased by 17% during this time frame, however prognosis is sub-type specific, as only small gains in 5-year survival have been achieved for mesothelioma, and cancers of the brain, pancreas and lung (1).

Although basal and squamous cell carcinomas of the skin are the most frequently diagnosed cancers in Australia, incidence data from non-melanoma skin cancer (NMSC) is not included as part of the aforementioned analyses. Cancer diagnosis information is collected by law as part of the national cancer registry, however unlike all other cancers, basal and squamous cell carcinoma diagnoses are not notifiable under this system. Thus the health and economic burden of NMSC is frequently underrepresented in reports documenting cancer statistics and data trends over time. Although mortality from NMSC is comparatively low (~2.8/100,000 individuals), treatment is painful and disfiguring, and consequently represents a significant health burden (2).

Despite concerted efforts to reduce the incidence of skin cancer by sun protective measures with public education programs (3), squamous cell carcinoma (SCC) and basal cell carcinoma (BCC) continue to be the most common cancer diagnoses (2), with approximately 2% of the Australian population affected by non-melanoma skin cancer (NMSC) (4). Although not as lethal as melanoma, the cost of treatment for NMSC is predicted to increase substantially (22% by the year 2015) – particularly for individuals over 70 - each year and therefore is anticipated to become a significant public health burden during this time frame (estimated at more than $700 million by 2015) (5).

For those diagnosed with premalignant lesions, recurrence rates are high (4). Surgical excision is the current gold standard management strategy for all intra-epidermal keratinocyte dysplasias. As the majority of lesions occur in the head and neck area, treatment options are limited and commonly disfiguring (6), and therefore development of an effective chemopreventative strategy is an attractive prospect for health care practitioners and skin cancer patients.

In order to reduce the disease burden due to non-melanoma skin cancer, both incidence and prognosis needs to be addressed. This can be achieved by reducing modifiable risk factors (behaviour- and lifestyle-related) and by developing more efficient targeted treatment regimes.

### 1.1.2 Carcinogenic Transformation

Carcinogenesis is a complex multistep process during which cells undergo progressive functional changes, progressing from initiation to a malignant phenotype which is capable of escaping its site of origin and populating alternative regions of the body. During this process, patterns of gene expression are disrupted as a result of altered signal transduction activity, epigenetic changes, and gene mutations (7-9). Two of the more critical stages in carcinogenic transformation are the ability to successfully adopt genetic changes acquired during initiation (7); and the ability to manifest phenotypic changes which promote metastatic dissemination (epithelial-mesenchymal transition) (10). The consequence of these changes is a shift to a cellular phenotype which bears the hallmarks of cancer – replicative immortality, sustained proliferative signalling, self-sufficient growth/abnormal responses to regulatory signals, apoptotic resistance, inflammation, angiogenesis, tissue invasion, and metastasis (11, 12). Recently, the search for novel biomarkers and therapeutic targets has led to an overhaul of these categories to include evasion of immune surveillance, disrupted cellular energetics, genomic instability

and mitogenic dysfunction as emerging and/or enabling characteristics of carcinogenesis (12-14).

The tumour microenvironment has a unique role to play in providing a selective pressure which promotes growth and transformation of mutated cells (15). Driven by persistent exposure to endogenous and external stress, tumour cells are forced to adapt to chronic inflammation, replicative and mitotic stress, oxidative stress and/or hypoxia, metabolic and proteotoxic stress, and genetic instability (16)

Many of these changes are facilitated by alterations to the epigenome, with epigenetic repatterning contributing to tumour cell heterogeneity and reinforcing the neoplastic phenotype by silencing tumour suppressors (17), increasing epithelial/mesenchymal plasticity and reducing chromosomal stability (18, 19). Additionally, impaired maintenance of epigenetic imprinting is associated with increased cancer risk (20). Epigenetic dysregulation in cancer is an important biomarker for tumour progression and therapeutic resistance, and will be discussed further later in this chapter.

### 1.1.3 The DNA Damage Response

The imperative to maintain genomic integrity has driven eukaryotic cells to develop a complex and integrated system for detecting and repairing lesions in its sequence. These lesions occur most frequently during cell division, as the unravelling of its secondary structure leaves DNA vulnerable to both endogenous replication errors and also to environmental insult.

The cell reacts to inconsistencies in the DNA sequence by mounting a coordinated series of actions which facilitate repair of lesions in the genome by pausing replication and recruiting DNA repair complexes. Sustained genotoxic stress or irreparable damage triggers cell cycle arrest and stimulates proapoptotic cell death, preventing mutations from being perpetuated in daughter colonies (21, 22). As

such, the DNA damage response classically modulates the activity of four cellular processes – control of cell cycle transitions (checkpoints), gene regulation, DNA repair, and apoptosis (23, 24).

The ability to detect, and to coordinate an effective response to DNA damage is considered to be an important barrier to carcinogenesis (23-28). Disrupted expression and/or function of intermediates in the DNA damage response are associated with many, if not all, cancers. Consequently, these regulatory components have pharmaceutical potential as antineoplastic targets. This review will focus on effectors of the DNA damage response, and in particular the DNA damage effector p53 and its role as a tumour suppressor.

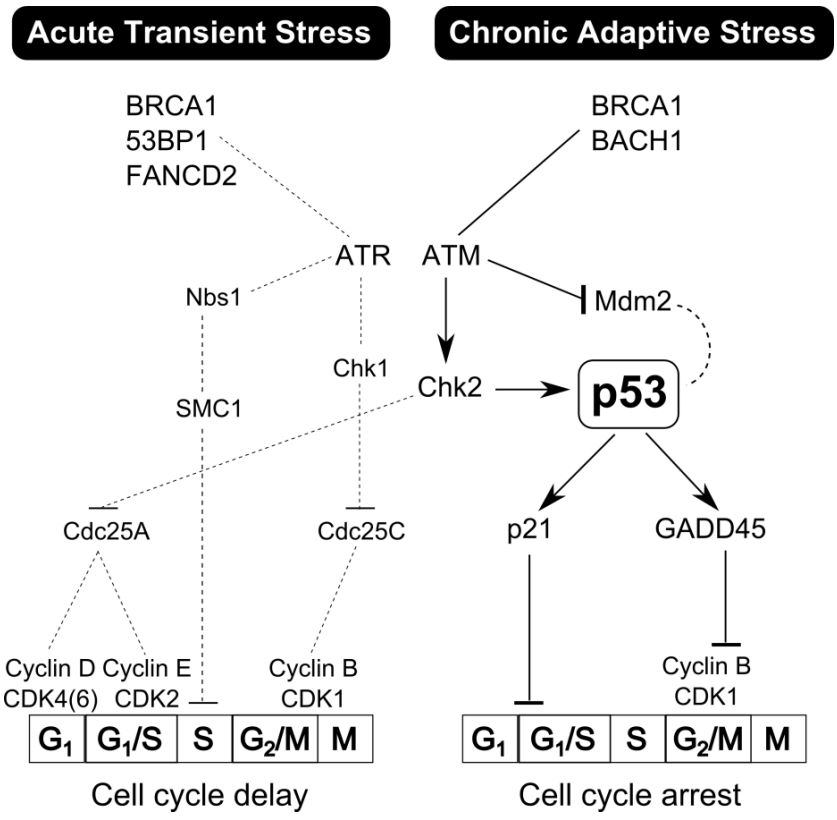


*Figure 1:1 Acute Transient vs Chronic Adaptive Stress Signalling*

Acute DNA damage pauses the cell cycle at the $G_1$ phase, stimulating DNA repair through the ATR/Nbs1/SMC1 pathway before resuming growth and division. Extended genotoxic damage arrests the cell cycle at the $G_2$M phase and coactivates proapoptotic signaling via p53

Key: BRCA1/2: breast cancer susceptibility protein 1&2; 53BP1 – p53-binding protein 1; FANCD2: Fanconi anaemia protein 2; ATM: ataxia-telangiectasia-mutated protein; ATR: ATM and Rad3-related protein; Nbs1: Nijmegen Breakage Syndrome protein 1; Mdm2 – murine double minute protein 2; Chk1&2 – checkpoint kinases 1&2; SMC1: structural maintenance of chromosome 1; Cdc25: cell division cycle 25; CDK1-4 cyclin-dependent kinases 1-4; GADD45 – growth arrest and DNA damage-inducible protein 45; $G_1$ – growth phase 1; $G_2$ – growth phase 2; S - synthesis; M - mitosis

#### *1.1.3.1 Effectors of the DNA Damage Response*

Effectors of the DNA damage response are transcription factors, DNA repair proteins, chromatin remodelling factors, cyclin-dependent kinases and the Cdc25 family of phosphatases (29-32). Short-term damage pauses the cell cycle at the $G_1$ checkpoint by activating Cdc25A and Cdc25C signalling cascades and allowing DNA repair complexes to operate (33). With sustained DNA damage, p53-mediated transcriptional targets (p21, 14-3-3σ, GADD45α) are up-regulated, arresting proliferation by blocking the cell cycle at $G_1$S and $G_2$M phases and sensitising the cell to apoptotic signalling [Figure 1:1]. Although both mechanisms are interrelated, adaptive changes induced by p53-mediated responses are more commonly disrupted during neoplastic progression, culminating in apoptotic resistance and loss of cell cycle control (34). Consequently, activation and/or restoration of the DNA damage response is a key chemotherapeutic strategy for most cancers (35).

### 1.1.4 Tumour Suppressor Protein p53

The tumour suppressor p53 is a transcription factor which has a central role in mediating cellular responses to genotoxic stress and hyperproliferative signalling (36), leading to a functional reputation as the ‘guardian of the genome’.

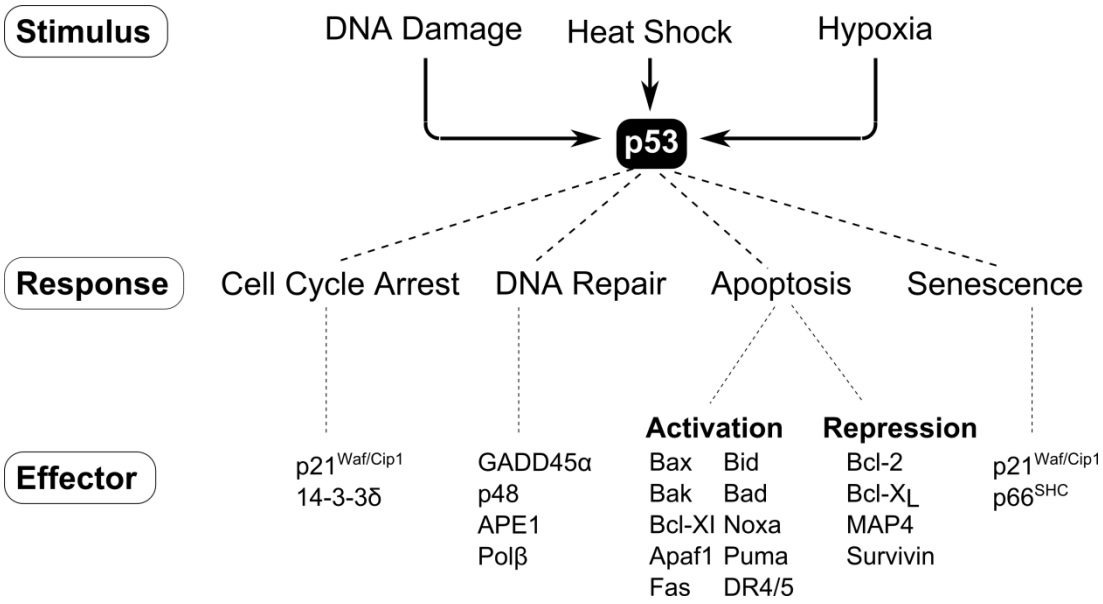


*Figure 1:2 p53-Mediated Stress Responses*

Nuclear accumulation of p53 increases transcription of downstream target genes – including cell cycle checkpoint regulators, DNA repair genes, cell death, and senescence genes (22, 23, 37, 38)

Canonical p53 responses regulate a diverse range of cellular processes which inhibit the perpetuation of mutated genomic material and thus tumour growth by triggering cell cycle arrest, coordinating DNA repair, initiating differentiation or senescence, and inducing cell death signalling and apoptosis (35) [Figure 1:2].

More recently, p53 activity has been implicated in wider spectrum of stress responses which contribute to tumour suppression, including oxidative stress, nutrient deprivation, hypoxia, ribonucleotide depletion, replicative stress and telomere attrition (39). Thus p53 transactivation is important for modulating additional cellular processes such as autophagy, metabolic reprogramming, invasion and metastasis, and regulation of stemness – all of which become impaired during tumorigenesis.

### *1.1.4.1 Transactivation*

p53 has a sequence-specific DNA binding domain with a consensus double stranded DNA sequence consisting of two tandem copies of a decameric motif separated by a

0–13 bp spacer RRRC(A/T)\(T/A)GYYY, where R represents purines, and Y represents pyrimidines (40, 41). P53 binds its response element as a homotetramer, which induces transactivation of target genes by generating a conformational shift in their gene promoter (42). p53-targeting genes have a variety of recognition sequences which influence the affinity and kinetics of gene transactivation and consequently p53 produces a wide range of transcriptional responses (43). Binding sites that conform to the consensus sequence form a strong protein-DNA complex and rapid transcriptional activation, however p53 binding sites which deviate from the consensus with a TC/GA/TG/CA/GC/GG/CC/CG core or mismatches in the flanking triplet sequences produce transcriptional repression in their target genes (44, 45).

#### *1.1.4.2 Posttranslational Modifications*

The outcome of p53-dependent signalling is dependent on the quality and duration of the initiating stimulus (46, 47). Post-translational p53 modifications drive transcriptional activation by promoting conformational stabilisation, tetramerisation and nuclear translocation (36, 46, 48) [Figure 3]. Amongst these, modifications to p53 lysine residues (acetylation and methylation, in particular) extend the half-life of p53 protein by inhibiting MDM2 and Pirh2-mediated ubiquitinylation (49, 50), and promote DNA binding by enhancing the affinity of p53 for its response element (51, 52).

DNA damage transducers stabilise cellular p53 by interfering with p53-MDM2 binding, after which the protein undergoes further posttranslational modifications which lead to both direct and indirect cellular actions (50). Activation of the DNA damage response pathway phosphorylates key serine residues (15, 20, 30 and 33) in the p53 activation domain (C-terminal regulatory domain) (37). Outcomes of p53 targeting by DNA damage response mediators are further directed by acetylation and deacetylation of lysine residues in the DNA-binding domain, tetramerisation, and C-terminal regulatory domains (51, 53) [Figure 1:3].

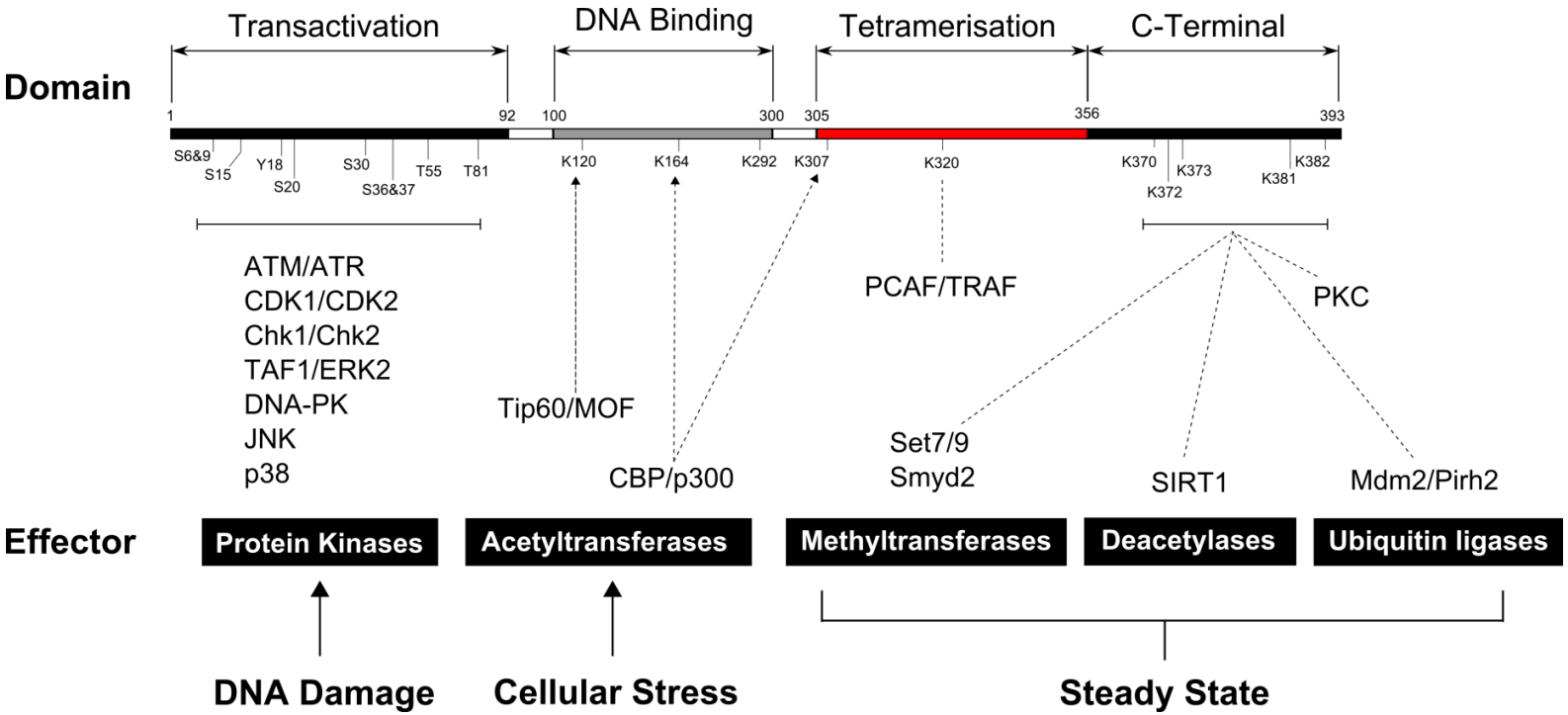


*Figure 1:3 Posttranslational Regulatory Control of p53*

P53 activity is regulated via phosphorylation and acetylation by genotoxic stress response mediators (32, 54). Maintenance of basal p53 expression and activity is controlled by deacetylation and ubiquitin-mediated proteolytic breakdown (46, 47, 55), as well as methylation of lysine residues in the regulatory domain (56-58).

Key: ATM - ataxia-telangiectasia-mutated protein; ATR - ATM and Rad3-related protein; Mdm2 - murine double minute protein 2; TAF1/ERK2 - extracellular signal-regulated kinase 2; Chk1&2 - checkpoint kinases 1&2; CDK1/2 - cyclin-dependent kinases 1&2; DNA-PK – DNA protein kinase; JNK – c-Jun N terminal kinase; PKC – protein kinase C; CBP/p300 - CREB-binding protein; PCAF - CBP/p300-associated factor; TRAF - Tip60/MOF-associated factor; Tip60 - Tat interacting protein; SIRT1 - silent information regulator2 protein 1

Lysine acetylation is a posttranslational modification which plays a key regulatory role in cellular processes dependent on signal transduction and gene transcription. Proteins which target p53 lysine residues are ubiquitous and have substrates with multiple cellular functions, including chromosomal remodelling, cell cycle control, DNA damage and repair, cytoskeletal remodelling, RNA splicing/ribosomal activity and signal transduction (59, 60). Of these, p300/CREB-binding protein (CBP), hMOF, and TIP60 are well characterised lysine acetyltransferases (KACs), and target residues in the p53 C-terminal and DNA binding domains, increasing p53-mediated functional activity (61). Conversely, deacetylation of C-terminal residues by lysine deacetylases (KDACs) down-regulates p53 transactivation and suppresses p53-mediated cellular responses, such as cell growth and apoptosis (55, 62).

Posttranslational lysine acetylation provides an additional qualitative level of regulatory control over p53-mediated responses by introducing a spectrum of conformational states and DNA binding affinities. These enable p53 to be differentially directed to p53 target genes, and to generate a suite of physiological outcomes according to the residue(s) modified (54), and the initiating stimulus (63)[Figure 1:3]. Partial acetylation by KACs at lysine residues 164, 373 and 382 promotes cellular survival by upregulating DNA repair enzymes and triggering cell cycle arrest (64-66). Further acetylation at lysine 120 alters the DNA binding characteristics of p53, switching the cellular outcome from survival to apoptosis (67). Modulation of p53 acetylation status, therefore, is considered to be critical to a cell's capacity to cope with environmental toxicity whilst maintaining genomic integrity, and generates different outcomes (survival, differentiation, senescence or apoptosis) relating to the stressor of interest.

#### *1.1.4.3 TP53 Mutations in Cancer*

The p53-dependent DNA damage response is considered to be an important barrier to tumorigenesis (68), and functional loss of its intermediates is a feature of the neoplastic phenotype. Impaired p53 activity and expression is considered to be

necessary for the progression of all human malignancies and may occur via numerous routes. These include disturbances in upstream pathway regulation, increased MDM2 expression, or *TP53* mutation (34). *TP53* is mutated in ~ 50% of cancers with inactivating mutations to its core DNA-binding domain or with destabilizing mutations to its tetramerisation domain (69-72). Additionally, loss of heterozygosity in the *TP53* gene may generate partial loss of function and genomic instability. Consequently, cancers with mutations to *TP53* are frequently accompanied by the loss of the second allele as a result of p53 haploinsufficiency (73).

Carcinogenic TP53 mutations generate a diverse range of alterations which affect p53 protein conformation, DNA binding affinity, tetramerisation, and protein-protein interactions (69, 70). The physiological outcome of these mutations are to a) generate a gain or loss of function phenotype – both of which contribute to tumorigenesis (74-78); and b) decrease genome-wide DNA stability and increase the rate of sporadic mutations (79). In cells with heterozygous p53 mutations, mutant p53 can have a dominant-negative effect on any non-mutated functional p53 within the cell by forming functionally inactive aggregates which inhibit DNA binding (80-82). Consequently, mutant forms of p53 contribute to tumour aggressiveness and resistance to chemotherapy (83).

Pharmaceutical p53 activation is an emerging strategy for enhancing the efficacy of chemotherapy. This approach exploits p53-specific functional differences between cells with wild-type p53 and those with p53-inactivating mutations. Early results from clinical trials indicate that a combinatorial approach is required for chemotherapy to effectively overcome p53 inactivating mutations

*Table 1:1 p53-Mediated Therapeutic Approaches*

| P53 Expression | Strategy/Description | Drug |
|---|---|---|
| Downregulated | Recombinant p53 | Gendicine |
| | Adenovirus | Advexin |
| | | SCH 58500, SCH 529074 |
| | Nuclear Export Protein CRM1 Inhibitors | Leptomycin B, Leptomycin A, Kasuzamycins |
| | MDM2 E3 Ligase Inhibitors | HLI 198 series |
| | Mdm2/MdmX Binding Blockers | Nutlin 3a/RG 7112 |
| | | Benzodiazepines |
| | | NSC 162908 [RITA] |
| | | MI series of Spiro-oxindoles |
| | | Quinolinols |
| Inactive/ Partially active | Conformation Restoration | Peptide Inhibitors: C369-383; C61-382; CDB3 |
| | | CDB3 (Molecular chaperone) |
| | | WR-1065, WR-2721 [amifostine] |
| | | PRIMA-1/PRIMA$^{MET}$ |
| | | MIRA-1 |
| | | PhiKan083 |
| | | CP-31398 |
| | | Ellipticine, NSC 176327, 9-hydroxy-ellipticine [9HE] |
| Gain of Function | SIRT1 Inhibitors | JJ78:12 series |
| | | Sirtinol |
| | | Tenovins 1 & 6 |

[Taken from (84-90)].

Current strategies developed to overcome dominant-negative and gain-of-function effects of p53 include stimulation of p53 degradation pathways, siRNA-mediated ablation of mutant p53 protein, blocking co-association with effector proteins, and reactivation of mutant p53 by restoration of wild-type function (82, 91, 92)[Table

1:1]. Importantly, the efficacy of these approaches is highly variable because the dominant-negative effect of mutant p53 depends on its propensity to inactivate circulating wild-type p53, and this is directly related to the site of mutation (93, 94).

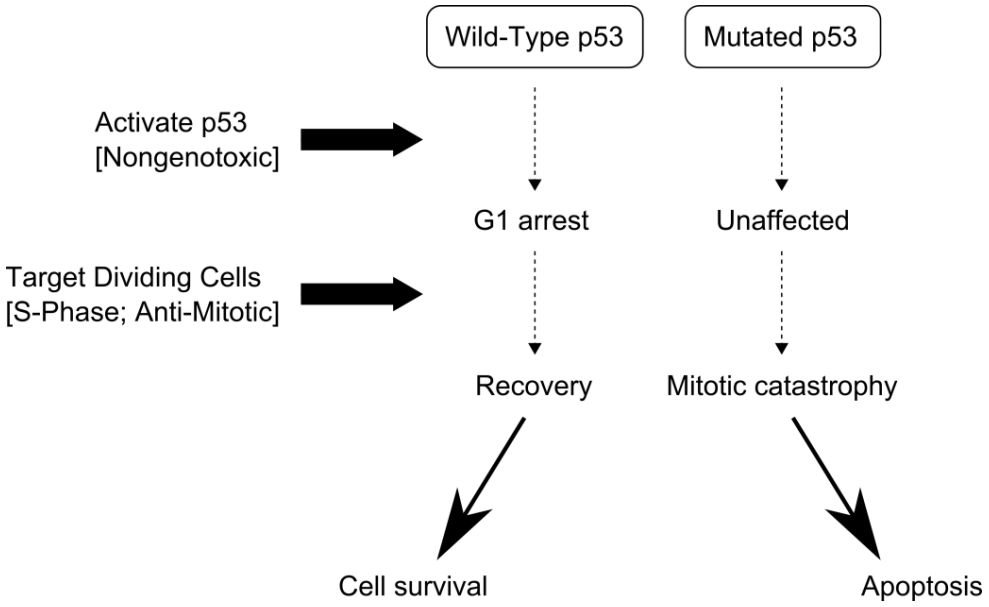


*Figure 1:4 p53-Based Cyclotherapy*

Pretreatment with a p53 activating drug halts the cell cycle in G1/G2 in normal cells carrying wild-type p53, whereas p53-mutant cancer cells continue cycling into S and M phase. S-phase or M-phase chemotherapy then specifically targets p53-mutant cancer cells to induce apoptosis, whilst having no effect on cell cycle-arrested normal cells (95).

Cyclotherapy is an alternative therapeutic strategy which exploits p53-based phenotypic differences in cancers expressing mutant p53. Cyclotherapy enhances the specificity of anti-mitotic chemotherapy by reducing toxicity in normal tissue and thereby improving chemotherapeutic dose tolerance for the patient. Here, the p53 activator treatment is optimised to induce a cytoprotective, but not cytotoxic, response. To achieve this, a pretreating dose of p53 activator is used to induce G1 arrest in normal cells whilst leaving cancer cells with mutated p53 unaffected [Figure 1:4] (89, 95, 96).

For p53-directed chemotherapy to be successful, the strategy employed is specifically tailored to the phenotypic characteristics generated by the mutation. Traditional pharmaceutical techniques exploit the increased rate of replication as a way of targeting cancer cells. However, normal cells which are rapidly dividing are also susceptible to the toxic effects of mitotic poisons, and thus unpleasant side effects are commonly experienced by patients during chemotherapy. Additionally, treatments which target tumour cells during division can have off-target effects which can cause resistance and induce secondary mutagenic outcomes. Therefore alternative techniques which exploit cancer-cell specific differences in order to enhance the efficacy of traditional regimens and reduce the risk of resistance and recurrence are attractive foci in the field of cancer therapies.

## 1.2 EPIGENETICS

### 1.2.1 Processes and Mechanisms

The human genome contains information which is encoded in the DNA sequence and is directly transferred to daughter cell lines during division, whereas the epigenome relates to the way cells express encoded genetic information and may, or may not, be heritable. Epigenetics is an overarching term which broadly encompasses DNA methylation, histone posttranslational modifications, chromatin remodelling, and the activity of small non-coding RNAs. The principal unifying tenet proposed by epigenetic regulation is that combinations of covalent modifications cause a structural rearrangement of chromosomal regions so as to register, signal or perpetuate altered activity states (97). As such, epigenetics describes information which is not directly encoded by the nucleotide sequence and which confers defined and gene-specific regulatory outcomes. These processes allows cells to respond and adapt to changes in their environment by altering the pattern of gene expression, and are now considered to have critical roles in both the prevention, and pathogenesis of disease (98).

### *1.2.1.1 DNA Methylation*

Human DNA is most commonly methylated by the activity of DNA methyltransferase enzymes, which catalyse the addition of a methyl group to the 5-carbon of cytosines, particularly those within CpG dinucleotides. Imprinted genomic methylation patterns are established at the time of implantation by DNA methyltransferases 3a and 3b (DNMT3a & b) and maintained between parent to daughter cell lines by DNA methyltransferase 1 (DNMT1) during replication (99).

CpG islands are genomic regions of ~ 0.2-1 kb rich in CpG dinucleotides. Of the ~28,000 CpG islands in human haploid cells, approximately 40-50% span the promoter and first exon region of genes. In normal cells, the majority of CpG dinucleotides are methylated, whereas CpG islands are predominantly unmethylated with the exception of inactivated X chromosomes, imprinted genes, repetitive and transposable elements (100). These established methylation patterns are responsible for regulation of cell type-specific gene expression, and the methylation status of regions associated with CpG islands in gene promoters inversely correlates with gene expression (101).

### *1.2.1.2 Histone Modifications and Chromatin Remodelling*

Nucleosomes form the core structural component of chromatin, each containing 147bp of DNA wrapped around an octamer of the core histone proteins H3, H4, H2A and H2B. Basic residues within histone H4 tails interact with acidic patches on adjacent H2A histones, coiling nucleosomes into 1.67 left-handed superhelical turns (102). Nucleosomal coiling regulates the degree of chromatin condensation and influences gene transcription – looser packing (euchromatin) is associated with gene transcription, whereas tighter packing (heterochromatin) silences gene transcription (103).

Modifications to histone N-terminal residues (phosphorylation, acetylation, methylation, sumoylation, ADP ribosylation, ubiquitination, deimination and proline

isomerisation) influence chromatin dynamics during metabolic processes such as DNA repair and replication, and regulate gene transcription by controlling accessibility of binding sites for transcription factors (104, 105)[Table 1:1].

*Table 1:2 Functional Properties of Histone Posttranslational Modifications*

| Histone | Modification | Residues | Outcome | Ref |
|---|---|---|---|---|
| H3 | Phosphorylation | T3, T11, T32 | Chromatin condensation | |
| | | S10, S28 | Transcriptional activation | (106) |
| | Acetylation | K4, K9, K14, K18, K23, K27 | Transcriptional activation | (106, 107) |
| | | K14, K18, K23, K56 | DNA repair | (108) |
| | Methylation | K4, R17, K79 | Transcriptional activation | (109) |
| | | K4 | Maintenance of DNA methylation patterns | (110) |
| | | K4, K9, K27 | Transcriptional repression | (106, 109) |
| H4 | Phosphorylation | S1 | Chromatin condensation | |
| | Acetylation | K5, K8, K12, K16 | Transcriptional activation | (106) |
| | | K5, K8, K12, K16 | DNA repair | (108) |
| | Deacetylation | K16 | Maintenance of telomeric chromatin | (111) |
| | Methylation | R3 | Transcriptional activation | (106) |
| | | K20, K59 | Transcriptional repression | (108) |
| H2A | Phosphorylation | S1, T119 | Mitosis | (112) |
| | | S129, S139 | DNA repair | (108) |
| | Acetylation | K4, K5, K7 | Transcriptional activation | (113) |
| | Ubiquitination | K119 | Mitotic & Meiotic Growth | (108) |
| | | K119 | Transcriptional repression | (106) |
| H2B | Phosphorylation | S14 | Chromatin condensation, apoptosis | (113) |
| | | S33 | Transcriptional activation | |
| | Acetylation | K5, K11, K12, K15, K16, K20 | Transcriptional activation | (109, 113) |
| | Ubiquitination | K123 | Mitotic & Meiotic Growth | (108) |
| | | K120 | Transcriptional activation | (106) |

Nucleosomal positioning at gene promoters is influenced by acetylation of histone H3 at lysine 9 (H3K9), which is directly associated with transcription factor accessibility and gene expression levels (114), whereas di- and trimethylation of H3K9 (H3K9me2, H3K9me3) promotes binding of heterochromatin protein 1 and is associated with transcriptional repression and heterochromatin formation (115, 116). In general, H4K20me3 and H3K27me3 marks are associated with increased chromatin packing and gene silencing; and H3K4me3 and H3K36me3 marks are associated with looser chromatin structures and active gene transcription (102, 107, 109).

#### *1.2.1.3 Epigenetic Regulation of Gene Transcription*

Cytosine methylation and histone posttranslational modifications contribute directly to the control of gene expression and the maintenance of genomic integrity. These processes are directly regulated by epigenetic modifiers (histone writers, readers, and editors) (117), DNA methylators, and chromatin remodellers, which function together to integrate the activity of signal transduction signalling intermediates with transcriptional activation (118).

Epigenetic readers (trans-acting factors) influence local chromatin structure of inducible genes through nucleosomal positioning or by modifying histone residues at the posttranslational level. These proteins operate by targeting specific histone motifs (chromodomains or bromodomains) near gene promoters (119-121). Chromodomain acting factors preferentially target methylated lysine residues and maintain patterns of histone methylation (histone demethylases, KDMs) (122), whereas bromodomain-targeting effector proteins target acetylated lysine residues (histone acetyltransferases, KATs) (123, 124) [Figure 1:5]. Current evidence suggests that trans-acting factors work cooperatively to maintain DNA methylation and histone patterns.

DNA methyltransferases form part of multi-protein chromatin remodeling complexes (Polycomb repressor group complexes, PRG) which include a variety of

epigenetic readers, including methyl CpG binding proteins, histone methyltransferases, and acetyltransferases (125). These PRGs are recruited to the chromatin of target genes which bear specific epigenetic patterns, and consequently, pro-carcinogenic changes in DNA methylation are dynamically linked to altered histone posttranslational modifications (126, 127). Furthermore, temporal models of gene silencing indicate that shifts in the pattern of histone acetylation provide the primary initiating event which precedes CpG island methylation (128).

Patterns of transcriptional activation and repression are regulated by a synergistic relationship between DNA methylation patterns and histone modifications. Regulation by DNA methylation or histone modification is dynamic, with specific combinations of epigenetic marks establishing transcriptional behaviour. DNA methylation is thought to silence gene transcription by restricting transcription factor binding and/or altering regional chromatin packing by increasing affinity for methyl-CpG binding proteins. Studies investigating the temporal order of epigenetic events associated with transcriptional silencing suggest that repressive histone marks are acquired at specific loci prior to changes in DNA methylation (129, 130). Less clear is how these histone marks drive patterns of CpG dinucleotide methylation. Since chromatin decondensation is required for cis-acting factors such as DNMTs to associate with DNA, it is likely that local nucleosomal remodelling facilitates accessibility of DNMTs to promoter CpGs. Nucleosomal remodelling factors are recruited to CpG islands by Methyl CpG Binding proteins (MeCPs), which co-associate at gene promoters with histone modifying enzymes as part of Polycomb group repressor complexes (125).

#### *1.2.1.4 Functional Roles of Epigenetic Regulators*

The chromatin of developmental genes is facultatively silenced by condensation, and becomes poised for transcriptional activation during differentiation. ATP-driven nucleosomal remodelling factors such as SWI/SNF actively affect higher order

chromatin structure by regulating nucleosomal positioning across regions of the chromosome (131) [Figure 1:5].

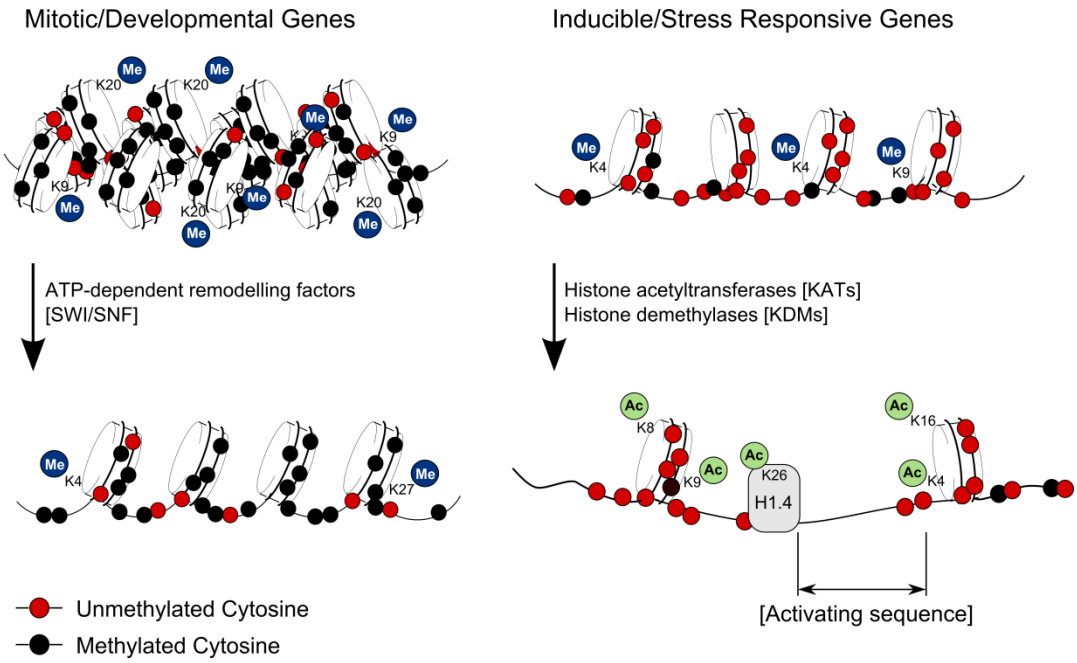


*Figure 1:5 Chromatin Remodelling*

The histones of tightly packed heterochromatin bear an abundance of trimethylated lysine residues at lysine 9 for H3 and lysine 20 for H4. ATP-dependent remodelling enzymes such as SWI/SNF release condensed chromatin from its higher order structure during mitosis and differentiation, generating bivalent domains by methylating lysines 4 and 27 of H3. The chromatin of inducible genes is trimethylated at lysines 4 and 9 of H3 and exists in a poised, but inactive state. Removal of trimethylated marks by histone demethylase activity and acetylation of lysines by histone acetyltransferases exposes gene promoter sequences during transcriptional activation.

These remodeller proteins are vital during active rearrangement of chromatin structure during DNA replication; chromosome segregation during meiosis; regulation of transcriptional repression and initiation; and DNA repair and recombination (132). Regionally acting histone modifiers are unable to penetrate the highly condensed chromatin of silenced genes without this initial remodelling process. Consequently, inducible genes exist in a transcriptionally 'poised' and

inactive state generated by a bivalent pattern of histone marks which facilitates regional access to epigenetic readers.

These remodeller proteins are vital during active rearrangement of chromatin structure during DNA replication; chromosome segregation during meiosis; regulation of transcriptional repression and initiation; and DNA repair and recombination (132). Regionally acting histone modifiers are unable to penetrate the highly condensed chromatin of silenced genes without this initial remodelling process. Consequently, inducible genes exist in a transcriptionally 'poised' and inactive state generated by a bivalent pattern of histone marks which facilitates regional access to epigenetic readers.Reestablishment of histone marks during replication is particularly important for maintaining epigenetic patterns of gene silencing. Genes are replicated according to their chromosomal position, such that housekeeping genes are constitutively localised in pericentromeric regions, and replicate early, whereas inducible genes tend to replicate late (133). DNMTs and HDACs are recruited at replication foci during the S phase of the cell cycle (134), and consequently, tissue-specific and stress-responsive genes are more susceptible to processes which impair maintenance CpG methylation and which alter posttranslational histone modifications during growth and proliferation (135, 136).

#### *1.2.1.5 MicroRNAs*

MicroRNAs (miRNAs) are small non-coding RNAs which regulate gene expression at the post transcriptional level and are derived from genomic sequences coding for stem-loop precursors. MicroRNA-mediated interference is facilitated by complementary base pairing to target mRNAs, mostly at the 3' UTR region. MicroRNAs have documented roles in the regulation of cell proliferation and metabolism, developmental timing, cell death, hematopoiesis and neuronal development (137, 138).

With the exception of those within the Alu repeats transcribed by polymerase III (Pol III), most miRNA genes are derived from primary miRNA transcripts (pri-

miRNAs) produced by Pol II and containing a 5’ cap and a poly(A) tail (139). The primary sequence is cleaved within the nucleus by a multiprotein complex composed of the RNAse III enzyme Drosha and the double-stranded RNA-binding domain (dsRBD) protein DGCR8/Pasha into a 70-nt hairpin precursor (pre-miRNA) (140). Following cytoplasmic export by the Exportin-5 (141, 142), pre-miRNAs are processed into mature 22-nt miRNA:miRNA* duplexes by the RNAse Dicer (143). The miRNA strand of this duplex is incorporated into an RNA-induced silencing complex (RISC), which guides the complex to its mRNA targets and contains the endonuclease Argonaute2 in its catalytic core (144, 145).

Both the regulation and processing of miRNAs are linked via Drosha and Dicer activity regulators; and *cis*-acting modifications and *trans*-acting proteins which control enzyme activity and the stability of mature microRNAs (146)[Figure 1:6].

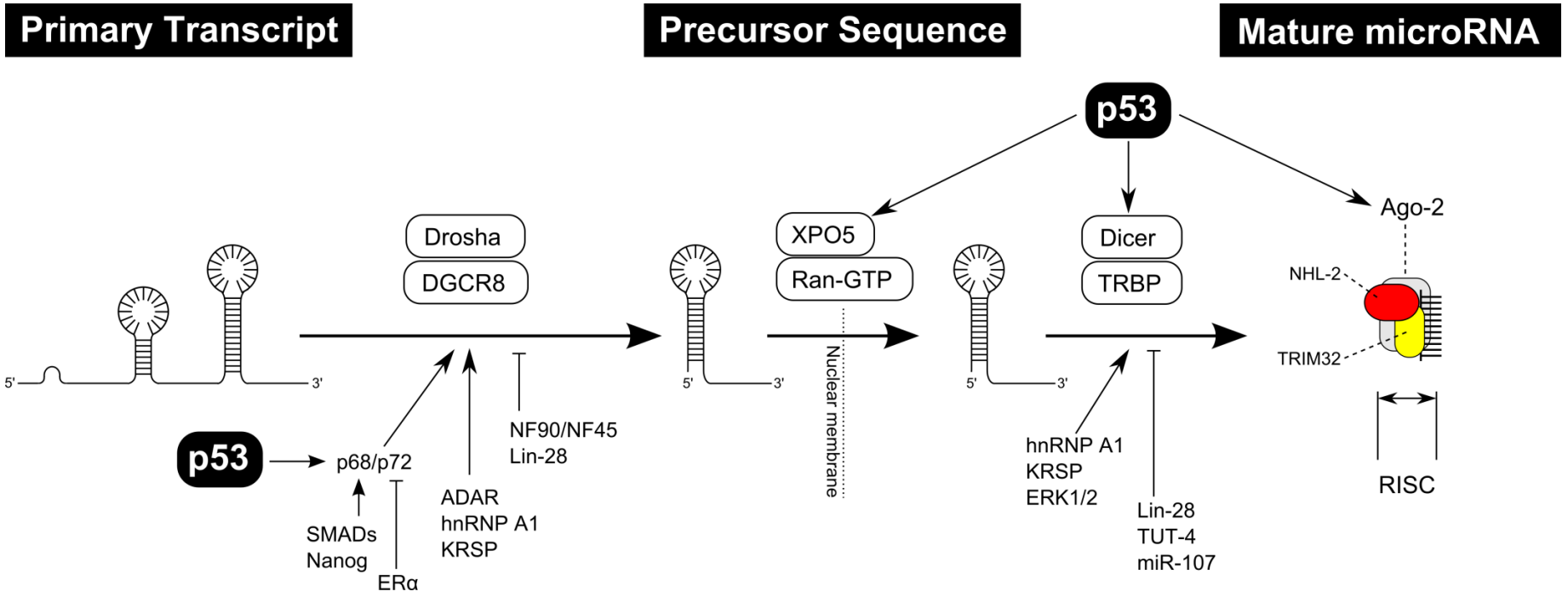


*Figure 1:6 Regulation and Processing of microRNAs*

Following transcription, primary sequences are cleaved into precursor microRNAs by Drosha and translocated from the nucleus to the cytoplasm by Exportin 5. Precursor sequences are further cleaved into ~22 nucleotide duplexes by Dicer, following which the mature microRNA is incorporated into a RISC complex by Argonaute. Control of microRNA maturation is mediated by regulation of Drosha and Dicer RNase activity and expression (147, 148). These processes are directly or indirectly modulated by p53 (149, 150).

Key: RISC - RNA-induced silencing complex; ADAR - adenosine deaminase acting on RNA enzymes; DGCR8 - DiGeorge syndrome critical region gene 8; ERα - estrogen receptor alpha; hnRNP A1 - heterogeneous nuclear riboprotein A1; KSRP - KH-type splicing regulatory protein; SMADs - signal transducers of TGF; NF90/NF45 – nuclear factors 90 & 45; TUT4 - terminal uridylyl transferase; XPO5 – Exportin 5; ERK1/2 – Extracellular signal regulated protein kinases 1 & 2; Ago-2 – Argonaute 2; TRIM32 – Tripartate motif-containing protein 32

Although this field is still in its infancy, it appears that miRNA interference provides a critical means for moderating cellular responses. In particular, p53-mediated effectors are tightly regulated by microRNA-mediated self-regulatory feedback loops which are activated during genotoxic stress (149, 151, 152). Additionally, expression of miRNA regulatory factors is functionally linked to p53-mediated signaling (150). miRNAs regulate the expression of DNA repair proteins and effectors of the DNA damage response (153, 154) and consequently impaired miRNA-mediated regulation of cellular growth and survival signaling is a common feature of disease pathology (155).

### 1.2.2 Epigenetics and Carcinogenesis

It is increasingly evident that maintaining epigenetic control is vital to genomic integrity during an organism's lifespan. A strong association exists between altered epigenetic imprinting and the pathophysiology of chronic disease states (156-158). Despite this, a causal link between disrupted epigenetic control and cancer initiation is a matter of debate. Numerous epigenetic events have been identified as cancer hallmarks. On a global scale, these include disruptions to the nuclear architecture, the CpG island methylator phenotype, and inactivation of DNA repair mechanisms (9, 17, 20, 159). Regional chromatin reorganization in cancer cells occurs in response to altered expression or activity of epigenetic modifiers and chromatin remodelers (160, 161). Thus manipulation of epigenetic factors such as DNA methylation, histone modifications and miRNAs provides the potential for intervening in pathological processes or monitoring disease progression (162, 163).

#### *1.2.2.1 Cancer and DNA Methylation*

During the past twenty years, a strong link between epigenetic reprogramming and carcinogenesis has been revealed – partly through genomic analysis of imprinting disorders, but also due to the association between cancer development and

germline mutations of DNA methylation control enzymes (164). Since then, a consistent pattern of global demethylation, juxtaposed against hypermethylation of CpG islands in gene promoter sequences has been uncovered in many cancer types (157, 165). As our understanding of carcinogenesis has evolved, Knudson's 'two hit hypothesis' has been revised to reflect both the loss of heterozygosity and the loss of imprinting observed in cancer (166, 167). To this end, disrupted DNA methylation patterns and microsatellite instability have both been proposed as stage-specific biomarkers for individual cancer subtypes (158, 168, 169). More than 40 tumour suppressor genes are known to be silenced by hypermethylation in both solid cancers (prostate, breast, GIT) and haematological malignancies (leukemia, lymphoma, myelodysplastic syndromes) (168). Importantly, any defects which affect expression of DNA repair genes or DNMT activity facilitate the acquisition of phenotypic characteristics which drive cancer (170-173).

Imprinted methylation patterns are altered during carcinogenic transformation, causing genomewide hypomethylation and promoter hypermethylation (167, 174). Cancer-associated hypomethylation generally occurs within intergenic and intronic regions of the DNA at microsatellite repeat sequences and transposable elements, and is believed to promote chromosomal instability (158). This is particularly evident for impairments which influence the DNA damage response, as chromatin dynamics facilitate the process of DNA repair and regulate epigenetic patterning following genotoxic damage (108).

#### *1.2.2.2 Cancer and Histone Modifications*

Altered patterns of histone modifications are increasingly recognized as important epigenetic features of cancer, with histone lysine acetylation and methylation being the best characterized. The role of HAT and HDAC activity in modifying acetylation status is vital for regulating gene expression and epigenetic memory, and thus over- or under-expression of these enzymes leads to the aberrant histone acetylation patterns associated with carcinogenesis (175-177). Early in carcinogenic

transformation, levels of monoacetylated H4-K16 and trimethylated H4-K20 decrease, and this characteristic increases with tumour progression (178, 179). These alterations in turn influence recruitment of chromatin remodeling proteins (such as Polycomb group complexes), and promote the cancer phenotype by altering tumour suppressor gene transcription (180-182).

### *1.2.2.3 Cancer and MicroRNAs*

The role of non-coding RNAs in the coordination of cellular responses remains to be fully characterised, however many miRNAs have targets whose regulatory control is disrupted during carcinogenesis (183-185) [Table 1:2].

*Table 1:3 Neoplastic microRNA Targets*

| MicroRNAs | Targets | Role |
|---|---|---|
| miR-221, miR-222, miR106a, miR-290 cluster | p27(Kip1), p21(Cip1), Cdk6, Cdc25A, Cyclin D2, Cyclin E2, Cdk4, pRb, p130/RBL2 | Cell cycle regulators |
| miR-29b, miR-34 family, miR-15a, miR-16 | Mcl-1, Bcl-2, p53 | Antiapoptotic gene repression |
| miR-10b, miR-21, miR-127, miR-199a, miR-210, miR-373, miR-520c | HOXD10<br>PTEN | Metastatic inducers |
| Let-7 family, miR-100, miR-126, miR-218, miR-335 | Ras family<br>HMGA2 | Metastatic suppressors |
| miR-17-92 cluster (miR-17, miR-18a, miR-19a, miR-20a, miR-19b-1, miR-92a-1), miR-378, miR-27a, miR-126 | Tsp-1, CTGF | Angiogenesis |
| miR-200 family, miR-429, miR-30 family | | Cell Migration, Invasion, E-M transition |
| miR-34 family, miR-181, miR-21, Let7 family | | Cancer stem cells |
| miR-9, miR-181, miR-34a, miR-340 | | Invasion |
| miR-205, miR-326, miR-21, miR-335, miR-92a, miR-141 | | Serological diagnosis |

PTEN: phosphatase and tensin homologue

CLL: chronic lymphocytic leukemia

Bcl2: B cell lymphoma

HCC: hepatocellular carcinoma

pRb: Retinoblastoma protein

The significance of these observations is twofold – first, miRNAs have a key role in regulating oncogene expression; and second, promoter regions in miRNA genes are frequently affected by mutation and/or changes in epigenetic patterns of expression (155, 186, 187). These alterations have potential clinical applications as diagnostic and prognostic biomarkers in cancer (188, 189).

Defective microRNA biogenesis is linked to the pathogenesis of chronic disease, and is an emerging finding in cancer subtypes. Dicer1 haploinsufficiency promotes tumour progression in mouse models (190, 191), and Dicer/Drosha expression correlates with tumour severity and therapeutic outcomes (192-195). As a consequence, global patterns of miRNA expression are frequently altered in cancer (138, 196, 197).

### 1.2.3 Epigenetic Antineoplastics

Epigenetic repatterning is associated with the pathology of many diseases – particularly cancer – and these changes have implications for improved diagnosis and the efficacy of treatment regimes. Uncovering the regulatory mechanism which governs epigenetic repatterning is important to our understanding of disease processes, and in particular, those disorders which are associated with ageing or exposure to environmental toxins (128). Equally important is to understand how epigenetic regulation processes can be manipulated to enhance pharmaceutical efficacy and prevent resistance. Use of histone modifiers and DNMT inhibitors in chemotherapy is in its infancy, however results are promising.

A combinatorial strategy which targets epigenetic modifiers is emerging as a way to improve remission rates during cancer chemotherapy. Epigenetic antineoplastic drugs currently under review predominantly target DNMTs and Class I and II HDACs, albeit via a variety of different biochemical mechanisms. The use of epigenetic modulators to target epimutations in cancerous tissue has rapidly gained support amongst the medical community. DNA methyltransferase inhibitors such as

Suberoylanilide hydroxamic acid (SAHA, Vorinostat) are currently used in clinical settings as chemotherapeutic agents (198). These studies have also demonstrated HDACi-induced downregulation of DNA repair and cell survival proteins, which is thought to render tumorigenic cells more susceptible to other modalities of cancer therapy than 'normal cells'. The intention of this treatment strategy is to 1) restore sensitivity to intracellular oxidative and metabolic stress associated with carcinogenesis, and 2) synergistically enhance the cytotoxicity of commonly used antineoplastics (175, 199).

SIRT1 is an NAD+ dependent lysine deacetylase which has nuclear and cytoplasmic substrates, of which p53 is the most extensively characterised (200). SIRT1 suppresses p53-regulated transcriptional activity by stabilising p53 in its non-acetylated form (201). SIRT1-mediated deacetylation inhibits p53 transactivation (202), blocks nuclear translocation (203) and down-regulates expression of p53 transcriptional gene targets. Modulation of SIRT1 activity has been proposed as a strategy for reducing the pathological features of diseases associated with ageing (204, 205), and for overcoming resistance in diseases with p53 inactivation as part of their etiology (90, 206). However, as yet, few in vitro studies have been performed to test the efficacy of SIRT1 activity modulators as adjuvants in chemotherapy regimens (207). The effect of SIRT1 on cellular physiology and the use of SIRT1-targeting pharmaceuticals will be explored in more detail later in this chapter.

## 1.3 HISTONE DEACETYLASES

Histone deacetylases (HDACs) belong to a family of enzymes which modulate chromatin structure by altering the acetylation status of nucleosomal histones. Their general cellular role is to regulate transcriptional activity by opposing the action of histone acetyltransferases. These enzymes also influence the activity of non-histone proteins, including transcription factors and glucocorticoid receptors;

and perform functional roles in maintaining genomic integrity by recruiting and stabilizing DNA methylation and repair complexes. Thus HDACs are considered to be integral to the coordination of the epigenetic machinery.

Mammalian HDACs are categorised into four classes based on their homology to histone deacetylases in yeast. Members of Classes I, II (subdivided into IIa and IIb) and IV have metal ion-dependent catalytic activity, whereas Class III HDACs are NAD+-dependent. Although all classes are specific for acetylated lysine residues, individual family members have unique subcellular localisation, tissue specificity and cellular function (208) [Table 1:3].

*Table 1:4 Classification of Histone Deacetylases*

| *Class* | *Enzyme* | *Subcellular Localization* | *Site/Expression* | *Function* | *Refs* |
|---|---|---|---|---|---|
| Class I (yRpd3-like) | HDAC1 | Nucleus | Sin3, NuRD, CoREST, PRC2 | Transcriptional Repression | (113) |
| | HDAC2 | Nucleus | | | (209) |
| | HDAC3 | Nucleus/cytoplasm | N-CoR-SMRT | | |
| | HDAC8 | Nucleus | | | |
| Class IIa (yHda1-like) | HDAC4 | Nucleus/cytoplasm | Brain, skeleton | Transcriptional repression | (113) |
| | HDAC5 | Nucleus/cytoplasm | Muscle, heart, brain | Coordinate extracellular signals with gene expression during development and disease | (209) |
| | HDAC7 | Nucleus/cytoplasm | Endothelium, thymocytes | | |
| | HDAC9 | Nucleus/cytoplasm | Muscle, heart, brain | | |
| Class IIb (yHda1-like) | HDAC6 | Cytoplasm | α-Tubulin, cortactin, interferon receptor IFNαR, chaperones | Cytoskeletal remodeling, membrane translocation | (209) |
| | HDAC10 | Nucleus/cytoplasm | | | |
| Class III (ySir2-like) | Sirtuins | Nucleus/cytoplasm/Mitochondria | SEE TABLE 1.4 FOR DETAILS | | |
| Class IV | HDAC 11 | Unknown | Brain, heart, muscle, kidney, testis | Unknown | (209) |

yRpd3 - yeast Reduced potassium dependency 3; yHda1 - yeast Histone deacetylase-A1; ySir2 - yeast Silent information regulator 2

### 1.3.1 Class III Histone Deacetylases

Sirtuins belong to a conserved family of NAD+-dependent deacetylases which share homology with silent information regulator 2 (Sir2) enzymes from yeast. Sirtuins couple the enzymatic cleavage of NAD+ to the deacetylation of key acetyl-lysine residues to generate nicotinamide and 2'-O-acetyl-ADP-ribose (189-191) [Figure 1:7]. Although the majority of sirtuins have NAD+-dependent deacetylases activity, two Sir2 family enzymes (SIRT4 and SIRT6) predominantly catalyse ADP-ribosylation reactions, which proceed via cleavage of NAD+ with the subsequent production of nicotinamide (210, 211).

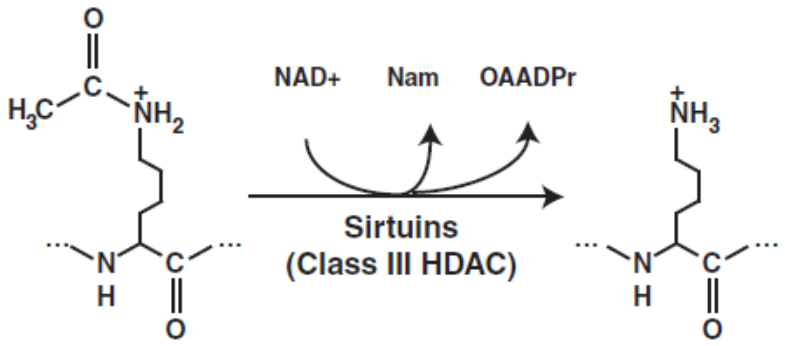


*Figure 1:7 Class III Histone Deacetylase Catalytic Mechanism*

Sir2 family NAD+-dependent deacetylases couple the hydrolysis of NAD+ to the deacetylation of acetyl-lysine residues of protein substrates to yield nicotinamide (Nam) and the metabolite *O*-acetyl-ADP-ribose (OAADPr). (212, 213).

Sirtuins are functionally important for numerous cellular processes, including cell cycle regulation, nutrient metabolism, and cellular ageing (214). The cellular outcome of sirtuin-mediated regulatory control is activation of cellular adaptive responses to environmental change [Table 1:4]. Sirtuin activity realigns cellular imprinting patterns, causing long-term adaptive change which reactivates oncogenes and/or down-regulates tumour suppressor gene expression (209, 215).

*Table 1:5 Functions of Class III Deacetylases in Humans*

| | Localisation | Targets | Function |
|---|---|---|---|
| SIRT1 | Nuclear/Cytoplasmic | P53, NF-κB, FOXO1, FOXO3, Bax, HIF1α, MyoD, Ku70, β-Catenin, c-Myc, FXR, TORC2, SREBP, PER2, LXR, PPARγ, p300, Tat, PCAF, ERα, AR, SMAD7, p73, Sox9, HSF1, PGC1α, HEY2, NCoR/SMRT, E2F1, CLOCK, RelA/p65 | Energy metabolism<br>Fatty acid and cholesterol mobilisation<br>Circadian rhythm regulation<br>DNA damage response |
| SIRT2 | Nuclear/Cytoplasmic | αTubulin, FOXO3a, H4 | Cell cycle control |
| SIRT3 | Mitochondrial | AceCS2, GDH Complex 1, LCAD, HMG-CoA Synthase 2, IDH2, MnSOD, SOD2 | ATP production<br>Regulation of mitochondrial proteins<br>Thermogenesis |
| SIRT4 | Mitochondrial | GDH, IDE, ANT | Insulin secretion<br>Fatty acid oxidation |
| SIRT5 | Mitochondrial | CPS1 | Urea cycle |
| SIRT6 | Nuclear | NF-κB, HIF1α, Helicase, DNA Polymerase β, CtIP, H3K9, H3K56 | Telomeric stability<br>DNA repair<br>Inflammation |
| SIRT7 | Nucleolus | RNA Polymerase Type I, E1A, SMAD6 | RNA polymerase I transcription |

Key - P53: tumour suppressor protein p53; FOXO: Forkhead box O; Bax: Bcl2-associated protein 2; HIF: Hypoxia-inducible factor; HSF1: Heat shock factor 1; PGC-1α: Peroxisome proliferator-activated receptor gamma coactivator 1α; NF-κB: Nuclear factor kappa B; TORC2: Transcriptional coactivator for CREB; LXR: liver X receptor; FXR: farnesoid X receptor; SREBP: Sterol regulatory element binding protein; PER2: period circadian homologue 2; NCoR/SMRT: nuclear corepressor/silencing mediator for retinoid and thyroid receptors; H4: histone 4; AceCS2: Acetyl-CoA synthase 2; LCAD: long chain Acyl-CoA dehydrogenase; HMG-CoA synthase 2: 3-hydroxy-3-methylglutaryl CoA synthase 2; IDH2: isocitrate dehydrogenase 2; MnSOD: Mn-superoxide dismutase; SOD2: superoxide dismutase 2; GDH: Glutamate dehydrogenase; CPS1: carbamoyl phosphate synthase 1; CtIP: C-terminal binding protein interacting protein; H3K9: histone 3 lysine 9; H3K56: histone 3 lysine 56. (Based on reviews by 200, 210, 216, 217)

### 1.3.2 SIRT1

Human SIRT1 shares the closest homology with its yeast counterpart, and its cellular and physiological roles have been the most extensively characterized. The rest of this chapter will focus on biochemical features of SIRT1, with particular emphasis on the role SIRT1 plays in regulating cellular responses to genotoxic damage, and the potential use of SIRT1 modulators in therapeutic disease intervention.

SIRT1 is predominantly localised in the nucleus, and has both histone and non-histone substrates (218). Identified in the 1990s, SIRT1 rapidly gained a reputation as an anti-ageing enzyme for its role in prolonging lifespan in yeast, worm and fly models. Since then, numerous physiological effects of SIRT1 in various cell types have been identified. To date, the most extensively studied effects of SIRT1 activity are those which influence adaptive responses to metabolic, oxidative and oncogenic stress. Non-histone substrates of SIRT1 regulate transcriptional activation, cell cycle progression, survival and senescence, DNA damage and DNA repair responses, metabolic activity, gene expression and signal transduction. These induce physiological changes which affect fat storage and mobilisation, insulin sensitivity, glucose tolerance, neuroprotection, cardioprotection, inflammation and stress resistance in a tissue-specific manner [Table 1:5].

SIRT1 influences gene transcription and genomic stability by modifying the activity of chromatin remodelling complexes, DNA methyltransferases, and histone regulatory enzymes. Furthermore, in its role as a histone deacetylase, SIRT1 is recruited to sites of genotoxic DNA damage and regulates the acetylation status of histones in proximity to the lesion. Thus SIRT1 maintains genomic integrity by activating and recruiting the DNA repair machinery and by remodelling regional areas of chromatin when cells are exposed to mutagens (219).

*Table 1:6 Physiological Roles of SIRT1*

| Tissue | Target | Physiological Effects | Organismal Outcome |
|---|---|---|---|
| Liver | ↑PGC1α, ↑FOXO1, ↓TORC2, ↓STAT3 | ↑ Late Gluconeogenesis, ↓Glycolysis | Metabolic homeostasis |
| | ↑PGC1α, ↑PPARα | ↑Fatty Acid Oxidation | ↑Insulin sensitivity |
| | ↑LXRα, ↑FXR, ↓SREBP | ↑Cholesterol Efflux | ↑Glucose tolerance |
| | ↓NF-κB | ↓Inflammation | ↓Fatty Liver |
| Adipose Tissue | ↓PPARγ | ↑Lipolysis | ↓Fat storage |
| | ↓PPARγ | ↑Mobilisation of FFAs | ↑Insulin sensitivity |
| | ↓PPARγ | ↓Lipogenesis | ↓Macrophage infiltration |
| Pancreas (β Cells) | ↓Ucp2 | ↑Insulin Secretion | ↑Glucose tolerance |
| Brain/CNS | ↑AgRP | ↓Leptin Signaling | ↓Neurodegeneration |
| | ↓POMC | ↓Energy Expenditure | |
| | ↑CLOCK:BMAL1, ↑PER2 | ↑Stabilization of Circadian Rhythm | ↑NAD Biosynthesis |
| Heart | ↓PPARγ | ↑Insulin sensitivity | ↑Cardioprotection |
| Skeletal Muscle | ↑PGC1α | ↑Mitochondrial fatty acid oxidation | Improved insulin sensitivity |
| | ↓PTP1B | ↓Inflammation | |

Key - PGC1α: peroxisome proliferator-activated receptor-γ coactivator 1α; PPARα: peroxisome proliferator-activated receptor α; LXRα: liver X receptor α; FXR: farnesoid X receptor; SREBP: steroid receptor binding protein; Ucp2: uncoupling protein 2; FOXO1: forkhead box O1; TORC2: transcriptional coactivator for CREB; STAT3: signal transducer and activator of transcription 3; POMC: propiomelanocortin; BMAL1: brain and muscle aryl hydrocarbon receptor nuclear translocator (ARNT)-like; CLOCK: Circadian Locomotor Output Cycles Kaput; PER2: Period circadian protein homologue 2. (Based on reviews by 220, 221-224)

### *1.3.2.1 Modulation of SIRT1 Activity*

SIRT1 binds a consensus peptide sequence [K(V/S)(V/T)GG**K**KXXK], however specificity for the target lysine residue within this region varies between substrates, with the greatest affinity shown for histone H4 acetylated at lysine 16 [H4 Ac(K16)], and p53 acetylated at lysine 382 [p53 Ac(K382)] [Table 1:6]. Based on relative SIRT1 substrate affinities acetylation of p53 at residue 382 was used as a marker for p53 activity in this study.

*Table 1:7 Binding affinity for SIRT1 substrate sequences*

| Substrate | Sequence | $K_m$ (μM) |
|---|---|---|
| Consensus | K(V/S)(V/T)GG**K**KXXK | |
| p53 Ac(K382) | HLKSKKGQSTSRHK**K**LMFKTEG | 4.3 ± 0.5 |
| H3 Ac(K9) | ARTKQTAR**K**STGGKAPRKQL | ~239 |
| H3 Ac(K14) | KSTGG**K**APRKQ | 420 ± 40 |
| H3 Ac(K115) | HA**K**RVTIQKKD | 9.2 ± 1.6 |
| H4 Ac(K5) | SGRG**K**GGKGLGKGGAKRHRK | 140 ± 32 |
| H4 Ac(K8) | SGRGKGG**K**GLGKGGAKRHRK | 54 ± 17 |
| H4 Ac(K12) | SGRGKGGKGLG**K**GGAKRHRK | 105 ± 15 |
| H4 Ac(K16) | SGRGKGGKGLGKGGA**K**RHRKILRD | 1.1 ± 0.3 |
| H4 Ac(K77) | HA**K**RKTVTSLD | 13.1 ± 1.8 |
| H4 Ac(K79) | HAKR**K**TVTSLD | 10.5 ± 1.4 |
| H2B Ac(K82) | YN**K**KSTISARE | ND |

(from 225, 226), Target lysine residue is marked in bold; ND: Not Determined

Structurally, SIRT1 is more open in its unbound apo- state, and adopts a closed conformation during entry of target substrates into the binding site [Figure 1:8]. Affinity for NAD+ entry into the catalytic core increases when SIRT1 is in its closed conformation, and thus conformational changes are induced upon substrate binding which enhances catalytic turnover (227).

Since the discovery of SIRT1's anti-ageing potential, there has been a drive to develop novel SIRT1 activity modulators as therapeutic agents. Nutritional

compounds were amongst the original SIRT1 modulators identified, however their pharmacokinetic properties proved a hindrance to therapeutic efficiency. Synthetic SIRT1 modulators which increase the V*max* or lower the K*m* for substrates are considered to have the most attractive clinical potential, with EX-527 reaching the clinical trial stage in recent months [Table 1:7].

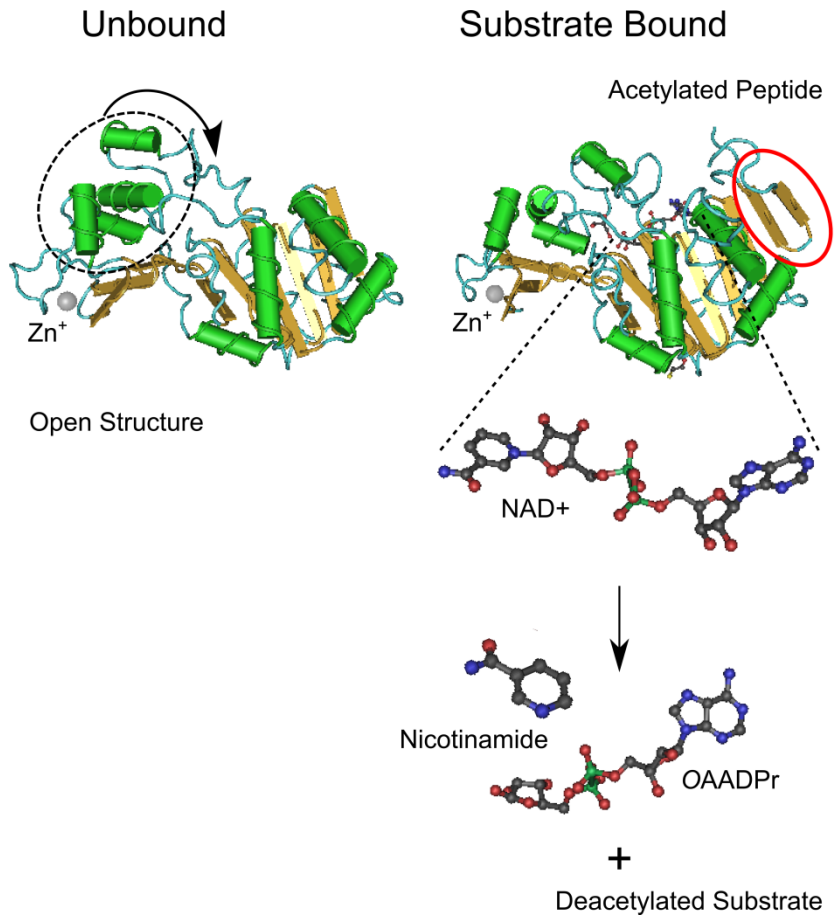


*Figure 1:8 SIRT1 undergoes conformational changes during inhibition and substrate binding*

Figure was created using 3D protein structures uploaded to the Molecular Modelling Database by Zhao et al. and Davenport et al (228, 229). Data files were manipulated with Cn3D 4.3.1 software produced by the National Center for Biotechnology Information (230). The SIRT1 enzyme reaction proceeds via an alkylamidate intermediate, formation of which facilitates transfer of the acetyl moiety from the substrate lysine residue. 2'-*O*-acetyl-adenosine diphosphoribose (*O*AADPr) is released from the catalytic site along with the deacetylated substrate and nicotinamide (212, 231-233). NAD+: Nicotinamide adenine dinucleotide; EX-527: 6-Chloro-2,3,4,9-tetrahydro-1H-carbazole-1-carboxamide; *O*AADPr: 2'-*O*-acetyl-adenosine diphosphoribose

EX-527 is an indole analogue which was developed to target human SIRT1 in a concentration-dependent manner, with an $IC_{50}$ of 38 nM measured using an *in vitro* Fluor de Lys assay (234). EX-527 has some inhibitory effect on other members of the sirtuin family, with much lower potency (SIRT2, $IC_{50}$ = 19.6 µM; and SIRT3, $IC_{50}$ = 48.7 µM)(235). On entry to the hydrophobic binding pocket, EX-527 interacts with the $NAD^+$ ribose moiety and stabilises SIRT1 in its closed structure, forcing $NAD^+$ to extend into an inactive conformation (229) and blocking substrate release (236) [Figure 1:9].

*Table 1:8 SIRT1 Activity Modulators (Based on reviews by 214, 237, 238-241)*

| Type | Modulator | Kinetics/Function |
|---|---|---|
| Nutraceuticals | Sulforaphane | Inhibitor |
| | Resveratrol | Activator |
| | Quercetin | Activator |
| | Butein | Activator |
| Inhibitors | Nicotinamide | $IC_{50}$: 50-100 µM |
| | 2-Anilino-benzamide | $IC_{50}$: 17 µM |
| | Suramin | $IC_{50}$: 2.42 µM |
| | $Cu^{2+}/Zn^{2+}$ | $IC_{50}$: 1 µM |
| | EX-527 | $IC_{50}$: 0.098-1 µM |
| | Sirtinol | $IC_{50}$: 37.6-131 µM |
| | Meta-sirtinol | $IC_{50}$: 63 µM |
| | Para-sirtinol | $IC_{50}$: 13 µM |
| | Salermide | $IC_{50}$: 76 µM |
| | Tenovin-1 | $IC_{50}$: 21 µM |
| | Cambinol | $IC_{50}$: 56 µM |
| | Splitomicin | $IC_{50}$: 5 µM |
| Activators | $NAD^+$ | $K_m$: 90 µM |
| | SRT1720 | $K_m$: 0.16 µM |
| | SRT2183 | |
| | Pyrroloquinoxaline | $EC_{1.5}$: 10 µM |
| | Oxazolopyridine | $EC_{1.5}$: 0.09 µM |

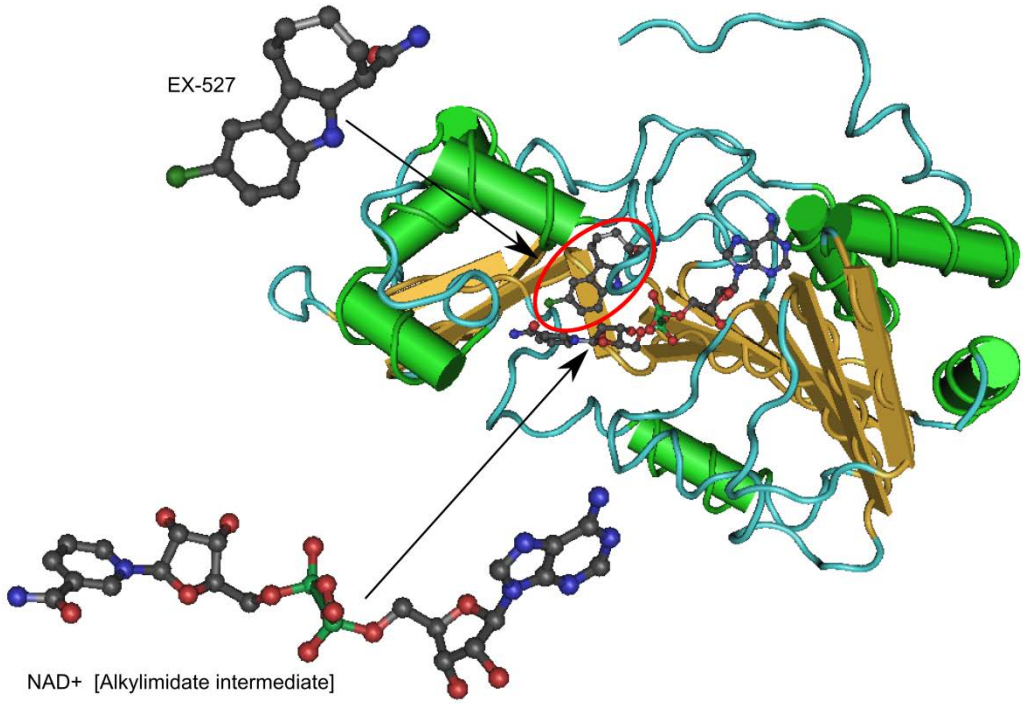


*Figure 1:9 EX-527 and NAD+ interact within the SIRT1 catalytic cleft*

EX-527 occupies the C-binding pocket in the catalytic cleft of SIRT1, and interacts with the NAD+ ribose moiety to block catalysis (229, 236).

### *1.3.2.2 Biological Regulators*

SIRT1 activity is coupled to substrate usage by its relationship with NAD+ availability and the NAMPT/NMNAT1 salvage pathway for NAD+ regeneration (242-244), and has three main classes of endogenous protein regulators – protein kinases, catalytic domain binders and sumoylation regulators. Phosphorylation of SIRT1 at Thr522 by Dual specificity regulated kinases (DYRK1A or DYRK3) increases SIRT1 activity, promoting cell survival during genotoxic stress (245).

Casein kinase 2 (CK2) increases SIRT1-mediated p53 deacetylation by phosphorylating Ser 154, 649, 651 and 683 residues (246), and phosphorylation of Ser27 by c-Jun N-terminal kinase 2 (JNK2) increases SIRT1 activity by promoting stabilisation (247). N-terminal domain binding of active regulator of SIRT1 (AROS)

also promotes SIRT1 activity by lowering its $K_m$ (248), whereas deleted in breast cancer (DBC-1) acts as a SIRT1 catalytic domain inhibitor (249). Interestingly, the catalytic activity of SIRT1 is enhanced by sumoylation of lysine 734 during DNA damage, and yet is suppressed by SENP1 (sentrin-specific protease)-mediated desumoylation during chronic stress conditions (239), indicating that SIRT1 may modulate different cell survival responses depending on the intracellular environment. SIRT1 expression varies according to tissue type and its metabolic requirements, with transcription regulated by p53, hypermethylated in cancer (HIC1) and E2F1 response elements in its promoter region. HIC1 is a transcriptional repressor which is activated by p53, and whose inhibition of SIRT1 transcription is thought to act as a regulatory feedback loop (250). E2F1-mediated pro-apoptotic signaling during the DNA damage response is also mediated by SIRT1. Activation of E2F1 by ATM stimulates SIRT1 transcription, and SIRT1-mediated deacetylation of E2F feeds back to suppress its transcriptional activity (251). Additionally, SIRT1 expression is regulated at the level of protein translation via HuR-mediated stabilization of SIRT1 mRNA (252), and non-coding RNA-induced interference by microRNAs miR34a, miR199 and miR200a (253).

#### *1.3.2.3 Targets*

SIRT1 is predominantly known for its effect on cellular growth and survival via inactivation of p53-mediated apoptosis and cell cycle arrest (201, 202, 254). However SIRT1 also induces p53-independent effects on survival signaling. SIRT1 deacetylation of Smad7 at Lys64 and 70 inhibits TGFβ-induced apoptosis in mesangial cells, and also plays a role in regulating Smad7 expression through Smad ubiquitination regulatory factor (SMURF)-mediated proteolysis (255). SIRT1 also acts as a negative regulator of the histone acetyltransferase p300 by deacetylation and subsequent sumoylation of lysines 1020 and 1024. Both SIRT1 and p300 co-regulate a subset of common substrates which are important for cellular growth and proliferation via this mechanism (256). Additionally, mTOR-mediated

phosphorylation of SIRT1 at serine 47 inhibits SIRT1 activity and promotes cellular senescence rather than growth during genotoxic damage (257). SIRT1 also blocks inflammatory signaling by deacetylating the RelA/p65 subunit of NF-κB at lysine 310, promoting TNFα-induced apoptosis (258) and STAT3 transcriptional activity (259).

SIRT1 influences epigenetic control of gene transcription through histone-mediated chromatin remodeling (219). This is achieved, in part, by modulation of histone methyltransferase SUV39H1 targeting, which promotes accumulation of trimethylated histone H3 at lysines 9, 79 and 20 (260); deacetylation of histone H4 at lysine 16 and histone H3 at lysine 9 (261); and recruitment of histone H1b to facultative heterochromatin (262). This may be associated with maintenance of CpG island imprinting patterns and gene silencing through co-recruitment of DNA methyltransferase 3b (DNMT3b) (263). SIRT1 is also thought to influence the structural maintenance of chromatin within the nucleus. In this model, heterochromatin islands within the nuclear architecture are destabilized by environmental insult, and depend on SIRT1 activity for restoration (264).

The role of SIRT1 as a histone deacetylase has implications for embryonic growth and development, with the SIRT1 null genotype proving to be lethal in the perinatal period (265-267). Future work to uncover the role of SIRT1 in Notch signaling may provide clues as to why this is the case. In *Drosophila*, SIRT1 forms a co-repressor complex with Lysine-specific demethylase 1 (LSD1) to remove H4K16 acetylation marks in genes regulated by the Notch signaling pathway by associating with CSL in Notch target genes (268). Interestingly, although the *SIRT1*$^{+/-}$ genotype in mice is compatible with life, SIRT1 haploinsufficiency is associated with tumorigenesis, particularly in conjunction with impaired p53 or PARP1 expression. Primary tumours in these mice demonstrate numerous chromosomal abnormalities, including extensive aneuploidy, translocations, dicentricity, strand breaks and deletions (266). Also, SIRT1 expression is reduced in certain human carcinomas,

suggesting that loss of functional SIRT1 interferes with the DNA damage response and contributes to genomewide instability.

### *1.3.2.4 SIRT1 and the DNA Damage Response*

SIRT1 plays numerous roles in the maintenance of genomic stability and plays an integral role in the coordinated repair of stress-induced DNA damage. (269, 270). In the DNA damage sensing complex, SIRT1 deacetylates Nijmegen breakage syndrome 1 (NBS1), activating ATM and ATR cell cycle checkpoint kinases (271, 272), and promoting γH2AX foci formation (273). SIRT1 also promotes and integrates the activity of different types of DNA repair. Increased UV-induced strand break repair is associated with SIRT1-mediated Ku70 activation (274), and deacetylation of XPA (Xeroderma Pigmentosum Group A) by SIRT1 at lysines 63 and 67, indicating a role in nucleotide excision repair (NER) (275).

Additionally, SIRT1 deacetylates Apurinic endonuclease/redox-factor 1 (APE/Ref1) at lysines 6 & 7, facilitating its binding to X-ray Repair Cross Complementing 1 (XRCC1) during base excision repair (BER) (269), and is recruited to double strand breaks, where it promotes homologous recombination by deacetylating Werner helicase (WRN) (276, 277). SIRT1-mediated regulation of signaling targets produces a differential effect on cell cycle control and apoptotic signalling. SIRT1 potentiates p53-, p73 and FOXO-mediated growth arrest and up-regulates DNA repair genes whilst attenuating stress-induced apoptosis (202, 278-280); and triggers cell cycle arrest and senescence by deacetylating Rb and c-Myc (281, 282) [Figure 1:10].

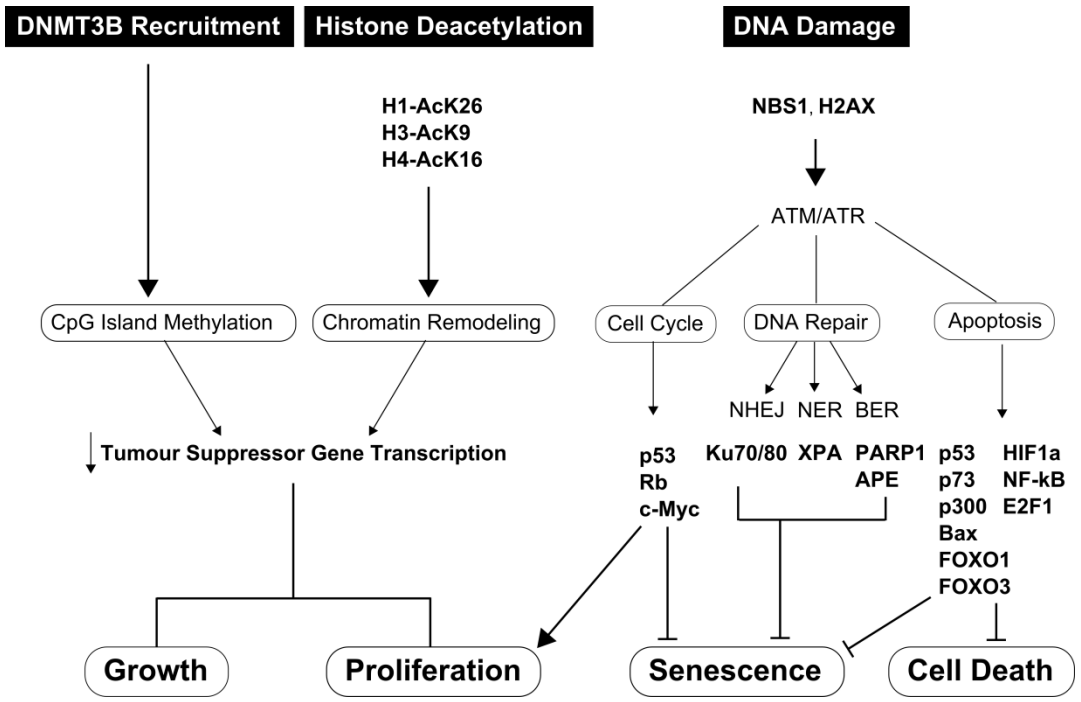


*Figure 1:10 SIRT1 and the DNA Damage Response*

SIRT1 influences cellular adaptation to genotoxic stress by deacetylating mediators of the DNA damage response. By promoting cellular growth and DNA repair, SIRT1 primes cells to overcome DNA damage. SIRT1 also blocks p53-mediated cell cycle arrest and apoptosis, preventing DNA damage-induced senescence and allowing progression through cell cycle checkpoints

Key – DNMT3B: DNA methyltransferase 3B; NBS1: Nijmengen Breakage Syndrome protein 1; H2AX: histone 2AX; ATM: ataxia-telangiecatesia-mutated protein; ATR: ATM and Rad3-related protein; NHEJ: non-homologous end joining; NER: nucleotide excision repair; BER: base excision repair; XPA: Xeroderma Pigmentosum Group A; PARP1: poly(ADP-ribosyl) polymerase; APE: ; FOXO1 & 3: forkhead box O 1 & 3; HIF1α: hypoxia-inducible factor 1α; NF-κB: nuclear factor kappaβ

### *1.3.2.5 The role of SIRT1 in cancer*

According to current mechanistic evidence, SIRT1 activity can be tumour-promoting or tumour-suppressing, and thus classification of SIRT1 as either a tumour suppressor or oncogene is ambiguous. SIRT1 prevents tumorigenesis in normally functioning cells by maintaining DNA fidelity (264, 265). Once initiation has occurred, however, SIRT1 promotes cancer progression by enabling neoplastic cells to adapt to the tumour microenvironment (266), and can facilitate cancer evolution

through the accumulation of genetic alterations (267), evasion of growth suppression and resistance to cell death signalling (245, 268, 269).

Additionally, SIRT1 promotes multidrug resistance by inducing enzymes which regulate drug metabolism and by activating cellular detoxification mechanisms (183, 270, 271). Neoplastic cells frequently overexpress SIRT1 (272, 273), and consequently inhibition of SIRT1 is a potential pharmaceutical strategy for sensitising resistant cancer cells to cytotoxic drug therapy (274).

## 1.4 ARSENIC-MEDIATED CARCINOGENICITY

Arsenic is classified as a Class 1 human carcinogen by the International Agency for Research on Cancer (IARC) monographs (283, 284). Based on criteria outlined in the IARC Preamble (285), the general consensus is that that there is sufficient epidemiological evidence for the carcinogenicity of inorganic arsenic compounds, including arsenic trioxide, arsenite, and arsenate, and these agents cause cancer of the lung, urinary bladder, and skin (283, 286, 287). Yet regardless of a clear association between arsenic exposure and cancer risk determined in epidemiological studies, the nature of arsenic-induced cancer remains a complex and incompletely understood process. Consequently, investigators are keen to uncover mechanistic data which provides evidence for arsenic carcinogenesis which may reduce the uncertainty introduced in meta-analyses.

So far, the consensus opinion is that arsenic does not directly interact with cellular DNA, although it appears to introduce conditions which promote mutagenesis. These include induction of oxidative DNA damage (288, 289), aneuploidy (290), destabilisation of the genome (microsatellites), and suppression of DNA repair. Additionally, although arsenic does not cause point mutations, it acts as a co-mutagen with UV or ionising radiation (291), and in the presence of DNA alkylating agents such as methyl methanesulfonate (292). These investigations support epidemiological findings of an increased cancer risk with sun exposure and for individuals who ingest tobacco smoke or who chew betel nut (293-295). For exposed populations, risk of arsenic-induced skin lesions is significantly related to prolonged sun exposure (296), polymorphisms of glutathione-S-transferase (GST), methylene tetrahydrofolate reductase (MTFR), and DNA repair genes (297, 298), folate deficiency/vitamin B intake (299, 300), and clearance capacity of urinary metabolites (301-303). Thus, epidemiological and experimental studies indicate that several different mechanisms may be involved.

Oral administration of arsenate will cause cancer in mice, rats or hamsters; however there are questions as to the relevance of animal models of carcinogenesis when applied to human cancer risk. The main issue with these studies is how arsenic-induced carcinogenesis in animals should be interpreted in the context of human exposure (304, 305), as biotransformation and detoxification capacity differs between humans and animals (306). Ultimately, these analyses reveal problems inherent in confirmation of causality in toxicological studies performed with animal models.

Cell transformation assays are an alternative to animal studies for investigations into arsenic carcinogenicity. Using anchorage-independent growth, colony formation and tumour formation in SCID mice as endpoints, these studies demonstrate that arsenic induces transformation in culture. Investigations into human cell transformation use genetically altered cell lines, rather than primary cultures, in which the cells have acquired an immortalised phenotype through mutations to the p53 gene, introduction of TERT genes, or by SV40 viral infection. During carcinogenesis, cell populations undergo a sequential process in which cells with procarcinogenic mutational changes are retained, whilst non-immortalised (finite lifespan) cell strains senesce before they have acquired all the genetic changes necessary for transformation (307). To date, *in vitro* arsenic exposure models have shown that at least 20 weeks of treatment is required in order for arsenic-exposed cells to acquire a malignant phenotype. However in none of these studies was a primary cell strain used. The most likely reason for using an adapted cell line is that a limited number of divisions achievable from primary cells is prohibitive for use in extended treatment regimes. Therefore it could be argued that these are not actual models of carcinogenesis but instead describe changes to cells with pre-existing mutations which have adapted them for culture.

### 1.4.1 Carcinogenic Properties of Arsenic

Arsenic does not interact directly with the DNA in a manner such as direct carcinogens, although it can introduce intranuclear conditions by which mutagenesis is more likely. These include induction of oxidative DNA damage (288, 289), aneuploidy (290), interference with DNA repair and genomic instability (microsatellite formation). Additionally, arsenic produces phenotypic changes which appear to promote cellular transformation. Patterns of gene expression are altered in arsenic exposed tissues as a consequence of epigenetic changes to gene promoters (308, 309), dysregulated signal transduction pathway activation (310-313), and shifts in steroid receptor binding (314). Moreover, arsenic influences mitochondrial function such that cells adopt an anaerobic profile consistent with oncogenic reprogramming of nutrient use and energy production (315).

Long-term low level exposure to arsenic induces other pro-carcinogenic cellular changes, many of which are adaptive responses to arsenic toxicity (316, 317). These include dysregulated energy metabolism, altered genomic fidelity and pathological gene expression (286). In combination with extracellular conditions which facilitate clonal selection, arsenic toxicity produces gradual genotypic, phenotypic and morphological changes which progress to tumour formation.

Dose-response data further complicates our understanding of arsenic-induced carcinogenesis. Whilst sublethal concentrations of arsenic (generally 0-5 μM, depending on cell type) generate protective responses consist with stress adaptation (antioxidant gene expression, DNA repair, pre-inflammatory cytokines, proliferative signalling) (310, 318-320), higher concentrations (5-100 μM) induce genes which trigger cell cycle arrest and apoptosis (321-324). From these data, it appears that lower arsenic doses induce phenotypic changes which promote carcinogenesis, and evidence for this this is supported by in vitro transformation studies.

#### *1.4.1.1 Gene Expression*

Arsenic exposure interferes with oncogene and tumor suppressor gene expression, producing an outcome which depends on cell type, concentration and duration of exposure. Microarray analyses of gene expression in arsenic treated cells have identified hundreds of affected genes, most of which fall within these specific categories: cellular stress response, cell cycle control, redox regulation, and DNA repair (325-328).

Arsenic exposure influences cell cycle control by disrupting the p53-Mdm2 axis (329), inhibiting the activity of checkpoint proteins, and by altering cyclin D1 expression (330). However the outcome of arsenic-induced cell cycle dysregulation is dose- and duration- specific. Prolonged arsenite exposure at higher concentrations causes p53 to accumulate, increasing expression of the cyclin-dependent protein kinase inhibitors (CDKIs) p21 WAF1 and p27, and stalling the cell cycle at $G_1$/S (331). Non-lethal (submicromolar) arsenite concentrations, however, have the opposite effect, causing an up-regulation of cyclin D1 transcription which disrupts cell cycle control (332). Intermediate doses of arsenic (5-25 uM) also induce proliferation by activating Elk1 and ATF2 (333); and by increasing cyclin D1 levels (334).

In tissue systems, arsenic promotes cellular invasiveness and tumour migration by stimulating extracellular matrix remodeling, anchorage-independence and neovascularization. Arsenic stimulates matrix metalloproteinase production (335, 336), although this observation appears to be limited to lower treatment doses (337). In vitro vascularization studies demonstrate low-dose stimulation and high-dose inhibition of vascular endothelial growth factor (VEGF) secretion and endothelial cell proliferation with arsenic exposure (338, 339). In vivo studies correlate with these findings, demonstrating increased vessel growth and density in chicken chorionic membrane and murine studies conducted at arsenic

concentrations between 0.033 and 1 μM (340, 341); however tumour vasculature breaks down at higher (> 1 μM) doses (342).

Arsenic exposure generates a dose- and duration-dependent effect on cell survival. Acute high doses activate intrinsic apoptotic pathways through p53 and JNK-induced production of proapoptotic proteins. Long-term exposure to submicromolar concentrations of arsenic, however, induces transformational changes in cells which promote apoptotic resistance (343). Apoptotic resistance is linked to shifts in signal pathway flux, with preferential activation of PI3K-Akt/PKB signaling in arsenic treated cells and dampening of proapoptotic NF-κB and JNK signaling (310, 313). The transcription factors AP-1 and NF-κB are regulated by arsenic, presumably as a result of signal transduction pathway activation by reactive oxygen species (ROS) (344, 345). Acute low-dose arsenite up-regulates AP-1 and NF-κB expression in human fibroblasts, while chronic exposures down-regulates AP-1 and NF-κB (346). Also, in aortic endothelial cells and rat lung tissue, acute low dose arsenic treatment promotes nuclear accumulation of NF-κB (347, 348). Cell survival-modulating changes to telomerase activity and telomere length have also been documented in cells treated with arsenic. Submicromolar doses of arsenite maintain telomere length by increasing telomerase activity; whereas higher concentrations promote telomere attrition and apoptotic cell death by inhibiting telomerase (349, 350).

Arsenic disrupts redox state and re-routes metabolic activity within the cell (315). Metabolic reprogramming is now considered to be a hallmark/driver of cancer (12) which enhances cellular use of glycolytic metabolic pathways for energy production in aerobic conditions (351, 352). This process disrupts the provision of one-carbon intermediates to downstream metabolites through folate and methionine cycling pathways. One-carbon metabolism integrates cellular nutrient status by cycling carbon units from amino acid inputs to generate diverse outputs, including nucleotide metabolism, cellular biosynthesis and maintenance of redox homeostasis by restoring NADPH status and glutathione content (353).

Shifts in metabolic pathway flux have an indirect effect on gene expression programs through their impact on the activity of epigenetic modifiers, which rely on one carbon metabolism to maintain cofactor availability. Consequently, the epigenetic status of cells transformed by arsenic seems to be directly linked to one-carbon metabolism through its influence on histone acetylation and nucleic acid methylation.

### 1.4.2 Arsenic as an Epimutagen

Arsenic-induced carcinogenesis is associated with epigenetic changes which influence the entire genome. Long-term, low-dose arsenic exposure is known to induce genome-wide changes to the epigenetic landscape in cultured cells, and these changes appear to mirror those observed in epidemiological studies. A causal relationship between arsenic-induced epigenetic damage and/or cancer risk in exposed populations, however, has yet to be established. Although the rate of epigenetic change varies somewhat between cell lines, histone posttranslational modifications occur within 24 hours (354, 355) and DNA methylation changes within 2-3 days of low-dose arsenic treatment (309, 356, 357). Long-term in vitro arsenic treatment generates epigenetic changes which are consistent with carcinogenic progression. These studies also indicate that exposure for 8-20 weeks is required for these changes to be associated with pre-carcinogenic transformation (358-360), however a mechanism for arsenic-induced epimutagenesis is yet to be uncovered.

#### *1.4.2.1 Methylation Damage*

Widespread modifications to genomic DNA methylation patterns are associated with arsenic exposure. Dose-dependent hypermethylation of gene promoters was first noticed in regions of the p53 gene following exposure of cultured cells to either As(III) or As(V) (309). Similarly, the p53 promoter region was shown to be hypermethylated in basal cell carcinomas (BCCs) from arsenic exposed individuals

relative to BCCs from non-exposed patients (361). In contrast, chronic treatment of rat liver cells with arsenic causes global hypomethylation of promoters and malignant transformation (360, 362). Changes to methylation patterns induced by arsenic are persistent, destabilizing (290), and have the potential to promote aberrant expression of genes involved in cell development and regulation, creating a procarcinogenic state (363).

Activity and expression of p53 is dysregulated in arsenic-induced BCC and up-regulated in sporadic (UV-induced) BCC, and this is thought to result from differences in the mutagenic mechanism of the agents involved (361, 364). Arsenic impairs the pattern of p53 expression by increasing DNA methylation at its promoter region (308), whereas characteristic UV-induced mutational lesions inactivate the DNA binding domain and extend its half-life by altering protein stability (365-368). This mutational fingerprint is characteristic of UV-induced NMSC, and so it appears that these cases may have resulted from combined arsenic and UV exposure.

At this point in time, arsenic-induced DNA methylation changes are thought to result from impaired nucleotide methylation during replication. DNA methyltransferase-1 (DNMT1) is primarily involved with the maintenance of genomic imprinting patterns by transferring methyl groups from *S*-adenosyl methionine (SAM) to cysteine nucleotides (369). Extended arsenic exposure directly inhibits DNMT activity and expression in vivo and in vitro, and many studies also demonstrate decreased SAM availability and reduced global DNA methylation (370-372). The most widely cited mechanism for CpG hypomethylation in arsenic-transformed cells is competition for available methyl groups by DNMT1 and arsenite methyltransferase during arsenic biomethylation (360, 362). An alternative mechanism proposes that glutathione synthesis during oxidative stress redirects cellular stores of homocysteine from pathways which recycle DNMT cofactors, such as SAM (373, 374). However, although there is plenty of evidence to support a causative link between SAM insufficiency and DNA hypomethylation (375), some

inconsistencies and confounders exist – mostly due to the concomitant impact of B-group vitamin availability on SAM synthesis. Human population studies are particularly contradictory, in part due to a wide range of exposure duration and dose in recorded populations, but also due to the significant impact of dietary folate on methylation capacity in exposed groups (376, 377).

Adding to the epimutagenic nature of arsenic exposure, there is some evidence that DNMT1 plays a role in strand discrimination during DNA mismatch repair (378). Reversal of DNA methylation damage is most likely to proceed via the BER pathway, with GADD45α implicated in its coordination (379-381). Given the critical nature of the BER pathway for the repair of methylation changes and DNA damage created by oxidative stress, arsenic-induced disruption of BER has the potential to seriously impact cellular maintenance of epigenetic and genomic integrity, contributing to the procarcinogenic properties of arsenic.

#### *1.4.2.2 Chromatin Modifications*

Arsenic is known to influence histone posttranslational modifications, although investigations in this area are scant. Microarray experiments demonstrate global changes to histone methylation and promoter-specific shifts in histone H3 acetylation with long-term exposure to arsenite (356, 382). Analysis of the relationship between arsenic-induced gene upregulation and histone H3 modifications at a single promoter region during malignant transformation shows a significant reduction in trimethylated lysine 27 and dimethylated lysine 9, and significantly increased H3 acetylation and dimethylated lysine 4 (357, 383). Additionally, arsenite-induced histone H3 phosphoacetylation is associated with ERK-mediated c-fos and c-jun upregulation and caspase-10 induction (354, 355).

Our hypothesis is that disruptions to metabolic and redox homeostasis in arsenic-exposed cells are responsible for epigenetic reprogramming by modulating the activity of chromatin remodeling enzymes. Cellular metabolic activity influences the supply of cofactors for posttranslational histone modifications such as acetylation

and methylation (384, 385). Additionally, histone modifying enzymes are commonly redox sensitive (213, 386, 387), and maintenance of deacetylase activity in cancer is dysregulated by altered NAD availability (388). Thus environmental toxins which induce oxidative stress (such as arsenic) therefore promote cancer indirectly as a consequence of epigenomic remodeling during metabolic reprogramming. To test our hypothesis, this investigation aims to interrogate the relationship between the epigenetic effects of arsenic toxicity and histone deacetylase activity.

#### *1.4.2.3 MicroRNA Expression*

Investigations into the impact of arsenic on microRNA expression are in their infancy, however a handful of studies indicate that arsenic exposure significantly alters the cellular miRNA profile. Arsenic treatment (4 µM, 24 hours) upregulated miR-24, miR-29a, miR-30a and miR-210 in HepG-2 cells (389); and was associated with down-regulation of miR-19a and up-regulation of miR-222* in T24 cells (390). The microRNA expression profile changes in cells transformed with As(III), and interestingly, these changes appear to be cell line-specific [Table 1:9].

As yet, a mechanism of action for arsenic-mediated changes in miRNA regulation has not been uncovered. Also, whether arsenic-induced carcinogenesis in exposed human populations is characterized by specific changes in microRNA expression is yet to be determined. However, considering the relationship between arsenic exposure and DNA methylation, there may be a causal link between arsenic-induced promoter hypermethylation and miRNA precursor expression. We intend to investigate this hypothesis during the course of this study.

*Table 1:9 microRNA expression profiles in arsenic-exposed cell lines*

| As(III) (µM) | Duration | Cell line | miRNA | Change | miRNA | Change | Ref |
|---|---|---|---|---|---|---|---|
| 4.0 µM | 24 hr | HepG2 | miR-30a | 3.84 | miR-744 | 0.64 | (389) |
| | | | miR-210 | 3.09 | miR-296-5p | 0.63 | |
| | | | miR-29a | 2.99 | miR-663 | 0.59 | |
| | | | miR-24 | 2.9 | miR-675 | 0.58 | |
| | | | miR-886-3p | 1.8 | | | |
| 2.5 µM | 16 wks | HBEC | miR-200b | 0.0049 | miR-141 | 0.013 | (391) |
| | | | miR-200a | 0.11 | miR-429 | 0.015 | |
| | | | miR-200c | 0.018 | | | |
| 4.0 µM | 24 hr | T24 | miR-19a | 0.420 | miR-222* | 2.32 | (390) |
| 1.0 µM | 15 wks | HELF | miR-21 | 6.8 | | | (392) |
| 2.0 µM | 48 hr | HL-60 | let-7d | 0.45 | | | (393) |
| | | NB4 | miR-766 | 0.6 | | | |
| 5.0 µM | 29 wks | RWPE-1 | miR-134 | ↓14.6 | miR-125a-5p | ↓2.6 | (394) |
| | | | miR-127-5p | ↓13.2 | let 7b | ↓2.6 | |
| | | | miR-373 | ↓10.6 | miR-181b | ↓2.6 | |
| | | | miR-9 | ↑7.4 | miR-98 | ↓2.4 | |
| | | | miR-34c-5p | ↓5.9 | let-7i | ↓2.1 | |
| | | | miR-146b-5p | ↓5.7 | miR-34a | ↓2 | |
| | | | miR-135b | ↓5.4 | miR-196a | ↓2 | |
| | | | miR-222 | ↓5 | miR-181a | ↓2 | |
| | | | miR-155 | ↓4.4 | miR-183 | ↑2 | |
| | | | miR-138 | ↓4.2 | let-7e | ↓1.9 | |
| | | | miR-205 | ↓4.1 | miR-181c | ↓1.9 | |
| | | | miR-218 | ↓2.9 | let-7c | ↓1.8 | |
| | | | miR-10b | ↓2.9 | miR-125c | ↓1.8 | |
| | | | miR-181d | ↓2.8 | miR-126 | ↓1.6 | |
| | | | miR-96 | ↑2.7 | | | |
| 5.0 µM | 18 wks | WPE | miR-9 | ↓2.6 | miR-143 | ↓4.8 | |
| | | | miR-34c-5p | ↓2.4 | let-29b | ↑1.9 | |
| | | | miR-135b | ↓5 | miR-193b | ↑1.8 | |
| | | | miR-138 | ↓1.8 | miR-355 | ↓1.8 | |
| | | | miR-205 | ↓2.4 | miR-7 | ↑1.7 | |
| | | | miR-218 | ↓4.4 | miR-148a | ↓1.7 | |
| | | | miR-34a | ↑2.3 | | | |

*Table 1:10 Arsenic-Induced Epimutagenesis*

| Cell Line/Species | Concentration | Duration | Epigenetic Change | Reference |
|---|---|---|---|---|
| Mouse lung | 50 ppm As(V) | 12 weeks | ↓ methylation in promoter regions, no change in coding domain | (395) |
| Mouse liver | 45 ppm | 48 weeks | Global hypomethylation; ↓ methylation of the ER-α promoter | (362) |
| HepG2 & Huh-7 | 2 & 10 uM As(III) | 24, 48, 72 hours | Reversal of hypermethylation - p16INK4a, RASSF1A, E-Cadherin, GSTP1 | (371) |
| A/J mouse lung | 1, 10, 100 ppm As(V) | 18 months | ↑ in promoter methylation of p16INK4a and RASSF1A | (370) |
| Molt4, MUTZ-1, U937, U266, CA46 | 0.5, 1 and 2 uM As(III) | | Demethylation of CDKN2B and CDKN2A promoter sequences | (372) |
| UROtsa | 1 uM As(III); 50 nM MMAs(III) | 24, 52 weeks | ↓ H3 acetylation *DBC1*, *FAM83A*, *ZSCAN12*, *C1QTNF6*, ↑ H3 acetylation *NEFL* | (356) |
| | | | ↑ AcH3K9, AcH3K14 and me2H3K4; ↓ me3H3K27 and me2H3K9 | (357) |
| | | | Promoter hypermethylation (single copy elements), hypomethylation (microsatellites) | (383) |
| NB4 | 0.2, 0.4, 0.8, 1.6 uM As(III) | 24-72 hrs | ↑ H3 phosphorylation (S10) and H3 acetylation (K14) of caspase-10 associated chromatin | (354) |
| WI38 | 50, 100, 200, 400 uM As(III) | 10, 30, 60 min | ↑ H3 phosphorylation (S10) and H3 acetylation (K14) of c-fos and c-jun | (355) |
| A549 | 0.08-2 uM As(III); 30-300 uM As(V); 2-2000 uM DMAs(III) | 1-2 weeks | ↑ CCGG methylation status; ↑ in 5-MeC content [p53 promoter] | (309) |
| HaCaT | 0.2 uM; 25 uM As(III) | 1 - 72 hrs | Global hypomethylation (reduced 5-methyl-dCMP) [0.2 uM, 10 passages] | (396) |
| V79-C13 | 10 uM As(III) | 24 hrs | Genome-wide DNA hypomethylation | (290) |
| TRL1215 | 0.125, 0.25, 0.5 uM As(III) | 8, 18 weeks | Dose-dependent genomic hypomethylation | (360) |
| A549, BEAS-2B | 0.1, 1, 2.5, 5, 10 uM As(III) | 24 hours | ↑ me3H3K4; ↑ me2H3K9, ↓ me3H3K27 | (382) |
| SK-MEL5, SK-MEL28, SK-MEL31, RPMI7951 | 1, 2.5, 5 uM As(III) | 24 hours | Dose-dependent increase in H2AX phosphorylation (S139) | (397) |

Exposure to sub-lethal doses of arsenite promotes the genotoxicity of mutagens. One of the more critical stages in carcinogenic transformation is the ability to successfully adopt genetic changes acquired during initiation. Arsenic exposure facilitates the transition from initiation to promotion stages in carcinogenesis by generating a combination of oxidative DNA damage, altered regulation of cellular stress responses, and inhibition of DNA repair. For these changes to progress it has been generally accepted that a secondary contributing mutagen (such as UV exposure) is necessary for arsenic to produce malignant clonal lines. However, more recent insights into the role of epimutagenesis in cancer indicate that arsenic-induced epigenetic damage may provide the requisite changes necessary for autonomous progression.

Long-term *in vitro* arsenic treatment generates epigenetic changes consistent with this model of carcinogenesis, progressively increasing chromosomal instability and epigenetic changes with exposure [Table 1:10]. Maintaining control over gene transcription is particularly important to cellular function. Equally important is the cell's ability to maintain and perpetuate its genetic code. Alterations to both of these processes are common to most, if not all cancers. How these changes develop in the presence of carcinogenic stimuli and how cellular stress responses influence epigenetic patterns are major questions addressed by our investigation.

*Overview*

TP53 is the most frequently mutated gene in cancer, indeed p53-mediated regulation of cell cycle control and cell death signalling is a barrier which must be overcome for cancer to progress. However, p53 mutations which contribute to cancer are complex and produce a heterogeneous suite of cellular responses. The conformation and expression of mutated p53 proteins is highly variable and consequently, the efficacy of p53-based cancer therapy is dependent on p53 mutational status.

Mediators of the DNA damage response pathway in tumour cells are attractive targets for chemotherapeutic development. In particular, treatments which generate DNA damage-dependent responses have the potential to overcome apoptotic resistance and/or trigger functional senescence in cells with functional mutations to p53. This is a valuable property in targeted cancer therapy, considering the ubiquitous nature of *TP53* loss of function mutations in human tumours.

Altered epigenetic expression patterns are common features of tumourigenesis and contribute to the development of the cancer phenotype. The maintenance of normal epigenetic imprinting across cell generations is intrinsically linked to the DNA damage response, and thus disrupted regulation of effector activity impacts on the epigenetic code. As such, changes in promoter methylation, chromatin condensation patterns and microRNA expression are useful biomarkers for cancer development and prognosis. Our understanding of SIRT1 and miR-34a as key regulators of adaptive responses to cellular stress has increased dramatically during the past 10 years. Consequently, impairments to miR-34a-mediated feedback regulation of SIRT1 are intrinsically associated with the pathology of chronic disease.

Arsenic exposure disrupts established patterns of DNA methylation and posttranslational histone modifications; however the relationship between arsenic-induced epigenetic dysregulation and carcinogenesis has not been conclusively established. Our hypothesis is that arsenic interferes with the regulatory activity of epigenetic modifying enzymes such as SIRT1. This thesis explores the mechanism by which an effective cellular response to chronic stress is affected by the lysine deacetylase SIRT1 in keratinocytes with p53 mutations. Specifically, this investigation will address the role of SIRT1 in arsenic-mediated keratinocyte transformation and skin cancer development.

*Overall aims of this project:*

1. To determine the influence of p53 mutational status on p53/SIRT1/miR-34a axis activity by comparing cellular stress responses in normal and p53-mutated keratinocytes
2. To observe the influence of arsenic on keratinocyte growth and replication in culture
3. To investigate the effect of arsenic exposure on feedback regulation of the p53/SIRT1/miR-34a axis in human keratinocytes
4. To document the effect of arsenic exposure on epigenetic regulation of the p53/SIRT1/miR-34a axis by measuring histone modifications and CpG island methylation changes at SIRT1 and miR-34a gene promoters

## *Structure of the Thesis*

A review of the relevant literature is presented in Chapter 1, followed by a general description of experimental materials and methods used during the investigation (Chapter 2). Chapter 3 covers initial work performed in order to characterise cell lines and optimise culture conditions prior to investigating the research aims.

Chapters 4 and 5 describe the relationship between SIRT1 activity, p53 acetylation status and genotoxic stress responses in human keratinocytes (Research Aim 1). These investigations used RNAi and pharmaceutical techniques to alter target gene expression and activity, and assayed apoptotic signalling in wild-type and p53-mutated keratinocytes.

Chapter 6 evaluates the effect of arsenic on histone acetylation status and chromatin condensation at target gene promoters using a 24 hour exposure period (Research Aims 3 and 4).

Long term studies in Chapter 7 were designed to explore a correlation between procarcinogenic effects of arsenic exposure on epigenetic regulation of SIRT1 and miR-34a gene expression in cultured human keratinocytes by documenting CpG dinucleotide methylation at gene promoters (Research Aims 2, 3, 4).

Research Chapters 3-7 are followed by a General Discussion and Summary of the thesis. The last sections describe buffer solutions and procedures performed to optimise experimental methods (Supplementary Material), and abstracts from manuscripts and presentations produced during the course of the investigation.

# Chapter 2 -
# General Materials and Methods

## 2.1 GENERAL PROCEDURES

### 2.1.1 Biological Containment and Sterilisation

Buffer solutions for use in cell culture, and consumables contaminated with biological material were sterilised by autoclaving at 121°C (115 kPa) for 20 minutes. Heal labile solutions such as growth media and bovine serum albumin (BSA) were sterilised by passing the solution through a sterile disposable 0.2 µm filter unit. Frequently used sterile solutions for use in cell culture were stored in aliquots.

### 2.1.2 Maintaining Sample Integrity

Procedures involving nucleotide extraction, reverse transcription and PCR setup were all carried out using filtered pipette tips to prevent between-sample cross-contamination. When purified nucleotide extracts were used, all procedures were performed in a controlled airflow cabinet to minimise aerosol production. Prior to RNA extraction, workbenches were treated with RNaseZap® to reduce RNase contamination.

### 2.1.3 Stock Solutions

Commonly used solutions and buffers were prepared as stock concentrates and stored at room temperature or −20°C as indicated. Recipes are provided in the Supplementary Materials.

The vendors, catalogue numbers, lot numbers and dilutions of antibody solutions used in this study are as follows:

## 2.2 SPECIFIC MATERIALS

Vendors, catalogue numbers, lot numbers and dilutions of antibody solutions used in this study are as follows:

| Target Antibody | Vendor | Location | Catalogue # | Lot # | Dilution |
|---|---|---|---|---|---|
| SirT1(C14H4) Rabbit mAb | Cell Signaling Technology | Beverly, MA | 2496 | Lot 1 | 1:1000 |
| Acetyl-p53 (Lys382) Antibody | Cell Signaling Technology | Beverly, MA | 2525 | Lot 10 | 1:500 |
| X-Actin Antibody | Millipore | Billerica, MA | MAB 1501R | LV1519577/LV 1368255 | 1:5000 |
| p53 Antibody | Cell Signaling Technology | Beverly, MA | 9282S | Lot 4 | 1:1000 (WB); 1:100 (ChIP) |
| Anti-Involucrin Antibody | Abcam | Cambridge, UK | ab97764 | | 1:1000 |
| Anti-Cytokeratin 10 Antibody | Abcam | Cambridge, UK | ab53112 | | 1:500 |
| Anti-Filaggrin Antibody | Abcam | Cambridge, UK | ab81468 | | 1:1000 |
| Nanog (D73G4) | Cell Signaling Technology | Beverly, MA | 4903 | | 1:1000 (WB) |
| p53 Antibody (Pab 1801) [N-terminal aas 32-79] | Santa-Cruz Biotechnology | Santa-Cruz, CA | sc-98 | D2009 | 1:1,000 (WB); 1:100 (IP) |
| SirT1 (D739) Antibody | Cell Signaling Technology | Beverly, MA | 2493S | 0002 | 1:1000 (WB) |
| p53 (7F5) Antibody | Cell Signaling Technology | Beverly, MA | 2527S | 0006 | 1:1000 (WB) |
| Anti-acetyl Histone H4 (Lys16) | Millipore | Temecula, CA | 07-329 | 2178420 | 1.0 mg/ml |
| Anti-Histone H4 antibody - ChIP Grade | Abcam | Cambridge, UK | ab10158 | GR103452 | 2 ug/25 ug chromatin |
| Anti Histone H4 (acetyl K16) antibody - ChIP Grade | Abcam | Cambridge, UK | ab61240 | | 0.1 ug/ml |
| HRP-Conjugated anti-Rabbit IgG | Cell Signaling Technology | Beverly, MA | 7074P2 | 20 | 1:10000 |
| HRP-Conjugated anti-Mouse IgG | Cell Signaling Technology | Beverly, MA | 7076S | 22 | 1:10000 |
| Mouse Anti-Rabbit IgG (Light Chain Specific) (L57A3) mAb | Cell Signaling Technology | Beverly, MA | 2525S | | 1:1000 |
| p53 Antibody | Cell Signaling Technology | Beverly, MA | 9282S | Lot 4 | 1:1000 (WB); 1:100 (ChIP) |
| PARP Antibody | Cell Signaling Technology | Beverly, MA | 9542 | | 1:1000 |

## 2.3 CELL CULTURE

### 2.3.1 Cultured Cells

#### *2.3.1.1 Primary Keratinocytes (NHEKs)*

Primary human epidermal (NHEK) keratinocytes isolated from neonatal foreskin and cryopreserved at the end of primary culture were obtained from Cascade Biologics (Life Technologies Corporation, Carlsbad, CA) [Figure 2:1]; and maintained in EpiLife® Medium supplemented with Human Keratinocyte Growth Supplement (HKGS) and 100 ng/ml kanamycin sulfate in a humidified incubator at 37°C and 5% $CO_2$. Cells were seeded at a density of ≥ $2.5 \times 10^3$ cells/$cm^2$ and the culture medium replaced every 2-3 days.

NHEK cells were passaged when confluence reached ≤70% in the following manner: growth medium was aspirated from the culture flask, and the cells washed in 20 ml of pre-warmed Hank's balanced salt solution (HBSS, $Ca^{2+}$ and $Mg^{2+}$ free). Adherent cells were detached from the culture flask by incubation for 3-5 min in 0.025% trypsin-EDTA, and the reaction quenched by adding an equivalent volume of 0.5 mg/ml soybean trypsin inhibitor in PBS to the suspension. Culture flasks were re-seeded with 1:10 of the harvested cells in complete media, and the remainder used to seed plates for subsequent experimental treatments.

#### *2.3.1.2 HaCaT Keratinocytes*

The HaCaT cell line is a spontaneously transformed adult keratinocyte cell line which is non-tumorigenic and considered immortal due to its ability to proliferate beyond passage 140 in culture (398) [Figure 2:1]. HaCaTs are compound heterozygotes with mutations to the conserved domains of the *P53* gene. These were identified as a C → T transition in codon 179 of exon 5 in one *P53* allele, and consecutive CC → TT transitions in codons 281 and 282 of exon 8 in the other *P53* allele (Lehman 1993). The codon 179 mutation causes a histidine residue to be replaced with tyrosine in the DNA binding domain of the p53 protein, whereas the codon 282 mutation results in replacement of arginine with tryptophan. Codon 282

of *P53* is a frequently mutated CpG site which is considered to be particularly vulnerable to sunlight-induced UV damage. This mutation is associated with accumulation of p53 protein, possibly as a result of structural changes to the Mdm2 binding site.

Mutations to the p53 gene in our HaCaT cell line were confirmed by sequencing PCR product amplified from cDNA following reverse transcription from RNA (sequencing experiments are described in detail in Chapter 3). Additionally, no mutations were found in the p53 sequence of NHEK cells. These results allow us to be confident that the assumptions we made with regards to p53 status in both HaCaT and NHEKs which informed our experimental model are sound.

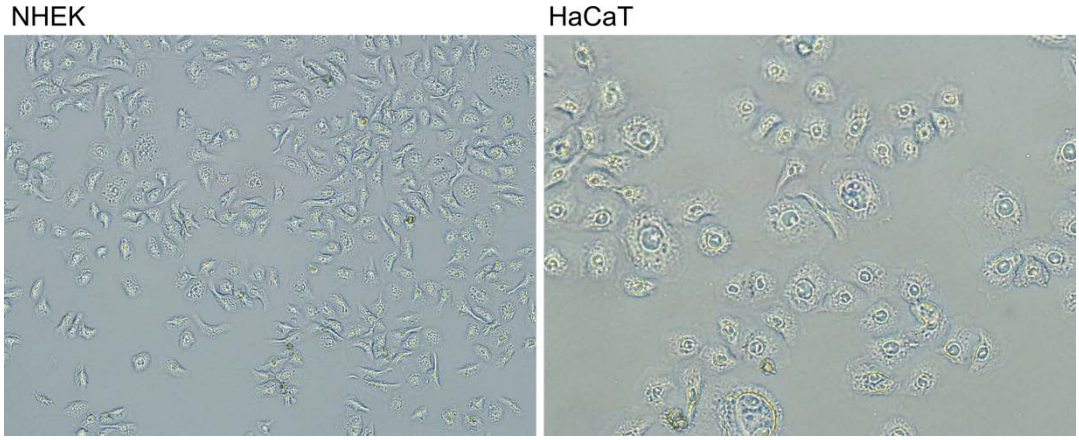


*Figure 2:1 Neonatal human (NHEK) and p53-mutated (HaCaT) keratinocytes – Morphology in Culture*

Human keratinocyte cells were seeded in 6 well culture plates at a density of $4 \times 10^5$ cells/cm$^2$ and allowed to recover overnight. The culture medium was removed and the cells fixed in ice-cold 3.7% formaldehyde/PBS solution prior to staining with 0.05% crystal violet solution for 30 minutes. Stained cells were magnified with an Olympus IX71 inverted microscope (Olympus, Center Valley, USA) and photographed using an Optronics digital camera (model 60800, Goleta, USA). Images were generated using Optronics Magnafire software (version 2.1, Goleta, USA).

HaCaT cells were cultured in Dulbecco's Modified Eagle's Medium (DMEM) with Ham's Nutrient Mixture F-12 (D-MEM/F-12) supplemented with 7.35 mg/L GlutaMAX™, 100 ng/ml kanamycin sulfate and 5 % foetal bovine serum (FBS) or EpiLife® Medium supplemented with Human Keratinocyte Growth Supplement (HKGS) and 100 ng/ml kanamycin sulfate in a humidified incubator at 37°C and 5%

$CO_2$. The HaCaT cell line was passaged at ≤80% confluence in the following manner: growth medium was aspirated from the culture flask, and the cells washed in 20 ml of pre-warmed phosphate buffered saline (PBS, $Ca^{2+}$ and $Mg^{2+}$ free). Adherent cells were detached from the culture flask by incubation for 3-5 min in 0.025% trypsin-EDTA, and the reaction quenched by adding an equivalent volume of complete media to the suspension. Culture flasks were re-seeded with 1:20 of the harvested cells in complete media, and the remainder used to seed plates for subsequent experimental treatments.

### 2.3.2 Performing Cell Counts

Detached cells were pelleted by centrifugation at 150×g for 5 min at room temperature, the supernatant aspirated and the cells resuspended in a known volume of liquid. Ten microliters of a 1:10 dilution of cell suspension stained with 0.1% Trypan Blue solution was loaded into a haemocytometer chamber and viable cells counted using an inverted microscope. Harvested cells were equal to the outer square count multiplied by 10 (dilution factor) × $10^4$ cells/ml. Active dye exclusion enabled viable cells to be differentiated from blue stained dead cells, and the viable cell count estimated from the percentage of live cells within the total population.

### 2.3.3 Cryopreservation and Reconstitution of Cell Lines

Early passage (P1/P2) cells were harvested, pelleted, and the viable cell count determined using techniques outlined above. The cell pellet was resuspended at a density of 1 × $10^6$ cells per ml in cold freezing medium [10% FBS & 7.5% dimethyl sulfoxide (DMSO) in D-MEM/F12 (HaCaT) or 5% DMSO in EpiLife® with HKGS (NHEK, HaCaT)] and divided into 1 ml aliquots in Greiner BioOne cryovials. The cryovials were placed in a NALGENE® Cryo 1°C Freezing Container containing isopropanol and frozen overnight in a −80°C freezer before transferring to liquid nitrogen.

Cells were revived by thawing the cryovials rapidly in a 37°C waterbath the cell suspension diluted in 10 ml of prewarmed complete medium (dropwise with gentle

agitation for the initial 2 ml, gradually thereafter) and the suspension was triturated slowly for 5 minutes to promote DMSO expulsion. Revived cells were pelleted by centrifugation at 150g for 5 minutes, the cryopreservation medium aspirated and the pellet reconstituted in growth medium for incubation at 37°C and 5% $CO_2$.

## 2.4 MICROPLATE ASSAYS

### 2.4.1 Viability Assays

#### *2.4.1.1 AlamarBlue*

Prior to each experiment, a within-well assay was used to titrate treatment doses for each culture. The alamarBlue® assay measures innate metabolic activity of viable cells with an oxidation-reduction indicator (resozurin) that both fluoresces and changes colour in response to chemical reduction (399, 400). Cells were exposed to test compounds and alamarBlue® reagent added to each well at 10% of the treatment medium volume at the end of the treatment period (typically 24 hrs). Culture plates were incubated with alamarBlue® reagent for 3 hours, after which fluorescence emission was measured at 595 nm using excitation at 540 nm using an Infinite M200-Pro plate reader [Tecan, GmbH, Grödig, Austria]. Positive and negative (medium only) control wells were included on each plate to calibrate the fluorescence reading and to allow for between-plate standardisation.

#### *2.4.1.2 CyQUANT*

Since alamarBlue was unable to discriminate between apoptotic and necrotic cell death, more specific multiwell cytotoxicity assays which use target-bound fluorophores or target-triggered chemiluminescence were required to quantitate apoptosis. As the signal generated in these assays is sensitive to cell number as well as apoptotic activity, two cell proliferation assays were used in order to standardise the signal for variations in seeding density. Toxicity assays were normalised for metabolically active cell number using a fluorescent assay for cellular DNA content

(CyQUANT® NF assay [Molecular Probes, Inc. Eugene, OR]), and a chemiluminescent assay for cellular ATP content (ATPLite assay [Perkin Elmer, Boston, MA. USA]).

The CyQUANT assay uses fluorescent dye binding to cellular DNA as a quantitative measure of cell number [Figure 2:2 (a)]. To perform the analysis, microplates were removed from incubation and equilibrated to room temperature. Treatment media was aspirated and replaced with working CyQUANT NF dye reagent (1:500 dilution of DNA dye binding solution in Hank's Balanced Salt Solution (HBSS). Fluorescence was read using an Infinite M200-Pro plate reader [Tecan, GmbH, Grödig, Austria] with an excitation wavelength of 485 nm and an emission wavelength of 530 nm after 60 min incubation at 37°C. The signal was analysed relative to a no cell/medium only background reading.

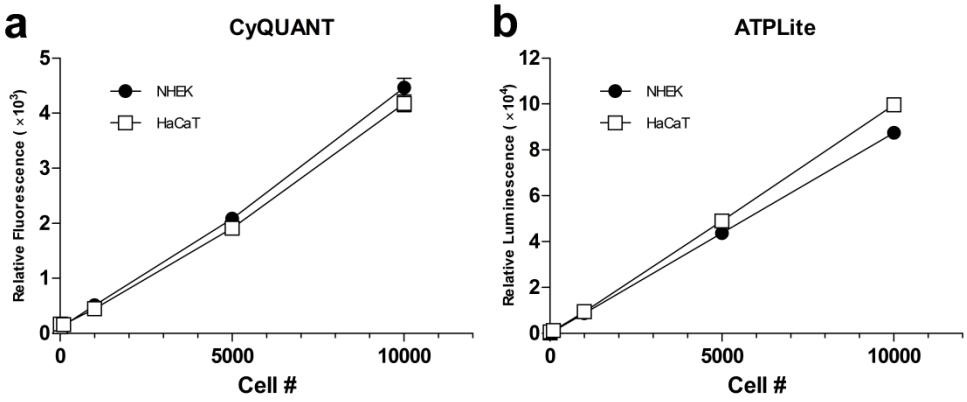


*Figure 2:2 Cell Proliferation assays – Linearity*

Primary keratinocyte (NHEK) and p53-mutated (HaCaT) cells were seeded into microplate wells using a suspension series from 0-10,000 cells/well and incubated overnight at 37°C and 5% $CO_2$. Cell number was analysed by relative fluorescence and chemiluminescence using CyQUANT and ATPLite viability assays according to the manufacturer's instructions. Both CyQUANT and ATPLite assays generated a linear analytical response from 0-10,000 per well in a 96 well microplate.

### *2.4.1.3 ATPLite*

The ATPLite assay provides a quantitative determination of cell viability through detection of ATP content using luciferase and D-luciferin according to the following reaction scheme:

$$\text{ATP + D-Luciferin + } O_2 \xrightarrow[Mg^{2+}]{\text{Luciferase}} \text{Oxyluciferin + AMP + PPi + } CO_2 \text{ + Light}$$

To perform the assay, microplates were removed from incubation, equilibrated to room temperature and cells lysed with mammalian lysis solution for 5 min prior to addition of luciferin substrate. Luminescence was read a using an Infinite M200-Pro plate reader [Tecan, GmbH, Grödig, Austria] after 5 min incubation on an orbital shaker. The signal was analysed relative to a no cell/medium only background reading [Figure 2:2 (b)].

### 2.4.2 Cytotoxicity Assays

The Topoisomerase I inhibitor, camptothecin (CPT), is a well-established S-phase-specific component of chemotherapeutic management strategies which activates the cell death program in cancer cells by generating DNA strand breaks (401, 402). CPT-mediated apoptosis is predominantly p53-dependent (37), and has been widely characterised in cultured cell systems. For this study, 24 hr exposure duration was used to be more efficient time-wise.

Colorimetric, fluorimetric and chemiluminescent assays were used to measure metabolic activity, caspase 3/7 activity, LDH release and PARP cleavage as apoptotic endpoints. Care was taken to minimise variability by using identical growth medium constituents for both cell cultures (see Chapter 3 for details), and by standardisation of inter-assay treatment and sampling parameters.

#### *2.4.2.1 Apo-ONE Caspase 3/7 Assays*

Apoptotic cells can be recognised by a characteristic pattern of morphological, biochemical and molecular changes. Broadly speaking, the apoptotic fraction of a population is determined by i) measuring membrane changes, ii) assaying changes in mitochondrial and/or cytoplasmic enzyme activity, and iii) analysing DNA fragmentation. For this study, the Apo-ONE Homogeneous Caspase-3/7 Activity Assay [Promega, Madison, MI, USA], the CytoTox-ONE™ Assay [Promega, Madison,

MI, USA] and relative PARP cleavage were employed to assay cytotoxicity and to discriminate between apoptotic and necrotic effects on treated cells.

The Apo-ONE assay uses the caspase 3/7 substrate rhodamine 110, bis-(N-CBZ-L-aspartyl-L-glutamyl-L-valyl-L-aspartic acid amide); [Z-DEVD-R110], which exists as a profluorescent substrate prior to the assay. Upon sequential cleavage and removal of the DEVD peptides by cellular caspase-3/7 activity and excitation at 499 nm, the rhodamine 110 leaving group fluoresces with an emission wavelength of 530 nm. The amount of fluorescent product generated is proportional to the amount of caspase-3/7 cleavage activity present in the sample. To perform the assay, Apo-ONE reagent was added to pre-equilibrated microplates and incubated at room temperature for 30 min while protected from light. Fluorescence intensity was measured using an Infinite M200-Pro plate reader [Tecan, GmbH, Grödig, Austria].

#### *2.4.2.2 CytoTox-ONE LDH Release Assay*

The CytoTox-ONE assay measures lactate dehydrogenase (LDH) release from cells with a damaged membrane. Release of LDH from damaged cells is measured by supplying lactate, NAD+, and resazurin as substrates in the presence of diaphorase. Generation of the fluorescent resorufin product is proportional to the amount of LDH in the culture medium.

To perform the assay, CytoTox-ONE reagent was added to pre-equilibrated microplates and incubated at room temperature for 10 min while protected from light. The reaction was quenched with Stop solution to stabilise the signal and fluorescence read at an emission wavelength of 590 nm after excitation at 560 nm using an Infinite M200-Pro plate reader [Tecan, GmbH, Grödig, Austria]. LDH release was analysed by subtraction of background fluorescence from all values.

#### *2.4.2.3 PARP Cleavage*

Relative PARP cleavage was determined by immunoblotting cell lysates from treated NHEKs and HaCaTs cultured in 6-well plates. PARP1 binds to breaks in the sugar-phosphate backbone of DNA, modifying surrounding histones to induce

chromatin relaxation. Additionally, contact with DNA strand breaks triggers autoribosylation and recruits DNA repair enzymes to the site of DNA damage. During apoptosis, PARP undergoes caspase 3-mediated proteolytic cleavage from a full-length 116 kDa protein to 89 kDa (carboxy-terminal catalytic domain) and 24 kDa (amino-terminal DNA binding domain) fragments. Thus PARP1 acts as a DNA damage sensor within the cell, and can be used as a molecular biomarker for apoptotic activity.

Homogenisation of cells releases proteolytic enzymes into the lysate and shears DNA. PARP1 undergoes autoribosylation in these conditions, even in the presence of protease inhibitors. Posttranslational modification by polyribosylation alters the molecular weight of full length and cleaved PARP during immunoblotting, making quantitation difficult. This can be abrogated by including urea in the sample extraction buffer, which dissociates PARP from any DNA in the lysate, preventing activation of the ribosylation reaction [Figure 2:3].

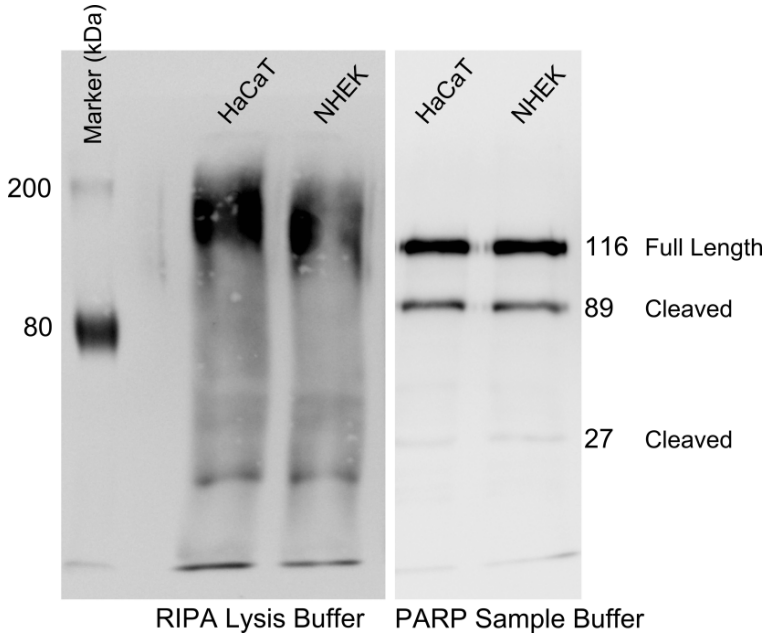


*Figure 2:3 Immunoblotting of apoptotic samples extracted in RIPA or PARP lysis buffer solutions*
Primary keratinocyte (NHEK) and p53-mutated (HaCaT) cells were grown in 6-well culture plates and treated with 5 µM CPT for 24 hr. Protein was isolated using Radioimmunoprecipitation assay (RIPA) and PARP lysis buffer solutions and separated on 8% polyacrylamide by SDS-PAGE. Full-length and cleaved PARP subunits were detected using anti-PARP1 antibodies by immunoblotting.

In order to include all apoptotic cells for analysis of PARP cleavage, the detached fraction of cells in treatment medium was aspirated separately from each well, pelleted by centrifugation at 500 rcf for 5 min and washed in ice-cold PBS, repelleted and lysed using 50 µL of PARP sample buffer [62.5 mM Tris/HCl, pH 6.8; 6M urea; 10% glycerol; 2% SDS; 0.00125% bromophenol blue; 5% β-mercaptoethanol, protease and phosphatase inhibitors]. The adherent fraction of cells was washed in PBS and lysed in situ on ice using a further 100 µL of PARP sample buffer. The two fractions of lysed cells were combined, and the DNA sheared by passing the sample 6-7 times through a 25 gauge needle. These samples were boiled for 10 min and loaded onto 8% polyacrylamide for separation by SDS-PAGE. Expression of full-length and cleaved PARP was detected using polyclonal antibodies directed towards the PARP1 cleavage site (Asp214-Gly216) [Cell Signaling Technology #9542; Beverly, MA] by western protein analysis according to the protocol outlined below.

## 2.5 WESTERN PROTEIN ANALYSIS

### 2.5.1 Sample Preparation

#### *2.5.1.1 Cell Lysates*

Treatment media was aspirated from the culture vessel and cells washed once in ice-cold PBS. Chilled lysis buffer was added (150 µl per well) and plates incubated for 20 minutes on ice. Wells were scraped with a cell scraper and detached cell samples aspirated into 1.5 ml microcentrifuge tubes. Homogenisation was completed by passing the lysate through a 25 gauge needle 5-6 times. Lysates were clarified by centrifugation at 15,000g for 10 minutes in a chilled centrifuge, and the supernatant transferred to a fresh tube. Total protein was assayed and the lysates stored at −20°C until use.

### *2.5.1.2 Determination of Total Protein*

Working BCA assay reagent was prepared according to the manufacturer's specifications [4% copper (II) sulphate pentahydrate solution diluted 1:50 in bicinchoninic acid solution]. Two hundred microliters of working solution was mixed with 25 µl cell lysate diluted 1:5 in lysis buffer in a 96 well microtiter plate and incubated at 37°C for 30 minutes. Absorbance was measured at 595 nm using a microplate reader, and protein readings were determined against a standard curve prepared by diluting bovine serum albumin (BSA) in lysis buffer.

## 2.5.2 SDS-PAGE (Sodium dodecyl sulfate polyacrylamide gel electrophoresis)

Polyacrylamide gels were prepared in a BioRad casting module using the following formulations. During polymerisation, the separating gel was overlaid with water-saturated butanol, after which the butanol was aspirated and replaced with a 4.5% stacking gel into which the comb was placed. After complete polymerisation (approx. 1 hour), gels were assembled in a BioRad Mini-PROTEAN® Tetra Cell electrophoresis module and equilibrated in SDS-PAGE running buffer for 5 minutes.

| Separating Gel; 37.5:1 | Stack | Resolving | | | |
|---|---|---|---|---|---|
| Component | 4.5% | 10% | 15% | 8% | X% |
| 40% Acrylamide | 240 ul | 2.43 ml | 3.51 | 1.944 ml | 2.34*[Vol (ml)]*(X%) |
| 2% Bisacrylamide | 130 ul | 1.34 ml | 2.01 | 1.072 ml | 1.34*[Vol (ml)]*(X%) |
| 0.5 M Tris-HCl (6.8) | 630 ul | | | | |
| 1.5 M Tris-HCl (8.8) | | 2.5 ml | 2.5 ml | 2.5 ml | Total/4 |
| 20% SDS | 25 ul | 100 ul | 100 ul | 100 ul | Total/100 |
| H2O | 1.46 ml | 3.58 ml | 1.825 ml | 4.329 ml | |
| 10% APS | 12.5 ul | 50 ul | 50 ul | 50 ul | Total/200 |
| TEMED | 2.5 ul | 5 ul | 5 ul | 5 ul | Total/2000 |
| Total | 2.5 ml | 10 ml | 10 ml | 10 ml | |

Samples were prepared by boiling for 5 min at 99°C in 4× Laemmli reducing buffer, and the equivalent of 10 µg total protein was loaded onto the gel. A dye-conjugated

molecular weight marker was loaded onto each gel for reference. Proteins were separated by electrophoresis at 120V for 2 hours.

### 2.5.3 Immunoblot Preparation and Analysis

SDS-PAGE gels were removed from the electrophoresis tank and equilibrated in cold transfer buffer for 15 minutes prior to transfer sandwich assembly. PVDF membranes were pre-wetted in 100% methanol for 30 seconds and the gels placed next to PVDF membrane between cellulose blotting paper. Proteins were transferred to the membrane at 1.5 Amps and 25 V in a BioRad Trans-Blot Turbo® electrophoretic transfer system. Following transfer, the membranes were incubated in blocking buffer (5% non-fat milk powder in Tris-buffered Tween-20 [TBST]) for 30 minutes at room temperature, rinsed briefly in TBST and placed in 50 ml Falcon tubes with primary antibody solution for overnight incubation at 4°C on a roller. Membranes were then washed three times for 5 minutes each in TBST, and incubated for 2 hours in horseradish peroxidase-conjugated (HRP) secondary antibody solution at room temperature. Residual secondary antibody was removed from the membrane by washing four times for 5 minutes each in TBST, and the membranes were developed in chemiluminescent HRP substrate (Millipore, Billerica, MA) for 5 minutes. The chemiluminescent signal was detected using a Las-3000 Luminescent Image Analyser (Fujifilm, JPN), and MultiGauge software (Fujifilm, JPN) used for densitometric analysis of the signal.

## 2.6 GENE EXPRESSION

### 2.6.1 RNA Extraction

Cellular RNA was extracted from treated samples using a MO-BIO Ultraclean® Tissue & Cells RNA Isolation kit according to the manufacturers' instructions with minor changes. Briefly, approximately $5 \times 10^5$ cells were disrupted in 250 µl Solution TR1 with 1% β-mercaptoethanol, scraped into a 1.5 ml microcentrifuge tube and

homogenised by passing the solution through a 25 gauge needle 5-6 times. An equal volume of Solution TR2 was added to the lysate, mixed thoroughly by pipetting and the sample transferred to a spin column. The spin column was centrifuged at ≥ 10,000 rpm for 1 min in a microcentrifuge and the flow-through discarded. The spin filter was washed by adding 500 µl Solution TR3 and centrifuging at ≥ 10,000 rpm for 1 min and transferred to a fresh collection tube. The spin column was washed twice using 500 µl of Solution TR4 with centrifugation at ≥ 10,000 rpm for 1 min after each step. The spin filter was thoroughly dried by centrifugation at 13,000 rpm for 2 min and transferred to a new collection tube. Sample RNA was eluted from the membrane by adding 30 µl of Solution TR5 directly to the membrane; incubating at room temperature for 1 minute and centrifugation ≥ 10,000 rpm for 2 min. Eluted RNA was stored at −20°C (1 month) or −80°C (6 months).

#### *2.6.1.1 Total RNA*

Working RNA assay solution was prepared by diluting Qubit™ RNA BR Reagent 1:200 in Qubit™ RNA BR Buffer. A 1:10 dilution of each sample was added to working RNA assay reagent to a final volume of 200 µl, vortexed thoroughly and incubated at room temperature for 2 minutes prior to reading fluorescence with a Qubit™ fluorometer. RNA concentration was determined relative to a standard curve prepared using a 100 ng/µl standard solution.

#### *2.6.1.2 RNA Integrity*

The integrity of extracted RNA was analysed using the Experion™ automated electrophoresis system according to the manufacturer's instructions (BioRad). Briefly, StdSens RNA analysis reagents were allowed to come to room temperature and the analysis chip was primed by adding 9 µl of Gel Stain solution into the priming well, and running the priming program. The chip was prepared with Gel and Gel Stain solution, and buffer added to each sample well. RNA ladder and sample were denatured by heating for 2 minutes at 70°C and cooling on ice for 5 minutes, and loaded onto the chip. Each electrophoretogram was analysed for RNA

concentration and integrity on an Experion analyser using the Experion software [Figure 2:4].

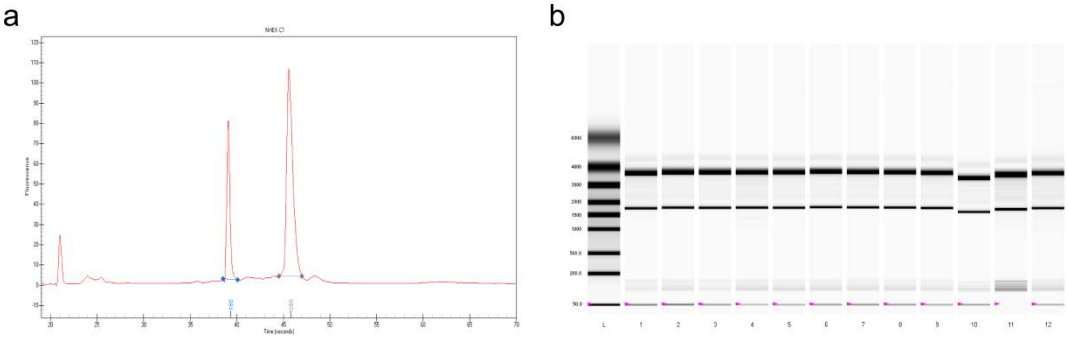


*Figure 2:4 Quantification and determination of RNA integrity*

Electrophoretogram (a) and Virtual Gel (b) of RNA extracts analysed using the Experion Automated Electrophoresis System

### 2.6.2 Reverse Transcription

First strand cDNA was synthesised using a Tetro cDNA Synthesis Kit (Bioline). One microgram of total RNA from each sample was incubated with 1 µl Oligo $(dT)_{18}$ and 1 µl of 10 mM dNTP mix in 10 µl total volume at 70°C for 5 min and chilled on ice for 1 min. To this primer premix, 10 µl of RT master mix (4 µl of 5X RT Buffer, 1 µl of 10U/µl RNase inhibitor, 1 µl of 200U/µl H-MLV Reverse Transcriptase, 4 µl of RNase-free water) was added and incubated at 45°C for 60 min. Reactions were terminated by inactivating the enzyme at 85°C for 5 min, samples were diluted 1:10 in RNase-free water and stored at −20°C.

### 2.6.3 Quantitative Real-Time PCR

Sample cDNA was amplified on a BioRad iCycler MYiQ™ using iQ™ SYBR® Green Supermix. Primer concentration and annealing temperature was optimized by performing melt curve analysis for each primer set. Reactions without sample template were included with each Reverse Transcription (RT Negative) and PCR run

(PCR Negative) to screen for reagent contamination. PCR efficiency was determined by including a 3-fold dilution series in each PCR run. All standards and samples were amplified in triplicate. Results were analysed using the ΔΔCt method (403, 404):

Relative expression = 2^[Control Ct(normalised) – Treatment Ct(normalised)] where Ct of each sample is normalised to the input cDNA using 5S rRNA as an internal control gene:

$Ct_{(normalised)} = [Ct_{(target\ gene)} - Ct_{(5S\ rRNA)}]$.

### 2.6.4 Agarose Gel Electrophoresis

Agarose gels were used to resolve PCR product following amplification. Gels were prepared by dissolving high resolution agarose in TBE buffer with SYBR® Safe DNA Gel Stain. For PCR product, 3% gels were run at 100V for 2 hours; and for chromatin digests, 1% gels were run at 80V for 1 hour in a BioRad Mini-Sub Cell® GT at room temperature. Bioline EasyLadder I DNA standards were run with each gel and resolved DNA was visualised using a Las-3000 imaging system.

#### *2.6.4.1 Primers*

Primers for RT-PCR were designed from NCBI Reference sequences derived from the GRCh38 GenBank record with Primer3 software [365] using primer design parameters outlined by Dieffenbach et al [366]:

| Gene | HGNC ID | RefSeq | Sequence | Amplicon |
|---|---|---|---|---|
| 5S rRNA | 34362 | NR_023363 | GTAACCCGTTGAACCCCATTACAC CCATCCAATCGGTAGTAGCG | 151 bp |
| SIRT1 | 14929 | NM_001142498 | GCAGATTAGTAGGCGGCTTGAAGA TCTGGCATGTCCCACTATCA | 152 bp |
| miR-34a | 31635 | NR_029610 | CCAGCTGTGAGTGTTTCTTTGGCAG CCCACAACGTGCAGCACTTCTAG | 104 bp |
| P53 | 11998 | NM_000546 | CCATGTGCTCAAGACTGGCGCT AGTCTGGCTGCCAATCCAGGGAA | 161 bp |
| U6 snoRNA | 32688 | NR_003098 | CGCTTCGGCAGCACATATACTAA TATGGAACGCTTCACGAATTTGC | 97 bp |

## 2.7 ANALYSIS OF MATURE MICRORNA EXPRESSION

### 2.7.1 RNA Extraction

Mature microRNAs were isolated as part of the total RNA isolate extracted using a miRCURY RNA Isolation Kit [Exiqon, Vedbaek, Denmark]. Hsa-miR-34a expression was detected with a miRCURY Universal RT-PCR kit using LNA PCR primer sets for miR-34a with U6 snoRNA and 5S rRNA as internal controls. This kit discriminates between primary and mature sequences in 20 ng of the total RNA isolate by polyadenylation and first strand cDNA synthesis of mature microRNAs. LNA primers used in the PCR step are stabilised to be specific for the mature microRNA and not for its step-loop precursor and so can be detected using SYBR green dye during the PCR amplification process.

The cDNA template was diluted 1:80 in Nuclease-free water and amplified with ExiLENT SYBR green master mix [Exiqon, Vedbaek, Denmark] on an ABI 7500 StepOne Plus PCR Cycler according to the manufacturer's protocol. A synthetic control template (UniSp6 CP, RNA spike-in) was added to the polyadenylation and first strand synthesis reaction to control for differences in the efficiency of cDNA synthesis between samples. Primers for UniSp6 CP were used to amplify the RNA spike-in during PCR amplification.

### 2.7.2 Taqman PCR Assays

Primers and probes for TaqMan Gene Expression, TaqMan Pri-miRNA and TaqMan microRNA assays were obtained from Applied Biosystems (Life Technologies, Carlsbad CA). Assays were performed according to the provided protocols using cDNA template prepared as described previously.

### *2.7.2.1 Primers for Taqman PCR*

*Gene Expression Targets*

| Target | RefSeq Accession # | Location |
|---|---|---|
| 18SrRNA | NR_003286.2 | Chr.Un_NT_167214: 109078 - 110946 |
| BIRC5/Survivin | NM_001012270.1 | Chr.17: 76210277 - 76221716 |
| BCL2 | NM_000633 | Chr.18: 60790579 - 60986613 |
| DICER1 | NM_001195573.1 | Chr.14: 95552565 - 95623759 |

*Pri-miRNA Targets*

| Target | RefSeq Accession # | Location |
|---|---|---|
| hsa-miR-145 | MI0000461 | Chr. 5 - 148810209 - 148810296 [+] |
| hsa-miR-200c | MI0000650 | Chr.12: 7073260 - 7073354 [+] |
| hsa-miR-107 | MI0000114 | Chr.10: 91352504 - 91352584 [-] |
| hsa-miR-16-1 | MI0000069 | Chr.13: 50623255 - 50623337 [-] |

Taqman microRNA Assays [Applied Biosystems, Carlsbad, CA, USA] were used for detection of hsa-miR-145, hsa-miR-141, hsa-miR-107 and hsa-miR-15a expression. For these assays, differentiation of mature microRNAs from their precursors in total RNA isolates was achieved by using target-specific stem-loop primers at the first strand cDNA synthesis step.

In order to amplify multiple microRNA targets from each sample, the reverse transcription step was multiplexed by pooling the target primers (10 µl of each 5× stem-loop primer solution in 1 ml TE buffer). First strand synthesis was carried out using a TaqMan MicroRNA RT Kit [Applied Biosystems, Carlsbad, CA, USA] in the following manner:

| Component | Vol/Rx (µl) |
|---|---|
| RT Primer Pool | 6 |
| dNTPs (100 mM) | 0.3 |
| Multiscribe Reverse Transcriptase (50 U/µl) | 3 |
| 10× RT Reaction Buffer | 1.5 |
| RNase Inhibitor (20 U/µl) | 0.19 |
| Template RNA | 350 ng |
| Nuclease-free water | To 15 µl |

Reactions were prepared in PCR tubes, mixed by inversion and incubated on ice for 5 min and amplified using thermal cycling conditions outlined by the supplier.

*MicroRNA Targets*

| Target | RefSeq Accession # | Sequence |
|---|---|---|
| hsa-miR-34a | MIMAT0000255 | UGGCAGUGUCUUAGCUGGUUGU |
| hsa-miR-200a | MIMAT0001620 | UAACACUGUCUGGUAACGAUGU |
| hsa-miR-145 | MIMAT0000437 | GUCCAGUUUUCCCAGGAAUCCCU |
| hsa-miR-141 | MIMAT0000432 | UAACACUGUCUGGUAAAGAUGG |
| hsa-miR-107 | MIMAT0000104 | AGCAGCAUUGUACAGGGCUAUCA |
| hsa-miR-15a | MIMAT0000068 | UAGCAGCACAUAAUGGUUUGUG |

## 2.8 TRANSIENT GENE SILENCING BY RNAi

OnTarget siRNA targeting pools (Dharmacon, Thermo-Fisher) were used for transient p53 and SIRT1 knockdown. To achieve efficient ablation of target genes whilst minimising off-target effects, transfection protocol was optimised to find conditions which produce >80% depletion of target mRNA content while maintaining >80% cell viability (see Supplementary Material for details).

### 2.8.1 Sample Preparation

Following detachment, cells were pelleted by centrifugation at 500g for 5 minutes and resuspended in growth media with supplements and without antibiotics. For 24 hour treatments, cells were seeded into tissue culture plates at a density of 2×104 cells per well (96-well), 1×105 cells per well (12-well), or 2×105 cells per well (6-well) and allowed to recover in an incubator overnight at 37°C and 5% CO2.

### 2.8.2 Transfection Protocol

Cells were seeded in 6-well plates in antibiotic-free medium at a density of 1.5×105 cells per well and allowed to recover overnight.

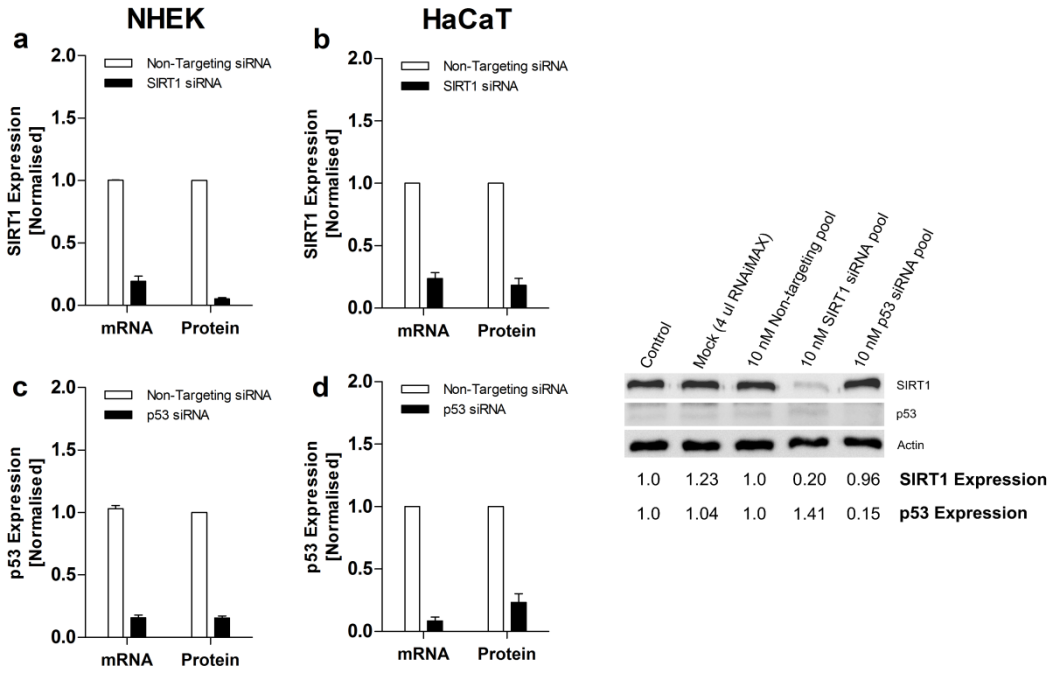


*Figure 2:5 Knockdown of SIRT1 and p53 in primary keratinocytes*

Transient transfection of primary human (NHEK) and p53-mutated (HaCaT) keratinocyts for 72 hr with 10 nM SIRT1 and p53 siRNA targeting pools was achieved using RNAiMAX as a transfection agent. RNA expression in transfected keratinocytes was measured by RT-PCR, and total p53 and SIRT1 protein by Western Blotting. 5S rRNA was used to normalise RNA expression and Actin was used as a loading control in immunoblotting. Results were analysed relative to expression in keratinocytes transfected with an equivalent concentration of a non-targeting siRNA pool.

On the day of transfection, the seeding medium was removed, the cells washed once with buffered saline solution and 1.5 ml of antibiotic-free medium added to each well. Transfection solution was prepared by combining diluted RNAiMAX solution (5 µl RNAiMAX + 250 µl reduced serum media) and siRNA solution (5 µl of 5 mM On-Target Smartpool siRNAs in 1X siRNA buffer) and incubating the mix at room temperature for 20 minutes. The solution was then overlaid onto the culture medium in each well and the transfection reaction incubated for 4-5 hours at 37°C and 5% CO2. After this time, the transfection medium was replaced with relevant cell treatments in antibiotic-free media and returned to the incubator. RNA was

extracted at 24 hours and protein extracted at 48 hours following treatment for functional assays. Using the optimised protocol, ≤ 25% ablation of SIRT1 [Figure 2:5(a, b)] and p53 [Figure 2:5(c, d)] was achieved in NHEK and HaCaT cells after 48 hours transfection with 10 nM siRNA targeting pool.

## 2.9 IMMUNOPRECIPITATION

Cell lysates were prepared in a non-ionic extraction buffer [50 mM Tris-HCl (7.4), 1 mM EDTA, 1% Triton X-100, 5 mM sodium pyrophosphate, 10 mM β-glycerophosphate, 0.1% β-mercaptoethanol, 50 mM NaF, 0.5 mM sodium orthovanadate, 0.1 mM PMSF, 1X protease inhibiter cocktail mix)], and antibody-bound magnetic beads were used to capture SIRT1:p53 protein complexes. SIRT1:p53 protein complexes were pulled down from the beads, and co-associated proteins detected by western blotting.

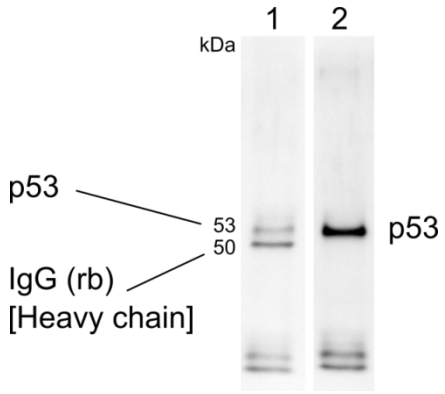


*Figure 2:6 Detection of p53 from immunoblot prepared with anti-p53 mouse mAb using anti-rabbit IgG secondary antibodies by isotype switching*

Lane 1: Eluate from a p53 immunoprecipitation experiment was separated by SDS-PAGE and visualised by immunoblotting using the same p53-targeting primary antibody and HRP-conjugated anti-rabbit IgG secondary antibodies for detection. The heavy chain IgG subunit (anti-p53 rabbit mAb) generates a band at ~50 kDa, in the same region as the target protein (p53).

Lane 2: The isotype for secondary antibody detection was switched by incubating the membrane in mouse anti-rabbit IgG (light chain specific) monoclonal antibody solution, and then using HRP-conjugated anti-mouse IgG secondary antibodies for immunodetection. Heavy chain IgG subunit is no longer present.

Antibodies obtained for use in this experiment were optimised for immunoprecipitation by the manufacturer and used at the recommended concentration. As the denatured rabbit IgG heavy chain of the SIRT1 primary antibody used for immunoprecipitation runs at approximately 50 kDa and p53 protein is 53 kDa, bands from the eluate on the subsequent western blot appear at approximately the same region. To differentiate between bands generated by the target (p53) and the antibody (IgG), and so accurately quantitate p53 protein, immunoblots were incubated with light chain-specific anti-isotype antibodies [Figure 2:6].

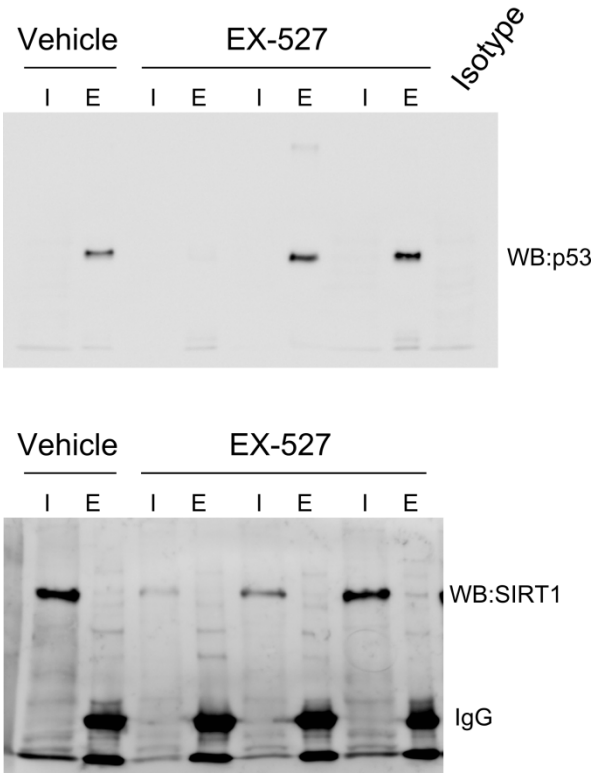


*Figure 2:7 SIRT1:p53 co-immunoprecipitation in EX-527 treated keratinocytes*

Primary human keratinocytes (NHEK) were grown to 75% confluence in 100 $cm^2$ culture plates and treated with 1 µM EX-527 for 24 h. Total protein was extracted in non-ionic lysis buffer and p53:SIRT1 immunocomplexes captured overnight at 4°C. WB – Western Blot; I – Input; E – Eluate.

Immunoprecipitation using this technique generated a wide degree of within-treatment variability occurred in replicate samples [Figure 2:7]. To compensate for this during analysis, results were normalised using densitometric data from the

input signal and the pull-down to accurately compare replicates and treatments. Firstly, the signal obtained from the eluate was standardised with 2% v/v of the sample lysate used for immunoprecipitation; and secondly, the eluate signal detected in the SIRT1 immunoblot was standardised to the quantity of pulled down immunocomplexes (detected by immunoblotting with anti-p53 antibodies).

This compensated for the between-sample variability inherent in lysate preparation and differences in efficacy of immunocomplex capture (including differences in antibody affinity, magnetic bead loading, bead washing, and elution).

## 2.10 CHROMATIN ACCESSIBILITY RT-PCR (CHART-PCR)

ChART-PCR detects structural differences in the chromatin of target regions using micrococcal nuclease (MNase) to create conditions for differential PCR amplification across nucleosomal boundaries. Unlike formaldehyde-mediated crosslinking used in ChIP, nucleosome-bound DNA is protected from MNase, enabling conformational variability in higher order chromatin structure to be detected (405). Chromatin remodelling is determined semi-quantitatively by the dropoff in PCR amplification (406).

### 2.10.1 Stabilisation of Chromatin and Nuclear Extraction

Treated cells were detached using TrypLE [incubated at 37°C for 5 min (Life Technologies Corporation, Carlsbad, CA)] and washed once in warmed PBS. Washed cells were pelleted by centrifugation at 500 g for 5 min. Nuclei were extracted by incubation in NP-40 lysis buffer [10 mM Tris.HCl (pH 7.4), 10 mM NaCl, 3 mM $MgCl_2$, 0.5% NP-40, 0.15 mM Spermine hydrochloride, 0.5 mM Spermidine, 1X Protease Inhibitor Cocktail] for 5 min on ice. Nuclei were pelleted at 1000 rpm for 5 min at 4°C, and washed once in calcium free MNase reaction buffer [10 mM Tris.HCl (pH 7.4), 15 mM NaCl, 60 mM KCl, 0.5% NP-40, 0.15 mM Spermine hydrochloride, 0.5 mM Spermidine]. Sensitivity was maximised in this assay by maintaining the

structural integrity of extracted chromatin prior to MNase digestion. Nuclear membrane damage was reduced by pelleting nuclei at ≤1000 rpm and minimal pipetting was used during resuspension steps. This was crucial to prevent nuclei from adhering to the wall of pipettes or from forming a solid pellet, as the nuclei were permeabilised during extraction to allow MNase digestion. To minimise endonuclease activity, samples were processed and prepared rapidly (within a 1 hour time frame) and kept on ice at all times. Spermine and spermidine were included in nuclear isolation and wash buffers to provide counter-ions for chromatin stabilisation (407).

### 2.10.2 Digestion of DNA with Micrococcal Nuclease

Each sample was resuspended in 200 µl reaction buffer and divided equally between two 1.5 ml microcentrifuge tubes. $CaCl_2$ was adjusted to 5 mM and one aliquot was digested with micrococcal nuclease (20 kU/ml) at room temperature whilst the other was placed on ice (as a digestion control). Reactions were quenched after 5 min by adding 20 µl Stop Buffer (100 mM EDTA + 10 mM EGTA).

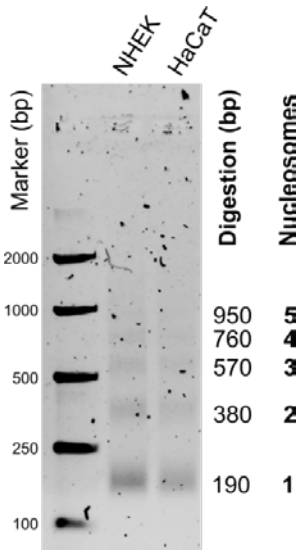


*Figure 2:8 Micrococcal nuclease digest of nuclear extracts*

Nuclei were isolated from NHEK and HaCaT cells and incubated with micrococcal nuclease at 37°C for 20 min. DNA fragments were separated on 1% agarose gel and visualised with SYBR Safe DNA stain.

DNA was released from the nuclei by adding 80 µl reaction buffer containing 4% SDS and incubating each sample at 65°C for 2 hrs with 3 µl Proteinase K, and purified using Bioline Isolate II DNA extraction columns. Twenty kU/ml of MNase enzyme was sufficient to cut chromatin into a nucleosomal ladder [Figure 2:8].

### 2.10.3 Measurement of Chromatin Accessibility by PCR Amplification

#### *2.10.3.1 Determination of Relative Chromatin Condensation*

DNA eluates were quantitated and diluted to a concentration of 5 ng/µl in nuclease-free water.

Primers were designed to amplify a nucleosome-spanning region of the promoter sequence for each gene (> 2 × 147 bp).

| Gene | ID | Coordinates | Sequence | Amplicon |
|---|---|---|---|---|
| Rhodopsin | 3q21 | chr3:129242616 chr3:129243256 | GCTAAGCCCCTAATCCACCG ACACAGTCATTACCATCAGCGA | 641 bp |
| SIRT1 | 10q21.3 | chr10:69643221 chr10:69643951 | GGCCAGAACCCATACTAGGC AAGAGAGGCAAAAGGAGGCG | 731 bp |
| miR-34a | 1p36.22 | chr1: 9241106 chr1: 9242223 | AAGATATCTCAGAACTGGGCAGAG TGGGCTTGCCTGGGCTTGTT | 1118 bp |

A total of 10 ng DNA was amplified using BioRad iQ SYBR Green Supermix (BioRad, Gladesville, NSW) with the following reaction conditions:

| | | |
|---|---|---|
| Denaturation | 95°C | 10 min |
| Anneal and Extend [40 cycles] | 95°C | 15 sec |
| | 60/65°C | 30 sec |
| | 72°C | 1 min |

MNase-mediated internucleosomal cutting was assayed using a standardised concentration of DNA template for each PCR reaction.

### *2.10.3.2 Calculations*

The ChART-PCR assay was standardised by equalising the concentration of DNA template used in each reaction and by normalising samples for endogenous DNase activity using undigested Input template. Chromatin accessibility was calculated using the following method:

Change in accessibility = 2^[Treatment Ct(adjusted) – Control Ct(adjusted)]

where Ct of sample DNA is adjusted by normalisation to the input template using the formula: $Ct_{(adjusted)} = [Ct_{(digest)} – Ct_{(input)}]$.

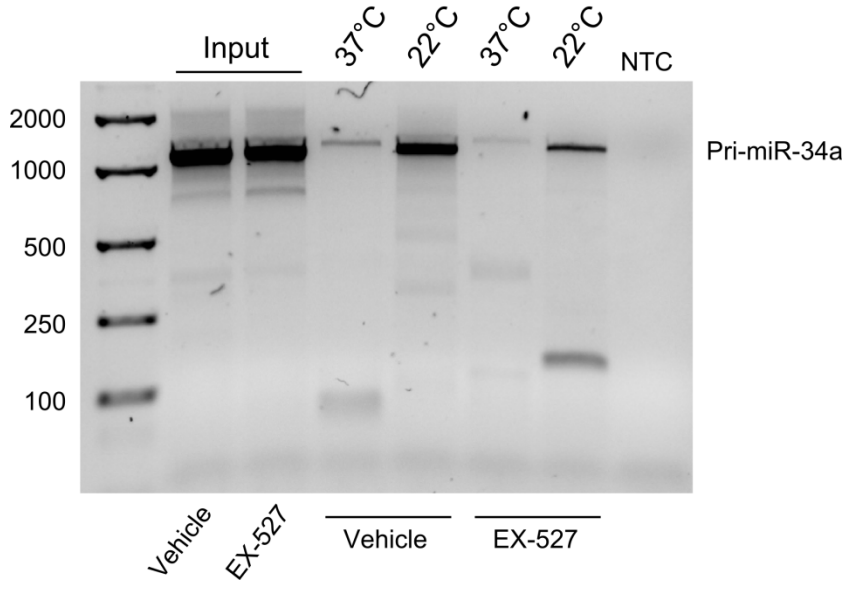


*Figure 2:9 Amplification of MNase digested chromatin after EX-527 treatment*

Nuclei were isolated from NHEK cells which had been treated for 24 hrs with 1 µM EX-527 or DMSO (vehicle) and incubated with micrococcal nuclease at 37°C or 22°C for 5 min. DNA was extracted according to the ChART protocol outlined in Chapter 2, and equal concentrations were amplified for 40 PCR cycles using *pri-miR-34a* ChART primers.

Undigested DNA from Vehicle and SIRT1-inhibited samples was amplified as a reference (Input). PCR product was run on 2% agarose gel and visualised with SYBR Safe DNA stain.

When SIRT1 was inhibited in NHEKs for 24 hrs, amplification of the pri-miR-34a gene promoter decreased when digested with MNase for 5 minutes [Figure 2:9]. This effect was more evident using a lower reaction temperature [Figure 2:9], and therefore MNase digestion was performed at 22°C to enhance assay sensitivity when used to measure chromatin accessibility.

The effect of SIRT1 inhibition on MNase accessibility in chromatin at the Rhodopsin gene promoter was quantified from Ct values generated during qPCR analysis [Figure 2:10(a)]. Quantification of these data using the previously outlined method demonstrates that inhibition of SIRT1 increases MNase accessibility in NHEKs [Figure 2:10(b)].

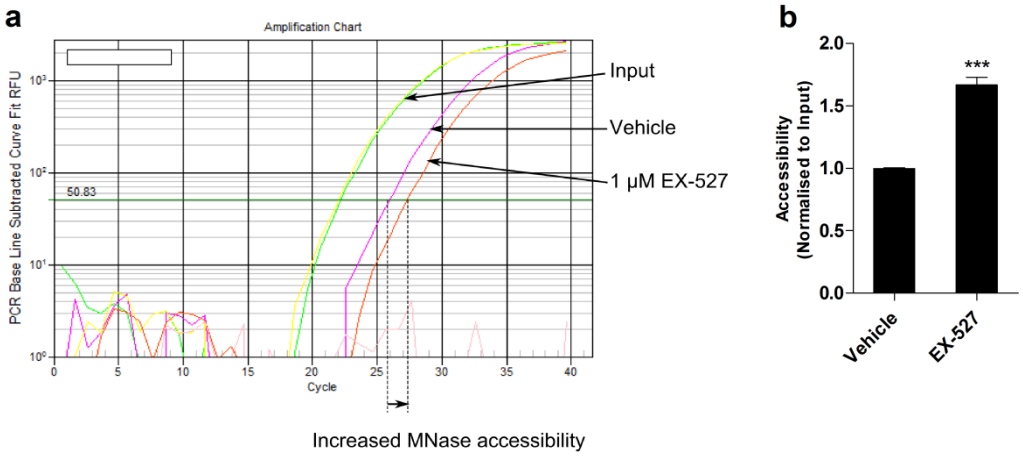


*Figure 2:10 Analysis of MNase accessibility by PCR amplification*

Primary (NHEK) keratinocytes were treated for 24 hrs with 1 µM EX-527 or DMSO (vehicle) and MNase-digested chromatin was prepared according to the ChART protocol outlined in Chapter 2. MNase-digested and undigested input DNA was analysed by qPCR with Rhodopsin primers using iQ SYBR Green Supermix (BioRad, Gladesville, NSW).

Panel a: qPCR amplification curves from Input and MNase digested chromatin

Panel b: Analysis of MNase sensitivity of the *Rhodopsin* gene in SIRT1 inhibited keratinocytes

EX-527-treated samples were analysed by paired *t*-test relative to vehicle control, with *** ($p$<0.001); $n$=3.

## 2.11 CHROMATIN IMMUNOPRECIPITATION (ChIP)

ChIP is a technique which enables analysis of DNA-protein interactions. Associations are measured by selective immunoprecipitation of DNA fragments crosslinked with the protein(s) of interest, after which the DNA fragments are purified. Here, RT-PCR was used to quantitate the association between gene locus and the protein of interest.

### 2.11.1 Preparation of Crosslinked Chromatin

Cells were grown to 80% confluence in 150 $cm^2$ culture plates and treated in 20 ml of media. DNA was crosslinked to the chromatin by incubation in 1% formaldehyde for 15 minutes on a rotator (40 rpm) at room temperature, after which the reaction was stopped by addition of 1M glycine solution to a final concentration of 0.125M. Culture medium was removed and the cells washed twice in ice-cold PBS prior to addition of cell lysis buffer [5 ml/plate; 20 mM Tris.HCl (pH 8.0), 85 mM KCl, 0.5% NP40 + 1× Protease Inhibitor Cocktail]. The cell suspension was scraped into 15 ml Falcon tubes and incubated on ice for 10 min with regular inversion. Samples were pelleted by centrifugation at 1500 rpm for 5 min at 4°C, and the supernatant aspirated. Nuclei were washed in 10 ml of ice-cold PBS, and repelleted by centrifugation at 1500 rpm for 5 min. Cells were resuspended in 1 ml of PBS and 10 µl removed for counting.

#### *2.11.1.1 Chromatin Fragmentation*

Nuclei were pelleted at 3,000 rpm for 5 min at 4°C, resuspended in Nuclear Lysis Buffer [50 mM Tris.HCl (pH 8.0), 10 mM EDTA, 1% SDS, 1× Protease Inhibitor Cocktail] at a concentration of approximately 3-4$\times 10^7$ nuclei/ml and incubated on ice for 10 min. Chromatin was sheared using a Sonics Ultrasonicator to generate DNA fragments of 300 – 1000 bp.

#### *2.11.1.2 Fragment Size Analysis*

Fifty microliters of nuclear lysate was incubated at 37 °C with 2 µl RNase A solution with 6 µl 5 M NaCl in 100 µl water for 20 min, after which 2 µl of 20 mg/ml

Proteinase K solution was added and crosslinks reversed at 65°C for 2 hours. DNA was purified using a BioLine DNA extraction kit into a final volume of 20 µl eluate. Total DNA extracts were resolved by submarine electrophoresis on 1% high resolution agarose gels at 80V for 1 hour. Resolved DNA was visualised using a Las-3000 imaging system.

### *2.11.1.3 Empirical Determination of Sonication Conditions*

Sonication was optimised by determining the conditions required for nuclear lysis and extending the sonication time incrementally to shear chromatin. Nuclear extracts in 250 µl aliquots were exposed to 5 min sonication sets (10 cycles of 30 seconds on/30 seconds off at the 100% amplitude setting) on ice to maintain protein:DNA interactions. After each set, 10 µl of the sample was viewed under a microscope to determine the degree of nuclear lysis.

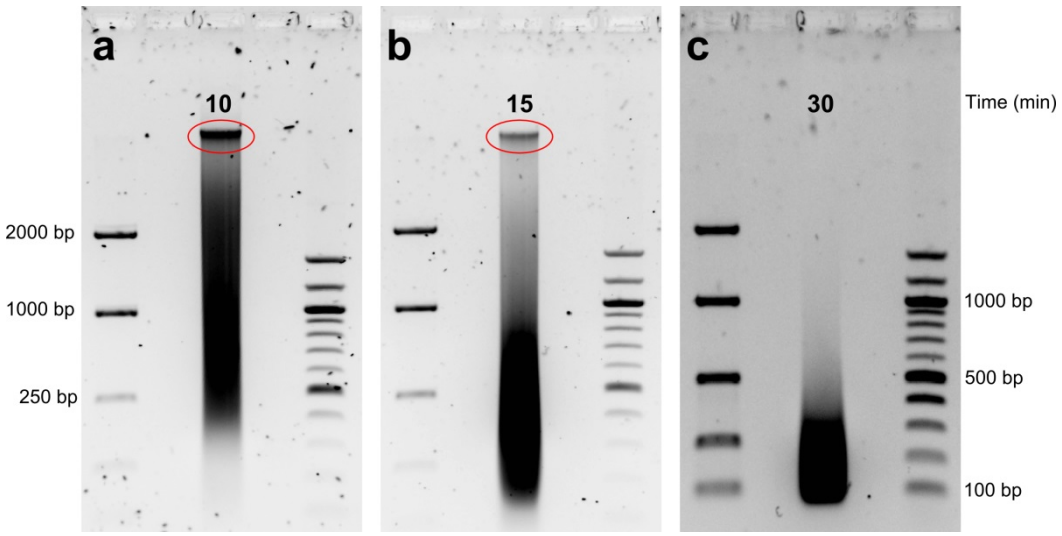


*Figure 2:11 Optimisation of chromatin fragmentation conditions.*

Nuclei from primary neonatal (NHEK) keratinocytes were isolated and sonicated on ice using 10 cycles of 30 seconds on/30 seconds off at the 100% amplitude setting. DNA fragments were purified from crosslinked chromatin and separated on 1% agarose by electrophoresis. Total sonication time is indicated.

Panel a: 10 minutes

Panel b: 15 minutes

Panel c: 30 minutes

Note: Non-lysed nuclei are circled (red)

For NHEK and HaCaT keratinocyte nuclei prepared using the above manner, whole nuclei remained in solution in solutions exposed to sonication energy for < 30 min, and 3 sets of 5 min sonication cycles (15 min total) was required to release crosslinked chromatin into solution [Figure 2:11]. Ten minutes of sonication time sheared DNA to a fragment size range between 250 and 2500 bp; at fifteen minutes, fragment size range was between 100 and 1000 bp; and after 30 minutes, DNA fragments were between 100 and 250 bp [Figure 2:11]. From these results, 15 minutes was decided on as the optimal sonication conditions.

## 2.12 IMMUNOPRECIPITATION

### 2.12.1 Antibody loading (magnetic beads)

Target antibodies were preloaded and crosslinked to Protein G-coupled Dynabeads (Dynal AS, Life Technologies, Oslo, Norway) with bis(sulfosuccinimidyl) suberate ($BS^3$) (ThermoFisher Scienctific, Rockford IL). Five µg antibody stock was diluted in 200 µl PBS + 0.02% Tween20 (PBST) and added to 1.5 mg Dynabeads in a 1.5 ml screwtop microcentrifuge. Antibody loading was carried out on a roller at room temperature for 60 minutes. The beads were washed twice in 200 µl Conjugation Buffer [20 mM phosphate buffer (pH 7.5), 150 mM NaCl] and resuspended in 250 µl of 5mM $BS^3$ solution [20 mM phosphate buffer (pH 7.5), 150 mM NaCl, 5 mM $BS^3$]. Antibody bound beads were crosslinked on a roller at room temperature for 30 minutes, and the reaction quenched by adding Tris.HCl (pH 7.5) to a final concentration of 20 mM. Following a 15 min incubation period, antibody-crosslinked beads were washed 3× in 200 µl PBST by gentle pipetting and stored in PBST at 2-8°C.

The crosslinked chromatin solution was diluted 1:10 in ChIP buffer [16.7 mM Tris.HCl (8.0), 167 mM NaCl, 1.2 mM EDTA, 1% Triton X-100, 1 × protease inhibitor cocktail]. A 100 µl aliquot was removed from the diluted preparation and stored at –20 °C to use as a 2% input sample. Immunocomplexes were captured by adding 25 µg of antibody-loaded magnetic beads (2.5 µg antibody solution per reaction) to 1

ml aliquots of diluted chromatin solution with overnight incubation at 4°C on a roller mixer. One sample from each preparation was incubated with magnetic beads loaded with 2.5 µg normal Rabbit IgG as a negative control.

Beads with captured immunocomplexes were washed once in 1 ml low salt wash [20 mM Tris.HCl (pH 8.0), 0.1 % SDS, 150 mM NaCl, 2 mM EDTA, 1% Triton-X100], 1 ml high salt wash [20 mM Tris.HCl (pH 8.0), 0.1% SDS, 500 mM NaCl, 2 mM EDTA, 1% Triton X-100], and twice each in 1 ml LiCl wash [10 mM Tris.HCl (pH 8.0), 250 mM LiCl, 1% Igepal/NP-40, 1% Sodium deoxycholate, 1 mm EDTA], and TE buffer [10 mM Tris.HCl (pH 8.0), 1 mM EDTA] for 5 minutes at 4 °C with rotation for each wash. Immunocomplexes were eluted by adding 150 µl ChIP elution buffer [100 mM $NaHCO_3$, 1% SDS] and incubating the beads for 30 minutes at 65 °C on a thermomixer at 1200 rpm. The supernatant was aspirated and transferred to a new tube.

### 2.12.2 Elution and Extraction of Crosslinked DNA

The salt concentration of each sample was raised to 200 mM by adding 6 µl of 5 M NaCl and the crosslinks reversed by incubating for 2 hr with 3 µl of 20 mg/ml Proteinase K at 65 °C on a thermomixer at 700 rpm. DNA was purified by spin column extraction, eluted into 50 µl buffer and stored at – 20 °C until PCR quantification.

### 2.12.3 PCR Analysis of Associated Genes

#### *2.12.3.1 Primer Design*

Nucleotide sequences were were retrieved using the NCBI/RefSeq database and screened for regulatory features with the Ensembl database. For each gene, the sequence was expanded to include regulatory regions upstream of the coding domain.

Primers were designed according to the following parameters:

| | |
|---|---|
| Primer Length | 24 nucleotides |
| Optimum Tm | 60°C (58-60°C) |
| Optimum CG content | 50% (30-80%) |
| Amplicon size | 80-160 bp |

| Gene | ID | Site | Coordinates | Sequence | Amplicon |
|---|---|---|---|---|---|
| RPL30 | 8q22 | | 99057030 | AAGGGCCAAACACCACAATCGCTA | 139 bp |
| | | | 99057144 | AATCGAAGAGACTGAACGGGCTTCG | |
| miR-34a | 1p36 | Upstream | 9241106 | AAGATATCTCAGAACTGGGCAGAG | 102 bp |
| | | | 9241207 | GCATGTGAAACTCTAGCAGATACC | |
| | | 1 | 9241825 | TAATGAAAACCCTGTTCAATTGTG | 153 bp |
| | | | 9241977 | CTGGAGATAGAGGAGGGAAGAAAG | |
| | | 2 | 9242156 | TCCAAATGCCCCCGATCTGCGT | 68 bp |
| | | | 9242223 | TGGGCTTGCCTGGGCTTGTT | |
| SIRT1 | 10q21 | 1 | 69643806 | TGTATACCACCCTACAAGTGATGG | 154 bp |
| | | | 69643959 | TAAGTAGGAAGAGAGGCAAAAGGA | |
| | | 2 | 69643284 | GATAGAAACGCTGTGCTCCAGGCA | 143 bp |
| | | | 69643426 | AAAGCCCTTCCACTTTCCTCTCTCCC | |
| | | 3` | 69674963 | CTTTGGAGAGAACTTGAGATAGGC | 195 bp |
| | | | 69675157 | TTGGGGTTTAAGTGAAAGAGTAGG | |

[see http://www.genenames.org/data/hgnc_data.php?hgnc_id=14929 (SIRT1) and http://www.genenames.org/data/hgnc_data.php?hgnc_id=31635 (miR-34a)]

Template DNA was amplified with target primer sets using 2× BioRad SYBR green reaction mix on an iCycler MYiQ™ [Bio-Rad Laboratories, CA, USA] using the following cycling conditions:

| | Temp (°C) | Time | |
|---|---|---|---|
| Activation | 95 | 10 min | |
| Denaturation | 95 | 10 sec | 40 cycles |
| Anneal and Extend | 60 | 60 sec | |

### 2.12.4 Calculation of Results

ChIP data were calculated by quantifying the RT-PCR results from the ChIP reaction relative to the Input reaction. Input Ct values were adjusted to the dilution factor (DF) [Ct-$Log_2$(DF)].

The amount of genomic DNA co-precipitated with the antibody was calculated as an IP:Input ratio using the following formula:

% total = $2^{\Delta CT}$ Where ΔCT = CT(adjusted Input) – CT(ChIP)

## 2.13 DNA METHYLATION ANALYSIS

Normal human keratinocytes (NHEK) were cultured for 10 weeks in EpiLife Keratinocyte growth medium into which had been added arsenite [As(III)] to a final concentration of 0.5 μM. Cells were grown in 75 $cm^2$ flasks using a seeding density of $5 \times 10^5$ cells and allowing an overnight settle prior to addition of the treatment medium. When the flasks had reached 75-85% confluence (approximately once per week), the cells were detached using TrypLE dissociation reagent (Invitrogen, Carlsbad, CA, USA), rinsed in Epilife and counted using a Haemocytometer. Half a million cells were passaged into a new flask and the remaining harvested cells washed in PBS. The harvested NHEKs were pelleted in aliquots of $1 \times 10^6$ cells and stored at −80°C until use. Untreated NHEK cells grown in EpiLife were harvested concurrently as passage matched controls.

### 2.13.1 Bisulfite Conversion

Methylated cytosine bases are differentiated from non-methylated bases by treatment with sodium bisulfite. Methylation of cytosine confers resistance to sodium bisulfite treatment, whereas unmethylated bases are converted to uracil and are amplified as thymine during PCR (408) [Figure 2:12].

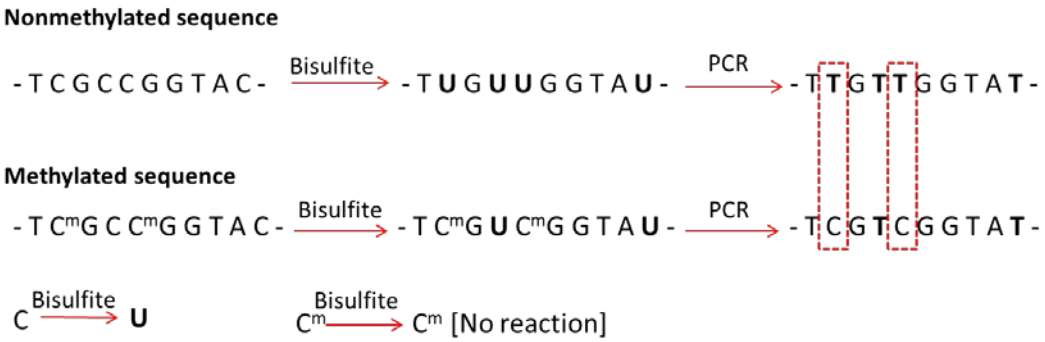


*Figure 2:12 Detection of cytosine methylation by bisulfite conversion*

Cytosine bases (C) are converted to uracil (U) by bisulfite treatment. These bases are subsequently converted to thymine (T) during the 1st round of PCR amplification. Methylated cytosine bases ($C^m$) are unaffected by bisulfite treatment, and remain cytosines during PCR amplification.

During conversion, bisulfite is added to the 5,6 double bond, generating cytosine sulfonate in equilibrium with cytosine. In acidic conditions, cytosine sulfonate is deaminated to uracil sulfonate. Removal of bisulfite in alkaline conditions removes the sulfonate group and covers the 5,6 uracil double bond. Methylation of cytosine at its 5' position inhibits sulfonation [Figure 2:13].

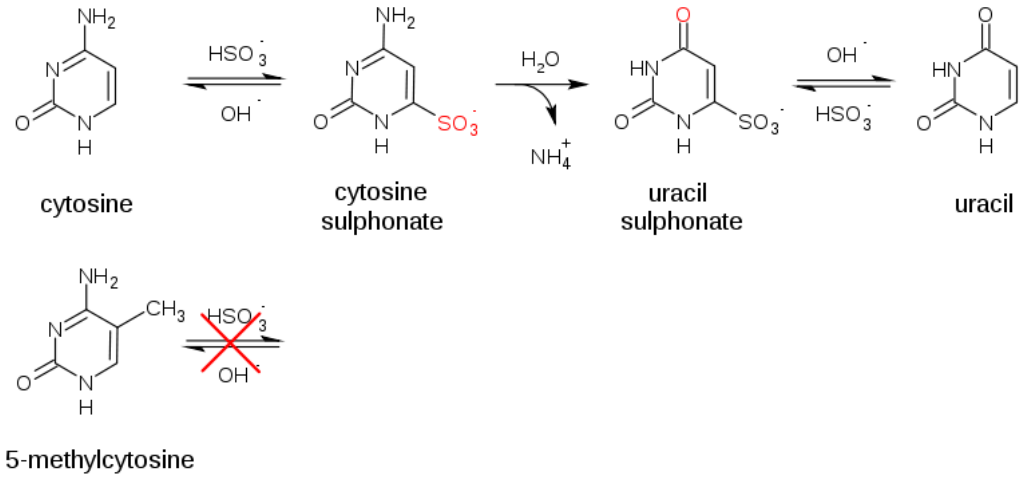


*Figure 2:13 Bisulfite Conversion of Cytosine to Uracil*

Bisulfite is added to the 5,6 double bond, generating cytosine sulfonate in equilibrium with cytosine. In acidic conditions, cytosine sulfonate is deaminated to uracil sulfonate. Removal of bisulfite in alkaline conditions removes the sulfonate group and covers the 5,6 uracil double bond. Methylation of cytosine at its 5' position inhibits sulfonation (408).

DNA from treated cells was bisulfite converted using a Cells-to-CpG Bisulfite Conversion Kit (Applied Biosystems, Foster City, CA, USA). The recommended protocol is optimized for conversion of 5000 to $10^5$ cultured cells, therefore a cell count was performed during harvest to optimise the concentration of input DNA. Cells were lysed and denatured at 50°C for 10 min prior to addition of the conversion reagent. The bisulfite reaction mix was added and the sample incubated according to cycling protocols in Table 2:1. Samples were desalted and desulfonated immediately following conversion, and the converted DNA stored at −80°C prior to use in PCR amplification reactions.

*Table 2:1 Bisulfite conversion protocol*

| Input DNA 100 ng - 2 µg | | Input DNA 50 pg - 100 ng | | Input DNA ≥ 2 µg | |
|---|---|---|---|---|---|
| Temp (°C) | Time (min) | Temp (°C) | Time (min) | Temp (°C) | Time (min) |
| 65 | 30 | 65 | 30 | 95 | 3 |
| 95 | 1.5 | 95 | 0.5 | 65 | 60 |
| 65 | 30 | 65 | 30 | 95 | 3 |
| 95 | 1.5 | 95 | 0.5 | 65 | 30 |
| 65 | 30 | 65 | 30 | 4 | Up to 4 hrs |
| 4 | Up to 4 hrs | 4 | Up to 4 hrs | | |

## 2.13.2 Bisulfite PCR

### *2.13.2.1 Primer Design*

Conversion-specific primers were designed to span CpG rich regulatory domains of target genes using Methyl Primer Express Software v1.0 (Applied Biosystems) (409) [Table 2:2].

The output from this program was screened for potential target candidates using primer design parameters described by Li and Dahiya (410) and Wojdacz et al. (411):

- Primer pairs were designed to amplify a CpG-rich region, and target loci contain a minimum number of non-CpG cytosines in their sequence.
- The target amplicon has a length of no greater than 450 bp and no less than 100 bp.
- The melting temperature of the primers are matched to within 1°C
- To ensure bisulfite-specific amplification, the 3' end of the primer contains one or more T corresponding to non-CpG cytosines.

Primers containing CpG dinucleotides were placed as close as possible to the 5' end of the primer and degenerate bases represent the methylated and unmethylated cytosines. Y was used to represent C and T in a forward primer, and R was used to represent G and A in a reverse primer.

*Table 2:2 Primers for Bisulfite Sequencing*

| Gene | Region | ID | Sequence | bp | % CG |
|---|---|---|---|---|---|
| SIRT1 | 10q21.3 | SIRT1BisF | GTGATTYGTAGTGTTGTGGTTT | 190 | 61.58 |
| | | SIRT1BisR | CCATCTTCCAACTACCTCTCTAAC | | |
| miR-34a | 1p36.22 | miR-34aBisF | AAGGGGATGAGGATTAGGAT | 346 | 45.09 |
| | | miR-34aBisR | AAACAAACCCAAACAAAACC | | |
| hMLH1 | 3p21 | hMLH1BisF | GGAGTGAAGGAGGTTACGGGTAAGT | 182 | 68 |
| | | hMLH1BisR | AAAAACGATAAAACCCTATACCTAATCTATC | | |

A CpG-rich region of the *hMLH1* gene was used as a methylation-sensitive control sequence during analysis. Candidate primer sets were checked and tested for bisulfite sequence sensitivity and specificity using gDNA controls [Cells-to-CpG Methylated and Unmethylated gDNA Control Kit (Applied Biosystems, Foster City, CA, USA)]. Quantitative PCR was performed on a StepOne PCR cycler (Applied Biosystems, Foster City, CA, USA) using BioRad iQ SYBR Green Supermix (BioRad, Gladesville, NSW).

Primer specificity was assayed by amplifying converted and non-converted (raw) DNA using conversion-specific PCR primers. Bisulfite converted DNA templates amplified with bisulfite-specific primers for both gene targets, whereas unconverted DNA was not amplified [Figure 2:14].

Although the primer sets are specific for bisulfite-converted DNA, Ct values were >30 for the methylated template amplified with miR-34a bisulfite primers. In order to achieve sufficient template amplification for analysis by gel electrophoresis, high resolution melt curve analysis or for sequencing, 60-80 cycles of amplification were required for future applications.

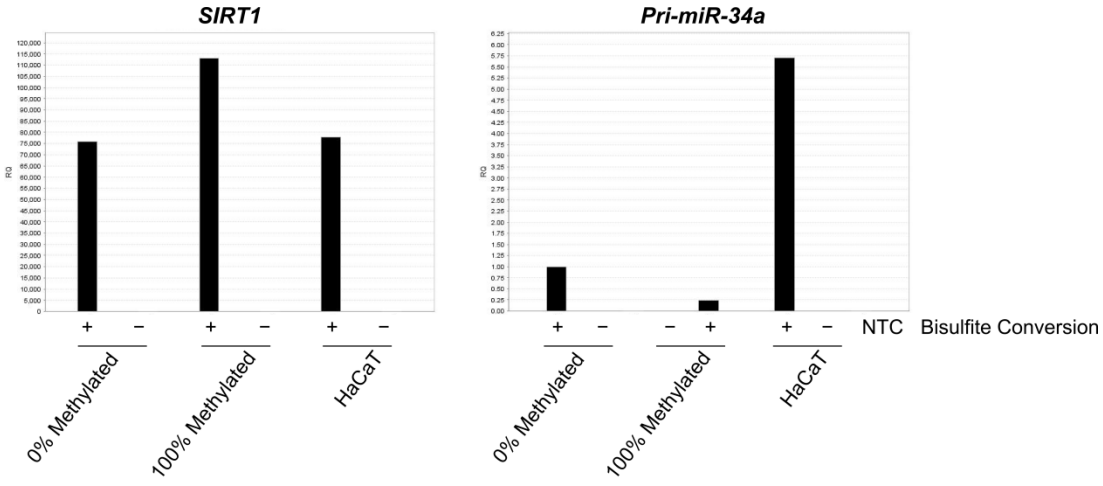


*Figure 2:14 Bisulfite Conversion Specificity*

Bisulfite converted DNA and unconverted (raw) sample templates were amplified using bisulfite-specific primer sets for SIRT1 and miR-34a targets, where Control 1 is unmethylated gDNA template and Control 2 is fully methylated gDNA template. Relative quantitation was determined using ΔCt values for each sample compared to Control 1 unconverted DNA (Raw). Quantitative PCR was performed on a StepOne PCR cycler (Applied Biosystems, Foster City, CA, USA) using BioRad iQ SYBR Green Supermix (BioRad, Gladesville, NSW). Note- both bisulfite PCR primer sets amplify templates in a conversion-specific manner.

### *2.13.2.2 Amplification Efficiency*

As bisulfite PCR uses CG rich regions of the gene as templates, target sequences are prone to secondary structure formation and mispriming which can inhibit

amplification. DMSO disrupts intra-strand reannealing, allowing the higher Tm associated with cytosine-guanine bonding to be overcome (412).

By including DMSO at a final concentration of 2% in each PCR reaction, amplification of target sequences improved significantly [Figure 2:15].

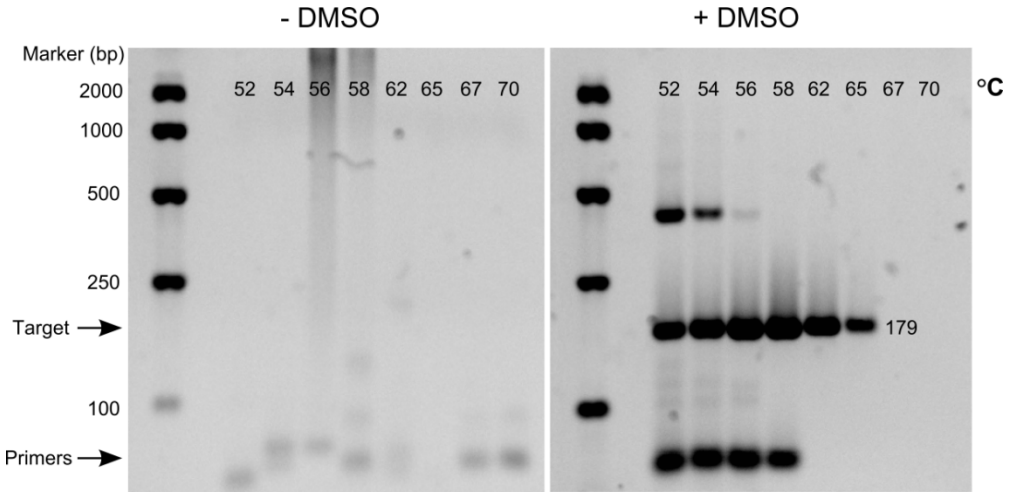


*Figure 2:15 Bisulfite PCR adjuvants – miR-34a Primers*

Bisulfite converted DNA template was amplified using a temperature gradient with miR-34a bisulfite primers for 80 cycles. PCR product was separated on 2% agarose gel by electrophoresis and visualised using SYBR safe DNA stain. PCR product was amplified with (Right panel), and without (Left panel) DMSO included in the PCR reaction mix at a final concentration of 2%. Note- off-target amplification increases with temperatures < 60°C.

### 2.13.3 High Resolution Melt Curve Analysis

Bisulfite converted sequences differ in their thermal stability in a methylation-dependent manner. Conversion of non-methylated cytosines to thymine following bisulfite treatment causes its PCR product to melt at a lower temperature than its methylated counterpart (385) [Figure 2:16]. Different melting properties of converted sequences were analysed using the relative fluorescence of a double-stranded DNA binding dye such as SYBR green (386).

As the effect of arsenic on SIRT1 or miR-34a methylation in keratinocytes was unknown prior to this investigation, high resolution melt curve analysis was

performed to screen for changes in the target regions prior to sequencing. To gauge the effect of arsenic on CpG methylation of the target genes, methylation-specific standards were prepared from fully methylated and unmethylated gDNA [Table 2:3 & Table 2:4] and treated by bisulfite for conversion prior to use in melt curve analysis studies.

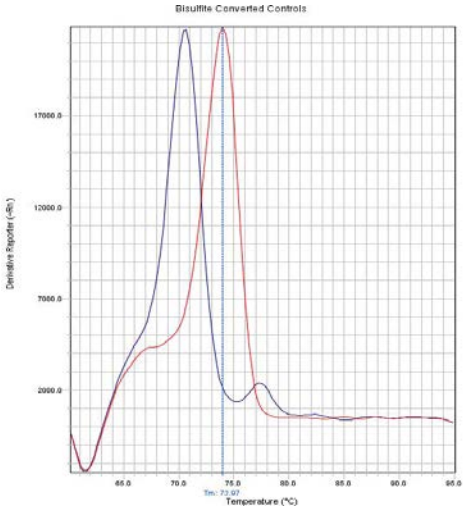


*Figure 2:16 Melting Properties of Methylated and Unmethylated DNA*

Pri-miR-34a sequences were amplified from unmethylated (0%, blue) and fully methylated (100%, red) control DNA following bisulfite conversion.

*Table 2:3 High % methylation standards*

| Control gDNA | Input volume (µl) | | | | | |
|---|---|---|---|---|---|---|
| Fully methylated DNA (20 ng/µl) | 10 | 7.5 | 5 | 2.5 | 1 | 0 |
| Non-methylated DNA (20 ng/µl) | 0 | 2.5 | 5 | 7.5 | 9 | 10 |
| Standard (% methylation) | 100 | 75% | 50% | 25% | 10% | 0% |

*Table 2:4 Low % methylation standards*

| | | | | | | | |
|---|---|---|---|---|---|---|---|
| Fully methylated DNA (20 ng/µl) | 10 | 0.75 | 0.5 | 0.25 | 0.1 | 0.01 | 0 |
| Non-methylated DNA (20 ng/µl) | 0 | 9.25 | 9.50 | 9.75 | 9.90 | 9.99 | 10 |
| Standard (% methylation) | 100 | 7.5% | 5% | 2.5% | 1% | 0.1% | 0% |

DNA was prepared for HRM analysis with a Cells-to-CpG Bisulfite Conversion Kit (Applied Biosystems, Foster City, CA, USA) according to the manufacturer's instructions. Genomic DNA from treated cells was amplified with MeltDoctor HRM reagents (Applied Biosystems, Foster City, CA, USA) using cycling conditions optimized for each individual primer set used, and then subjected to melt curve analysis. hMLH primer sets were designed to amplify bisulfite-converted methylation standards, and used to test the sensitivity of melt curve analysis to discriminate between high [Figure 2:17(a & c)] and low [Figure 2:17(b & d)] % methylation of PCR product.

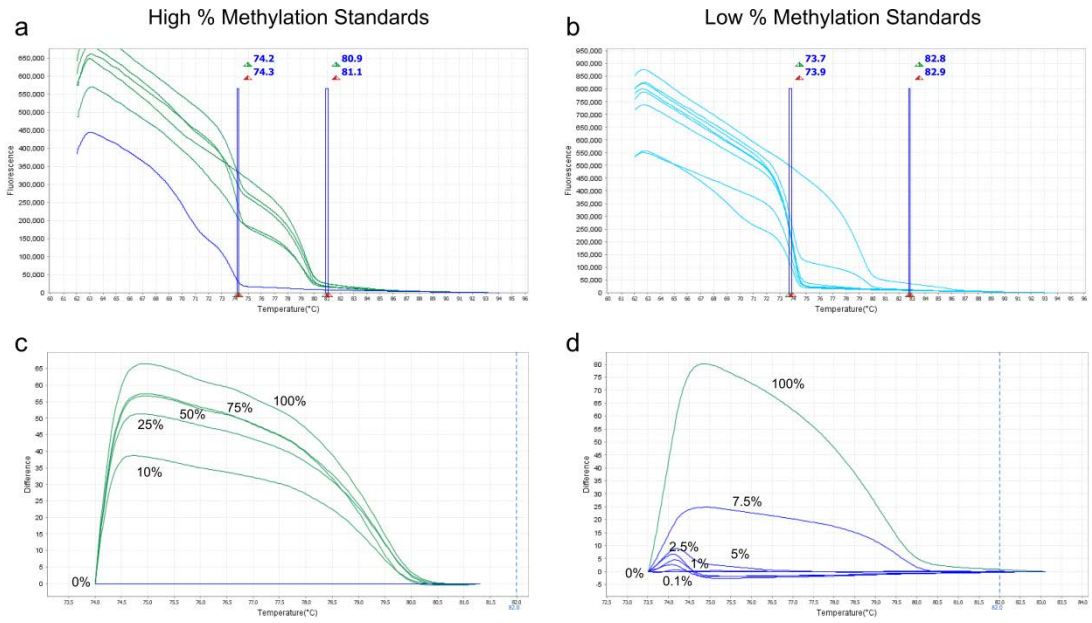


*Figure 2:17 Melt Curve Plots – Methylation Standards*

Methylation standards were prepared by mixing 100% methylated and unmethylated control DNA. Standards were amplified using hMLH primers and high resolution melting performed with MeltDoctor HRM Reagents. Melt curves (Panels a & b) were analysed and difference plots (Panels c & d) were generated from the data using High Resolution Melt Software v3.0 (Applied Biosystems, Foster City, CA, USA).

Once amplification conditions had been optimized for SIRT1 and miR-34a gene targets, methylation standards were used to generate high resolution melt curves for use as reference plots during analysis of arsenic-treated samples [Figure 2:18].

HRM analysis confirmed that 0.5 µM arsenic induced progressive changes in the methylation profile of the target genes when compared with untreated controls, and that a 10 week treatment schedule provides sufficient exposure time to create detectable results for bisulfite sequencing experiments (see Supplementary Material for Details).

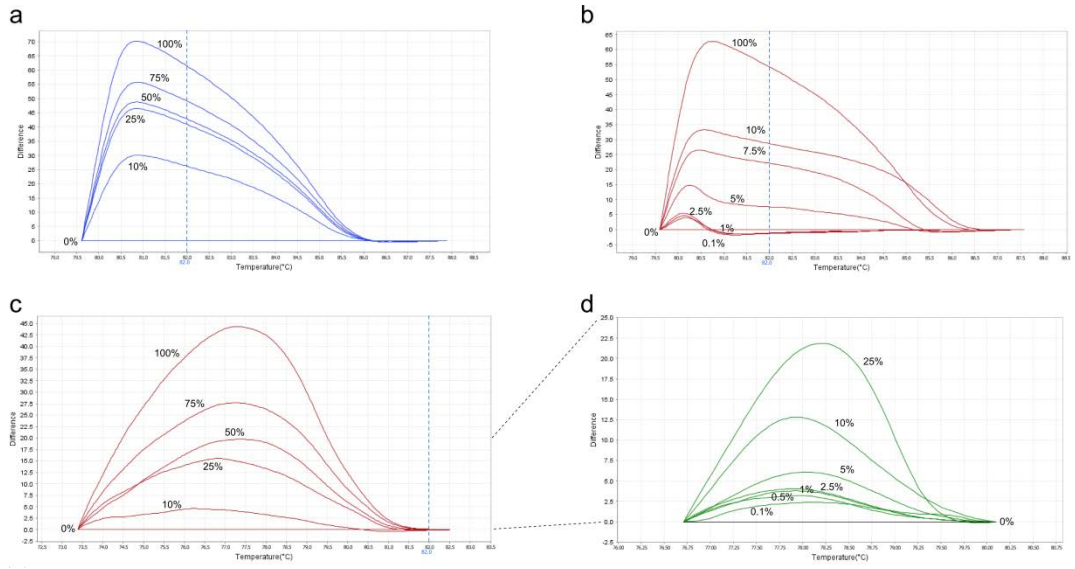


*Figure 2:18 Melt Curve Analysis – Sensitivity of HRM*

Methylation standards were amplified using SIRT1 and pri-miR-34a bisulfite primers. High resolution melting performed with MeltDoctor HRM Reagents and and difference plots generated from melt curve analysis data using High Resolution Melt Software v3.0 (Applied Biosystems, Foster City, CA, USA).

Panels a & b – Difference plots, SIRT1 methylation standards

Panels c & d – Difference plots, Pri-miR-34a methylation standards

### 2.13.4 Bisulfite Sequencing

When determining the effect of a treatment on methylation status at a locus, the gold standard technique is to insert a fragment of the target region into a plasmid vector and to analyse an aggregate of the cloned population. In this study, direct sequencing of the endogenous PCR product was used as an alternative. Although the sequences generated in this manner were from a heterogeneous population,

differences in chromatogram signal intensity were sensitive enough to provide a general comparison of CpG methylation between samples. Residual nucleotides, primers and salts were removed from PCR products using a MinElute PCR cleanup kit by following the manufacturer's instructions. The resultant purified PCR products were analysed for extracted DNA on a Qubit fluorometer using a dsDNA HS assay kit (Molecular Probes, Life Technologies). Total extracted PCR product was between 20 and 450 ng DNA for all samples.

### *2.13.4.1 BigDye Reaction Setup and Cycle Sequencing*

Sequencing reactions were set up in PCR tubes as follows:

| Component | Quantity/Rx (ul) |
|---|---|
| 5X Sequencing Buffer | 1.75 |
| BigDye Terminator | 0.25 |
| Template | to 100 ng* |
| Primer | 3.3 pmol |
| H2O | to 10 ul |

Reactions were spun down in a microcentrifuge and BigDye Terminator bound to the DNA template by placing the sample sequencing reactions on a thermocycler using the following conditions:

| | | |
|---|---|---|
| Denaturation | 96°C | 1 min |
| | 96°C | 10 sec |
| 25 cycles | 50°C | 5 sec |
| | 60°C | 4 min |
| Hold | 4°C | |

### *2.13.4.2 Cleanup and Analysis*

To remove unincorporated dye-labelled terminators, DNA was precipitated onto CleanSeq magnetic beads (10 µl/Rx) by adding 42 µl of 85% ethanol to each sample and mixing thoroughly by pipetting. The contaminated supernatant was aspirated by placing the PCR strips onto a magnetic plate and allowing the beads to settle for 3-5 minutes. Captured DNA was washed by adding 100 µl of 85% ethanol to the

beads, incubating for 30 seconds and aspirating the supernatant as before. Excess ethanol was removed from the DNA by air drying for 10 minutes, and captured DNA was eluted by incubating the beads in 40 µl of water at room temperature for 5 minutes. Thirty microliters of cleared DNA solution was aspirated for analysis on the ABI Prism 310 Genetic Analyser.

Unmethylated and fully methylated bisulfite converted sequences were aligned to the original (unconverted) sequence using the CLC Main Workbench application (Version 6.7.1) [Figure 2:19].

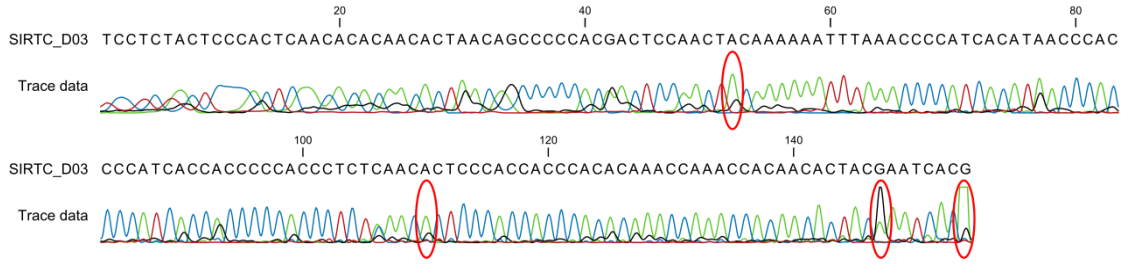


*Figure 2:19 Chromatogram of bisulfite-converted gDNA*

SIRT1 amplified PCR product. Bases with heterogeneous cytosine methylation in the sample are circled in red.

Note: Complementary DNA sequence is represented here [G→A replaces C→T]

### *2.13.4.3 Conversion Efficiency*

Sequencing of sample DNA was performed according to the protocol outlined in Chapter 2. Unmethylated and fully methylated bisulfite converted sequences and unknown samples were aligned to the original (unconverted) sequence using the CLC Main Workbench application (Version 6.7.1). When sequencing traces were analysed, whole cell samples processed in initial bisulfite conversion experiments proved to have a conversion efficiency of <100% [see Figure 2:20(a-b)]. To improve data accuracy, sequencing was repeated using samples generated with a separate DNA extraction step. Although the sequences generated in this manner were from a heterogeneous population, differences in chromatogram signal intensity were

sensitive enough to provide a general comparison of CpG methylation between samples.

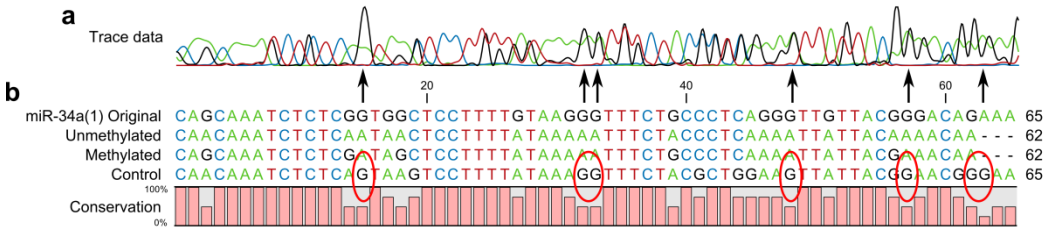


*Figure 2:20 Incomplete bisulfite conversion*

Panel **a**: Chromatogram of PCR product generated from normal keratinocytes bisulfite converted from cell extracts without a separate DNA isolation step.

Panel **b**: Sequence alignment. Mixed base signals are circled.

Key: Red – thymine (T); Green – adenosine (A); Blue – cytosine (C); Black – guanine (G)

### *2.13.4.4 Representation of Data from Methylation Analysis*

No consensus exists for the representation of bisulfite sequencing data. From the original sequence alignment [Figure 2:21(a)], methylated cytosines can be identified [Figure 2:21 (b)], and the relationship between cytosine methylation and CpG dinucleotides determined using the BiQ Analyser software program (413). CpG methylation is conventionally represented in a 'ball and stick/lollipop' format for shorter regions, or as frequency histograms for genomewide data [Figure 2:21 (c)]. For the short PCR amplified sequences analysed in this study, the ball and stick format provided the clearest representation of CpG methylation status across the region tested [Figure 2:21(d)].

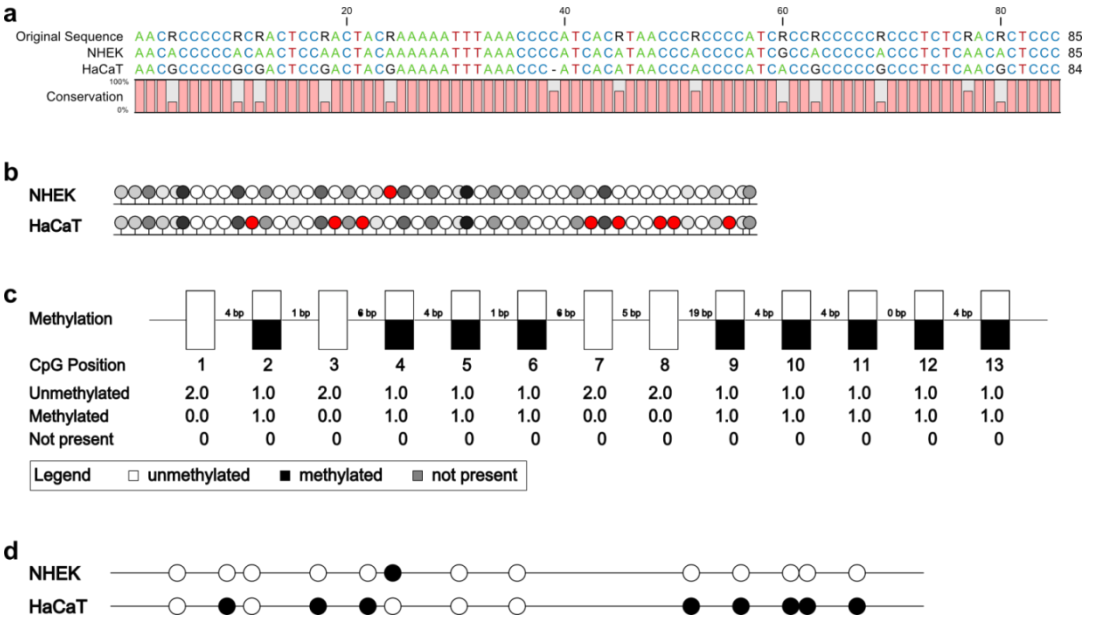


*Figure 2:21 Representation of Bisulfite Sequencing Data*

*Genomic DNA from primary neonatal (NHEK) and HaCaT keratinocytes was bisulfite converted and the SIRT1:p53 response element amplified and sequenced on an ABI Prism 310 Genetic Analyser.*

Panel **a**: Clustal W (1.83) multiple sequence alignment

Key: Red – thymine (T); Green – adenosine (A); Blue – cytosine (C); Black – guanine (G); Black - mixed bases A/G (R).

Panel **b**: Cytosine methylation – Lollipop Style Diagram

Key: Red – methylated cytosines; White/Grey/Black – unmethylated cytosines

Panel **c**: CpG Methylation Analysis - Aggregated Representation

Key: Black – methylated CpG; White – unmethylated CpG

Panel **d**: CpG Methylation Analysis – Bead Style Representation

Key: Black – methylated CpG; White – unmethylated CpG

# Chapter 3 -
# Cell Line Characterisation

## 3.1 ABSTRACT

The aim of this chapter was to define the parameters of the experimental model by differentiating cultured keratinocytes with characteristic UV-induced p53 mutations from wild-type keratinocytes by their genotypic and phenotypic properties. In order to achieve this aim, firstly the p53 mutational status of the HaCaT cell line was confirmed; secondly culture conditions were optimised for discrimination of p53-dependent phenotypic responses; and thirdly, expression and acetylation of p53 and p53-regulated genes was analysed in the HaCaT cell line by comparison with cultured keratinocytes expressing wild-type p53.

For this study, primary neonatal keratinocytes, NHEK, and the spontaneously immortalised human keratinocyte cell line, HaCaT, were used to demonstrate the relationship between SIRT1-mediated gene regulation and cellular stress responses. The HaCaT cell line was derived from the normal margin of an excised melanoma, and although non tumorigenic, contains mutations to each p53 allele which affect its expression and activity. The HaCaT cell line therefore acts as a model for the pro-carcinogenic effect of UV-induced p53 gene mutations in keratinocytes.

For detailed descriptions of the Materials and Methods, refer to Chapter 2: General Materials and Methods

## 3.2 INTRODUCTION

*Tumour Protein 53 (TP53) Mutations in Keratinocytes*

Carcinogenic TP53 mutations impede the pattern of p53 protein expression, block posttranslational modifications which promote nuclear translocation and oligomerisation, and/or interfere with DNA binding affinity (81, 414). The most frequently mutated bases (R175, R248, R249 and R273) make up 25% of all TP53 mutations, of which R248W and R273H impair DNA contact and R175H and R249S alter protein conformation (69, 70). A phenotype driven by p53 mutations differentiates normal cells from malignantly transformed cells in many cancer types, including 36% of all skin cancers (415). Features of the mutated p53 phenotype include: suppression of DNA repair, dysregulated cell cycle control and impaired survival/cell death signalling (83), and therefore p53 is an attractive target for anti-cancer treatments. Current p53-targeting therapies seek to rescue p53 function or block p53 overexpression in order to enhance the efficacy of chemotherapeutics.

Ultra violet radiation (UVR) is the primary mutagen responsible for skin cancer. UVB interacts directly with DNA in epidermal keratinocytes, forming 6-4 photoproducts and cyclopyrimidine dimers, whereas UVA acts indirectly by generating oxidative radicals (416). Repair of the resultant photolesions can create strand breaks and induce modifications to damaged pyrimidine bases such that the DNA sequence is permanently altered (417). These T→C or TT→CC transition mutations form the characteristic mutational signature of UVR damage in skin cancer (367, 418). The p53 gene in keratinocytes is susceptible to UV damage at 7 identified 'hotspots' – >30% of which are found at methylated CpG dinucleotides (165). UVB preferentially forms cyclobutane dimers at methylated CpG sites (419), and methylation of the cytosine residue at these CpG dinucleotides encourages hydrolytic deamination during repair of UV-induced DNA damage (72).

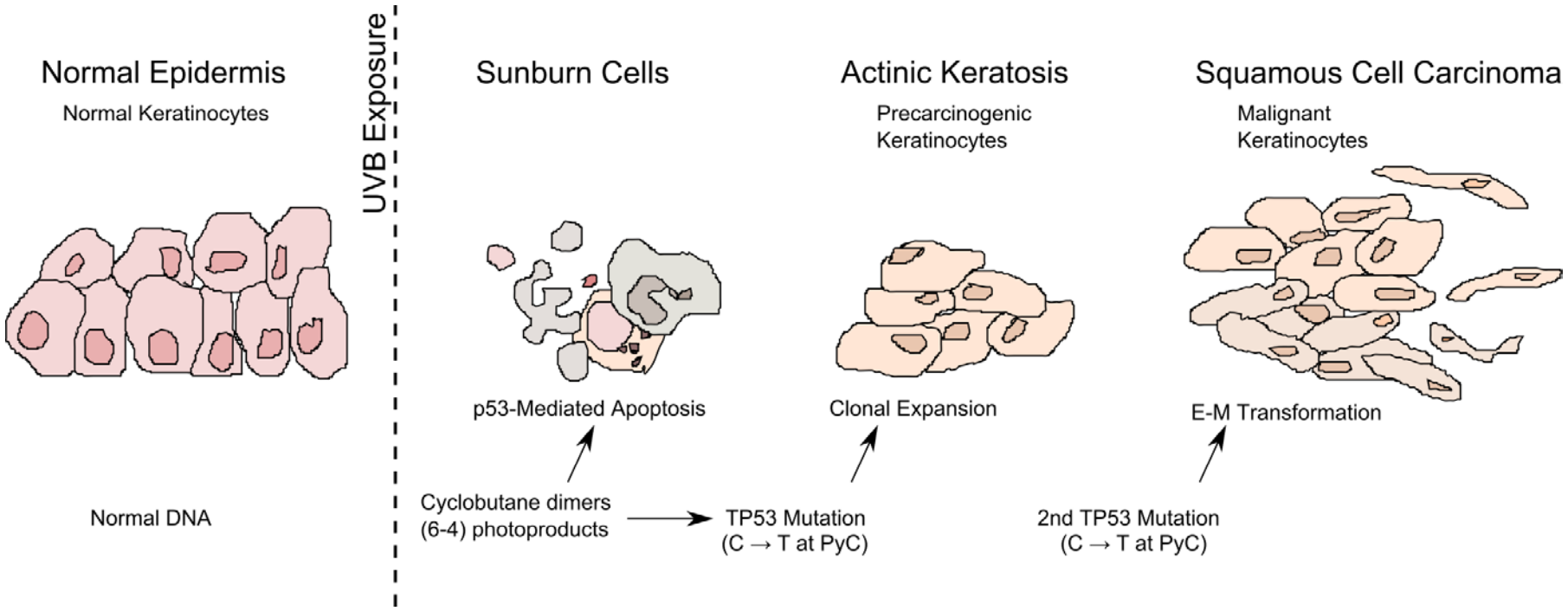


*Figure 3:1 Mutational Events in Skin Cancer*

Keratinocytes commonly undergo discrete steps as they progress to a carcinogenic phenotype. These events are precipitated by exposure to UV radiation, generating sunburn cells. UV-exposed keratinocytes with signature C→T transversions at TP53 mutational hotspots escape cell cycle regulatory control and p53-mediated apoptotic death. Clonal expansion of p53-mutated keratinocytes increases sensitivity to subsequent UV-induced DNA damage and drives malignant transformation from precarcinogenic actinic keratosis to squamous cell carcinoma (366, 420-422).

The number of keratinocyte colonies bearing missense and nonsense mutations in human skin increase with age and the level of sun exposure (423). On a physiological level, p53-mediated stress signalling is activated in keratinocytes exposed to UVR, which arrests cell cycle progression, induces the DNA damage response and activates cell death programs (producing sunburn cells) (366). If DNA repair is successful, replication is restarted, however if photolesions persist in the genome, cell death signalling culminates in apoptosis (418). Consequently, keratinocytes with impaired p53 expression and activity are unable to mount a normal response to UVR exposure, and can survive with additional UVR-mediated mutational damage [Figure 3:1].

### *In Vitro Culture of Keratinocytes*

Primary keratinocytes require a complex environment for growth *in vitro*. Keratinocyte culture systems have progressed with our understanding of epidermal growth and differentiation, from the use of feeder layers and supplementation with bovine serum solutions in the early 1980s to the defined media used today. A defined, serum-free medium supplemented with epidermal growth factor, insulin, hydrocortisone, ethanolamine and phosphoethanolamine was developed by Boyce and Ham for optimal propagation of keratinocytes in culture (424). These conditions enable primary keratinocytes to be maintained in culture for approximately 10-12 population doublings in a relatively undifferentiated state.

### *Keratinocyte Differentiation*

In human skin, keratinocytes undergo a process of terminal differentiation as they migrate from basal to suprabasal layers of the epidermis. As keratinocytes differentiate, their proliferative capacity and morphology alters, giving the outer layer of skin its structural and functional properties. The process of keratinocyte differentiation is associated with well-characterised changes in cytokeratin,

transglutaminase, involucrin and filaggrin expression. These shifts in gene expression are linked to the intracellular accumulation of keratohyalin granules, formation of a cornified envelope, and interconnecting desmosomal junctions.

The stratified layers of the skin develop within a calcium gradient which contributes to the progressive conversion of proliferative, undifferentiated keratinocytes in the basal layer to the non-proliferative phenotype characteristic of the suprabasal layers (425, 426). Increases in calcium concentration trigger formation of a cornified envelope in cultured keratinocytes by up-regulating involucrin expression and facilitating crosslinking by activation of transglutaminase (427-429).

### *The HaCaT Cell Line*

The HaCaT cell line has T→C and TT→CC mutations to codons 179, 281 & 282 of its TP53 alleles (430), which impairs DNA binding properties and increases cellular expression of mutant p53 proteins (431). Primary keratinocytes in culture rapidly enter replicative senescence and undergo terminal differentiation; however HaCaT cells retain their proliferative potential (even) in high calcium media. The loss of senescence that triggered the immortality of HaCaTs is attributed to a series of spontaneous events that occurred during *in vitro* culture of the cell line which resulted in the loss of chromosomes 3p, 4p and 9p, the gain of an isochromosome containing 9q, and the formation of a stable hypotetraploid population at passage 10 (398). Although the overall chromosomal content of the HaCaT cell line has remained stable, numerous additional rearrangements have occurred since (432). Importantly, the occurrence of phenotypic changes in the HaCaT cell line which contributed to its independent growth occurred after genotypic stabilisation when the chromosomes were no longer undergoing rearrangements (passage 70). This observation has been attributed to epigenetic modifications which enabled the cell line to adapt to culture conditions (432), and are therefore reversible. Despite concerns regarding the impact of these mutations on their phenotype, HaCaT cells

retain their morphological features and the capacity to differentiate into a polarised and stratified epithelium (433). This allows HaCaTs to be used as a representative model for keratinocyte responses in culture and is consistent with changes that are known to occur during the process of oncogenesis (formation of skin cancers).

For our investigations, two keratinocyte cell lines were used – primary neonatal human keratinocytes (NHEK; Cascade Biologics, cat# C-001-5C) purchased from Gibco-Invitrogen, (Life Technologies), and an immortalised HaCaT cell line which had been cultured in DMEM/F12 with added foetal bovine serum. NHEKs are fastidious to culture, requiring a complex defined medium for survival *in vitro*; however the HaCaT cell line displays unlimited population doublings in a less defined medium such as DMEM/F12. Prior to commencing experimentation, the HaCaT cell line was adapted to the same defined growth medium (low calcium, serum free) in order to minimise medium-specific variability in gene expression between the two keratinocyte cell lines. Phenotypic changes acquired by the HaCaT cell line during this process were monitored using keratinocyte differentiation markers.

## 3.3 RESULTS

### *Confirmation of the HaCaT Phenotype*

Our HaCaT cells were obtained as a live culture from a colleague who is well respected in the field of photobiology. Regardless of the source, we felt it was important to confirm the p53 mutational status of this cell line, as this assumption informed our hypotheses and conclusions based on the results obtained from experimentation. Contamination and misidentification of cultured cell lines has been an increasing issue in the field of research (434, 435). A recent Nature Methods retraction (436) has demonstrated the importance of cell line identification in the field of research. Although short tandem repeat (STR) profiling is recommended for cell line authentication (437), we considered the source of our cell lines was reliable enough to not warrant further investigation.

The HaCaT cell line was developed by Boukamp et al. from a skin sample which became spontaneously immortalised in culture following a replicative crisis between passages 6-10 (398). Acquisition of altered replication capacity in this cell line is attributed to an increase in telomerase expression resulting from hypotetraploidy triggered during this process (432, 438, 439). HaCaT keratinocytes are a useful *in vitro* cell line for modelling molecular mechanisms in the skin, partly due to their unlimited replicative potential, but also as they have retained their capacity for differentiation and are non-tumorigenic. A well-documented feature of HaCaT keratinocytes is its compound heterozygous mutations to each *TP53* allele. Although the HaCaT cell line was derived from morphologically normal skin, it had been exposed to UVR at a genotoxic level which was sufficient to produce the adjacent melanoma. The *TP53* mutations found in this cell line are characteristic of UVR damage and affect codon 179 of exon 5 in one allele and codons 281 and 282 of exon 8 in the other (430, 440). Since TP53 mutations are a common feature of non-melanoma skin cancer, our assumption is that these mutations generate a pre-carcinogenic phenotype which is related to UV-induced TP53 damage in the skin.

TP53 gene mutations in the cell line used for study experiments were identified by comparing its p53 cDNA sequence with the sequence obtained from wild-type human keratinocytes (NHEK, see Chapter 2 for details). The use of cDNA for sequencing p53 was challenging, due to the number of potential splice variants yielded by its 11 exons. Over 9 isoforms of this gene transcript have been identified, with the p53TA isoform representing the full-length transcript (441-443). The IARC TP53 Database [http://p53.iarc.fr/ProtocolsAndTools.aspx] (444, 445) recommends detection of p53 mutations by direct sequencing and outlines a protocol for targeting small (<500 bp) fragments. Although most p53 mutations are found within exons 5-8 (including those recorded for HaCaTs – see IARC TP53 Database (http://p53.iarc.fr/CellLines.aspx), we decided to screen the entire ORF sequence (exons 2-11) of isoform 1.

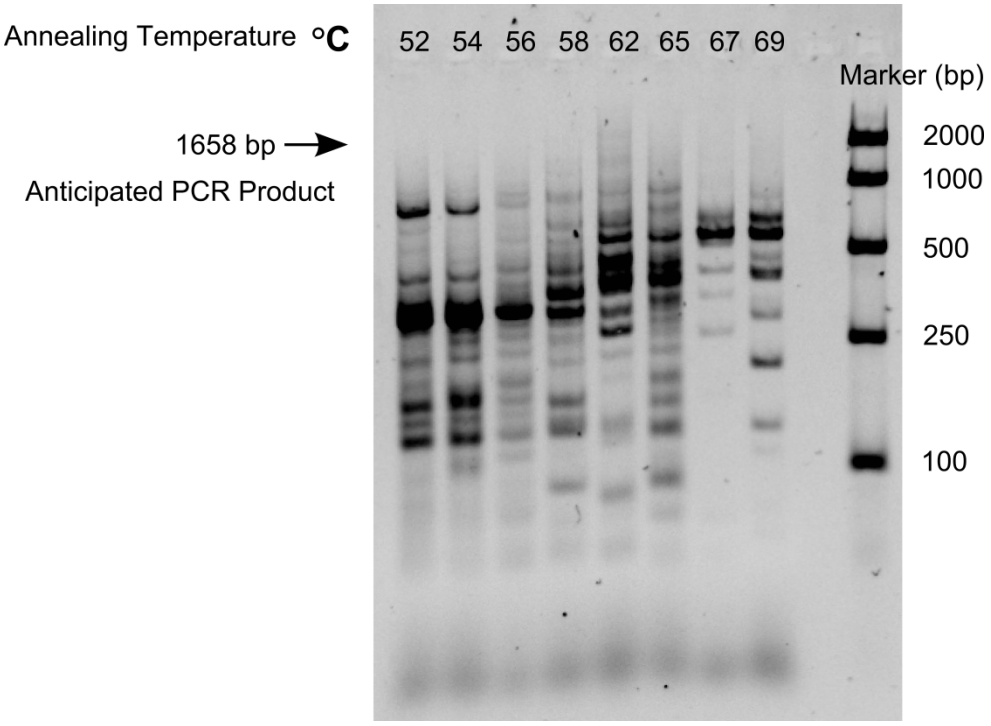


*Figure 3:2 Amplification Temperature Gradient*

Primers were designed to flank the p53 ORF in order to amplify the entire region of interest. Unfortunately, we were unable to amplify the entire region using this method – either because of the number of isoforms involved, or due to a high degree of secondary structure which impaired primer annealing [Figure 3:2].

To overcome this issue, the region was amplified in two overlapping sections of ~1000 bp each, and primers designed using transcript variant 1 for Homo Sapiens tumour protein p53 (TP53) mRNA (NCBI Reference Sequence: NM_000546.5) [Figure 3:3].

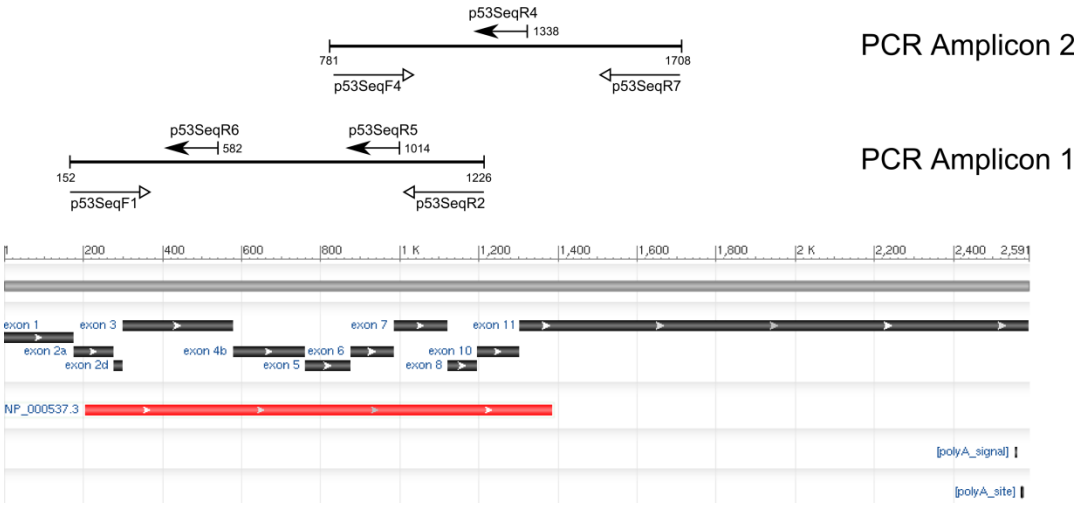


*Figure 3:3 Schematic for p53 primer walking*

Amplification scheme proposed for sequencing analysis of the p53 gene product in human keratinocytes. Diagrammatic representation of the TP53 gene and its transcribed mRNA product are shown for comparison.

Despite concerns about splice variants, a single band was obtained with these primer sets when amplified cDNA from NHEK and HaCaT cells was analysed via agarose gel electrophoresis [Figure 3:4]. Following purification of the amplified PCR product, ~500 bp regions of Amplicon 1 or 2 were sequenced by the Australian Cancer Research Foundation (AGRF) facility at the University of Queensland according to the primer schematic in Figure 3 [Table 3:1].

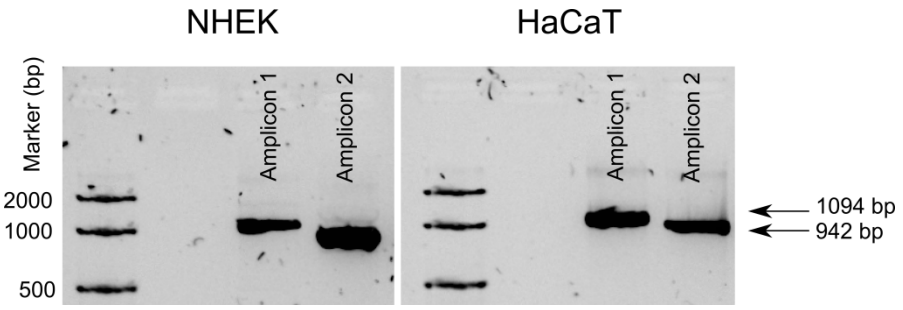


*Figure 3:4 p53 PCR Template for Sequencing*

P53 cDNA prepared from primary neonatal (NHEK) and p53-mutated (HaCaT) keratinocytes was amplified in two overlapping sections (PCR Amplicons 1 and 2). PCR product was purified for sequencing using a QIAquick PCR Purification Kit, and separated by agarose gel electrophoresis. Single bands obtained by PCR amplification were stained with SYBR Safe DNA stain (Molecular Probes, Eugene, OR) and visualised with a LAS-3000 Luminescent Image Analyser (Fujifilm, JPN).

*Table 3:1 Primers for p53 Sequencing*

| ID | Strand | Amplicon | Sequence | Site |
|---|---|---|---|---|
| P53SeqF1 | Forward | 1 | GGTGACACGCTTCCCTGGAT | 152..171 |
| P53SeqR2 | Reverse | 1 | AAGGCCTCATTCAGCTCTCG | 1226..1245 |
| P53SeqF4 | Forward | 2 | GCCCCTCCTCAGCATCTTAT | 781..802 |
| P53SeqR4 | Reverse | 2 | CGGGAGGTAGACTGACCCTT | 1338..1319 |
| P53SeqR5 | Reverse | 1 | TCAAAGCTGTTCCGTCCCAG | 1014..995 |
| P53SeqR6 | Reverse | 1 | TTGTTGAGGGCAGGGGAGT | 601..582 |
| P53SeqR7 | Reverse | 2 | GAAGTGGGCCCCTACCTAGA | 1708..1689 |

The ABI traces obtained from this facility were analysed using CLC Main Workbench software (CLC Bio Version 6.7.1). Inspection of the trace data demonstrated difficulties associated with direct sequencing of heterozygous mutations are not rapidly revealed by standard sequencing techniques, and must be discovered manually (446). Alternative sequencing methods (such as pyrosequencing) are recommended for high-throughput screening of multiple samples (447). Additionally, if the mutation is known, specific wild-type and mutant–targeting primers can be used to yield traces for each allele, however whilst this technique has been successfully used to differentiate p53 mutations in the HaCaT cell line

(440) [Figure 3:5], it has poor practical applications due to the highly variable nature of p53 mutations in a clinical setting.

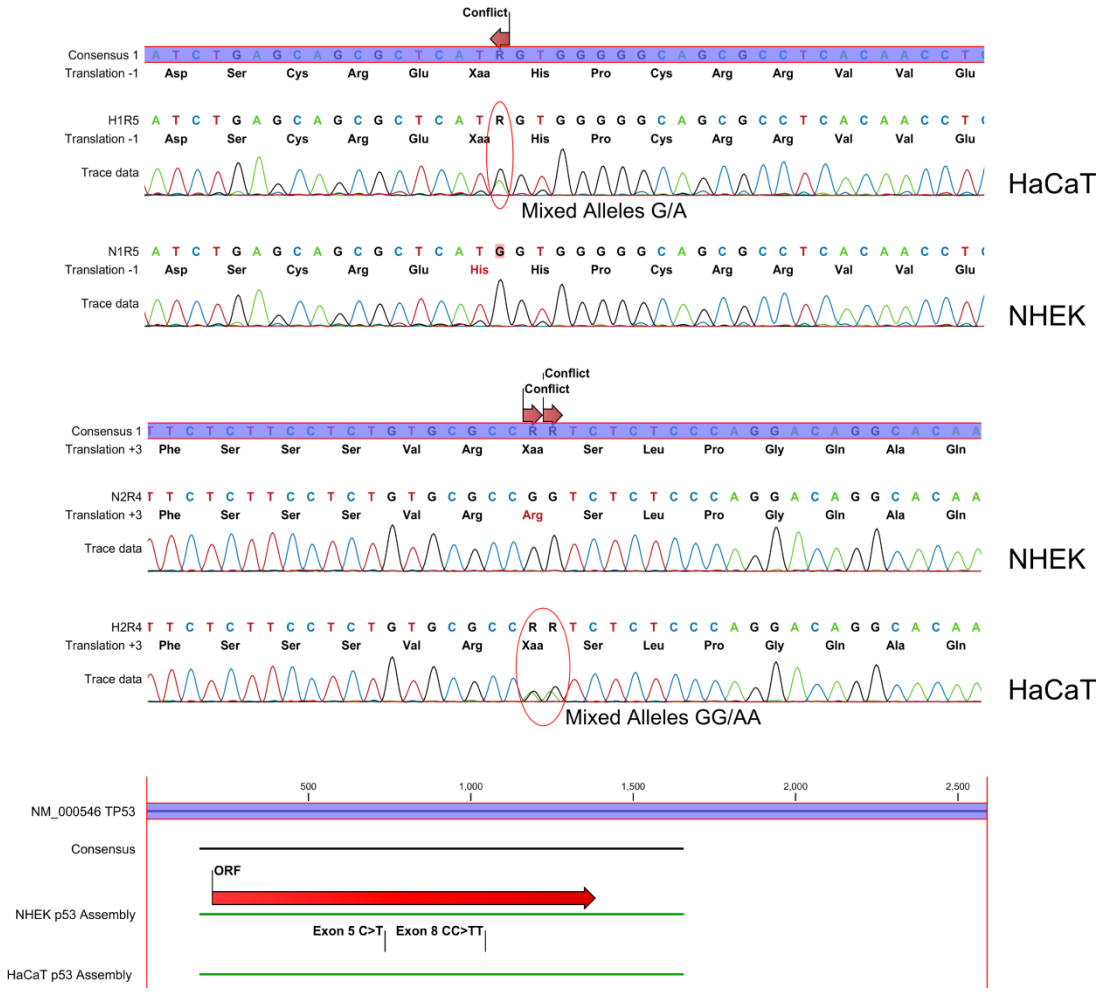


*Figure 3:5 Identification of mixed alleles from sequencing traces derived from p53 cDNA*

PCR product obtained from amplicons 1 & 2 were purified using a QIAquick PCR Purification Kit, and 60 ng of this template + 10 pmol primer oligonucleotides in 12 µl total volume were assayed by Sanger sequencing using a 3730xl DNA Analyser (Applied Biosystems). Regions of the HaCaT sequence displaying mixed bases on each allele are circled. Note – base data shown represents the cDNA complementary sequence. NHEK and HaCaT sequencing data was aligned with the NCBI TP53 gene sequence using CLC Main Workbench software (CLC Bio Version 6.7.1).

Analysis showed a single C > T and double CC > TT mutations at bases 600 and 1000 relative to the reference p53 sequence [NM_000546.5; Figure 3:5]. These findings correlate with the aforementioned mutations at exon 5 (H179Y) and exon 8 (R282W) (430), and confirmed the mutational status of p53 in our cell line has

remained consistent. Additionally, the NHEK cell strain did not display any mutations to its p53 sequence when analysed in comparison to NCBI-registered human p53 sequences, confirming that its p53 gene has 'wild-type' status. These results allowed us to be confident that the assumptions we made with regards to p53 status in both HaCaT and NHEKs which informed our experimental model were sound.

Next, growth conditions for *in vitro* culture were standardised to ensure any phenotypic features and physiological responses measured during investigations were unique to the cultured cells used in the study and not environmentally imposed by the composition of the culture medium.

### *Growth and morphology of HaCaT keratinocytes is dependent on growth medium*

Numerous investigations have shown that the primary trigger for differentiation of cultured keratinocytes is proximity during growth (448). To retain the replicative potential of primary keratinocytes, cells need to be maintained at a subconfluent density. In order to promote de-differentiation of HaCaTs in RPMI-1640 with 5% FBS, cells were seeded in 75T flasks at a density of $2.5 \times 10^4$ cells per $cm^2$ and flasks were passaged before 75% confluence was reached. Following adaptation, these cells were weaned to the defined keratinocyte medium (EpiLife supplemented with Human Keratinocyte Growth Supplement) containing 60 µM calcium for experiments. Epilife is a proprietary solution from Cascade Biologics. Although the exact concentration of its components is unavailable to consumers, it has been developed from MCDB 153 by modifying Ham's nutrient mixture F12 for growth of keratinocytes in culture (424, 449). Therefore the composition of MCDB 153 basal medium has been included for comparison with DMEM F12 and RPMI 1640 (Gibco Invitrogen) [Table 3:2].

*Table 3:2 Composition of Keratinocyte Culture Medium*

| | | DMEM-F12 | RPMI 1640 | MCDB 153 |
|---|---|---|---|---|
| Inorganic Salts | CaCl2 | 1.05 | | 0.06 |
| | Ca(NO3)2 • 4H2O | | 0.424 | |
| | CuSO4 • 5H2O | 0.0000052 | | 0.0000108 |
| | Fe(NO3)3 • 9H2O | 0.000124 | | |
| | FeSO4 • 7H2O | 0.0015 | | 0.005 |
| | MgCl2 | 0.301 | | 0.6014 |
| | MgSO4 | 0.407 | 0.407 | 0.00000125 |
| | Ammonium Metavanadate | | | 0.00000496 |
| | Molybdic Acid • 4H2O (ammonium) | | | 0.000001003 |
| | Nickel Chloride • 6H2O | | | 0.000000505 |
| | KCl | 4.16 | 5.33 | 1.49 |
| | NaHCO3 | 29.02 | 23.81 | |
| | NaCl | 120.68 | 103.45 | 131.02 |
| | Na2HPO4 | 0.5 | 5.63 | 2.00062 |
| | NaH2PO4 | 0.453 | | |
| | Sodium Metasilicate • 9H2O | | | 0.0004996 |
| | Sodium Acetate (anhydrous) | | | 3.6772 |
| | Sodium Selenite | | | 0.000022 |
| | Stannous Chloride • 2H2O | | | 5.008E-07 |
| | ZnSO4 • 7H2O | 0.0015 | | 0.0005 |
| Amino Acids | L-Alanine | 0.05 | | 0.1 |
| | L-Arginine • HCl | 0.699 | 1.15 | 0.9986 |
| | L-Asparagine • H2O | 0.05 | 0.379 | 0.1 |
| | L-Aspartic Acid | 0.05 | 0.15 | 0.03 |
| | L-Cystine • 2HCl | 0.1 | 0.208 | |
| | L-Cysteine • HCl • H2O | 0.0998 | | 0.2389 |
| | L-Glutamic Acid | 0.05 | 0.136 | 0.1 |
| | L-Alanyl-L-Glutamine (GlutaMax) | 2.5 | 2.06 | 4.042 |
| | Glycine | 0.25 | 0.133 | 0.1 |
| | L-Histidine • HCl • H2O | 0.15 | 0.0968 | 0.07986 |
| | L-Isoleucine | 0.416 | 0.382 | 0.015 |
| | L-Leucine | 0.451 | 0.382 | 0.5 |
| | L-Lysine • HCl | 0.499 | 0.219 | 0.0998 |
| | L-Methionine | 0.116 | 0.101 | 0.03 |
| | L-Phenylalanine | 0.215 | 0.0909 | 0.03 |
| | L-Proline | 0.15 | 0.174 | 0.3 |
| | L-Hydroxyproline | | 0.153 | |
| | L-Serine | 0.25 | 0.286 | 0.6 |
| | L-Threonine | 0.449 | 0.168 | 0.1 |
| | L-Tryptophan | 0.0442 | 0.0245 | 0.015 |
| | L-Tyrosine • 2Na • 2H2O | 0.214 | 0.11 | 0.013 |
| | L-Valine | 0.452 | 0.171 | 0.3 |
| Vitamins | D-Biotin | 0.0000143 | 0.00082 | 0.00005984 |
| | Choline Chloride | 0.0641 | 0.0214 | 0.0997 |
| | Folic Acid | 0.00601 | 0.00227 | 0.00179 |
| | myo-Inositol | 0.07 | 0.194 | 0.1 |
| | Niacinamide | 0.0166 | 0.0082 | 0.0003 |
| | D-Pantothenic Acid • ½Ca | 0.0047 | 0.000524 | 0.000499 |
| | Pyridoxal • HCl | | 0.0073 | |
| | Pyridoxine • HCl | 0.00986 | 0.00485 | 0.0002995 |
| | Riboflavin | 0.000582 | 0.000532 | 0.0001 |
| | Thiamine • HCl | 0.00644 | 0.00297 | 0.001 |
| | Vitamin B12 | 0.000502 | 0.0000037 | 0.0003 |
| | Adenine • HCl | | | 0.18 |
| Other | D-Glucose | 17.51 | 11.11 | 6 |
| | Lipoic Acid | 0.00051 | | 0.001 |
| | Hypoxanthine | 0.015 | | |
| | Linolenic Acid | 0.00015 | | |
| | Phenol Red • Na | 0.0215 | 0.0133 | 0.0033 |
| | Putrescine • HCl | 0.000503 | | 0.001 |
| | Pyruvic Acid • Na | 0.5 | | 0.5 |
| | Thymidine | 0.00151 | | 0.003 |
| | Glutathione | | 0.00326 | |

Exposure to a high calcium environment (>1 mM) promotes differentiation in primary keratinocytes (424, 450), however calcium is thought to have a permissive, rather than an initiating role in the differentiation process (451). Nonetheless, calcium concentration is a well-documented modulator of keratinocyte morphology. To adapt HaCaT keratinocytes previously cultured in DMEM, cells were grown in RPMI-1640 (0.424 mM calcium) for 4-5 weeks. During this time frame, FBS was maintained at 5% to ensure that any changes measured were specific to the altered calcium concentration.

After 10 days (2 passages) in RPMI-1640 + 5% FBS, decreased replication and increased detachment of senescent cells was observed. Calcium concentration is not considered limiting for keratinocyte growth (450), however when compared to normal keratinocytes, HaCaTs demonstrate an increase in proliferation and fraction of S and G2/M cells with higher calcium concentrations (452). Thus culture in RPMI-1640 + 5% FBS provides a selective pressure for survival of HaCaT clonal lines with a less differentiated phenotype as a consequence of the change in micronutrient concentration due to sloughing of differentiated squames into the growth medium.

### *HaCaT Keratinocytes are de-differentiated by culture in low calcium media*

HaCaTs cultured in DMEM/F12 display intracellular features of the granular and cornified epidermal layers, and these features are no longer evident after adaptation to EpiLife. When the HaCaT cell line is grown in DMEM-F12 + 5% FBS, cells display morphological features consistent with differentiated keratinocytes [cell-cell adhesion, stratification, flattening and spreading] [Figure 3:6]. Intermediate filaments and desmosomal junctions are features of suprabasal keratinocytes in the spinous layer. Keratohyaline granules predominantly form in the granular layer and contain profilaggrin, keratins 1, 2 & 10 and transglutaminase 3. The cornified envelope develops in the outer stratum corneum from loricrin, involucrin, trichohyalin, S100 proteins and small proline-rich proteins (453).

Interestingly, primary keratinocytes cultured from human foreskins also form a cornified envelope, and produce filaggrin-containing keratinohyaline granules when cultured in DMEM (454, 455). Involucrin is synthesised as a soluble precursor of the cornified envelope in the suprabasal epidermis. The cornified envelope is formed by transglutaminase-catalysed ε-γ-glutamyl-lysine bonding between involucrin and plasma membrane-bound proteins (456). Transglutaminase activity is calcium-dependent (457, 458); hence construction of a cornified envelope by keratinocytes grown in low calcium medium is limited.

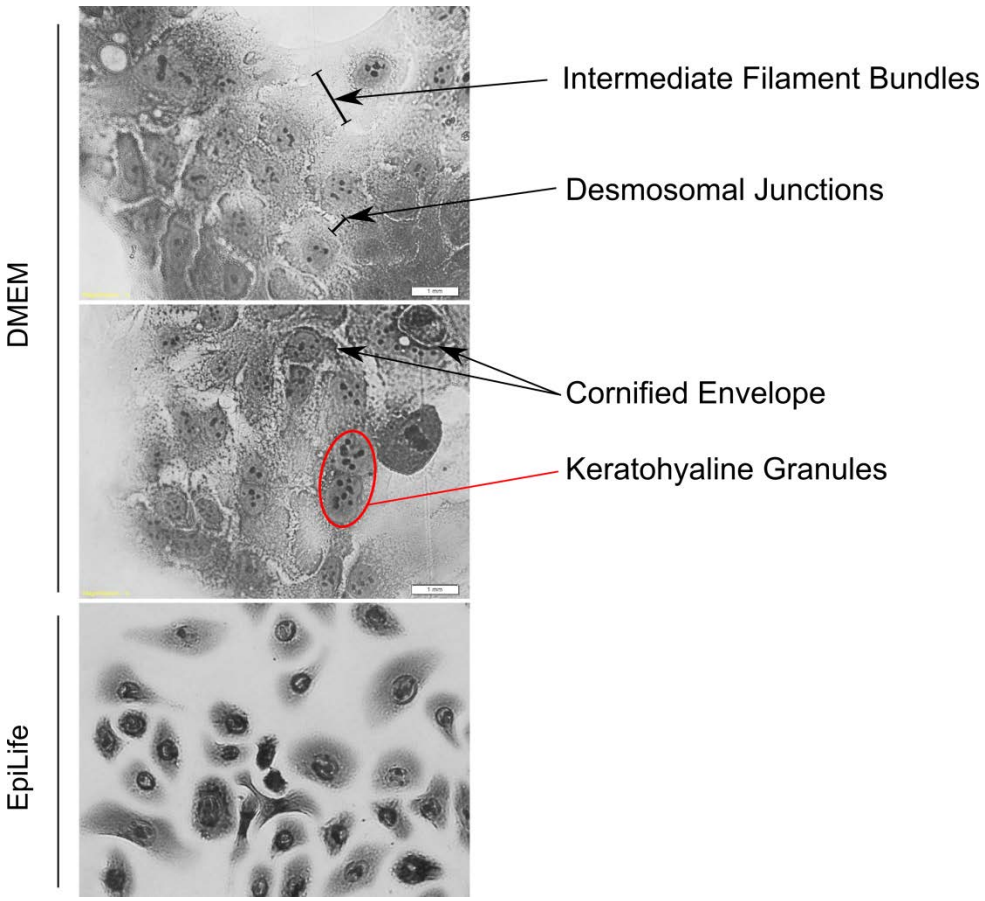


*Figure 3:6 Ultrastructure of HaCaT keratinocytes changes following adaptation*

HaCaT keratinocytes cultured in DMEM-F12 and 5% FBS or EpiLife with HKGS were seeded at a density of $5 \times 10^5$ cells per well in 6 well tissue culture plates and allowed to recover overnight. Microphotographs were prepared after staining with 0.05 % crystal violet in PBS.

Whilst HaCaT cells grown in DMEM-F12 produce colony-like clusters in culture [Figure 3:7(**a** & **d**], when this cell line is cultured in EpiLife [Figure 3:7 (**b** & **e**)], the growth pattern correlates more closely with NHEKs [Figure 3:7(**c** & **f**)].

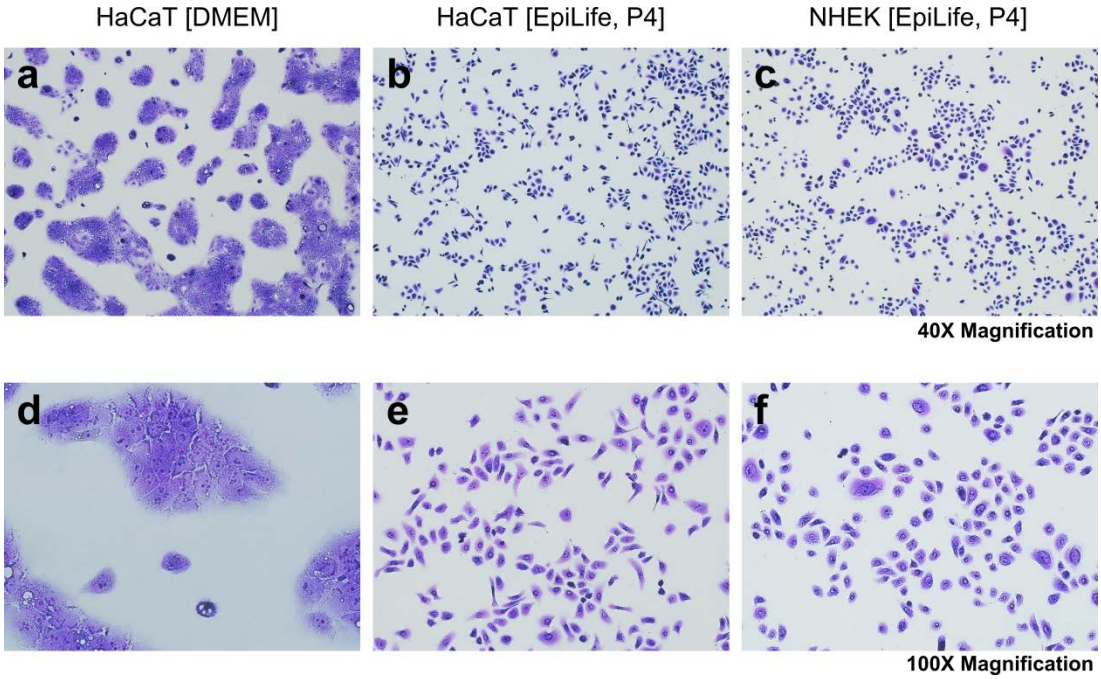


*Figure 3:7 Gross morphology of keratinocytes cultured in DMEM-F12 or EpiLife culture media*

Primary neonatal (NHEK) and HaCaT keratinocytes were seeded at a density of $5 \times 10^5$ cells per well in 6 well tissue culture plates and allowed to recover overnight. Microphotographs of keratinocytes were prepared after staining with 0.05 % crystal violet in PBS. Growth characteristics of (**a, d**) HaCaT keratinocytes cultured in DMEM-F12/ 5% FBS; (**b, e**) HaCaTs and (**c, f**) NHEKs seeded at identical density when cultured in EpiLife culture medium

As shown above, culture in EpiLife enables HaCaT keratinocytes to adopt growth characteristics and a morphology which more closely approximates the primary cell strain. To confirm that the observed morphological changes were related to de-differentiation of the HaCaT cell line, expression of representative differentiation markers was measured during adaptation to low calcium conditions.

As keratinocytes emerge from their stem cell precursors, they enter into a differentiation program as they migrate from the basal layer to the outer epidermal

layers. During this process, keratinocytes undergo numerous structural changes initiated by synthesis of differentiation-dependent marker proteins. Well established keratin markers for differentiation include keratins 5 and 14 in the basal layer, and keratins 1, 10, 6 and 16 in suprabasal layers of the epidermis. Loricrin and involucrin are expressed in the spinous layer, followed by filaggrin and transglutaminase in the granular layer (456). During terminal differentiation, the ~400 kDa profilaggrin polyprotein is dephosphorylated and rapidly cleaved by serine proteases to form monomeric filaggrin (37 kDa), which binds to and condenses the keratin cytoskeleton and thereby contributes to the cell compaction process that occurs during formation of the epidermal cornified layer (453).

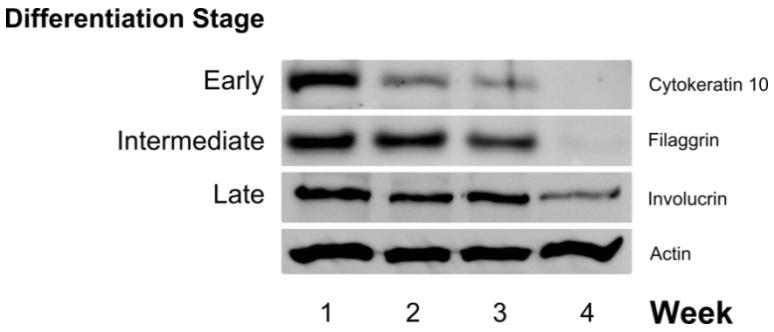


*Figure 3:8 De- differentiation of HaCaT keratinocytes in low calcium conditions*

TP53-mutated (HaCaT) keratinocytes were cultured for 30 days (4 weeks) in low-calcium, RPMI medium. Cell extracts were prepared weekly and differentiation marker proteins were detected by immunoblotting. Actin indicates protein loading.

In this investigation, cytokeratin 10 was used as a marker for early stage, filaggrin for intermediate stage, and involucrin for late stage differentiation. HaCaTs underwent a duration-dependent shift in involucrin, cytokeratin 10 and filaggrin expression during the initial 30 days of growth in low calcium conditions. After 4 weeks of adaptation, involucrin expression decreased by 30%, filaggrin expression decreased 10-fold and cytokeratin 10 was halved [Figure 3:8].

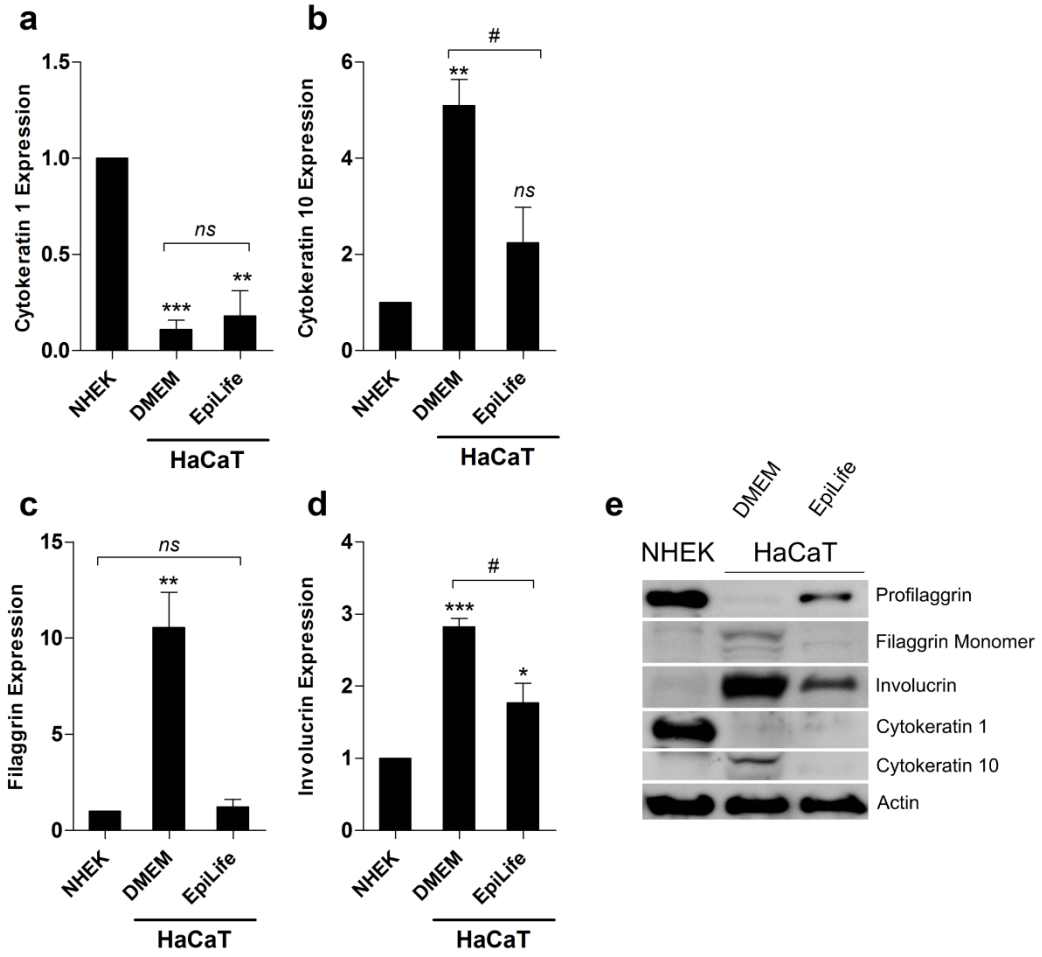


*Figure 3:9 Effect of growth medium on differentiation marker expression in keratinocytes*

Protein was extracted from untreated subconfluent HaCaT keratinocytes cultured in DMEM-F12 or EpiLife and used to compare differentiation marker expression with normal keratinocytes. Cytokeratin 1 (**a**), cytokeratin 10 (**b**), filaggrin (**c**), and involucrin (**d**) expression in HaCaT keratinocytes grown in DMEM-F12 or EpiLife was quantitated relative to expression in NHEKs. (**e**): Representative immunoblots of lysates from keratinocyte cells in their basal (unstimulated) state are shown for reference. Values represent mean expression relative to NHEKs from 3 independent experiments (± SD) and significant differences are represented as *, ** and ***; with $p < 0.05$, $p < 0.01$ and $p < 0.001$ respectively. Differences in expression between HaCaTs in DMEM-F12 and EpiLife were analysed by 1-way ANOVA with Bonferroni post-test and are indicated as # ($p < 0.05$).

A quantitative analysis of filaggrin, involucrin and cytokeratin expression was performed to compare the effect of growth medium on differentiation markers. HaCaTs grown in DMEM have 4-fold lower cytokeratin 1 [Figure 3:9(**a**)], 4.5-fold

greater expression of cytokeratin 10 [Figure 3:9(**b**)], 10-fold higher filaggrin [Figure 3:9(**c**)] and 3-fold higher involucrin [Figure 3:9(**d**)] when compared to normal keratinocytes grown in EpiLife.

Conversely, after adaptation to EpiLife, cytokeratin 10 and filaggrin expression in HaCaTs decreased to a level comparable to NHEKs [Figure 3:10 (**b**, **c**, **e**)]. Cytokeratin 1 expression was not altered in adapted HaCaTs [Figure 3:10 (**a**, **e**)], and although involucrin was still expressed in these cells, a significant reduction was observed [Figure 3:10 (**d**, **e**)]. This analysis demonstrates that adaptation to EpiLife has restored expression of filaggrin and cytokeratin 10 in HaCaT keratinocytes to a level comparable with primary keratinocytes. Although expression of involucrin in post-adapted HaCaTs remained higher than NHEKs, it was significantly reduced when compared to pre-adapted HaCaTs.

Although the NHEK samples in this study produced strong cytokeratin 1 and profilaggrin expression, the cells used for immunoblotting were harvested at a high confluence. NHEKs used in future experiments were used at lower seeding density, restoring cytokeratin 1 and profilaggrin expression in NHEK cells to a level which was analogous to post-adapted HaCaTs. Overall, differentiation marker expression demonstrates that growth of HaCaT keratinocytes in low calcium, serum free conditions allows the cell line to adopt a phenotype that correlates more closely with primary keratinocytes.

HaCaT keratinocytes cultured in defined medium undergo calcium-dependent changes in differentiation marker expression, although unlike normal keratinocytes, they retain their proliferative properties (452). HaCaT is a spontaneously immortalised cell line which is commonly used for *in vitro* studies due to its ease of growth in culture. However many investigators culture HaCaT keratinocytes in high calcium conditions and also supplement with bovine serum. The potential to influence the HaCaT phenotype by culture medium conditions is particularly important to studies which utilise the HaCaT cell line for preclinical investigations,

as treatment-based outcomes are dependent on the gene expression profile of the cell line used.

Consequently, HaCaT keratinocytes used in this study were cultured in reduced calcium, serum-free media to allow for more accurate comparisons to be made with primary keratinocytes during experimentation. The following results describe differences in the target gene expression profile of unstimulated primary cultured keratinocytes (NHEK) and the HaCaT cell line following adaptation to EpiLife.

*p53 is overexpressed in HaCaT keratinocytes*

As a transcription factor, p53 operates by binding to a canonical response element proximal to the transcriptional start site of target genes. This consensus sequence contains two tandem repeats of the RRRCWWGYYY motif separated by a 0-13 bp spacer region (R=purines; W=adenine/thymine; Y=pyrimidines) (40). In normal cells, wild-type p53 is synthesised in the cytoplasm, then assembled into dimers which are transported in the nucleus and assembled into tetramers at DNA binding sites for transcription. p53 binds to DNA in its tetrameric form (40, 414). Mutations to the C-terminal domain interfere with tetramerisation and alter the conformation of the nuclear export signal (71). This inhibits nucleocytoplasmic shuttling and reduces transcriptional activation (459). However, the majority of cancer–associated p53 mutations are found in the core domain and predominantly impair DNA binding affinity and/or protein conformation and stability (69).

p53 mutations cause genetic instability and polyploidy by 3 distinct mechanisms: Firstly, through loss of its tumour suppressor function; secondly by competitive inhibition of wild-type p53 targets; and thirdly through impaired cell cycle checkpoint control and inhibition of DNA repair pathways (78). These properties are exacerbated in cells with heterozygous p53 mutations (such as the HaCaT cell line). P53 haplo-insufficiency drives cancer formation in Li Fraumeni syndrome, and has a stronger effect on p53-mediated transrepression (in genes such as survivin) than

complete gene inactivation (73). When both mutant and wild-type p53 proteins accumulate at high concentration, inactive heterotetramers are formed that inhibit the formation of functional wild-type tetramers (42, 80, 81).

This attenuation of the tumour-suppressive property of p53 in the hemizygous phenotype increases tumorigenicity and metastatic potential, and contributes to chemotherapeutic resistance and poor treatment outcomes for patients (80).

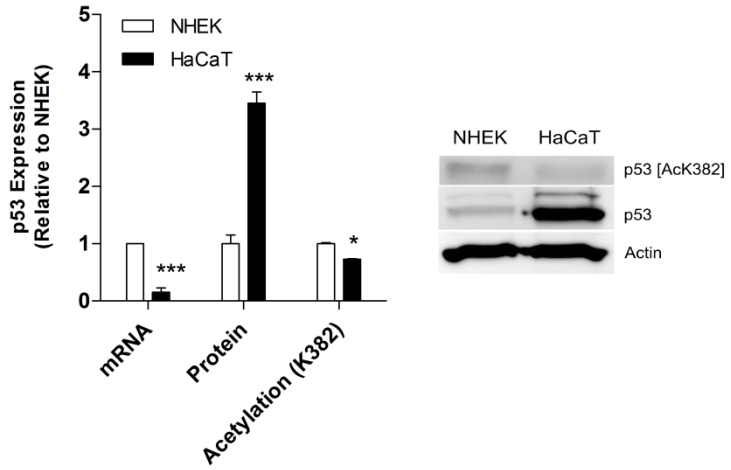


*Figure 3:10 Basal p53 Expression and Acetylation Profile*

Protein and total RNA was extracted from untreated subconfluent primary human (NHEK) and p53-mutated (HaCaT) keratinocytes. Expression of p53 mRNA was determined by qRT-PCR, acetylation and expression of total p53 protein was assayed by immunoblotting. All results are expressed relative to NHEK, and are expressed as mean ± SD, with $p<0.05$ (*); $p<0.001$ (***), using paired student's T-test for statistical analysis.

Consistent with NMSC samples (460), HaCaTs have 15% lower p53 mRNA expression and have over 3 times the cellular p53 protein content when compared to normal keratinocytes, (Figure 3:10; $p<0.001$). However although p53 is overexpressed in this cell line, acetylation of its active site residues is suppressed (Figure 3:10; $p<0.05$).

In addition to canonical functions of the p53/response element interaction, p53 functions as a transcriptional repressor at non-canonical DNA binding sequences.

Genes with a repressive p53 response element typically have alterations to the decamer motif (45), and p53-mediated transcriptional repression appears to regulate genes which are anti-apoptotic, regulate cell cycle checkpoint control and differentiation or senescence (44).

BCL-2 and Survivin are key proteins involved in cell death and survival signalling. Both are negatively regulated by wild-type p53 (461, 462), and are overexpressed in skin cancer (463, 464). When compared with NHEKs, expression of survival markers BCL-2 and BIRC5/Survivin in untreated HaCaTs is approximately 10-fold higher (Figure 3:11; $p<0.001$).

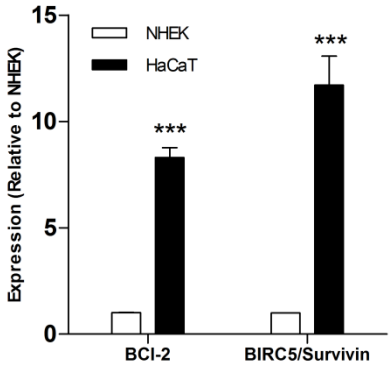


*Figure 3:11 Overexpression of survival markers in p53-mutated keratinocytes*

BCL-2 and BIRC5/Survivin mRNA expression in primary (NHEK) and p53-mutated (HaCaT) keratinocytes was determined by Taqman qRT-PCR. All results are expressed relative to NHEK, and are expressed as mean ± SD, with $p<0.001$ (***), using paired student's T-test for statistical analysis.

In conjunction with unlimited replicative potential in HaCaTs (398), overexpression of BCL-2 and Survivin contributes to the enhanced survival characteristics demonstrated by this cell line in culture.

## 3.4 DISCUSSION

The intention of this chapter has been to describe the process utilised to prepare, identify and characterise the phenotypic properties of the p53-mutated HaCaT keratinocyte cell line. In order to generate a model with p53 mutational status as its primary variable, HaCaT cells were adapted to growth in identical culture conditions as the keratinocytes used as a wild-type control, and the ORF of p53 isoform 1 was sequenced. To test the assumption that HaCaT mutations alter p53 expression and the transcriptional activity, p53 mRNA and protein expression were measured, and acetylation of p53 of lysine residue 382 was analysed in HaCaT and NHEK cells. Additionally, expression of BCL-2 and Survivin in NHEKs and HaCaTs was compared to assess the impact of p53 mutations on p53-DNA binding for p53 transcriptional repression targets. This chapter demonstrates some of the p53-specific phenotypic alterations in the HaCaT cell line which contribute to its precarcinogenic properties.

Use of *in vitro* systems to analyse and model cellular responses is standard practice in the fields of toxicology and clinical therapeutics. Findings from these studies shape our understanding of disease processes and inform animal studies and human clinical trials. Culture media is a critical mediator of keratinocyte phenotype, and therefore choice of growth conditions and the potential to influence cellular responses should be considered prior to conducting any *in vitro* investigation which utilises keratinocyte cell lines. Our investigations demonstrate that HaCaT keratinocytes can be successfully adapted to low calcium, serum-free growth environment following extended culture in high calcium and serum. When grown in these conditions, differentiation marker expression and morphology of HaCaTs shifts to approximate the profile measured in normal keratinocytes.

Mutations affecting the p53 gene of the HaCaT cell line were identified, and the location of these mutations in exons 5 and 8 confirmed by sequencing. An accumulation of p53 protein without a concomitant up-regulation of p53 mRNA in this cell line indicates that post-translational control of p53 expression is impaired.

Additionally, p53 acetylation is suppressed and p53-regulated anti-apoptotic markers BCL-2 and Survivin are overexpressed in HaCaTs, providing evidence of aberrant regulation of p53-mediated activation and DNA binding in this cell line. Of the HaCaT mutations, the H179Y mutation affects its zinc binding ligand, altering transactivation of p53; and both R281W and R282W mutations affect the major groove DNA binding domain (465).

HaCaT is a human keratinocyte cell line which is extensively used as an *in vitro* model to investigate keratinocyte cell physiology. Although this cell line was derived from a physiologically normal human skin source, both p53 alleles bear mutations and have undergone further cytogenetic changes after escaping replicative senescence. Additionally, cell lines which have adapted to survive in *in vitro* cell culture conditions develop properties which are phenotypically different from cells *in vivo*, and after >70 population doublings, the HaCaT cell line is no exception. Our model system was designed to minimise exogenous influences on growth and survival in culture so that the endogenous influence of p53 mutations on keratinocyte phenotype could be measured without the confounding effects presented by media composition.

In this chapter, the hypothetical framework for future experiments was defined by characterising the effect of p53 mutations in HaCaT keratinocytes on the p53 expression profile. Here we have determined that the HaCaT cell line has genotypic and phenotypic features which are consistent with precarcinogenic changes observed during the earliest stages of skin cancer initiation. Additionally, by standardising culture conditions for the growth of keratinocyte cell lines, media-dependent effects are minimised, and this enables our conclusions to be based on genotypic features of the keratinocytes used in experiment.

# Chapter 4 -
# SIRT1 Modulates MicroRNA Processing Defects in p53-Mutated Human Keratinocytes

## 4.1 ABSTRACT

Together with p53, the NAD-dependent lysine deacetylase SIRT1 and the microRNA miR-34a form a feedback loop which self-regulates SIRT1 expression and modulates p53-dependent responses. In addition to its well-described role in mediating transcriptional responses to genotoxic stress, p53 may also regulate microRNA processing and maturation. RNAi, miRNA target site blocking oligonucleotides and small molecule inhibitors were used to explore the functional relationship between p53, SIRT1 and miR-34a, and the influence of p53 and SIRT1 on microRNA biogenesis and maturation in primary (NHEK) and p53-mutated (HaCaT) keratinocyte cells.

Mature miR-34a decreased in p53-suppressed NHEK cells, whereas ablation of SIRT1 reduced the primary transcript (pri-miR-34a). When either SIRT1 expression or activity was inhibited in combination with p53 ablation, pri-miR-34a levels increased and mature miR-34a levels decreased. Under these same conditions, additional p53-regulated microRNAs (miRs 16-1/15, 145 and 107) also failed to mature. In HaCaT cells, primary microRNA transcripts for miR-16-1/15, miR-145 miR200c/141 and miRNA-107, but not miR-34a, were approximately 8-fold higher than in NHEK cells. However, the levels of mature microRNA sequences in HaCaT cells were only 1.5-2 fold higher (miR-16-1, miR-145), unchanged (miR-107) or decreased (miR-200c/141, miR-34a) compared to NHEK cells.

These results demonstrate that characteristic UV-induced TP53 mutations interfere with efficient microRNA biogenesis. Furthermore, SIRT1 functions in combination with p53 to establish microRNA expression patterns in human keratinocytes.

Much of the work in this chapter forms the basis of a manuscript published in the Journal of Dermatological Science:

SIRT1 Modulates MicroRNA Processing Defects in p53-Mutated Human Keratinocytes, 2014, *J Dermatol Sci*, **74**:142-9 http://dx.doi.org/10.1016/j.jdermsci.2014.01.008 (466).

## 4.2 INTRODUCTION

The transcription factor p53 has multiple tumour suppressor functions in the cell, including regulation of cell cycle progression, cell growth, DNA damage response and apoptotic signalling (467). Activation of p53 protein is influenced quantitatively and qualitatively by post-translational modifications which stabilise protein expression and facilitate DNA binding, and include phosphorylation, acetylation, methylation, ubiquitinylation, sumoylation and neddylation (48, 54). Acetylation of C-terminal lysine residues inhibits ubiquitin-mediated proteolysis, increases DNA binding affinity, and induces transcription of p53 regulatory targets (50-52). Post-translational modifications selectively affect p53-responsive promoter association and recruitment of transcriptional co-activators (43, 468-470), ultimately producing an analogue, rather than digital, transcriptional outcome in the cell. Mild p53 activation promotes cell cycle arrest and DNA repair (471), whereas increased induction of activated p53 triggers apoptotic signalling and cell death (54, 63, 472). Additionally, p53-mediated transcriptional repression influences stress responses by negative regulation of anti-apoptotic/pro-survival proteins. Impaired expression or functional activity of p53, therefore, drives carcinogenesis by interfering with endogenous p53-mediated responses to stress.

MicroRNAs are key regulators of downstream effectors of p53-dependent responses (473). As such, microRNAs maintain the functional integrity of the genome and acts as a tumour suppressor during exposure to carcinogenic stressors (149). Consequently, the widespread nature of p53 mutations in cancer has hinted at a relationship between p53 activity and microRNA biogenesis which precipitates and reinforces many of the changes to cellular biochemistry during carcinogenesis (149). During microRNA biogenesis, primary nuclear transcripts (pri-miRNAs) are processed into 70-nucleotide precursor sequences (pre-miRNAs) for cytoplasmic translocation and cleavage into ~22-nucleotide fragments (mature miRNAs) prior to incorporation into RNA-induced silencing complexes. This process is facilitated by two RNaseIII enzymes – nuclear Drosha and cytosolic DICER, as well as the RNaseIII-

associated proteins Di George syndrome critical region 8 (DGCR8) and the DEAD box RNA helicases p68 and p72 (474). p53 is found to be mutated in almost every cancer type, including those affecting the skin (415, 475).

The miR-34 family of miRNAs has recently emerged as an important regulatory component of p53-mediated signalling (476, 477), targeting substrates involved in cell cycle regulation and apoptosis (478). In particular miR-34a, whose expression is induced by p53-mediated transcriptional activation (149), regulates SIRT1 expression by base pairing with its 3'UTR (479). SIRT1, in turn, inhibits p53 activation through regulation of its acetylation status (201, 202). In this manner, SIRT1, p53 and miR-34a form a coherent feed-forward loop, referred to here as the p53/SIRT1/miR-34a axis, which influences cellular differentiation, senescence and apoptotic signalling (480-483).

Here, p53 expression and activity were manipulated to investigate the relationship between the p53/SIRT1/miR-34a axis and miRNA biogenesis in normal (NHEK) and p53-mutated (HaCaT) human epidermal keratinocytes. Expression of primary and mature miRNA targets was measured in a set of p53-regulated miRNAs to determine how p53 and SIRT1 contribute to miRNA maturation.

## 4.3 RESULTS

### *p53 and SIRT1 co-regulate miR-34a expression in human keratinocytes*

RNA interference (RNAi) was used to determine the relationship between SIRT1, p53 and miR-34a in normal (NHEK) keratinocytes. p53 is minimally expressed in normally growing keratinocytes (368) and has a half-life of < 12 minutes (484), thus siRNA-induced changes in unstressed keratinocytes were difficult to monitor and did not accurately represent knockdown efficiency in NHEKs. P53 is overexpressed in HaCaT keratinocytes however; so siRNA-induced ablation was easier to detect in this cell line. To confirm the efficacy of siRNA-induced p53 ablation during experiments, NHEKs were treated with a p53 expression inducer [camptothecin (CPT)]. P53 protein increased 6-fold in NHEKs after 24 hrs of CPT treatment, but not in p53-transfected cells [Figure 4:1].

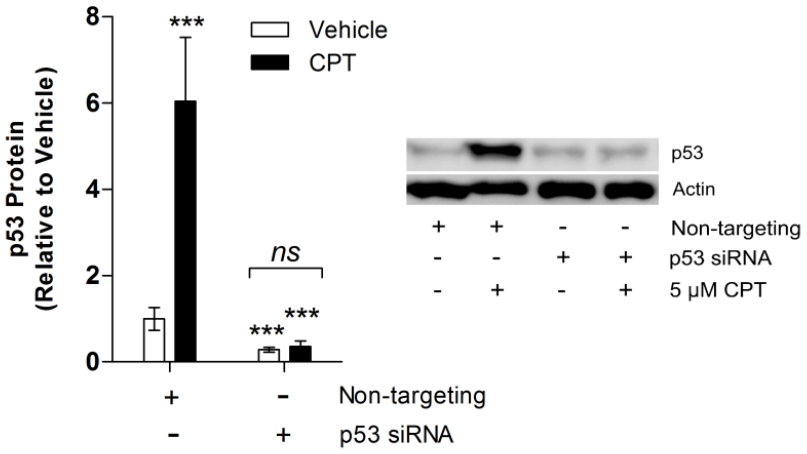


*Figure 4:1 Suppression of CPT-mediated p53 induction by RNAi in human keratinocytes*

Primary human keratinocytes (NHEKs) were transfected with a p53 siRNA targeting pool for 48 hours, and treated with 5 μM camptothecin (CPT, black bars) for 24 hrs. p53 expression was determined from extracted samples by qRT-PCR and immunoblotting. Actin was used as a loading control for immunoblotting, and RT-PCR results were normalised to 5S rRNA.

All data represent the mean ± SD of 3 independent experiments. Results significantly different from vehicle control (white bars) are represented as ***; $p < 0.001$ respectively.

Transfection of NHEK cells with p53-targeting siRNAs reduced p53 mRNA and protein expression by 45% [Figure 4:2(a-c); $p<0.001$] when compared to NHEKs transfected with non-targeting control siRNAs. Similarly, 48 hour transfection of NHEKs with SIRT1-targeting siRNAs reduced SIRT1 mRNA and protein by 60% when compared with the non-targeting siRNA pool [Figure 4:2 (c-e); $p<0.001$]. Using these p53- or SIRT1-specific targeting siRNA pools, we were able to selectively inhibit expression of either SIRT1 or p53 mRNA, with a slight reduction in SIRT1 protein generated by p53 knockdown [Figure 4:2 (e)].

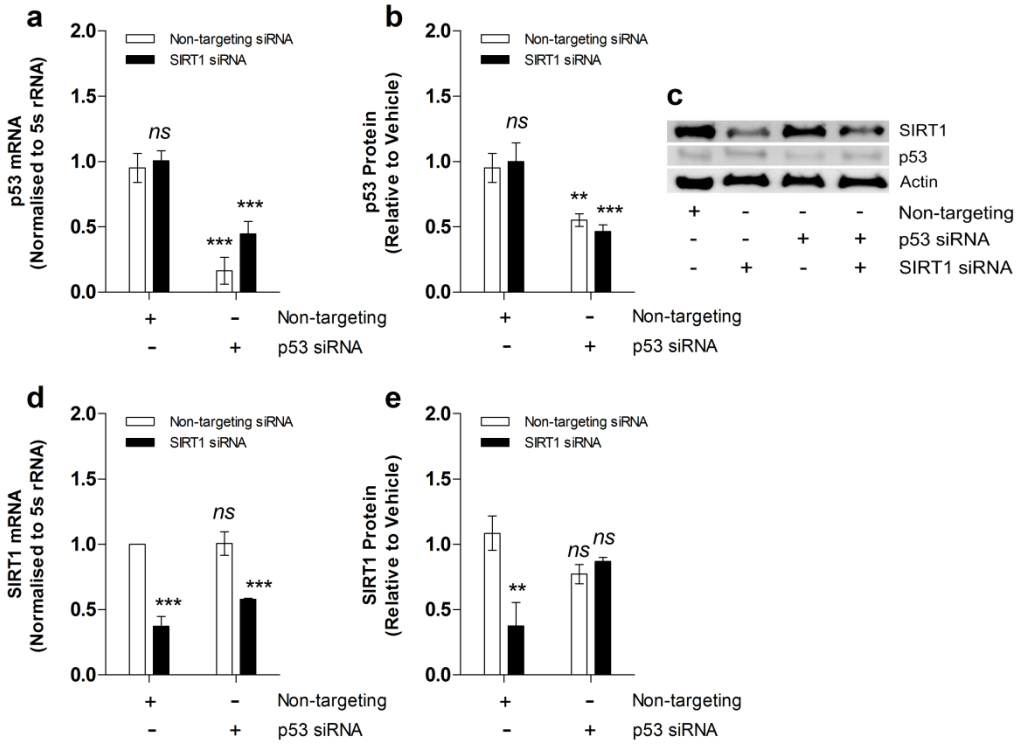


*Figure 4:2 Co-transfection of p53 and SIRT1 in human keratinocytes*

Primary human keratinocytes (NHEKs) were transfected with p53 (right Panel) and SIRT1 (black bars) siRNA targeting pools. Total RNA was extracted after 48 hrs and target genes assayed by RT-PCR. Results were normalised to 5S rRNA, and analysed relative to samples transfected with non-targeting control oligonucleotides (white bars).

All data represent the mean ± SD of 3 independent experiments and are represented as *, ** and ***; with $p < 0.05$, $p < 0.01$ and $p < 0.001$ respectively.

During combined p53/SIRT1 RNAi experiments, SIRT1 and p53 mRNA were both reduced in a manner comparable to p53 knockdown alone [Figure 4:2 (a & d)], although SIRT1 protein expression was not significantly suppressed by dual transfection [Figure 4:2 (c & e)].

In order to fully evaluate the influence of combined p53 and SIRT1 knockdown on the SIRT1-targeting microRNA, miR-34a, we specifically quantified abundance of both the primary transcript and its mature sequence after processing. Our results showed that p53 ablation alone did not significantly alter pri-miR-34a [Figure 4:3 (a)], but halved expression of its mature sequence [Figure 4:3 (b); $p$<0.001]. Conversely, SIRT1 knockdown halved pri-miR-34a [Figure 4:3 (a); $p$<0.001], but did not alter expression of mature miR-34a [Figure 4:3 (b)].

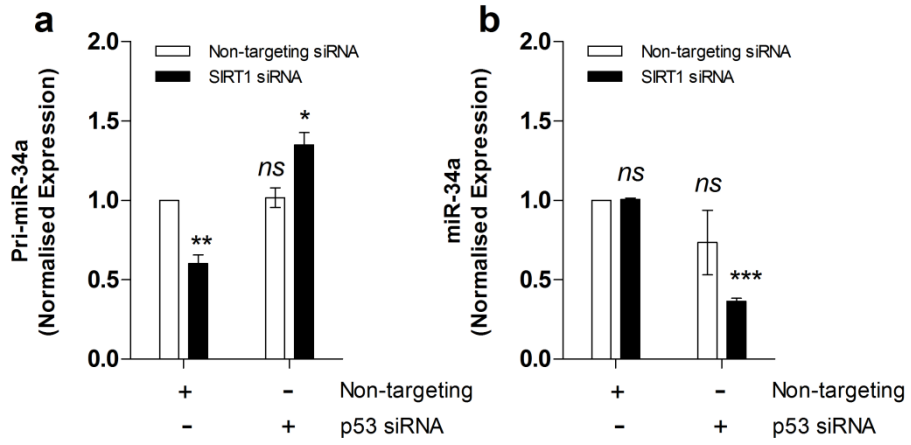


*Figure 4:3 p53 and SIRT1 co-regulate miR-34a maturation in human keratinocytes*

Primary human keratinocytes (NHEKs) were transfected with p53 (right Panel) and SIRT1 (black bars) siRNA targeting pools. Total RNA was extracted after 48 hrs and target genes assayed by RT-PCR. Results were normalised to 5S rRNA, and analysed relative to samples transfected with non-targeting control oligonucleotides (white bars).

All data represent the mean ± SD of 3 independent experiments and are represented as *, ** and ***; with $p < 0.05$, $p < 0.01$ and $p < 0.001$ respectively.

With combined p53 and SIRT1 transfection, pri-miR-34a expression in NHEKs increased by 30% [Figure 4:3 (a); $p$<0.001], but the mature miR-34a transcript did

not increase in a corresponding manner, and instead was depleted by 60% [Figure 4:3 (b); $p<0.001$].

### *Impaired post-transcriptional processing of miR-34a in p53 mutated keratinocytes*

To investigate the implications of our results in cancers with p53-inactivating mutations, SIRT1 was ablated in the p53-mutated keratinocyte cell line, HaCaT, using an identical siRNA transfection protocol as for NHEKs with dual p53 and SIRT1 knockdown. Abundance of p53, SIRT1, and miR-34a targets was measured using qRT-PCR and immunoblotting.

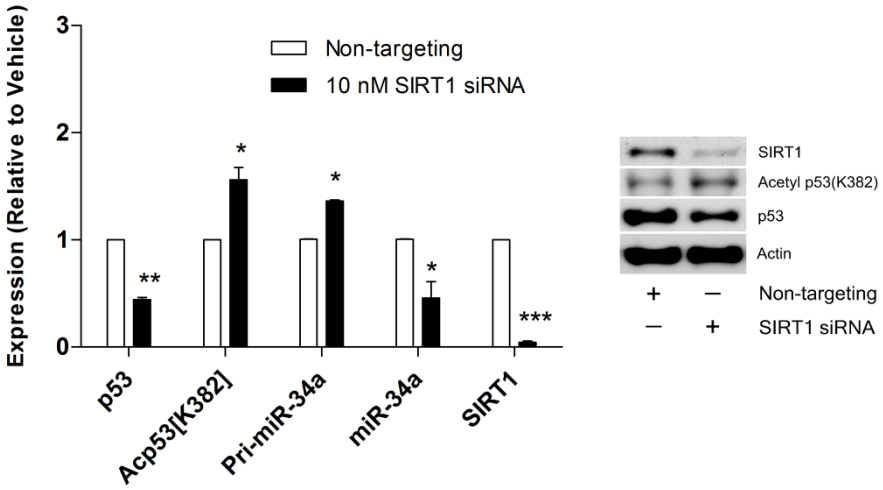


*Figure 4:4 SIRT1 knockdown suppresses miR-34a in p53-mutated keratinocytes*

SIRT1 was transiently ablated in p53-mutated keratinocytes (HaCaTs) with a SIRT1 siRNA targeting pool (black bars). Total protein and RNA was extracted after 48 hrs and target protein and mRNA expression assayed by immunoblotting or RT-PCR. Actin was used as a loading control for immunoblotting, and RT-PCR signals were normalised to 5S rRNA. Results were analysed relative to samples transfected with non-targeting control oligonucleotides (white bars).

All data represent the mean ± SD of 3 independent experiments and are represented as *, ** and ***; with $p < 0.05$, $p < 0.01$ and $p < 0.001$ respectively.

Knockdown of SIRT1 in the p53-mutated HaCaT cell line suppressed total p53 protein and increased relative p53 acetylation [Figure 4:4; $p<0.01$]. Additionally,

although the miR-34a precursor was induced in SIRT1-inhibited HaCaTs, expression of its mature sequence was down-regulated [Figure 4:4; $p<0.05$]. This experiment demonstrates that acetylation capacity in the DNA binding domain is not impaired by p53 mutations in HaCaT keratinocytes, and that pri-miR-34a transcription is effectively induced by p53 acetylation during SIRT1 ablation. However p53 mutations in this cell line suppress processing of the primary transcript to its mature miR-34a sequence.

### *A directed block of the miR-34a binding site enhances SIRT1 expression in human keratinocytes*

Our knockdown experiments have shown that both overexpression of SIRT1 and depletion of miR-34a are features of p53 mutations in the HaCaT cell line. Since SIRT1 is a well characterised target of miR-34a, the next step was to test the assumption that overexpression of SIRT1 in keratinocytes is related to altered miR-34a-mediated regulation. Target site blocking experiments were designed to measure cellular responses which are influenced by this relationship by interfering with miR-34a:SIRT1 mRNA binding. Based on the current understanding of miR-34a-mediated regulation of SIRT1 expression (479), our assumption was that inhibition of the interaction between miR-34a and SIRT1 at the target site would prevent microRNA-mediated degradation of SIRT1 mRNA, and promote its translation into SIRT1 protein.


*Figure 4:5 Schematic of Target site masking experiment*

LNA-modified oligonucleotides were designed to bind the miR-34a/SIRT1 target binding site within the SIRT1 3'UTR.These miR-34a:SIRT1 TSB oligonucleotides were used to interrogate cellular responses to miR-34a-mediated regulation of SIRT1 expression during p53-mediated signalling.

To confirm the relationship between miR-34a levels and SIRT1 expression, oligonucleotides were designed to specifically block the miR-34a complementary binding site within the 3' UTR of the SIRT1 mRNA [Figure 4:5].

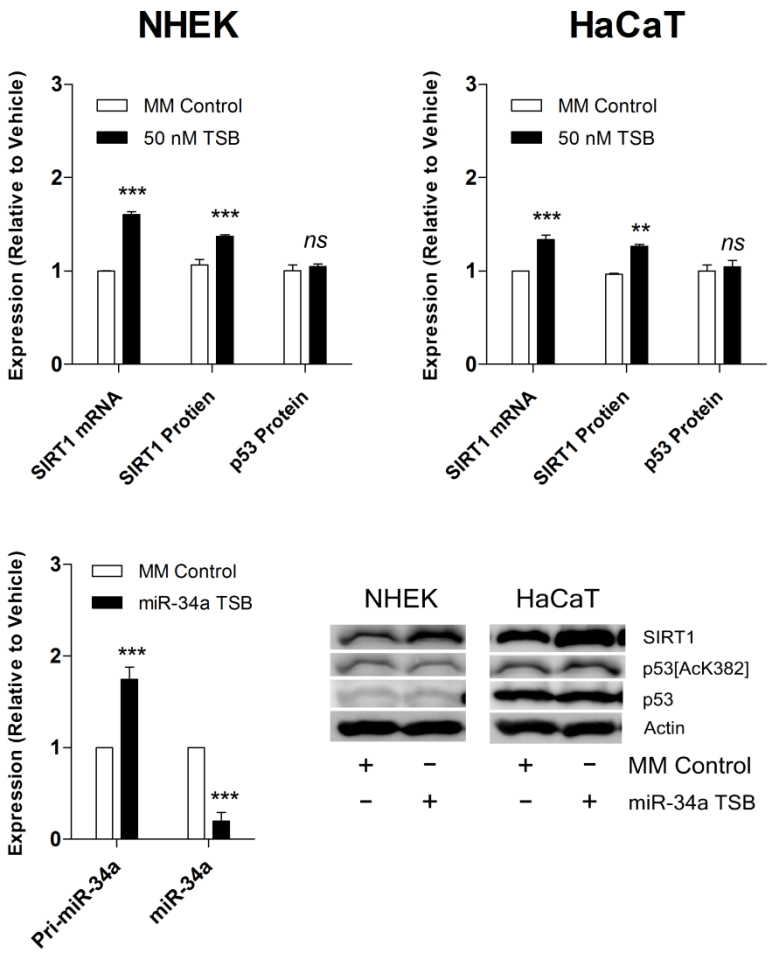


*Figure 4:6 Effective SIRT1 target site masking in human keratinocytes*

Primary human (NHEK) and p53-mutated (HaCaT) keratinocytes were transfected with 50 nM of a directed miR-34a:SIRT1 target site blocking (TSB) or mismatched control (MM Control) LNA-modified oligonucleotide pool. SIRT1 mRNA, SIRT1 protein, p53 protein expression and p53 acetylation was measured by qRT-PCR or immunoblotting after 72 hrs, and the effect of target site masking analysed relative to the mismatched control treatment. Protein loading was standardised using actin and PCR values were normalised using 5S rRNA as a control gene.

Results were analysed by paired *t* test; (** $p<0.01$; ***; $p<0.001$; $n=3$).

LNA-modified miR-34a:SIRT1 target site blocking oligonucleotides (TSB) were introduced into NHEK or HaCaT keratinocytes using RNAiMAX as a delivery system. The efficacy of miR-34a:SIRT1 target site masking was confirmed by assaying increases in SIRT1 expression following introduction of the miR-34a:SIRT1 target site blocking oligonucleotides.

After 72 hrs of treatment with 50 nM miR-34a:SIRT1 TSB oligonucleotides, SIRT1 mRNA expression in NHEK or HaCaT cells had increased significantly when compared to SIRT1 mRNA expression in keratinocytes treated with the same concentration of a mismatched control LNA-modified oligonucleotide pool [Figure 4:6; $p<0.001$]. Additionally, SIRT1 protein increased in TSB-treated NHEK and HaCaT cells after 72 hrs in addition to the accumulation of SIRT1 mRNA [Figure 4:6; $p<0.01$]. To confirm that SIRT1 mRNA is accumulating as a consequence of post-transcriptional stabilisation following the miR-34a:SIRT1 target site block rather than from cell stress-mediated transcriptional up-regulation, p53 protein expression and activation was assayed in treated cells.

No change in p53 acetylation or expression was measured in TSB-treated cells for either NHEK or HaCaT cells [Figure 4:6] therefore changes in SIRT1 expression resulting from a miR-34a:SIRT1 target site block are not related to p53-mediated transactivation.

Although the HaCaT genome is considered to be stable, mutations to the miR-34a-coding domain or to the 3'end of the SIRT1 gene could potentially be responsible for the altered regulation of SIRT1 by miR-34a observed in the HaCaT cell line. Target site blocking experiments in HaCaTs produced results consistent with findings in NHEKs, indicating that the interactions between miR-34a and the SIRT1 mRNA binding site in this cell line had not been compromised by extended growth in culture.

When miR-34a expression was assayed in these experiments, blocking the SIRT1 3' UTR miR-34a target site produced a 50% up-regulation of the primary miR-34a transcript [Figure 4:6; $p<0.001$], and suppressed mature miR-34a expression [Figure 4:6; $p<0.001$]. Taken together, these results demonstrate that the miR-34a:SIRT1 binding site is effectively blocked with 50 nM of LNA-modified oligonucleotides.

*Primary and mature miR-34a is differentially expressed by modulating p53 activity and expression*

The role of p53 and SIRT1 in miR-34a expression and biogenesis was further explored by altering p53 and SIRT1 activity using pharmaceutical agents. Wild-type p53 is minimally expressed in unstressed cells (estimated between 25 - 200 $\times$ $10^3$ molecules per cell, depending on the cell line) (485). P53 expression is suppressed by proteasomal degradation via the E3 ubiquitin ligase MDM2 (486, 487).

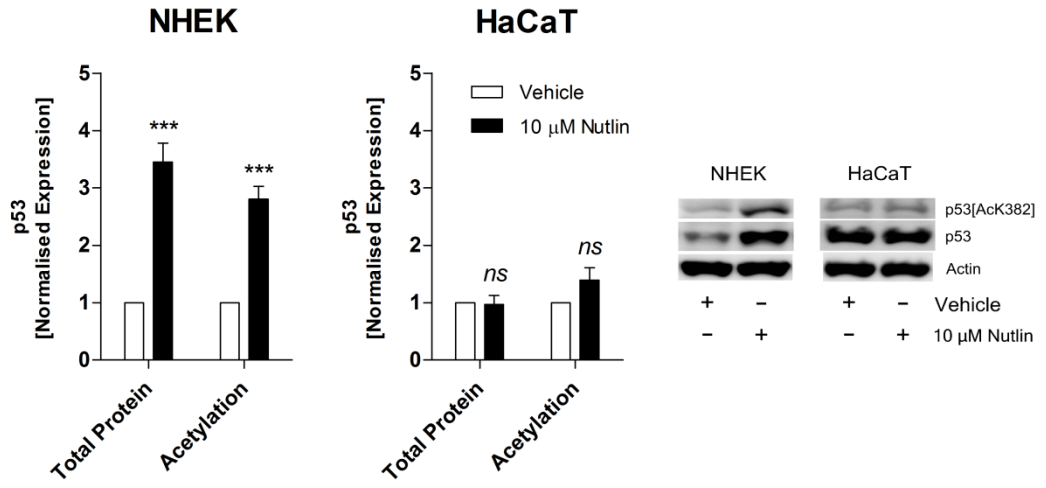


*Figure 4:7 Nutlin up-regulates p53 in wild-type, but not p53-mutated human keratinocytes*

Primary (NHEK) or p53-mutated (HaCaT) keratinocytes were treated with 10 μM Nutlin-3a for 24 hours. Expression of p53 (total protein) and p53 acetylated at lysine 382 [Acetyl p53(K382)] was measured by immunoblotting cell lysates. Densitometric data was analysed relative to vehicle controls, using actin to normalise protein loading.

All data represent mean ± SEM of 3 independent experiments. Results significantly different from vehicle are represented as ***; with $p < 0.001$.

Acetylation of p53 during cellular stress causes p53 protein to accumulate by dissociation of MDM2 from its p53 binding site (32). To increase p53 expression for our investigations, we used Nutlin-3a, a pharmaceutical MDM2 inhibitor. Nutlin-3a was developed for targeted chemotherapy in cancers which retain wild-type p53 (488, 489), however its efficacy as a p53 status-specific cancer therapy has been disappointing in clinical trials to date (490).

Nutlin-3a can reveal tumour-related changes in p53 signalling and induce senescence in fibroblasts by up-regulating the miR-34 family of microRNAs (491, 492). As miR-34a is one of the microRNA targets in this study, Nutlin-3a was an attractive choice for p53 induction during experiments. Firstly, the impact of Nutlin-3a on p53 expression and acetylation in keratinocytes was analysed by immunoblotting. Cellular p53 protein accumulated 4-fold and relative p53 acetylation increased 3-fold in NHEKs [Figure 4:7; $p$<0.01] however p53 protein and acetylation in HaCaT cells was unaffected by Nutlin-3a [Figure 4:7].

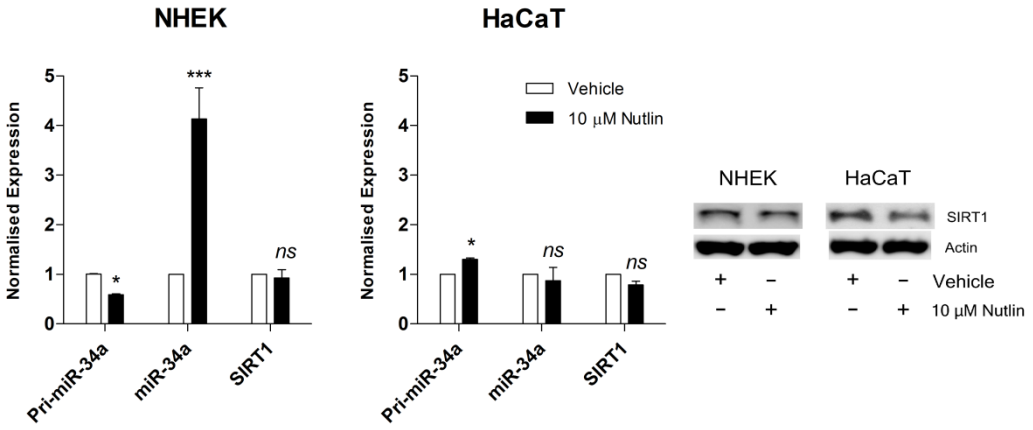


*Figure 4:8 Nutlin up-regulates miR-34a in wild-type, but not p53-mutated human keratinocytes*

Primary (NHEKs; left panel) and p53-mutated (HaCaT; right panel) keratinocytes were treated with 10 μM Nutlin (black bars). Total RNA was extracted after 24 hrs and expression of target genes was assayed by RT-PCR. Results were normalised to 5S rRNA, and analysed relative to vehicle controls (white bars).

All data represent the mean ± SD of 3 independent experiments and are represented as *, ** and ***; with $p < 0.05$, $p < 0.01$ and $p < 0.001$ respectively.

When p53 protein content in basal (untreated) NHEK and HaCaT keratinocytes was compared (Chapter 3; Fig 11) a 5-fold higher level of constitutive p53 was measured in the HaCaT cell line. This finding appears to be a consequence of a functional and structural change to the mutant p53 protein in HaCaTs which impedes ubiquitinylation and/or proteolytic breakdown. Thus p53 in HaCaT keratinocytes is maximally expressed in the intracellular environment, and is resistant to MDM2 inhibition by Nutlin-3a.

Furthermore, an increase in the cellular content of activated p53 with Nutlin treatment in NHEK cells was associated with a 4-fold induction of miR-34a [Figure 4:8; $p<0.001$]. Conversely, mature miR-34a expression was unaltered in Nutlin-treated HaCaTs, although expression of its primary sequence was slightly elevated [Figure 4:8; $p<0.05$]. These data demonstrate that enhanced acetylation, but not up-regulation, of p53 protein is associated with induction of miR-34a. Additionally, relative SIRT1 protein expression was not significantly different in Nutlin-treated keratinocytes for either NHEKs or HaCaTs [Figure 4:8].

### *Induction of p53 acetylation by treatment with a SIRT1 inhibitor*

To confirm the relationship between SIRT1 and miR-34a expression explored in earlier results, the SIRT1 inhibitor EX-527 was used to increase the level of p53 activation by promoting acetylation without altering the expression of p53.

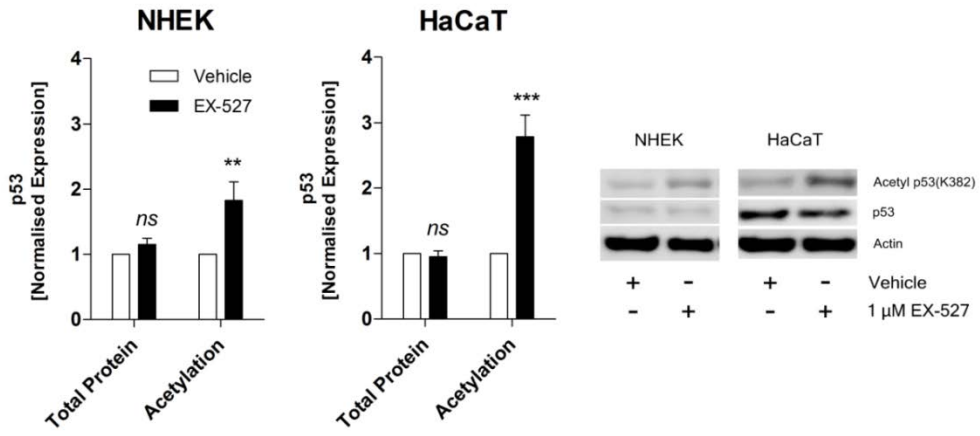


*Figure 4:9 Induction of p53 acetylation by SIRT1 inhibition in human keratinocytes*

SIRT1 activity in primary (NHEK) or p53-mutated (HaCaT) keratinocytes was inhibited with 1 µM EX-527 for 24 hours. Expression of p53 (total protein) and p53 acetylated at lysine 382 [Acetyl p53(K382)] was measured by immunoblotting cell lysates. Densitometric data was analysed relative to vehicle controls, using actin to normalise protein loading.

All data represent mean ± SD of 3 independent experiments. Results significantly different from vehicle are represented as *, ** and ***; with $p < 0.05$, $p < 0.01$ and $p < 0.001$ respectively.

Here, the effect of SIRT1 inhibition on p53 in keratinocytes was determined by immunoblotting using the acetylation of p53 at lysine 382 [Acp53(K382)] as a marker for SIRT1 catalysis. EX-527 increased p53 acetylation without a concomitant up-regulation of p53 protein for both cell cultures. EX-527-mediated induction of p53 acetylation in HaCaTs was significantly greater than for NHEKs [3-fold vs 2-fold; Figure 4:9].

Co-immunoprecipitation experiments were performed to further define the relationship between EX-527, SIRT1 activity and p53 acetylation. EX-527 enhanced the association between p53 and SIRT1 protein in NHEK and HaCaT cells [Figure 4:10; 6-fold for NHEK; 4-fold for HaCaT] after 24 hours of treatment. This experiment demonstrated that an association between p53 and SIRT1 persists with EX-527 treatment, and supports a catalytic mechanism for SIRT1 inhibition by EX-527 which indicates that EX-527 permits SIRT1-substrate binding (p53 in this study), but blocks substrate release.

Also, p53:SIRT interactions are not impeded by p53 mutations in the HaCaT cell line, as the relative increase in p53:SIRT1 association during EX-527 treatment is not significantly different than for wild-type (NHEK) keratinocytes [Figure 4:10].

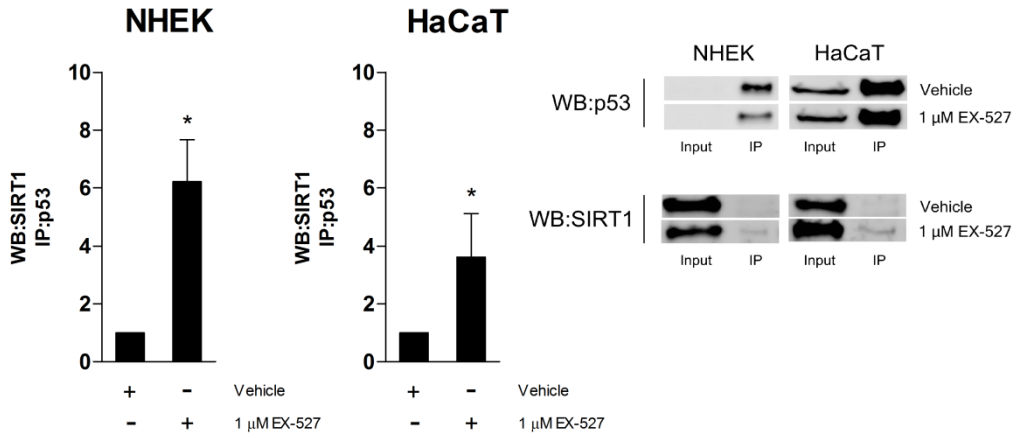


*Figure 4:10 Association between p53 and SIRT1 in EX-527 treated keratinocytes*

SIRT1 was inhibited in Primary human (NHEK) and p53-mutated (HaCaT) keratinocytes with 1 μM EX-527 for 24 hr. Protein was extracted in NP-40 lysis buffer and p53-SIRT1 protein complexes purified by immunoprecipitation using p53 as the target antigen. Co-association of SIRT1 with p53 was determined by immunoblotting and densitometric signal normalised to the input (raw lysate) signal.

The effect of SIRT1 inhibition on co-association between p53 and SIRT1 was calculated relative to vehicle control and analysed by paired t-test. Values represent the mean (± SD) from 3 independent experiments and significant differences are shown as * ($p < 0.05$).

Colocalisation of p53 and SIRT1 has been measured by others (201, 202, 493); however these investigations have been conducted using SIRT1 and p53 overexpression vectors and in tumour-derived cell lines. This study has confirmed this intracellular relationship between SIRT1 and p53 in keratinocytes using experimental conditions without off-target effects associated with plasmid insertion.

Altogether, EX-527 treatment experiments demonstrate that SIRT1 deacetylase activity suppresses p53 transactivation in keratinocytes by managing acetylation of its C-terminal lysine residues. Additionally, EX-527 generates differential responses in target cells depending on their p53 mutational status, and may therefore be useful as a p53-activating therapy in cancers with a p53 mutation profile similar to HaCaTs.

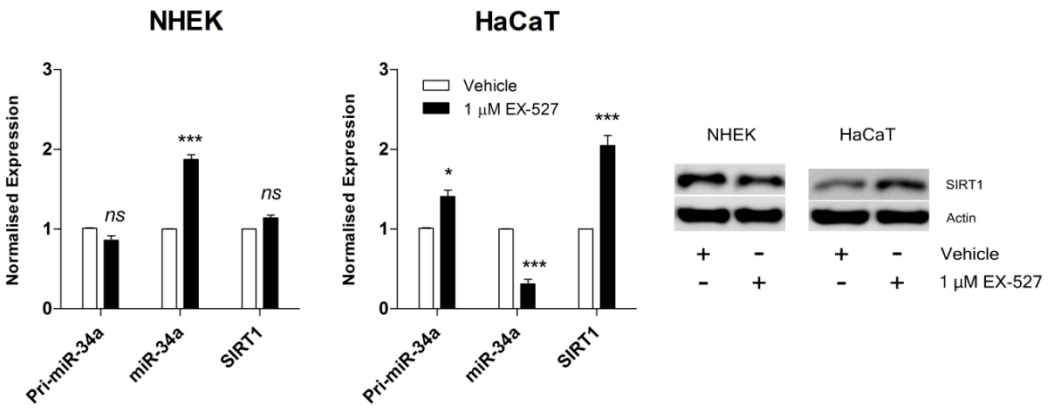


*Figure 4:11 miR-34a-mediated regulation of SIRT1 is impaired in p53 mutated keratinocytes*

Primary (NHEKs; left panel) and p53-mutated (HaCaT; right panel) keratinocytes were treated with 1 μM EX-527 (black bars). Total protein and RNA was extracted after 24 hrs and target protein or mRNA expression assayed by immunoblotting or RT-PCR. Actin was used as a loading control for immunoblotting, and RT-PCR signals were normalised to 5S rRNA. Results were analysed relative to vehicle controls (white bars).

All data represent the mean ± SD of 3 independent experiments and are represented as *, ** and ***; with $p < 0.05$, $p < 0.01$ and $p < 0.001$ respectively.

Mature miR-34a was induced in SIRT1-inhibited NHEK cells [Figure 4:11; $p<0.01$], although expression of the primary transcript was not altered. For the SIRT1-inhibted HaCaT cell line, however, an increase in p53 acetylation was associated with induction of pri-miR-34a but expression of the mature miR-34a transcript was suppressed [Figure 4:11; $p<0.001$]. Moreover, SIRT1 protein doubled in HaCaT cells treated with EX-527, whereas SIRT1 expression was not altered by SIRT1 inhibition in NHEK cells.

Taken with earlier results, these data show that p53 and SIRT1 are both critical to the maintenance of miR-34a expression in keratinocytes. Impaired maturation of the pri-miR-34a primary transcript appears to explain an overexpression of SIRT1 protein measured in the HaCaT cell line, which is augmented during p53 activation. To further model the effect of p53 insufficiency on miR-34a-mediated regulation of SIRT1 expression in HaCaTs, p53 was ablated in NHEKs prior to 24 hrs of EX-527 treatment to inhibit SIRT1 activity.

*P53 expression and SIRT1 activity regulate miR-34a biogenesis in keratinocytes*

In this experiment, when SIRT1 was inhibited in p53-ablated keratinocytes, SIRT1 protein increased in association with a suppression of mature miR-34a [Figure 4:12; $p<0.01$], however accumulation of SIRT1 protein following SIRT1 inhibition was not as pronounced in p53-ablated keratinocytes as it was for HaCaTs.

This outcome may have occurred as an off-target consequence of transfection stress in the model system. Nonetheless, SIRT1 inhibition produced a pattern of miR-34a dysregulation in p53-ablated NHEK cells consistent with the p53-mutated HaCaT cell line, i.e.- impaired miR-34a maturation which was associated with increased SIRT1 protein expression.

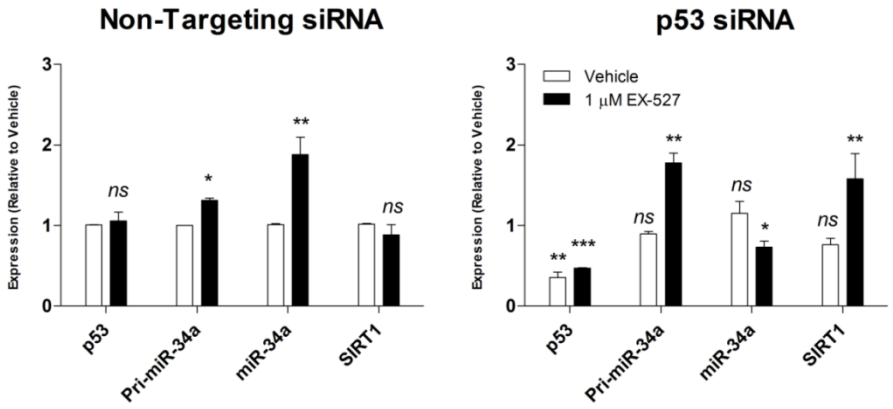


*Figure 4:12 SIRT1 inhibition suppresses miR-34a in p53-ablated human keratinocytes*

Primary human keratinocytes (NHEKs) were transfected with Non-targeting oligonucleotides (left panel) or p53 (right panel) siRNA targeting pools. After 24 hr knockdown, SIRT1 was inhibited with 1 μM EX-527 (black bars). p53 and SIRT1 protein expression, and pri-miR-34a or miR-34 expression was assayed by immunoblotting or RT-PCR, respectively. Actin was used as a loading control for immunoblotting, and RT-PCR signals were normalised to 5S rRNA. Results were analysed relative to vehicle controls (white bars).

All data represent the mean ± SD of 3 independent experiments and are represented as *, ** and ***; with $p < 0.05$, $p < 0.01$ and $p < 0.001$ respectively.

*SIRT1 activity modulates global microRNA maturation in human keratinocytes*

To further evaluate the impact of the p53/SIRT1/miR-34a axis on microRNA biogenesis, expression of several mature microRNAs was compared with their primary transcripts in NHEK cells transfected with p53 targeting siRNAs alone, EX-527-treatment alone, or both p53 siRNA and EX-527 treatment. For this purpose, we selected a small group of microRNAs with multiple gene targets which are key regulators of cell cycle control, differentiation and survival, and which included microRNAs miR-16-1/15, miR-145, miR-200c/141 and miR-107, all of which are established transcriptional targets of p53 (149). p53 knockdown reduced expression of the primary transcript for miRs 16-1 and 200c [Figure 4:13 (a); $p<0.001$], and increased expression of mature miR-107 [Figure 4:13 (b); $p<0.05$]. Inhibition of SIRT1 in NHEKs up-regulated microRNA expression for all mature transcripts [Figure 4:13 (d)]; and expression of the primary transcript increased for miRs 34a, 145 and 200c [Figure 4:13 (c)].

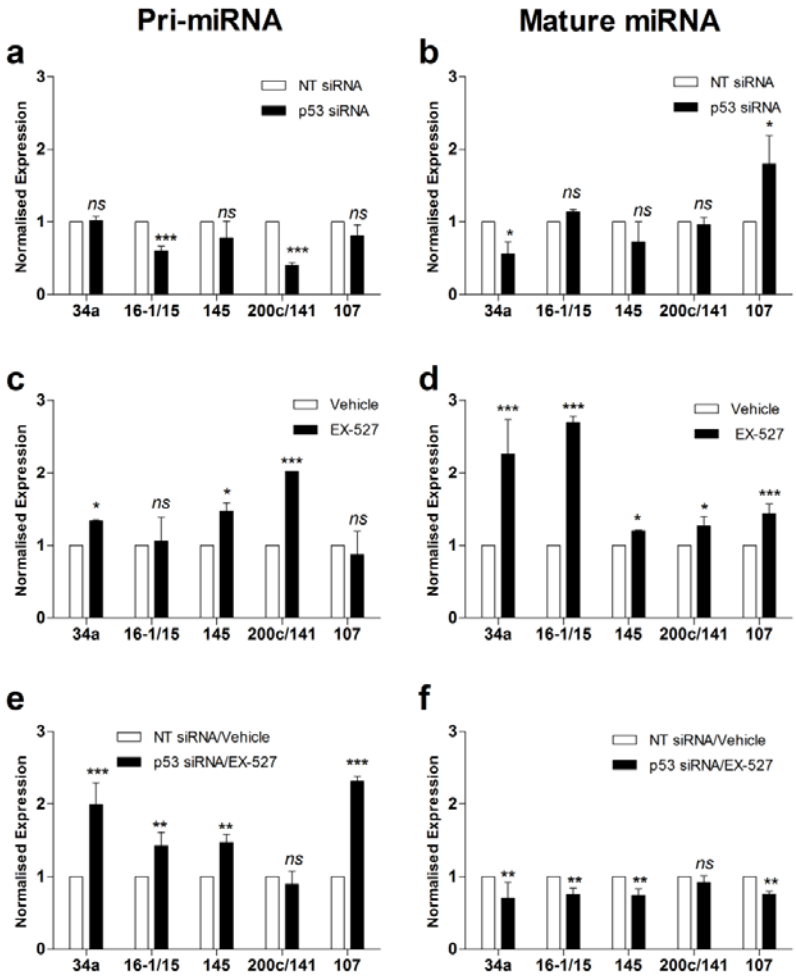


*Figure 4:13 p53 knockdown blocks microRNA maturation in SIRT1-inhibited human keratinocytes*

Primary human keratinocytes (NHEKs) were transfected with a p53 siRNA targeting pool and/or treated with 1 µM EX-527 for 24 hours. Expression of primary (left panels) and mature (right panels) microRNAs was determined by RT-PCR using Taqman probes. Results were normalised using 18S rRNA and U6 snoRNA. Panels **a** & **b**: p53 ablation alone; Panels **c** & **d**: SIRT1 inhibition; Panels **e** & **f**: Combined effect of p53 knockdown and SIRT1 inhibition.

All data represent the mean ± SD of 3 independent experiments. Results significantly different from samples treated with non-targeting oligonucleotides and/or vehicle (white bars) are represented as *, ** and ***; with $p < 0.05$, $p < 0.01$ and $p < 0.001$ respectively.

Treatment of p53-ablated NHEKs with EX-527 produced a more generalised response pattern, with an up-regulation of the primary transcript and suppression of the mature sequence observed in all microRNAs tested [Figure 4:13 (e & f)], with the exception of the primary miR-200c transcript.

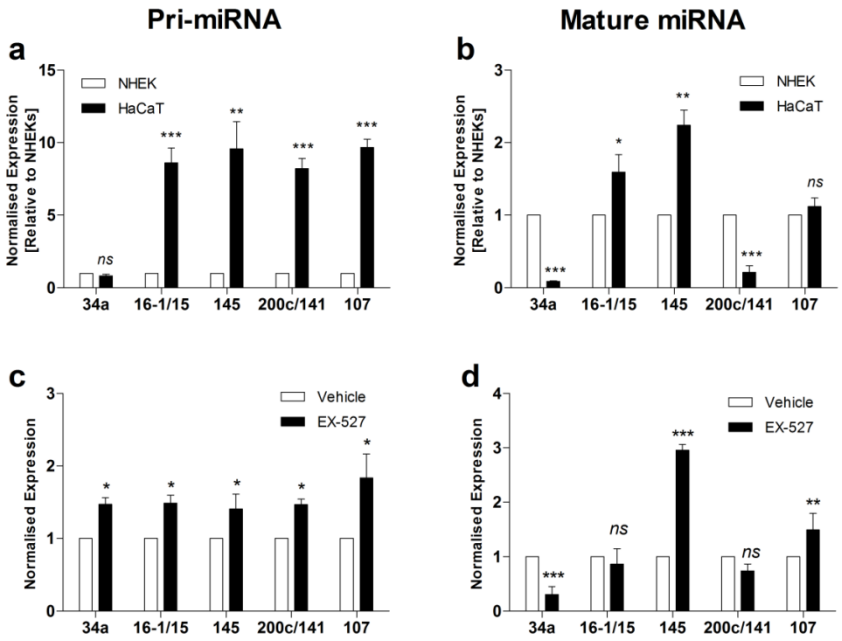


*Figure 4:14 p53 mutations block microRNA maturation in SIRT1-inhibited human keratinocytes*

Panels **a** & **b**: Analysis of microRNA expression in basal (unstimulated) p53-mutated keratinocytes (HaCaTs) relative to expression measured in unstimulated primary keratinocytes (NHEKs). Panels **c** & **d**: Primary and mature microRNA expression in HaCaT keratinocytes treated with 1μM EX-527 for 24 hrs. Expression of primary (left panels) and mature (right panels) microRNAs was determined by RT-PCR using Taqman probes. Results were normalised using 18S rRNA and U6 snoRNA.

All data represent the mean ± SD of 3 independent experiments. Results significantly different from vehicle (white bars) are represented as *, ** and ***; with $p < 0.05$, $p < 0.01$ and $p < 0.001$ respectively.

When HaCaT keratinocytes are grown in identical conditions, they display widespread alterations to their basal microRNA expression profile compared to NHEK cells. A 10-fold higher expression of primary transcripts was observed for all microRNAs tested, with the exception of pri-miR-34a [Figure 4:14 (a); $p<0.001$]. This was mirrored by overexpression of mature miRNAs 15 and 145 [Figure 4:14 (b)], however miR-34a and miR-141 expression was significantly lower than recorded for normal keratinocytes [Figure 4:14 (b); $p<0.001$], and miR-107 was not significantly different. Given our results in NHEKs transfected with p53-targeting siRNAs and co-treated with EX-527 [Figure 4:14 (e & f)], we lastly considered the effect on SIRT1 inhibition on microRNA maturation in HaCaT cells. Inhibition of SIRT1 in HaCaT

keratinocytes with EX-527 generated responses in microRNA primary transcripts which were consistent with, but not identical to, the expression pattern observed in p53-ablated and EX-527 treated NHEKs [Figure 4:14 (c); $p<0.05$]. Mature miR-34a was down-regulated; however in contrast to p53-ablated and EX-527 treated NHEKs, expression of mature miRs 145 and 107 increased in EX-527-treated HaCaTs [Figure 4:14 (d); $p<0.01$].

## 4.4 DISCUSSION

miR-34a is induced during p53 activation and has numerous downstream regulatory targets, of which SIRT1 is the most extensively characterised. SIRT1 expression is regulated at the posttranscriptional level by miR-34a-mediated binding of its 3' UTR. Suppression of SIRT1 by miR-34a during cellular stress responses reinforces p53 transcriptional activation by enhancing C-terminal regulatory domain acetylation. This constitutive feedforward loop is referred to as the p53/SIRT1/miR-34a axis [Figure 4:15].

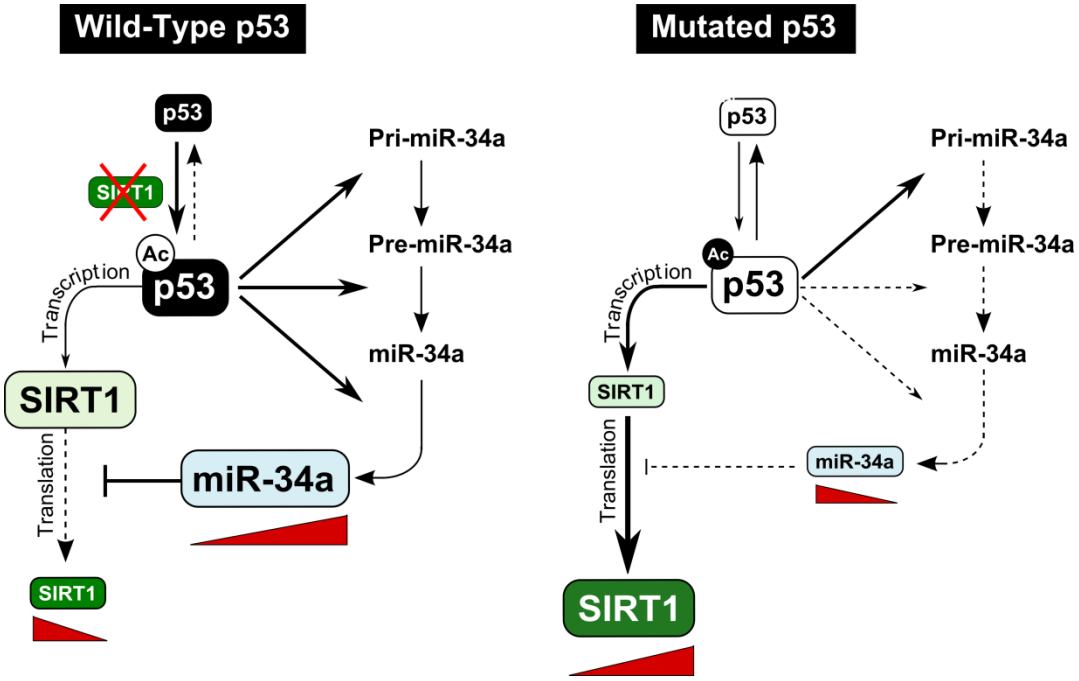


*Figure 4:15 Feedforward maintenance of p53 transactivation by miR-34a and SIRT1*

SIRT1 and p53 operate as a self-limiting negative feedback loop in which SIRT1-mediated deacetylation suppresses p53 transactivation and promotes proliferation and survival. Up-regulation of miR-34a interrupts this process during genotoxic stress by creating a feed-forward loop between p53 and SIRT1, which down-regulates SIRT1 expression and amplifies p53-mediated cell cycle control and apoptotic signaling.

SIRT1 expression increases in keratinocytes with p53 mutations as a consequence of impaired microRNA processing. During genotoxic stress, SIRT1 overexpression blocks feedforward regulation of p53-mediated cell stress responses by suppressing p53 activation, causing apoptotic resistance.

Our results correlate with the known functional relationship between p53 and miR-34a-mediated regulation of SIRT1 expression in other cell lines (HeLa, HEK (479); PC3PR (494), HUVEC (482)), and extend this functionality to the keratinocyte lineage.

In keratinocytes expressing wild-type p53, inhibition of SIRT1 with EX-527 up-regulates mature miR-34a. In p53-mutated keratinocytes, however, mature miR-34a was down-regulated during EX-527 treatment, contributing to an accumulation of SIRT1 protein [Figure 4:15]. miR-34a expression is impaired in tumour samples derived from multiple cancer types and is attributed to numerous mutational causes, including deletion of Chromosome 1 and/or inactivation of *TP53*. Although both p53 alleles are mutated in the HaCaT cell line, p53 retains partial function and responds to 24 hr of SIRT1 inhibition by producing a 3-fold increase in acetylation. The primary miR-34a transcript was up-regulated in SIRT1-inhibited HaCaT keratinocytes, indicating that although mature miR-34a was suppressed, EX-527-mediated p53 acetylation induces transcription of the miR-34a gene in this cell line.

Our findings with the HaCaT cell line supports a model in which mutant p53 interferes with the maturation of specific microRNAs when SIRT1 is inhibited. Interestingly, maturation of miR-145 and miR-107 was blocked in p53 knockdown/SIRT1-inhibited NHEKs but not in SIRT1-inhibited HaCaTs. This indicates an alternative, non-p53 dependent mechanism such as RNA sequence editing, mirtron-mediated splicing and post-translational regulation of stabilization complexes (474, 495) may also be operating for the maturation of these two microRNAs in the HaCaT cell line, possibly as an adaptation for survival in cells with mutated p53. Two predominant theories have been proposed to explain the impact of p53-mediated modulation of microRNA processing in cancer: 1) p53 mediates RNase III activity by associating with p68 (150), and therefore mutations to p53 suppress microRNA processing activity in Drosha and/or Dicer complexes; and 2) mutant p53 directly binds to and inactivates p63, inhibiting p63-mediated Dicer-1

expression (496). Regardless of the mechanism, regulation of Drosha and Dicer activity and expression is critical for ensuring microRNA biogenesis. Heterozygous deletion of Drosha and Dicer is known to promote cellular transformation and tumorigenesis in mouse models, and hemizygous loss of Dicer and/or Drosha is common in numerous human cancers (190, 497). The majority of microRNAs act as oncosuppressors, and thus downregulation of microRNAs is consistent with malignancy. One exception to this may be the Dicer-targeting miRNA, miR-107. Our investigation indicates that an increase in expression of miR-107 in p53 mutated cells may contribute to a pattern of impaired microRNA processing by blocking Dicer. High levels of miR-107 are associated with metastasis in breast cancers, and miR-107 is thought to induce epithelial-mesenchymal transitions by downregulating miR-200 family miRNAs (498, 499). In concordance with this, in p53 ablated and EX-527 treated NHEKs, expression of miR-200c/141 was significantly decreased, and was also significantly reduced in the p53-mutated keratinocyte cell line.

The activity and expression of multiple p53 transcriptional targets is regulated via microRNA-mediated feedback inhibition (149). miR-34a in particular is crucial to p53-mediated induction of pro-apoptotic signalling during cellular stress (479), and this property has consequences for carcinogenesis (476, 478). For example, acetylation performs numerous roles in signalling networks which regulate RNA splicing and nuclear transport (59), and it may be that SIRT1-mediated regulation of lysine acetylation directly regulates microRNA processor enzyme activity or contributes to the formation of functional signalling complexes. Further testing of this hypothesis is required to determine if this reflects a globalised phenomenon.

This investigation indicates that p53 and SIRT1 work co-ordinately to regulate miR-34a biogenesis. Although other p53-inducible miRNAs tested here generated a complex response pattern when exposed to alterations in p53 expression and acetylation, inhibition of SIRT1 activity alongside p53 ablation, either using RNAi in NHEK cells or in HaCaT cells with p53 mutations, consistently blocked processing of

the primary transcript, causing a concomitant decrease in mature microRNA expression. Our observations suggest that SIRT1 plays a role in maintaining and stabilising p53 in a form which promotes maturation of primary microRNA transcripts, however from these experiments alone, we cannot exclude other SIRT1-mediated mechanisms which may also contribute to microRNA processing.

Findings from this study have wider implications with regards to our understanding of the events which predispose cells to carcinogenic change. Here we demonstrate that p53 and SIRT1 co-ordinately regulate microRNA biogenesis. Since p53 is the most frequently mutated gene in cancer, novel insights into mechanisms which distinguish p53-mutated cells from their healthy counterparts may facilitate selective targeting of malignant cells during cancer therapy. Manipulation of SIRT1 activity influences the cellular microRNA profile in cells with reduced p53 function, and this knowledge has the potential to overcome chemotherapeutic resistance.

# Chapter 5 -
# SIRT1 Inhibition Restores Apoptotic Sensitivity in p53-Mutated Keratinocytes

# Chapter 5

## 5.1 ABSTRACT

Mutations to the p53 gene are common in UV-exposed keratinocytes, and contribute to apoptotic resistance in skin cancer. P53 acetylation is modulated, in part, by a complex, self-limiting feedback loop imposed by miR-34a-mediated regulation of the lysine deacetylase, SIRT1, and thus SIRT1 expression influences p53-mediated tumour suppressor activity. Additionally, expression of numerous microRNAs is dysregulated in squamous and basal cell carcinomas; however the contribution of specific microRNAs to the pathogenesis of skin cancer remains untested. Through use of RNAi, miRNA target site blocking oligonucleotides and small molecule inhibitors, this study explored the influence of p53 mutational status, SIRT1 activity and miR-34a levels on apoptotic sensitivity in primary (NHEK) and p53-mutated (HaCaT) keratinocytes.

SIRT1 and p53 are overexpressed in p53-mutated keratinocytes, whilst miR-34a levels are 90% less in HaCaT cells. HaCaT keratinocytes have impaired responses to p53/SIRT1/miR-34a axis manipulation which culminates in resistance to camptothecin-induced apoptosis. Inhibition of SIRT1 activity in this cell line increased p53 acetylation and doubled relative cell death. p53 mutations increase apoptotic resistance in keratinocytes by interfering with miR-34a-mediated regulation of SIRT1 expression. Thus, SIRT1 inhibitors may have therapeutic potential for overcoming apoptotic resistance during skin cancer treatment.

Much of the work in this chapter forms the basis of a manuscript published in Toxicology and Applied Pharmacology:

Herbert et al, 2014, SIRT1 inhibition restores apoptotic sensitivity in p53-mutated human keratinocytes, *Toxicol. Appl. Pharmacol*. http://dx.doi.org/10.1016/j.taap.2014.04.001 (500).

## 5.2 INTRODUCTION

Sun-exposed keratinocytes are particularly prone to DNA damage and thus adequate repair of UV-induced DNA lesions and elimination of sunburn cells remains an important barrier to carcinogenesis in the skin (367). These processes are primarily regulated by the transcription factor p53, however the *TP53* gene is one of the most frequently mutated tumour suppressor genes in skin cancer, with signature UV mutations affecting p53 activity in ~ 56% of basal cell and >90% of squamous cell carcinomas (501). Targeting p53 mutations, therefore, may be the key to overcoming pre-neoplastic proliferation and resistance to cell death signaling in non-melanoma skin cancer (502).

One of the hallmarks of cancer is evasion of apoptotic signalling which allows cells to proliferate in an uncontrolled manner (11, 12). This process is commonly related to loss or inactivation of the tumour suppressor p53 (35). During p53-dependent cell death signalling, destabilisation of the mitochondrial membrane releases cytochrome *c* into the cytoplasm which activates the Apaf-1/caspase 9 apoptotic pathway (predominantly via the Intrinsic Pathway) (64, 472). P53 regulates this process in a complex manner, through transactivation of p53-responsive genes coding for mitochondrial membrane proteins and downstream effectors (503). Notably, expression of downstream effectors is dysregulated in tumorigenic tissue (504, 505), and thus p53 mutations contribute to a failure of the cell death program to remove damaged cells when exposed to genotoxic stressors.

p53-mediated stress responses are facilitated by microRNAs, small non-coding RNAs which form a complex regulatory network controlling cell survival, senescence, growth and death (151). These feature a suite of microRNAs, including the miR-34a, miR-29, and let-7 families, miR-143, miR-145 and the miR-16-1/15a cluster (149, 151). The miR-34 family of miRNAs have recently emerged as important regulators of p53-mediated responses by directly targeting its downstream effector genes (476). The most widely characterised member of the

miR-34 family, miR-34a, targets SIRT1, an NAD-dependent deacetylase with numerous functional roles as a cell stress mediator (506). miR-34a expression is induced by p53-mediated transcriptional activation (476), and influences SIRT1 expression by complementary base pairing with its 3' UTR (479). SIRT1, in turn, regulates p53 activity via its acetylation status (201, 202). In this manner, SIRT1, p53 and miR-34a operate together to amplify cellular differentiation, senescence and apoptotic signalling (480-483).

Global alterations to the microRNA expression profile are common in dysplastic skin tissue and this in turn contributes to aberrant mRNA expression patterns observed in basal and squamous cell carcinoma (507). Additionally, dysregulation of post-transcriptional processing of microRNAs is thought to play a significant role in the mechanism of carcinogenic transformation (508), and microRNA . Despite the positive correlation between gain of function p53 mutations and chemotherapeutic resistance in squamous cell carcinoma (509), manipulation of the p53/SIRT1/miR-34a axis in order to enhance the efficacy of pharmacotherapy for skin cancer treatment has not previously been studied in keratinocyte cells.

In this chapter, activity and expression of SIRT1 and p53 was manipulated to differentiate apoptotic responses in wild-type and p53-mutated keratinocytes in order to 1) Determine if p53 mutations in the HaCaT cell line influence survival and sensitivity to cell death signaling; 2) Measure p53-related differences in microRNA-mediated regulation of anti-apoptotic gene targets for keratinocytes with wild-type and mutated p53; and 3) Investigate whether manipulation of the p53/SIRT1/miR-34a axis can influence sensitivity to apoptotic induction.

## 5.3 RESULTS

Camptothecin (CPT)-induced apoptosis is predominantly p53-dependent and has been extensively utilised in chemotherapy (402). Unfortunately, many tumours have proven resistance to CPT, in part due to the frequency of p53 inactivating mutations in malignant tissue (510). As such, CPT-induced apoptosis provides a method for studying the impact of p53 mutations on cell death and DNA damage signalling in this model system. PARP activity is p53 dependent and linked to DNA damage-induced cell death (511, 512). During apoptosis, PARP is inactivated by caspase-mediated cleavage into ~25 kDa and ~85 kDa fragments and is considered a characteristic marker for p53-dependent apoptotic signalling (513, 514).

Since miR-34a has a well characterised role in apoptotic signal amplification (515), and loss of miR-34a impairs p53-mediated cell death (478), we next tested if p53 mutations in the HaCaT cell line provide a survival advantage for precarcinogenic keratinocytes by comparing responses to genotoxic stressors with their wild-type counterparts.

### *TP53 mutations promote apoptotic resistance in human keratinocytes*

Initially, a time course for apoptotic induction by CPT was determined by exposing NHEK and HaCaT cells to CPT for 6, 12, 18 and 24 hr periods, using p53 induction and PARP cleavage as indicators of apoptosis. As expected, primary keratinocytes were significantly more sensitive than p53-mutated keratinocytes to CPT-induced apoptosis. CPT-mediated PARP cleavage in NHEKS was associated with DNA damage-induced induction of p53, which doubled cumulatively with each 6 hour period [Figure 5:1 (b, c)] and preceded PARP cleavage by approximately 6 hours. Conversely, p53 did not accumulate in CPT-exposed HaCaT keratinocytes [Figure 5:1 (b, c) ]and PARP cleavage was 3-fold lower than cleavage measured in NHEKs after 24 hrs [Figure 5:1 (a, c)]. These observations indicated that the mutations to p53 are impeding programmed cell death and apoptotic signaling in HaCaT cells.

We next investigated how p53 mutations in HaCaT cells may contribute to apoptotic resistance, and so quantified the expression of the p53-regulated anti-apoptotic genes Survivin/BIRC5 and BCL2. Both Survivin and BCL2 are repressed by wild-type p53 during p53-induced apoptosis (461, 462).

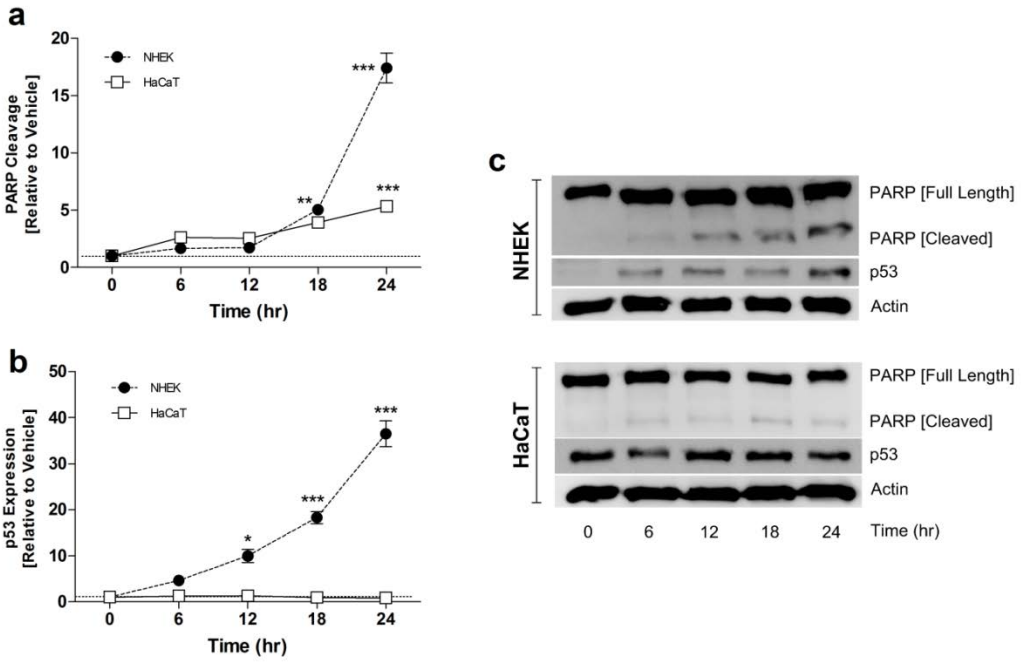


*Figure 5:1 Camptothecin resistance in p53-mutated keratinocytes*

Primary (NHEK, white bars) and p53-mutated (HaCaT, black bars) keratinocytes were treated with 5 µM camptothecin (CPT). PARP cleavage (Panel **a**) and p53 expression (Panel **b**) was measured at 6 hour intervals during the 24 hr exposure period by immunoblotting, using actin as a loading control (Representative immunoblot, Panel **c**).

All data represent mean ± SD of 3 independent experiments. PARP cleavage was determined by dividing the densitometric signal from the cleaved fraction by total PARP expression (full length + cleaved PARP). Results significantly different from vehicle are represented as *, ** and ***; with $p < 0.05$, $p < 0.01$ and $p < 0.001$ respectively.

## *TP53 mutations alter the cell death program in keratinocytes*

p53 negatively regulates expression of anti-apoptotic gene targets BCL-2 and Survivin by targeting repressive p53-binding sequences. Hence, a 6-fold induction of p53 in NHEKs [Figure 5:2 (a)] is associated with an 80% suppression of BCL-2 and

Survivin expression during 24 hrs of CPT treatment [Figure 5:2 (b & c)]. Conversely, BCL-2 and Survivin are up-regulated in the HaCaT cell line during CPT treatment [5-fold for BCL2; 2-fold for Survivin; Figure 5:2 (b & c)].

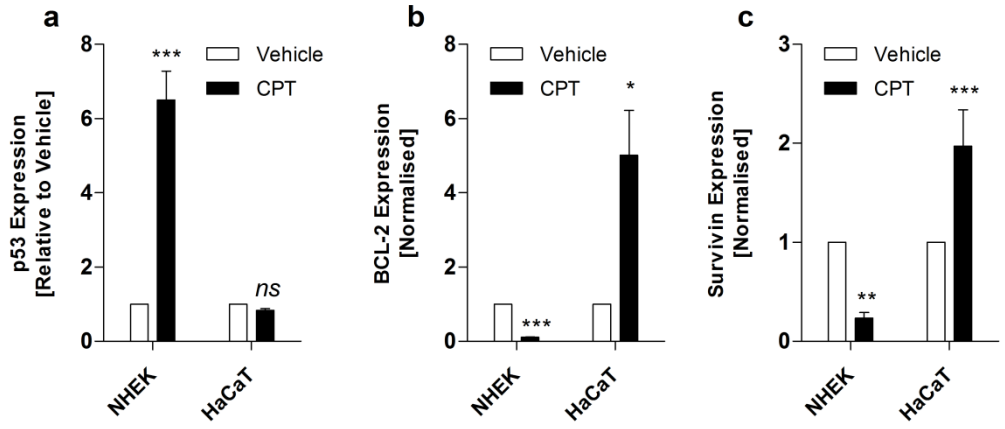


*Figure 5:2 Pro-survival target expression is impaired in p53-mutated keratinocytes*

Apoptosis was induced in primary (NHEK) and p53-mutated (HaCaT) keratinocytes using 5 µM camptothecin (CPT) for 24 hours. Total RNA was extracted for RT-PCR analysis of p53 (Panel **a**), BCL-2 (Panel **b**), Survivin (Panel **c**) expression. Values were normalised using 5S rRNA as a reference gene.

All data represent mean ± SD of 3 independent experiments. Results significantly different from vehicle are represented as *, ** and ***; with $p < 0.05$, $p < 0.01$ and $p < 0.001$ respectively.

Since expression of Survivin and BCL2 are both regulated by miR-34a (516, 517), we investigated if resistance to p53-dependent apoptosis in HaCaT cells was related to the changes in miR-34a expression and biosynthesis observed in Chapter 4. Pri-miR-34a was significantly up-regulated by CPT in NHEK and HaCaT cells [Figure 5:3 (a & b)], however only NHEKs showed an increase in the mature miR-34a sequence [Figure 5:3 (a)]. BCL2 is regulated by a group of microRNAs in addition to miR-34a – notably the miR-15a/miR-16-1 cluster (518) – so we next asked whether p53 mutations in HaCaTs affect expression of tumour suppressor microRNAs other than miR-34a. The miR-15a/miR-16-1 cluster is located within a 0.5 kilobase region of 13q14.3, and the microRNA products, miR-15a and miR-16-1, are processed from a single primary transcript during p53-mediated signaling (519). Here, pri-miR-16-1

provides a measure of primary transcript levels, and miR-15a has been assayed to represent expression of the mature microRNA.

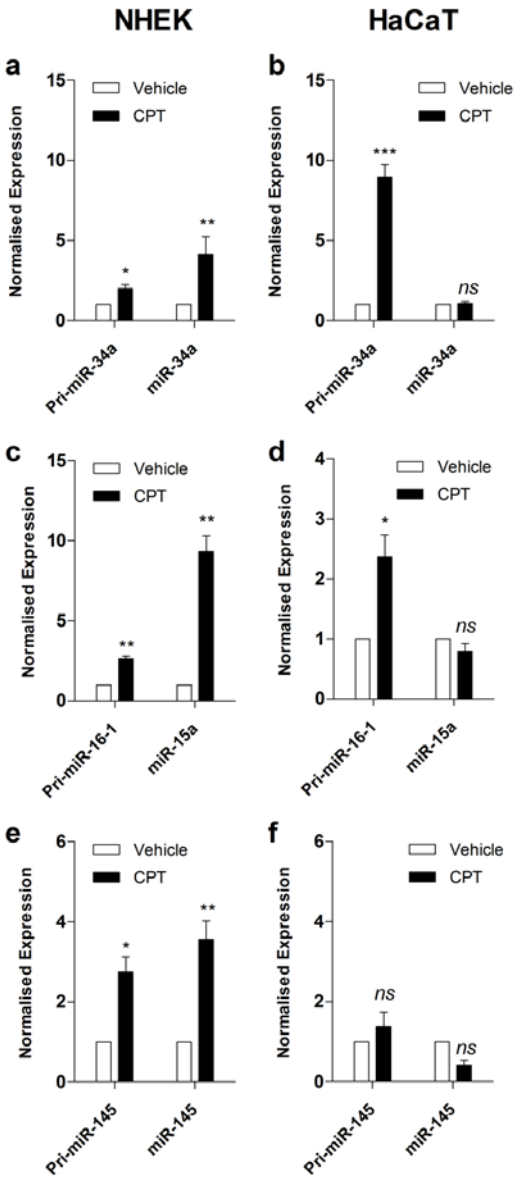


*Figure 5:3 Camptothecin-induced microRNA maturation is impaired in p53-mutated keratinocytes*

Apoptosis was induced in primary (NHEK, left panels) and p53-mutated (HaCaT, right panels) keratinocytes using 5 µM camptothecin (CPT) for 24 hours. Total RNA was extracted for RT-PCR analysis of microRNA sequences for miR-34a (Panels **a** & **b**), miR-16-1/miR-15a (Panels **c** & **d**), and miR-145 (Panels **e** & **f**) expression. For microRNA analysis, primers which were specific for either primary or mature sequences were used for reverse transcription and Taqman PCR assays. RN18S1 and U6 snoRNA were used as reference genes for pri-miRNA and microRNA assays, respectively.

All data represent mean ± SD of 3 independent experiments. Results significantly different from vehicle are represented as *, ** and ***; with $p < 0.05$, $p < 0.01$ and $p < 0.001$ respectively.

CPT significantly up-regulated expression of the primary transcript (pri-miR-16-1) in both cell cultures, however although the mature sequence (miR-15a) was significantly up-regulated in NHEKs [Figure 5:3 (c)], miR-15a was down-regulated in CPT-treated HaCaTs [Figure 5:3 (d)]. Additionally, although expression of the c-Myc targeting microRNA, miR-145, was up-regulated 4-fold by CPT in NHEKs, miR-145 was down-regulated in apoptotic HaCaTs [Figure 5:3 (e & f)]. These data correlate with aberrant expression of anti-apoptotic microRNA targets during CPT treatment in the p53-mutated cell line [Figure 5:2].

To further explore the relationship between p53 levels with respect to apoptotic sensitivity in these keratiniocytes, Nutlin-3a was used to block MDM2-mediated proteasomal targeting, and hence degradation of the p53 protein. p53 accumulated 4-fold in NHEKs treated with 10 µM Nutlin-3a for 24 hr [Figure 5:4 (a); $p < 0.001$; $n=3$], but no change in p53 content was achieved by Nutlin-3a treatment in the HaCaT cell line [Figure 5:4 (b)]. Notably, the 3.5-fold increase in p53 expression with Nutlin-3a treatment in NHEKs brings cellular p53 content to a level which correlates more closely with the cellular content of p53 protein measured in untreated HaCaT cells. When apoptosis was induced in NHEK and HaCaT cells following 30 min pretreatment with Nutlin-3a using CPT, p53 protein accumulated 5-fold in CPT-treated NHEKs [Figure 5:4 (a), $p<0.001$], however no significant change in p53 protein or acetylation was measured in CPT-treated HaCaTs [Figure 5:4 (b, d)]. This Nutlin-3a-induced increase in p53 protein was not associated with a change in acetylation of lysine 382 relative to total p53 protein content in NHEKs [Figure 5:4 (c)] or HaCaT cells [Figure 5:4 (d)].

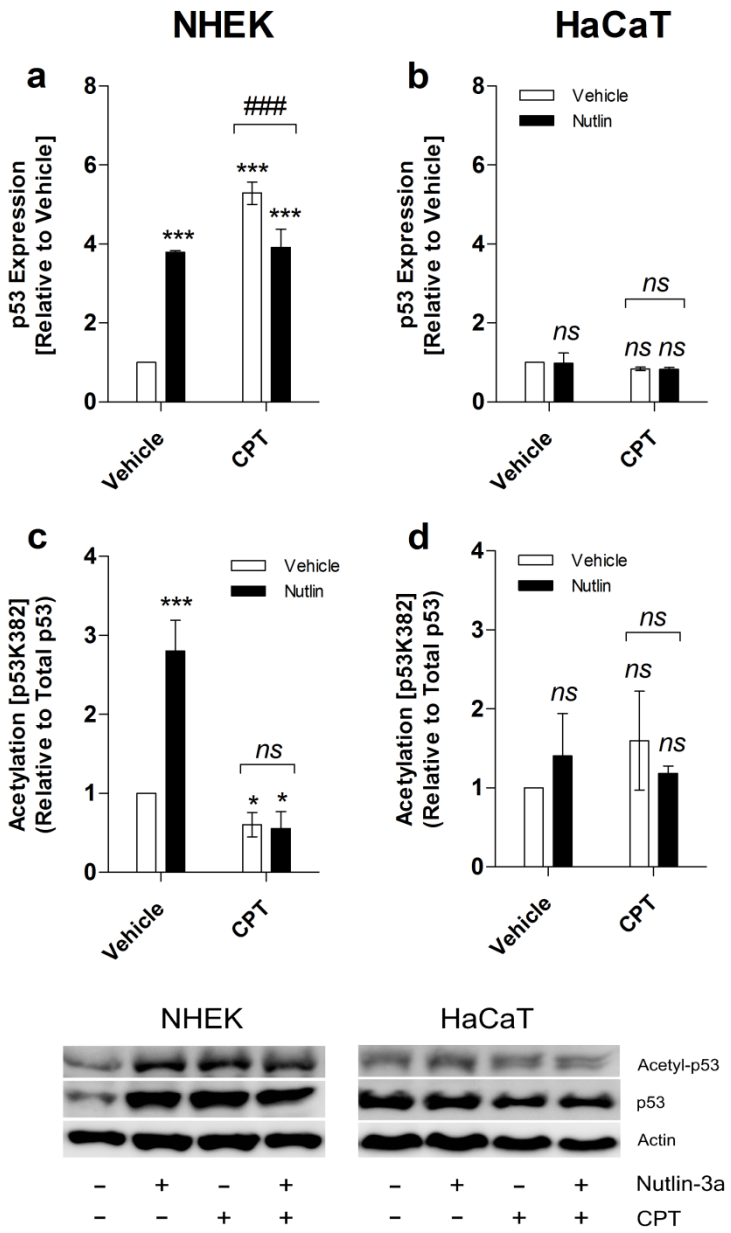


*Figure 5:4 Keratinocytes with p53 mutations are unresponsive to Nutlin-3a treatment*

P53 was stabilised in primary (NHEK, left panels) and p53-mutated (HaCaT, right panels) keratinocytes with 10 µM Nutlin-3a, and apoptosis was induced with 5 µM camptothecin (CPT) for 24 hrs. p53 expression and PARP (full length and cleaved) were detected by immunoblotting. Acetylated p53 (K382) (Panels **a** & **b**) and total p53 protein (Panels **c** & **d**) were analysed relative to vehicle controls, using actin to normalise protein loading.

All data represent mean ± SD of 3 independent experiments. Results significantly different from vehicle are represented as * ($p < 0.05$); *** ($p < 0.001$). Nutlin treatment-specific differences are expressed as ns (not significant), and ### ($p < 0.001$).

Moreover, Nutlin-3a treatment did not significantly alter CPT-induced PARP cleavage for either cell line [Figure 5:5 (a, b)]. So whilst CPT treatment triggers p53-dependent apoptosis for keratinocytes bearing either wild-type or p53 mutations, improving sensitivity of p53-mediated functional responses to DNA damage requires more than a stabilization of p53 protein. Furthermore, mutated p53 protein in HaCaT keratinocytes is resistant to MDM2-mediated proteasomal targeting, and hence Nutlin-3a is ineffective for recovering p53 functional responses in this cell line.

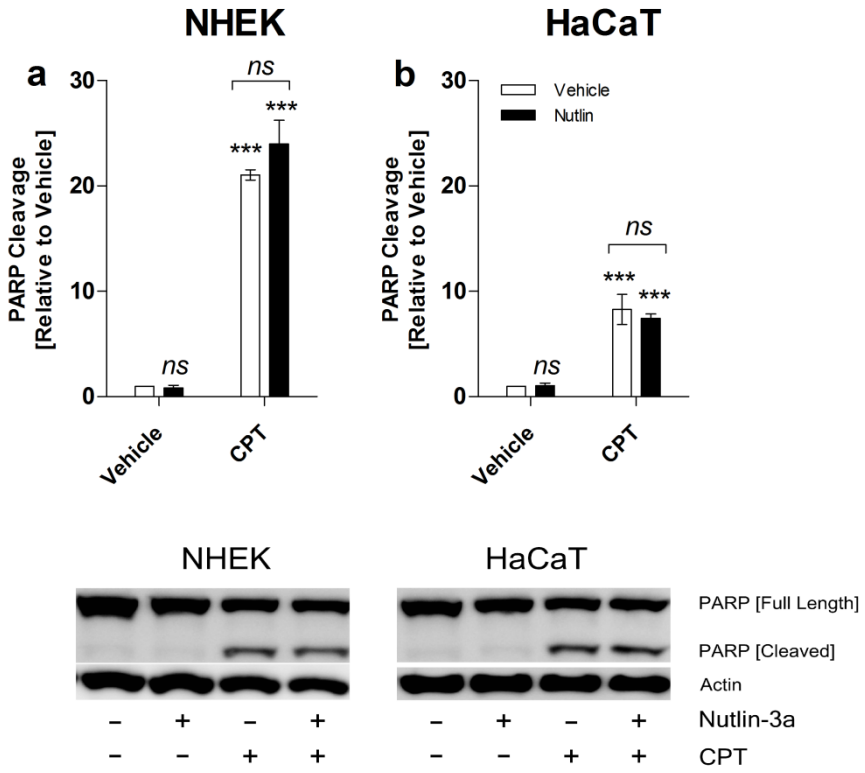


*Figure 5:5 Nutlin-3a treatment does not alter PARP cleavage in camptothecin-treated keratinocytes*

P53 was stabilised in primary (NHEK, Panel **a**) and p53-mutated (HaCaT, Panel **b**) keratinocytes with 10 µM Nutlin-3a, and apoptosis was induced with 5 µM camptothecin (CPT) for 24 hrs. PARP (full length and cleaved) were detected by immunoblotting and analysed relative to vehicle controls, using actin to normalise protein loading.

All data represent mean ± SD of 3 independent experiments. PARP cleavage was determined by dividing the densitometric signal from the cleaved fraction by total PARP expression (full length + cleaved PARP). Results significantly different from vehicle are represented as *** ($p < 0.001$). Nutlin treatment-specific differences are expressed as ns (not significant).

The intended pharmaceutical use for Nutlin 3a treatment is to act as an adjuvant in chemotherapy by increasing cellular p53 activity (488). Notably, the efficacy of Nutlin-3a depends on the nature of the gene lesion targeted – *in vitro* and *ex vivo* studies demonstrate that retention of some wild-type p53 activity is required for Nutlin-3a to enhance apoptosis in cancer cells (489, 492). Additionally, the outcome of Nutlin-3a treatment on p53-mediated responses is dependent on treatment concentration and duration of exposure, as well as p53 gene status. Whilst the concentration used here (10 μM) was greater than the dose sufficient to increase p53 content and to induce cell cycle arrest in RKO and LNCaP cell lines, a higher concentration (20 μM) is required to induce apoptosis (520), and thus it is possible that the dose and duration of exposure to Nutlin-3a in this study failed to lower the apoptotic threshold in HaCaT cells. However, considering that p53 expression is unresponsive to CPT in this cell line, it is more likely that overexpression of mutant p53 in HaCaTs prevents Nutlin-3a from having any pro-apoptotic effect.

We next considered whether manipulating SIRT1 expression levels could alter apoptotic sensitivity. Since regulation of SIRT1 expression is impaired in HaCaTs, RNAi was used to determine the relationship between SIRT1 and apoptotic signaling in this cell line. p53 expression was suppressed and acetylation increased slightly [1.5-fold; Figure 5:6 (a & b), $p<0.05$] when SIRT1 was ablated in HaCaTs [Figure 5:6 (c)]. When SIRT1-ablated HaCaT cells were treated with CPT, p53 protein decreased further, however relative acetylation was not altered [Figure 5:6 (a, b)], and no change in PARP cleavage was measured [Figure 5:6 (d)].

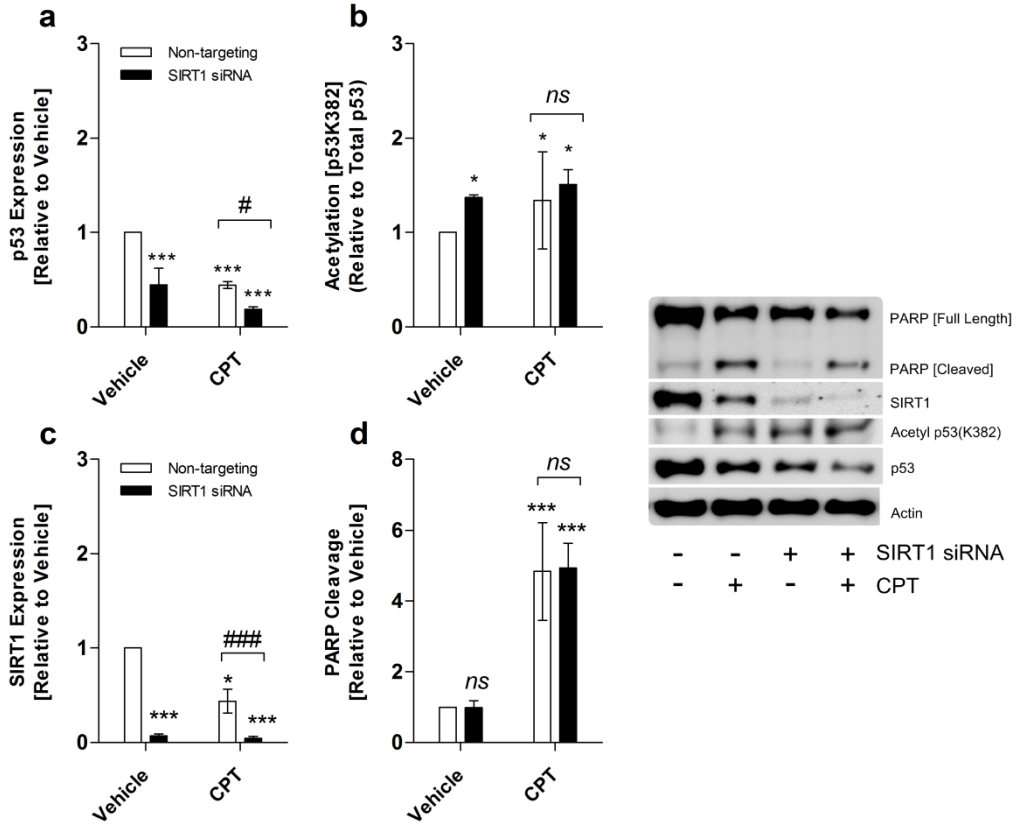


*Figure 5:6 SIRT1 knockdown is insufficient to overcome apoptotic resistance in keratinocytes with p53 mutations*

SIRT1 expression was transiently ablated in HaCaT keratinocytes using SIRT1 siRNA oligonucleotides (black bars) for 48 hr prior to induction of apoptosis with 5 µM camptothecin (CPT). p53 expression, p53 acetylation, SIRT1 expression and PARP (full length and cleaved) were detected by immunoblotting. Total p53 protein (Panel **a**), p53 acetylated at lysine 382 [p53K382] (Panel **b**), SIRT1 protein (Panel **c**) and PARP cleavage (Panel **d**) were analysed relative to vehicle controls, using actin to normalise protein loading.

All data represent mean ± SD of 3 independent experiments. PARP cleavage was determined by dividing the densitometric signal from the cleaved fraction by total PARP expression (full length + cleaved PARP). Results significantly different from vehicle are represented as * and ***; with $p < 0.05$ and $p < 0.001$ respectively. The effect of SIRT1 knockdown on CPT-treated samples was analysed relative to treatment with non-targeting control oligonucleotides by 2-way ANOVA and is expressed as *ns* (not significant), # ($p < 0.05$), and ### ($p < 0.001$).

To investigate the relationship between miR-34a-mediated regulation of SIRT1 expression and apoptotic resistance in keratinocytes, oligonucleotides were designed to specifically block the miR-34a targeting site within the SIRT1 3'UTR.

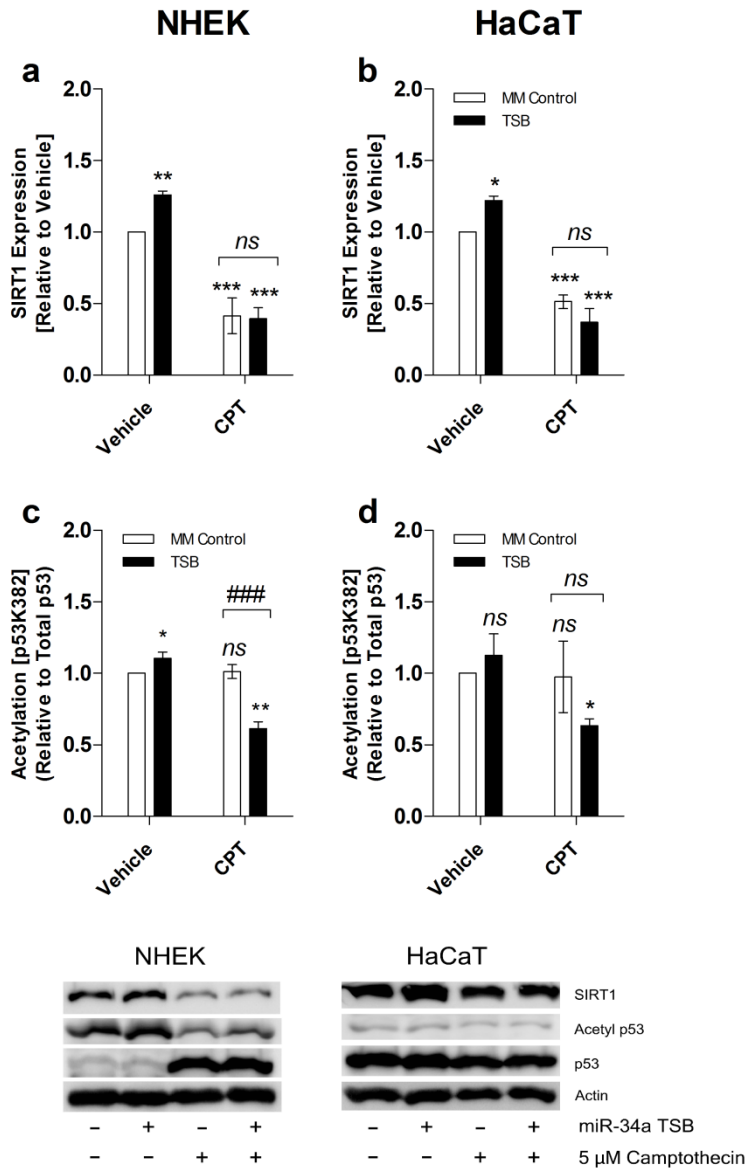


*Figure 5:7 SIRT1 protein expression is regulated by miR-34a in human keratinocytes*

Primary (NHEK, left panels) and p53-mutated (HaCaT, right panels) keratinocytes were transfected with oligonucleotides designed to mask the SIRT1/miR-34a target site (TSB, black bars) for 48 hr, after which apoptosis was induced with 5 µM camptothecin (CPT). SIRT1 expression (Panels **a** & **b**), and acetylation of p53 at lysine 382 (Panels **c** & **d**) was assayed by immunoblotting and analysed relative to vehicle control samples, using actin to normalise protein loading.

All data represent mean ± SD of 3 independent experiments. Results significantly different from vehicle are represented as *, ** and ***; with $p < 0.05$, $p < 0.01$ and $p < 0.001$ respectively. The effect of target site masking on CPT-treated samples was analysed relative to the mismatched control treatment by 2-way ANOVA and is expressed as *ns* (not significant), and ### ($p < 0.001$).

Cellular SIRT1 protein accumulated following a miR-34a target site block for both NHEK and HaCaT cells [Figure 5:7 (a, b); $p<0.05$], confirming that miR-34a post-transcriptionally regulates SIRT1 expression in wild-type and p53-mutated keratinocytes. SIRT1 was suppressed in CPT-treated NHEKs and HaCaTs, however SIRT1 did not accumulate when the miR-34a targeting site was blocked prior to CPT treatment [Figure 5:7 (a, b)].

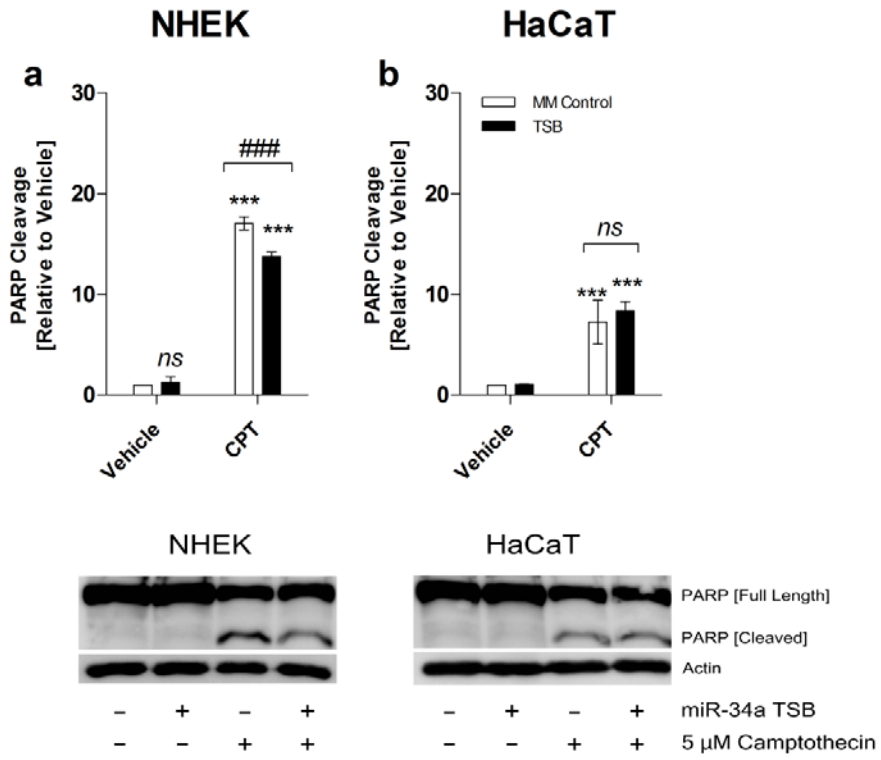


*Figure 5:8 miR-34a/SIRT1 mRNA target site block reduces apoptotic sensitivity in normal, but not p53-mutated keratinocytes*

The SIRT1/miR-34a target site was blocked in primary (NHEK, Panel **a**) and p53-mutated (HaCaT, Panel **b**) keratinocytes with target site blocking oligonucleotides (TSB, black bars) or mis-matched control oligonucleotides (MM control, white bars) for 48 hr, after which apoptosis was induced with 5 µM camptothecin (CPT). Immunoblots were prepared using anti-SIRT1 and anti-PARP1 antibodies, using actin to normalise protein loading.

All data represent mean ± SD of 3 independent experiments. PARP cleavage was determined by dividing the densitometric signal from the cleaved fraction by total PARP expression (full length + cleaved PARP). Results significantly different from vehicle are represented as ***; with $p < 0.001$. The effect of target site masking on CPT-treated samples was analysed relative to the mismatched control treatment by 2-way ANOVA and is expressed as *ns* (not significant), and ### ($p < 0.001$).

Although relative p53 acetylation was suppressed after 24 hours of CPT treatment in NHEKs [Figure 5:7 (c); $p<0.01$], no change in acetylation was measured in CPT-treated HaCaTs [Figure 5:7 (d)]. Additionally, the target site block did not produce a significant change in acetylation in CPT-induced NHEKs, however PARP cleavage decreased [Figure 5:8 (a); $p<0.001$]. No change in PARP cleavage was measured in the HaCaT cell line after a target site block [Figure 5:8 (b)].

### *SIRT1 inhibition overcomes apoptotic resistance in p53-mutated keratinocytes*

Because neither depletion of SIRT1 by RNAi nor the miR-34a/SIRT1 mRNA target site block were sufficient to influence p53-mediated apoptotic resistance in the HaCaT cell line, we lastly asked if inhibition of SIRT1 activity with EX-527 would increase apoptotic sensitivity. p53 acetylation was increased by 24 hr EX-527 treatment in both cell lines [Figure 5:9 (a, b); $p<0.01$].

Note that in the analysis, values for p53 acetylation are calculated relative to a measurement of total p53 in cells with each treatment. Thus, whilst p53 protein accumulated in CPT-treated NHEKs [Figure 5:9 (c); $p<0.01$], no change was detected for HaCaTs during CPT treatment [Figure 5:9 (d)] and EX-527 has increased the fraction of acetylated p53 in CPT treated HaCaT cells without increasing total protein. Conversely, EX-527 also increases p53 acetylation in NHEKs, however because total p53 protein is up-regulated during CPT treatment, the acetylated fraction (as calculated) remains unchanged.

To determine if EX-527-mediated changes in p53 acetylation influenced CPT-induced apoptosis, we assessed CPT- and EX-527-treated NHEK and HaCaT cells using markers of apoptosis (caspase 3/7 activity, PARP cleavage) and cell viability (ATP content).

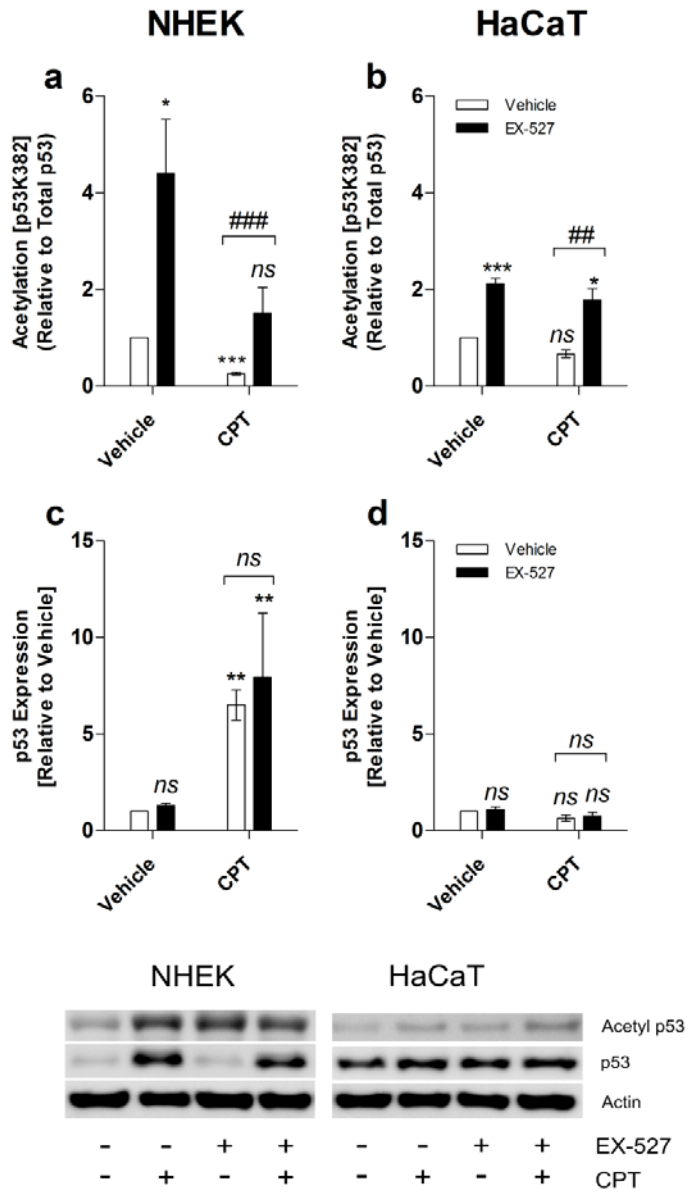


*Figure 5:9 p53 acetylation is enhanced in apoptotic p53-mutated keratinocytes*

SIRT1 was inhibited in primary (NHEK, left panels) and p53-mutated (HaCaT, right panels) keratinocytes with 1 µM EX-527, and apoptosis was induced using 5 µM camptothecin (CPT). p53 acetylated at lysine 326 and total p53 protein were detected by immunoblotting cell lysates after 24 hrs. Panels **a** & **b**: analysis of p53 acetylation; Panels **c** & **d**: analysis of total p53 protein. Protein loading was normalised using actin.

All data represent mean ± SD of 3 independent experiments. Results significantly different from vehicle are represented as *, ** and ***; with $p < 0.05$, $p < 0.01$ and $p < 0.001$ respectively. The effect of SIRT1 inhibition on CPT-treated samples was analysed relative to vehicle controls by 2-way ANOVA and is expressed as *ns* (not significant), ## ($p < 0.01$), and ### ($p < 0.001$).

In NHEK cells, CPT treatment reduced cell viability to 30% of the vehicle treated population, with no change in viability recorded during EX-527 treatment in this cell line [Figure 5:10 (a); $p<0.001$]. For HaCaTs, however, viability of CPT-treated cells was halved by inhibition of SIRT1 [Figure 5:10 (b); $p<0.001$].

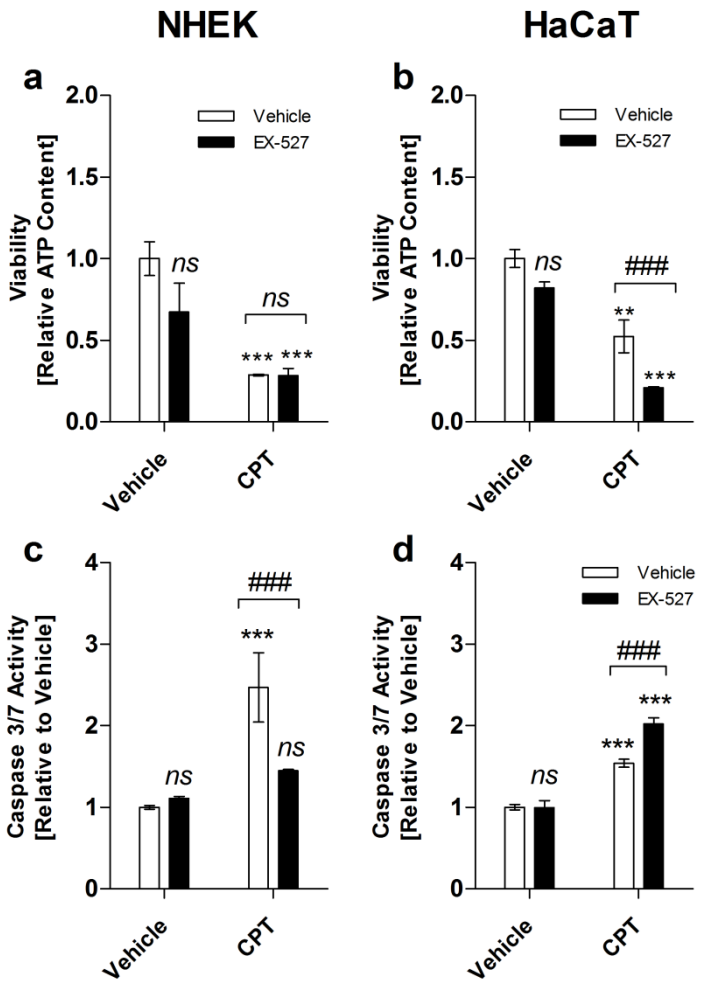


*Figure 5:10 SIRT1 inhibition overcomes apoptotic resistance in p53-mutated keratinocytes*

SIRT1 was inhibited in primary (NHEK, left panels) and p53-mutated (HaCaT, right panels) keratinocytes with 1 µM EX-527, and apoptosis was induced using 5 µM camptothecin (CPT). Viability (ATP Content) (Panels **a** & **b**), and Caspase 3/7 activity (Panels **c** & **d**) were assayed after 24 hrs.

All data represent mean ± SD of 4 independent experiments. Results significantly different from vehicle are represented as *, ** and ***; with $p < 0.05$, $p < 0.01$ and $p < 0.001$ respectively. The effect of SIRT1 inhibition on CPT-treated samples was analysed relative to vehicle controls by 2-way ANOVA and is expressed as *ns* (not significant), and ### ($p < 0.001$).

Although cell death was not altered by SIRT1 inhibition alone, caspase 3/7 activity doubled in NHEKs after CPT treatment [Figure 5:10 (c); $p<0.001$]. Additionally, a slight, but statistically significant increase in caspase 3/7 activity was observed for SIRT1-inhibited, CPT-treated HaCaTs [Figure 5:10 (d); $p<0.001$]. Consistent with these results, PARP cleavage doubled in SIRT1-inhibited HaCaT cells after 24 hours of CPT [Figure 5:11 (b); $p<0.001$], and was halved in similarly treated NHEK cells [Figure 5:11 (a); $p<0.01$].

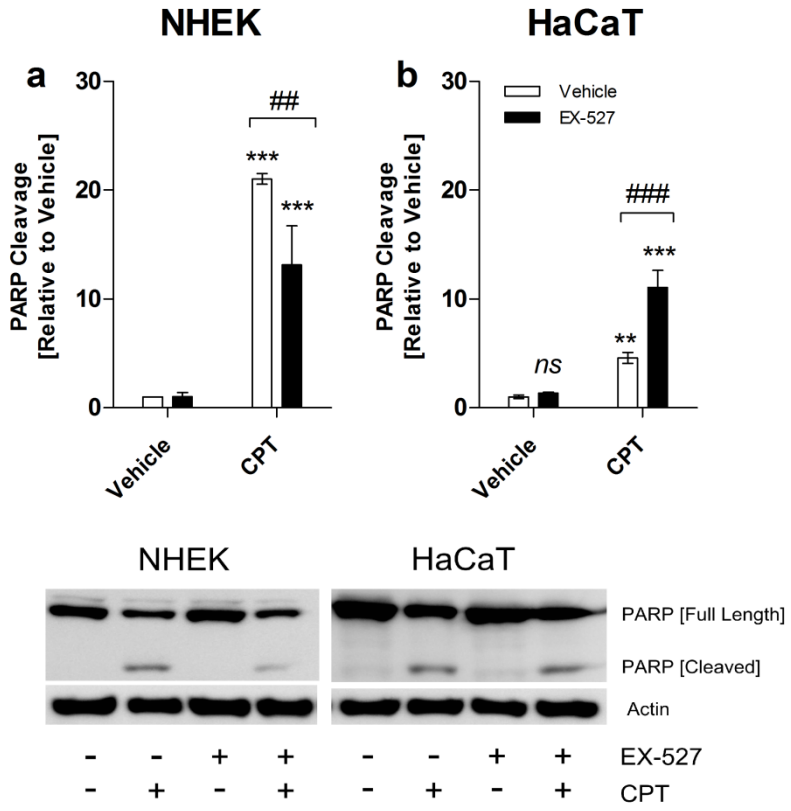


*Figure 5:11 SIRT1 inhibition restores p53-dependent cell death in p53-mutated keratinocytes*

SIRT1 was inhibited in primary (NHEK, Panel a) and p53-mutated (HaCaT, Panel **b**) keratinocytes with 1 µM EX-527, and apoptosis was induced using 5 µM camptothecin (CPT). PARP (full length and cleaved) was assayed after 24 hrs.

All data represent mean ± SD of 3 independent experiments. PARP cleavage was determined by dividing the densitometric signal from the cleaved fraction by total PARP expression (full length + cleaved PARP). Results significantly different from vehicle are represented as *, ** and ***; with $p < 0.05$, $p < 0.01$ and $p < 0.001$ respectively. The effect of SIRT1 inhibition on CPT-treated samples was analysed relative to vehicle controls by 2-way ANOVA and is expressed as *ns* (not significant), ## ($p < 0.01$), and ### ($p < 0.001$).

Collectively, these data indicate that inhibition of SIRT1 modulates cell death signalling in a p53-dependent manner, and preferentially promotes apoptosis in keratinocytes with p53 mutations.

## 5.4 DISCUSSION

HaCaT keratinocytes bear compound heterozygous mutations in each p53 allele which alters the activity and expression of p53 protein without complete loss of function (430, 431). Loss of a single functional p53 allele reduces cellular tumour suppressor capacity (73), and additionally, TP53 gain-of-function mutations (such as those found in HaCaT cells) can generate a phenotype with unique stress responses which promote carcinogenesis (521). By manipulating the activity and expression of p53 in the HaCaT cell line, we were able to uncover conditions by which this phenotype can be targeted to promote cell death in a differential manner. Apoptotic sensitivity was enhanced in HaCaT keratinocytes by increasing p53 acetylation through inhibition of SIRT1 activity (EX-527); but not by p53 or SIRT1 ablation (RNAi), blocking miR-34a-mediated regulation of SIRT1 (miR-34a TSB), or by stabilising cellular p53 protein (Nutlin-3a).

This study provides a mechanistic link between characteristic UV-induced p53 mutations, miR-34a insufficiency, and impaired regulation of SIRT1 expression in the skin. Increased SIRT1 expression is common in non-melanoma skin cancer (522). Consistent with this observation, SIRT1 protein accumulates in HaCaT keratinocytes as a consequence of failed miR-34a-mediated repression of SIRT1 at the translational level, culminating in reduced p53 acetylation and resistance to p53-dependent apoptosis [Figure 5:12]. Thus inhibition of SIRT1 in this cell line restores apoptotic sensitivity by partially overcoming the effects of miR-34a insufficiency. Together, these data indicate that p53 mutations contribute to apoptotic resistance in HaCaT keratinocytes by altering the regulatory capacity of the p53/SIRT1/miR-34a axis during apoptotic signaling. Whether this is a mechanism common to all keratinocytes with p53 mutations is yet to be determined, but the frequent occurrence of UV-induced p53 mutations and increased SIRT1 expression in skin cancers suggests it is likely to be widespread. Furthermore, low constitutive expression of miR-34a in p53-mutated keratinocytes supports the potential value of

miR-34a as a prognostic marker for skin cancer diagnosis and therapeutic monitoring (523).

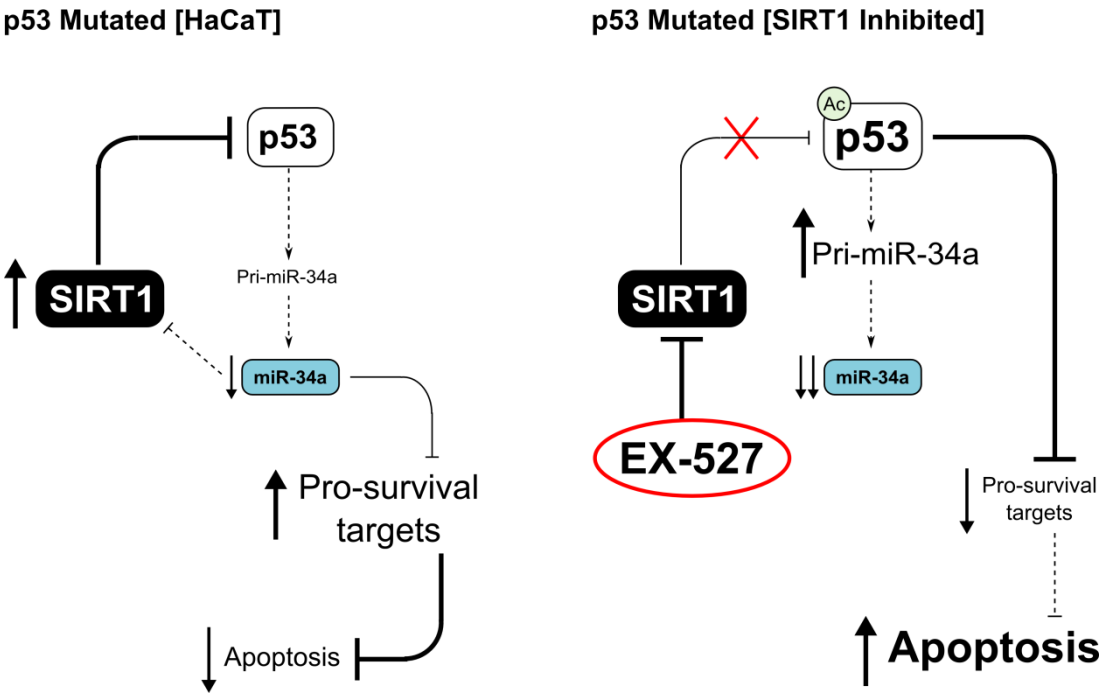


*Figure 5:12 EX-527 promotes p53-dependent apoptotic signalling in HaCaT keratinocytes*

SIRT1 accumulates in p53 mutated keratinocytes as a consequence of impaired miR-34a-mediated feedback regulation. Overexpression of SIRT1 and pro-survival proteins contributes to apoptotic resistance by suppressing p53 acetylation and inhibiting cell death signalling.

p53 acetylation is promoted in p53-mutated keratinocytes when SIRT1 is inhibited, enabling suppression of anti-apoptotic gene targets. Together, these changes restore sensitivity to CPT-induced cell death in the p53-mutated cell line.

Results from this study show that microRNA-mediated regulation of programmed cell death is altered in the HaCaT cell line. Induction of miR-34a, miR-16-1/15a and miR-145 during p53-dependent apoptotic signalling is suppressed in p53-mutated keratinocytes, and this has consequences for regulatory control of mRNA targets. Specifically, down-regulation of Survivin and BCL-2 during apoptosis is dependent on normal p53 activity. Aberrant microRNA expression is widespread in primary tumours, and is attributed to impaired post-transcriptional regulation of the

primary sequence (508, 524). We have previously found that p53 regulates biogenesis and maturation of microRNAs which have key downstream functions in p53-mediated signalling, and p53 mutations in HaCaTs interfere with this process (466). P53 modulates microRNA biogenesis by associating with the RNA helicase p68, which facilitates processing of the primary transcript by Drosha (150). In cells with mutant p53, formation of the Drosha complex is impeded, blocking processing of the primary microRNA transcript (152). Additionally, mutant p53 directly binds to and inactivates p63, inhibiting Dicer-1 expression and microRNA maturation (496). Basal and squamous cell carcinomas develop significant changes to the keratinocyte microRNA expression profile (525-527). Our results indicate that impairments to microRNA expression and target regulation in keratinocytes are driven by the dysregulating effect of p53 mutations on microRNA biogenesis and processing, and occur at the premalignant stage of carcinogenesis.

Exploitation of the mutational status of p53 in cancer has been an ongoing chemotherapeutic strategy for many years. Loss of a single functional p53 allele reduces cellular tumour suppressor capacity (73), and can generate a phenotype with unique stress responses which promote carcinogenesis (521). Numerous options, including gene-based therapy, manipulation of p53 expression by disruption of the p53-MDM2 axis, and reactivation of mutant p53 have been proposed as a means for restoring apoptotic sensitivity in chemotherapy (89, 490). Nutlin-3a is most effective when used in combination with inhibitors of S and M phase entry for selective targeting of cells with insufficient p53. However, as our results have demonstrated [Figure 5:1 (a & b)], p53 is overexpressed and underacetylated in the HaCaT cell line, indicating that p53 activity is suppressed. Moreover, although induction of MDM2 in the HaCaT cell line is sufficient to decrease p53 expression (528), our results show that HaCaT keratinocytes are resistant to MDM2 inhibition, and consequently Nutlin-3a does not promote cytotoxicity in these cells.

Early results from clinical trials indicate that a combinatorial approach is required for chemotherapy to effectively overcome p53 inactivating mutations (86, 96). Aside from loss-of function effects, p53 mutations increase protein stability and cause gain-of–function effects which increase resistance to p53-based therapeutic agents (75, 529), and hence reactivation of mutant p53 function has emerged as a strategy for improving the efficacy of traditional chemotherapy (530). In cells with heterozygous p53 mutations such as the HaCaT cell line, mutant p53 can have a dominant-negative effect on any non-mutated functional p53 within the cell by forming functionally inactive aggregates which inhibit DNA binding (80-82). Additionally, p53 mutations can produce a gain-of-function phenotype which results from the co-association of mutant p53 with other p53 regulatory proteins such as p63, p73 and the acetyltransferase p300 (531). This process is particularly problematic for cells exposed to genotoxic stress, during which p53 protein accumulates and tetramerisation increases exponentially (42). Current strategies developed to overcome dominant-negative and gain-of-function effects of p53 include stimulation of p53 degradation pathways, siRNA-mediated ablation of mutant p53 protein, blocking co-association with effector proteins, and reactivation of mutant p53 by restoration of wild-type function (82, 91, 92). Importantly, the efficacy of these approaches is highly variable because the dominant-negative effect of mutant p53 depends on its propensity to inactivate circulating wild-type p53, and this is directly related to the site of mutation (93).

Histone deacetylase (HDAC) inhibitors have recently been suggested as adjuvants for p53-based chemotherapy (532). Of the numerous HDAC-targeting therapies, only HDAC Class III (SIRT1) inhibitors, such as Tenovin-1 are exclusively p53-dependent (207). EX-527 is a SIRT1 inhibitor which induces conformational remodelling in the SIRT1 catalytic domain, and which inhibits enzyme activity by blocking substrate release (229). As a consequence of its p53 mutations, HaCaT cells express a mixture of p53 subtypes with functional anomalies affecting protein stability and transcriptional activation. However, some p53-dependent activity is

still retained in this cell line, albeit at highly suppressed levels. Based on its inhibitory mechanism, we postulate that EX-527 may trap mutant p53 in HaCaT keratinocytes by preventing its release from the catalytic domain of SIRT1. Removing a proportion of mutant p53 from circulation may relieve its dominant negative effect, and enable p53 to become transcriptionally active. This mechanism may also explain the discrepancy between the ability of EX-527 to increase apoptotic sensitivity in HaCaT cells, compared to the inability of SIRT1 knockdown to improve apoptotic sensitivity for HaCaTs .

p53 mutations in keratinocytes attenuate p53-dependent stress responses by blunting functional control of the p53/SIRT1/miR-34a axis. Defective miR-34a processing has widespread implications for cellular processes regulated by SIRT1 activity, there is some evidence that inhibiting SIRT1 sensitises pre-cancerous cells to apoptosis (533). Although loss of miR-34a alone does not appear to be oncogenic (534), impaired miR-34a-mediated regulation of p53 responses appears to be a hurdle which must be overcome to promote the efficacy of p53-based chemotherapy. Our results have wider chemotherapeutic potential as a treatment strategy in skin cancer. Up-regulation of cellular SIRT1 expression and inhibition of miR-34a processing in keratinocytes with p53 mutations causes apoptotic resistance and attenuation of p53-dependent stress responses when compared to wild-type cells. These changes may be overcome, in part, by synthetic SIRT1 inhibitors. By manipulating the activity of p53 with EX-527 in the HaCaT cell line, we were able to uncover conditions by which this phenotype can be targeted to promote cell death in a p53-dependent manner. Results from this investigation demonstrate the need for further investigation to explore the value of SIRT1 inhibition in the design of targeted chemotherapeutic regimens in tumours with p53-mutated genotypes.

# Chapter 6 -
# Sodium Arsenite Modulates Histone Acetylation at the miR-34a Gene Promoter

## 6.1 ABSTRACT

Expression of the histone deacetylase SIRT1 is altered in solid tumours and haematological malignancies; however its role in arsenic-induced pathology is unknown. In this investigation, the effect of arsenic on epigenetic regulation of the histone deacetylase SIRT1, and its targeting microRNA, miR-34a, was monitored in primary (NHEK) and p53-mutated (HaCaT) human keratinocytes. Arsenic produced dose-dependent responses in NHEK and HaCaT cells, increasing metabolic activity at concentrations ≤ 5 μM and causing cell death at higher concentrations. In NHEK cells, these changes were associated with concomitant shifts in SIRT1 expression and acetylation of histone H4 at lysine 16 (H4K16) and after 24 hours, 0.5 μM arsenic increased p53 and SIRT1 occupancy at *SIRT1* and *miR-34a* gene promoters and chromatin remodelling at the miR-34a gene. HaCaT keratinocytes, however, were resistant to arsenic-induced toxicity and did not display H4K16 acetylation changes or p53 recruitment at gene promoter regions after arsenic treatment.

Here we show that arsenic alters epigenetic regulation of SIRT1 expression in NHEK cells by modulation of SIRT1 activity and structural reorganisation of the chromatin at the miR-34a gene promoter. Conversely, HaCaT keratinocytes are resistant to arsenic toxicity, and appear to have altered structural organisation of the chromatin at gene promoters. Taken together, this investigation demonstrates that arsenic modulates SIRT1-mediated responses to cellular stress in human keratinocytes.

## 6.2 INTRODUCTION

Investigations within the past decade have demonstrated that arsenic influences the pattern of histone acetylation, methylation and phosphorylation in exposed cells, and these changes are associated with altered gene expression (535). These studies indicate that arsenic toxicity disrupts the regulatory function of chromatin remodelling complexes, and specifically, the activity of histone modifying proteins. Exposure to arsenic increases oxidative DNA damage and disrupts regulatory control over signal transduction and redox homeostasis (536). Additionally, arsenic exposure causes genomewide posttranslational histone modifications, particularly those associated with looser chromatin structures (537).

Carcinogenic changes to the epigenome can contribute to genomic instability and mutational DNA damage, and cultured cells undergo genome-wide restructuring of the epigenome with arsenic exposure. These changes appear to impair cellular stress responses such that the genotoxic damage imposed by carcinogens is enhanced, and sustained across replicative generations.

Histone deacetylases (HDACs) are particularly important regulators of chromatin conformation. Acetylation of the ε-amino group of lysine residues neutralises the positive charge of histone proteins, reducing DNA-binding affinity and loosening the chromatin structure (106, 538). This open configuration provides accessibility for transcriptional regulators at gene promoters (102, 539), and the DNA repair machinery during the DNA damage response (108). Additionally, bromodomain-binding proteins such as HDACs associate with acetylated histone lysine residues, enabling selective targeting of transcriptional regulators and chromatin remodelling complexes to gene promoter regions (119). Thus the role of HDACs is to suppress gene transcription and to promote a non-permissive/condensed conformation in chromatin by removal of histone acetyl residues (540, 541). Destablisation of chromatin causes genetic instability and increases the risk of mutational damage (542). Consequently, HDACs protect the genome against mutational damage by

establishing global chromatin environments and stabilising the structural integrity of the genome.

Acetylation and deacetylation of histone H4 at lysine 16 is a mark which is associated with genomewide changes in chromatin condensation and the patterns of transcriptional activation and repression (540, 543, 544). H4K16 is a substrate of the NAD-dependent lysine deacetylase SIRT1 (226, 261), and thus changes in the expression and activity of SIRT1 may be associated with genomewide shifts in acetylation of this mark (176, 545). Our hypothesis is that arsenic exposure induces histone posttranslational modifications by disrupting the regulatory function of SIRT1 and these changes alter cellular stress responses to arsenic toxicity by impairing regulation of tumour suppressor genes.

Arsenic-induced epigenetic changes are thought to promote the mutagenic damage which leads to carcinogenic transformation. Here, *in vitro* cell culture of non-immortalised (primary) human keratinocytes was used to investigate the epimutagenic properties of arsenic exposure. Acetylation of histone H4 and micrococcal nuclease accessibility were used as biomarkers for epigenetic effects, and expression of SIRT1 and miR-34a genes was used as an endpoint.

## 6.3 RESULTS

*Metabolic activation by sublethal arsenic exposure is affected by p53 status and SIRT1 activity.*

Assays were performed to determine the effect of short-term arsenic exposure on cellular metabolic activity in keratinocytes with wild-type p53 (NHEK), and keratinocytes bearing p53 mutations (HaCaT). The role of SIRT1 in regulating cellular responses to arsenic stress was investigated by specific inhibition of SIRT1 activity with EX-527.

Using the alamarBlue® assay as a fluorometric measure of cellular metabolic activity, we found that arsenic generates concentration-dependent toxicity in NHEK and HaCaT keratinocytes, with significant cell death occurring after exposure at higher concentrations (> 10 µM) [Figure 6:1 (a & b)]. HaCaT keratinocytes are resistant to cell death at higher arsenic concentrations, producing an $IC_{50}$ of ~60 µM As(III) after 24 hours of exposure [Figure 6:1 (b)], as opposed to an $IC_{50}$ of < 20 µM for NHEKs [Figure 6:1 (a)]. These data correlate with the $LD_{50}$ values determined for NHEK and HaCaT cells by other investigators using the MTT assay and by the Neutral Red assay (546-549). Inhibition of SIRT1 enhanced the toxicity of arsenic at higher concentrations, resulting in a lowering of the $IC_{50}$ [Figure 6:1 (a & b)]. These data indicate that SIRT1 performs a protective function in keratinocytes during cellular stress, as shown by the shift in $IC_{50}$ with EX-527 treatment.

Resozurin reduction was elevated in both cells lines when treated with arsenic at concentrations ≤ 5 µM for 24 hours [Figure 6:1 (a & b)]. When keratinocytes are exposed to sublethal concentrations of arsenic, expression of glutathione-related genes and antioxidant enzymes increase in response to reactive oxygen species production (548-551), and thus an increase in metabolic activity measured in arsenic-exposed keratinocytes during this experiment represents an increase in cellular reducing power. For the HaCaT cell line, this up-regulation of metabolic activity at submicromolar arsenic concentrations was suppressed significantly by

EX-527 treatment [Figure 6:1 (b)]. Thus it appears that in p53-mutated keratinocytes, aberrant constitutive expression of antioxidant enzymes, and overexpression of SIRT1 enhances metabolic responses to environmental toxicant exposure.

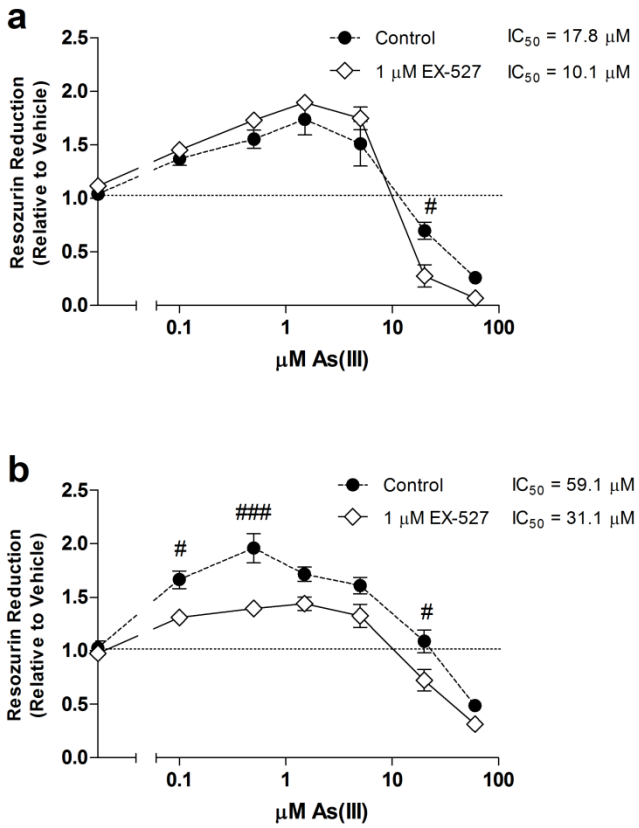


*Figure 6:1 Effect of SIRT1 on arsenic toxicity in human keratinocytes*

Primary (NHEK, Panel **a**) and p53-mutated (HaCaT, Panel **b**) keratinocytes were treated for 24 hours with arsenite [As(III)], and assayed for relative viability using resozurin reduction as a determinant of metabolic activity. SIRT1 was inhibited by treatment with 1 μM EX-527 during the 24 hr exposure period.

All data represent mean ± SD of 4 independent experiments. Cell-specific differences were analysed by 2-way ANOVA with Bonferroni post-tests, represented as # ($p$<0.05), ## ($p$<0.01), ### ($p$<001). $IC_{50}$ values were determined using non-linear regression.

These data show that cellular responses to As(III) are dose-dependent, therefore to further characterise the effect of arsenic on p53/SIRT1/miR-34a axis activity, p53 activation and expression, induction of SIRT1, and miR-34a expression was measured in arsenic-exposed keratinocytes.

### *Arsenic modulates SIRT1 and p53 gene expression in keratinocytes*

By measuring mRNA and protein expression in NHEKs exposed to a range of arsenic concentrations over a 24 hour time frame, we found that p53 expression was induced 2-fold by arsenic at submicromolar concentrations, and p53 mRNA was down-regulated in cells exposed to > 5 µM As(III) [Figure 6:2 (a)].

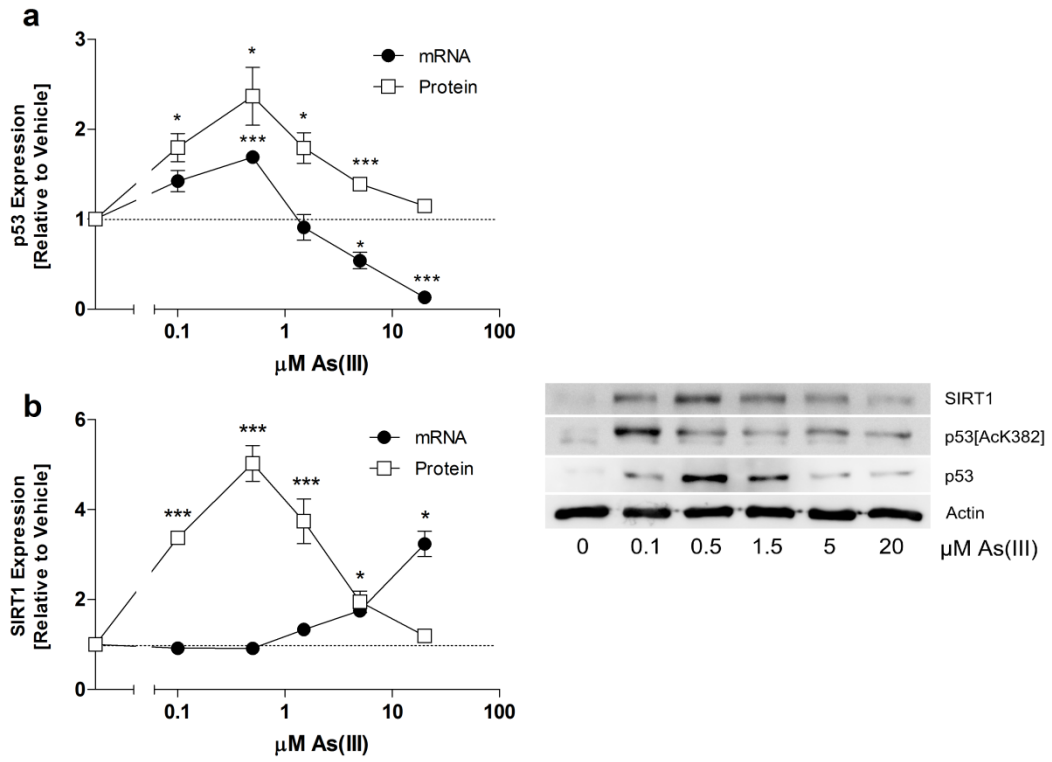


*Figure 6:2 Dose-dependent p53 and SIRT1 expression in human keratinocytes treated with arsenic*

The effect of As(III) on p53 (Panel a) and SIRT1 expression (Panel b) was detected by qRT-PCR and immunoblotting, using 5S rRNA to normalise qRT-PCR results and actin to normalise protein loading.

All data represent mean ± SD of 3 independent experiments. Results significantly different from vehicle are represented as * and ***; with $p < 0.05$ and $p < 0.001$ respectively.

Arsenic exposure increased SIRT1 protein 6-fold at sub-lethal concentrations, peaking at 0.5 µM [Figure 6:2 (b)]. SIRT1 mRNA, however, was not altered by arsenic at lower concentrations, and was up-regulated at doses ≥ 20 µM [Figure 6:2 (b)]. SIRT1 protein was not increased in NHEKs exposed to arsenic at concentrations higher than 5 µM, so based on these findings, the sublethal dose of arsenic (0.5 µM) which induced accumulation of SIRT1 protein was used for future experiments.

### *Arsenic up-regulates miR-34a gene expression in keratinocytes*

In order to fully evaluate the relationship between SIRT1 mRNA and arsenic exposure, expression of the SIRT1-targeting microRNA, miR-34a, was measured using primers targeting the precursor sequence, pri-miR-34a. Exposure to submicromolar concentrations of As(III) triggered a slight, but significant up-regulation of miR-34a after 24 hrs [Figure 6:3; $p < 0.05$], whereas treatment with > 5 µM As(III) induced > 10-fold increase in miR-34a abundance [Figure 6:3; $p < 0.001$].

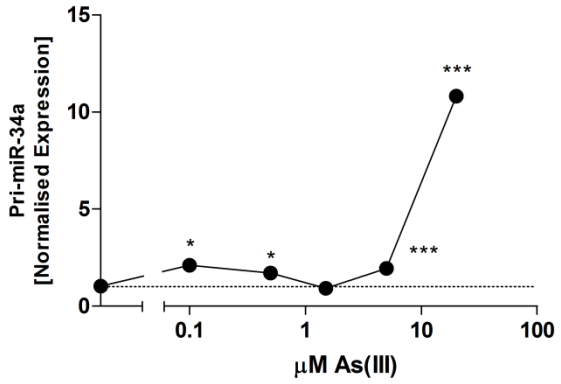


*Figure 6:3 Induction of miR-34a in human keratinocytes treated with arsenic*

Primary (NHEK) human keratinocytes were treated with arsenite [As(III)] for 24 hr. The effect of As(III) on pri-miR-34a expression was detected by qRT-PCR, using 5S rRNA and U6 snoRNA to normalise qRT-PCR results.

All data represent mean ± SD of 3 independent experiments. Results significantly different from vehicle are represented as * and ***; with $p < 0.05$ and $p < 0.001$ respectively.

Taken together, these data show that p53, SIRT1 and miR-34a (the p53/SIRT1/miR-34a axis) influence cellular responses to arsenic in a dose-dependent manner. At submicromolar concentrations, arsenic up-regulates p53, inducing a 2-fold increase in miR-34a transcription. At concentrations greater than 5 µM, a different response pattern emerges, and this is associated with cellular toxicity rather than metabolic activation. miR-34a is a well-characterised regulator of apoptotic signalling (476), and thus a 10-fold upregulation of miR-34a correlates with arsenic-induced cell death measured in toxicity assays at concentrations >5 µM [Figure 6:1 & Figure 6:3].

In oxidative conditions, SIRT1 is regulated by microRNA-targeted degradation of its mRNA (552, 553). Here we show that p53 is activated in keratinocytes exposed to arsenic in the 0.1-1 µM range, inducing a 2-fold increase in miR-34a expression. Paradoxically, SIRT1 protein accumulates in keratinocytes exposed to submicromolar concentrations of arsenic without a concomitant increase in SIRT1 mRNA. Arsenic is believed to inhibit ubiquitin E3 ligase activity (554-556), altering protein levels by interfering with targeted proteolysis (557). Consistent with this evidence, our findings suggest that sublethal concentrations (≤ 5 µM) arsenic blocks proteolytic degradation of SIRT1 in human keratinocytes.

### *Histone H4 is hyperacetylated by arsenic exposure in normal, but not p53 mutated human keratinocytes*

Next, whole cell lysates of As(III)-treated cells were analysed to determine if modulation of SIRT1 expression by arsenic influences acetylation of histone H4 at lysine 16 (H4K16) in keratinocytes.

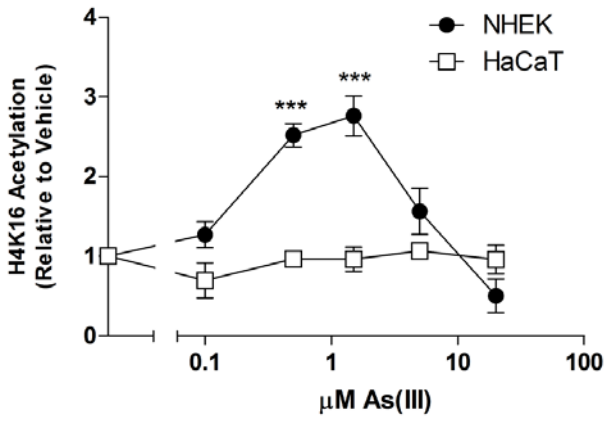


*Figure 6:4 Histone acetylation in arsenic-treated keratinocytes is p53-dependent*

Primary (NHEK) and p53-mutated (HaCaT) human keratinocytes were treated with arsenite [As(III)] and protein was extracted after 24 hours according to protocols outlined in Chapter 2. The effect of As(III) on histone H4 acetylation at lysine 16 was detected by immunoblotting. Protein loading was normalised using actin and acetylation was calculated relative to total H4 expression.

All data represent mean ± SD of 3 independent experiments. Results were analysed by 2-way ANOVA and values significantly different from untreated, passage matched controls are represented as ***; with $p < 0.001$.

Treatment with 0.5 and 1 μM As(III) increased acetylation of the SIRT1 substrate H4(K16) in NHEK cells [Figure 6:4; $p < 0.001$]. Taken with results from Figure 6.2, these data indicate that SIRT1 activity is also inhibited by arsenic exposure.

### *P53 is recruited to SIRT1 and pri-miR-34a gene promoters during arsenic exposure*

Both SIRT1 and miR-34a have p53 response elements in their gene promoters (479). In each case, the p53 response element identified in other studies was situated within upstream CpG islands (515, 558).

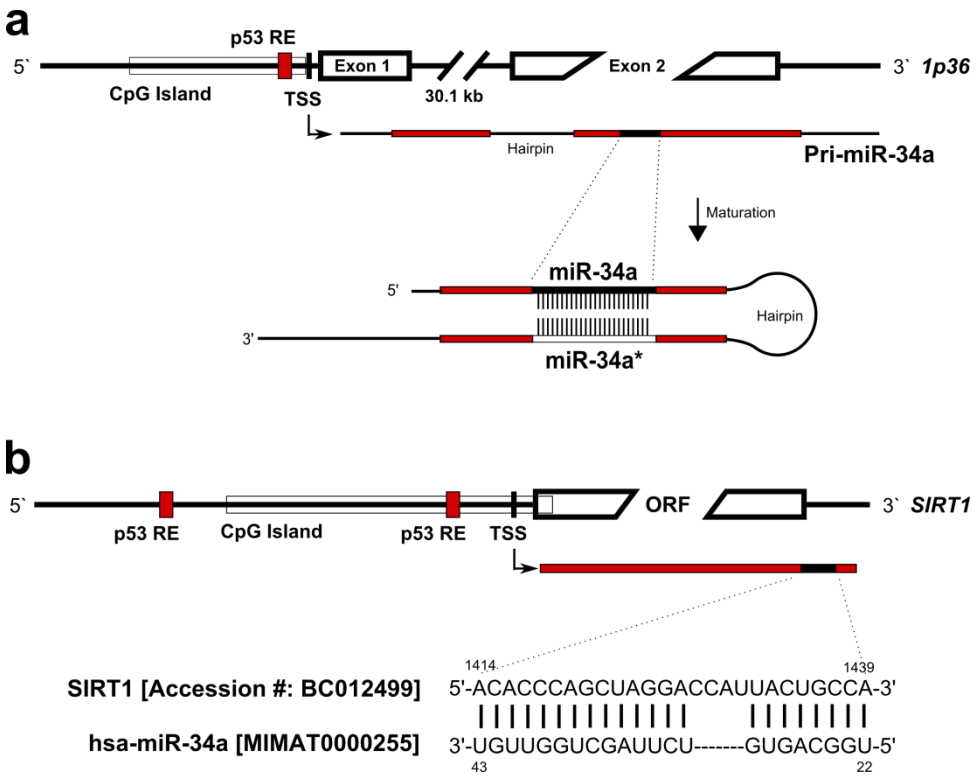


*Figure 6:5 Pri-miR-34a and SIRT1 Regulatory Features*

The Ch1p36 primary transcript (pri-miR-34a) is processed from exons 1 and 2 form to pre-miR-34a, which generates the loop-stem precursor to mature miR-34a (Panel a). Mature miR-34a inhibits translation of SIRT1 by complementary pairing to the SIRT1 primary transcript at its 3' UTR (Panel b).

These criteria were used to select suitable nucleotide sequences responsible for p53-dependent transcriptional regulation. Pri-miR-34a expression is regulated by a CpG island upstream from exon 1 which contains a p53 response element [Figure 6:5 (a)]. SIRT1 transcription is also regulated by an upstream p53 response element and a CpG island which spans the transcription start site (TSS) [Figure 6:5 (b)].

For promoter remodelling experiments, 2 loci within each gene promoter were used for analysis, and a third region was used as a control locus – upstream of the gene promoter for the miR-34a gene, and within the 3`UTR for SIRT1 [Figure 6:6].

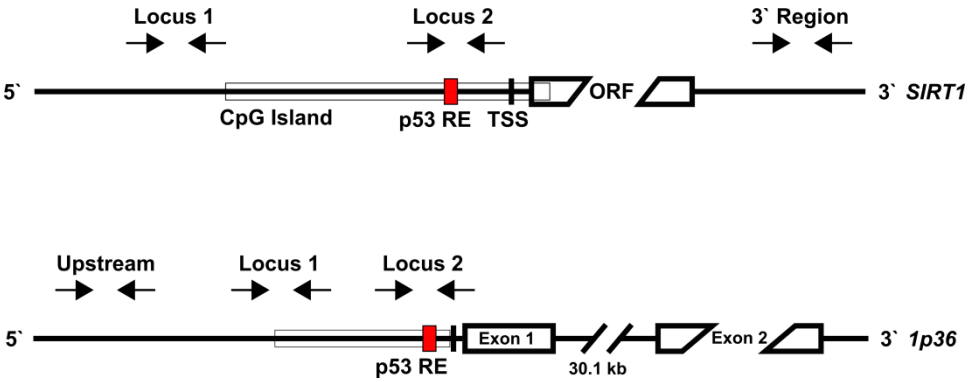


*Figure 6:6 Diagrammatic representation of gene loci for ChIP primers in SIRT1 and pri-miR-34a genes.*

NHEK and HaCaT cells were treated for 24 hours with 0.5 µM As(III) and analysed for changes in p53 binding to its target recognition sequence in SIRT1 and pri-miR-34a genes using chromatin immunoprecipitation (ChIP) coupled to RT-PCR. After 24 hrs of arsenic exposure, p53 is recruited to SIRT1 and miR-34a promoter regions in NHEK cells [Figure 6:7 (a & c)]. In the HaCaT cell line, no significant change in p53 recruitment was measured for miR-34a and SIRT1 promoter regions [Figure 6:7 (b & d)].

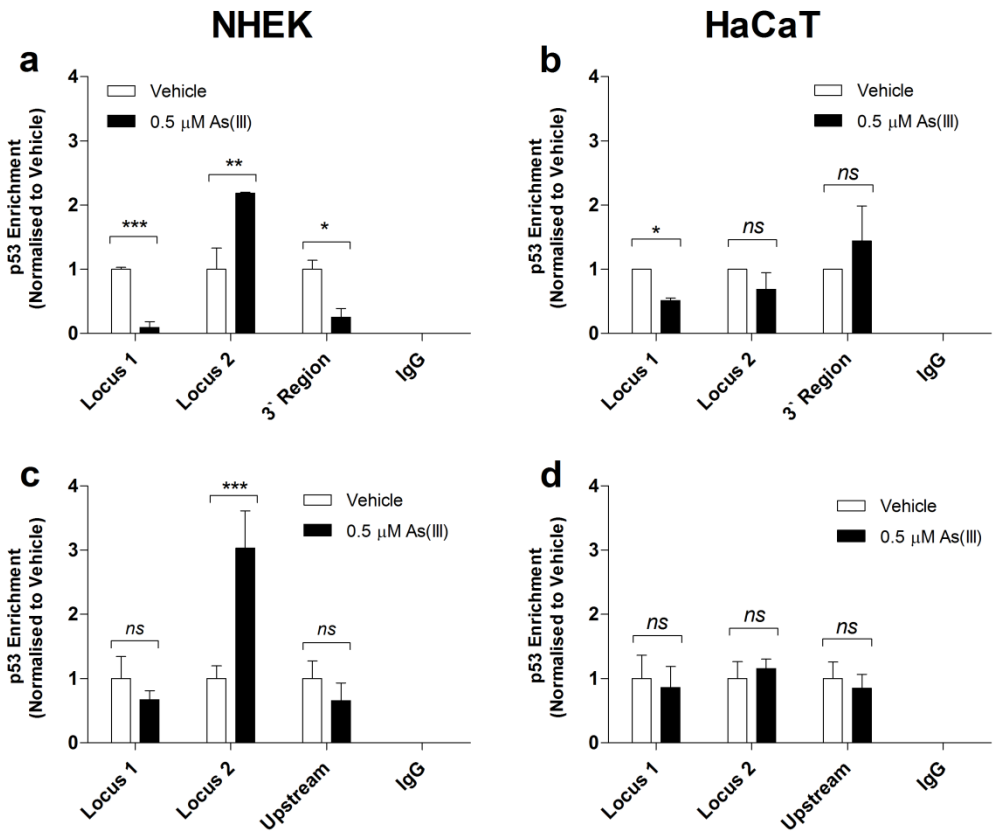


*Figure 6:7 Recruitment of p53 to SIRT1 and pri-miR-34a gene loci during arsenic exposure*

Crosslinked chromatin was isolated from normal (NHEK) and p53-mutated (HaCaT) keratinocytes treated with As(III) for 24 hrs and p53-associated chromatin was captured with antibody-bound magnetic beads. Occupancy at the SIRT1 (Panels a and b) and pri-miR-34a (Panels c and d) promoter loci was analysed by quantitative PCR relative to input DNA. Isotype matched IgG-bound beads were used as a control for immunoprecipitation, and 3' or upstream primer loci were used as PCR controls.

All data represents the mean ± SD from three independent experiments with * ($p < 0.05$), ** ($p < 0.01$) and *** ($p < 0.001$) respectively.

We have previously found that TP53 mutations in HaCaT keratinocytes generate structural and functional defects which alter responses to genotoxic stress (Chapter 5). Taken together with Chapter 5 findings, these experiments demonstrate that arsenic induces p53-mediated transcriptional activation, and this response is impaired in the HaCaT cell line.

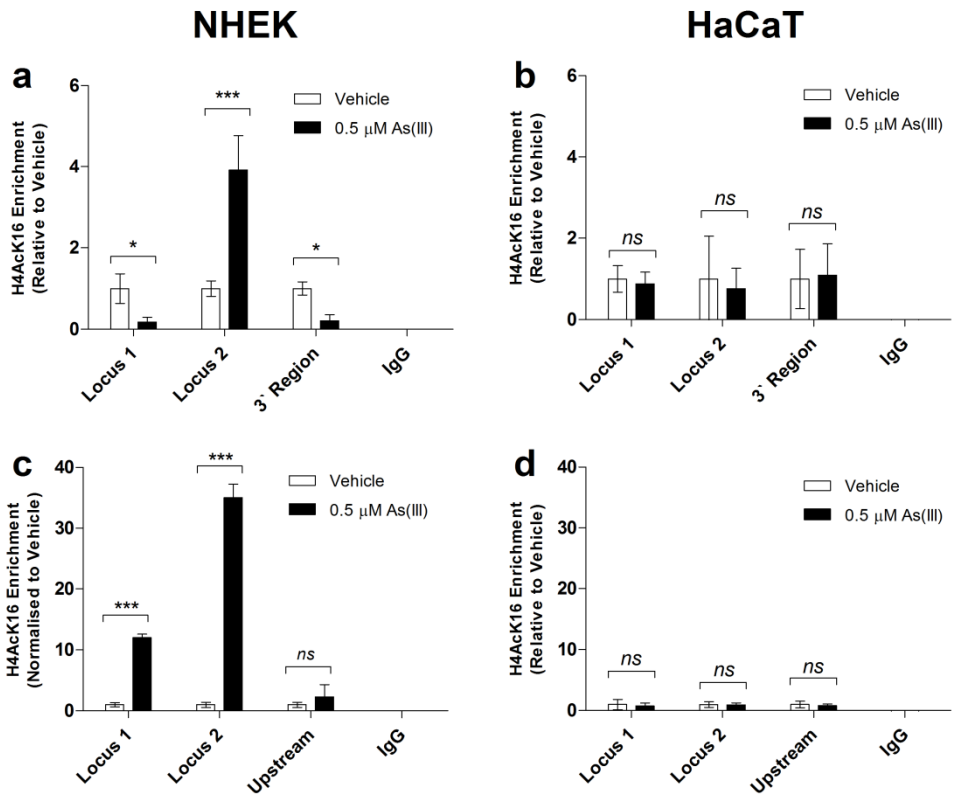


*Figure 6:8 Arsenic-Induced Acetylation of H4[AcK16] in Human Keratinocytes*

Crosslinked chromatin was isolated from normal (NHEK) keratinocytes treated with As(III) for 24 hrs and chromatin associated with SIRT1 or histone H4 acetylated at lysine 16 was captured with antibody-bound magnetic beads. Occupancy at *SIRT1* (Panels a amd c) and *pri-miR-34a* (Panels b and d) promoter regions were analysed by quantitative PCR relative to input DNA. Isotype matched IgG-bound beads were used as a control for immunoprecipitation, and 3' or upstream primers were used as PCR controls.

All data represents the mean ± SD from three independent experiments with * ($p < 0.05$), ** ($p < 0.01$) and *** ($p < 0.001$) respectively.

Next we asked if arsenic exposure influences remodelling of the chromatin at these promoters. First we looked at acetylation of lysine 16 in histone H4, as this mark is the predominantly characterised nuclear SIRT1 substrate. Additionally, SIRT1 occupancy at the same loci was assayed to determine the relationship between H4K16 acetylation and SIRT1 recruitment in arsenic-exposed NHEK cells. H4K16 acetylation in NHEK cells treated with the 0.5 µM concentration of arsenic increased 4-fold at the p53 RE within the SIRT1 promoter and 30-fold at the p53 RE within the

miR-34a promoter after 24 hours [Figure 6:8 (a & c)]. In arsenic-exposed HaCaT cells, however, acetylation of H4K16 at the SIRT1 and miR-34a promoters did not change during this time frame [Figure 6:8 (b & d)].

Finally, experiments were performed to determine if these changes in histone acetylation were associated with changes in chromatin condensation.

*Analysis of chromatin accessibility by RT-PCR (ChART)*

To test whether the changes we have seen are associated with chromatin remodelling, a MNase sensitivity assay was performed on the SIRT1 and miR-34a promoters in arsenic-exposed NHEK and HaCaT keratinocytes. The Rhodopsin gene was used as a control in these experiments.

In NHEK cells, a 3-fold increase in MNase accessibility across the miR-34a promoter was measured after 24 hrs arsenic exposure [Figure 6:9 (a)]. This correlates with the increase in acetylation of the H4K16 mark measured for the miR-34a target during arsenic exposure [Figure 6:8(c)], and indicates that this gene has undergone promoter-wide chromatin remodelling. For the SIRT1 promoter, no change in MNase accessibility was measured for arsenic-treated NHEKs [Figure 6:9 (c)], regardless of the change in histone acetylation [Figure 6:8 (c)]. For HaCaT cells, however, a slight, but significant decrease in accessibility was measured across both the miR-34a and SIRT1 promoter regions after arsenic treatment [Figure 6:9 (b & d)]. For both cell lines, the Rhodopsin gene was resistant to MNase digestion during arsenic exposure [Figure 6:9 (e & f)].

These data demonstrate that induction of miR-34a expression in NHEK cells is associated with structural remodelling at the miR-34a gene promoter during low-dose arsenic exposure.

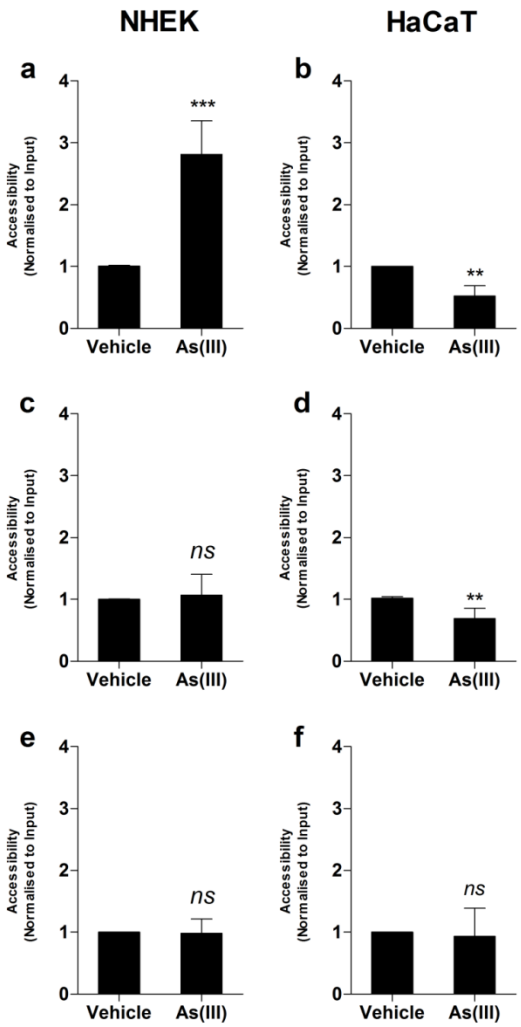


*Figure 6:9 Arsenic alters the pattern of chromatin condensation in human keratinocytes*

Primary human (NHEK) and p53-mutated (HaCaT) keratinocytes were treated with 0.5 µM As(III) for 24 hours. Chromatin was digested with micrococcal nuclease and DNA fragments were assayed for accessibility at *pri-miR-34a* (Panels **a** and **b**), *SIRT1* (Panels **c** and **d**), and *Rhodopsin* (Panels **e** and **f**) gene promoters by ChART-PCR using nucleosome-spanning primers. Results were normalised using undigested input DNA.

All data were analysed relative to vehicle controls by pairwise t-test and represent the mean ± SD from three independent experiments with *ns* (not significant); ** ($p < 0.01$) and *** ($p < 0.001$).

No structural change was detected in the region of the SIRT1 gene assayed in this experiment, and although H4K16 acetylation increased 4-fold during arsenic exposure, the change was not sufficient to influence nucleosomal positioning.

Collectively, these data suggest that for NHEKs, chromatin of the SIRT1 promoter is in a poised, or transcriptionally ready state. During arsenic exposure, *pri-miR-34a* becomes primed by acetylation of H4K16 and chromatin remodelling at its promoter, facilitating transcriptional activation. This epigenetic pattern correlates with SIRT1 inhibition. To further determine the relationship between SIRT1 activity and chromatin structure, acetylation of H4K16 and MNase accessibility was assayed at target gene promoters after SIRT1 activity was inhibited using EX-527.

### *Arsenic-mediated SIRT1 inhibition loosens chromatin by H4 hyperacetylation*

Inhibition of SIRT1 caused a 6-fold increase in acetylation of histone H4 at lysine 16 for the pri-miR-34a gene [Figure 6:10 (a)], and a 4-5 fold increase in acetylation for the SIRT1 gene after 24 hours [Figure 6:10 (c)]. These results were associated with a doubling in MNase accessibility for the *pri-miR-34a* promoter [Figure 6:10 (b)], and a slight increase in accessibility for the *SIRT1* promoter after 24 hours [Figure 6:10 (d)]. Taken together, ChIP and ChART results demonstrate that EX-527-induced hyperacetylation of H4K16 is associated with chromosomal loosening, and that inhibition of SIRT1 activity increased acetylation of this histone mark in keratinocytes with wild-type p53. Next, to determine how arsenic affects SIRT1 occupancy at gene promoter loci, SIRT1 ChIP was performed in arsenic-treated NHEK and HaCaT cells.

SIRT1 occupancy increased for all loci at both genes (4-fold in the case of pri-miR-34a, and ~3-fold for SIRT1) in the NHEK cell strain [Figure 6:11 (a & c)], and a slight increase was measured for 2 of the SIRT1 loci and locus 1 of the pri-miR-34a gene in the HaCaT cell line after 24 hours of arsenic treatment [Figure 6:11 (b & d)].

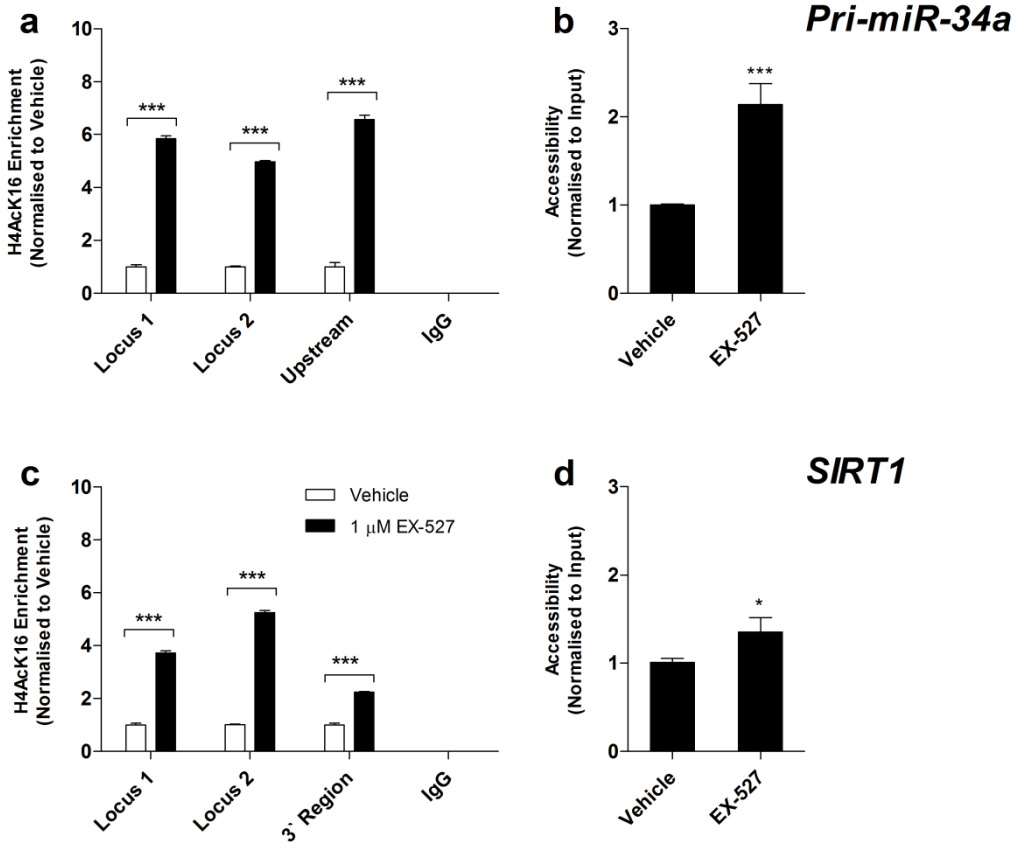


*Figure 6:10 SIRT1 inhibition enriches acetylation of H4 at lysine 16, increasing chromatin accessibility*

SIRT1 activity was inhibited in Primary human (NHEK) keratinocytes with 1 μM EX-527 for 24 hours. Panels a & c: Crosslinked chromatin associated with histone H4 acetylated at lysine 16 was captured with antibody-bound magnetic beads. Occupancy at pri-miR-34a and SIRT1 gene promoters was analysed by quantitative PCR relative to input DNA. Isotype matched IgG-bound beads were used as a control for immunoprecipitation, and upstream or 3' primers were used as PCR controls.

Panels b & d: Chromatin was digested at 22 °C for 5 min with micrococcal nuclease and DNA fragments were assayed for accessibility at pri-miR-34a and SIRT1 gene promoters by PCR using nucleosome-spanning primers. Results were normalised using undigested input DNA.

All data were analysed relative to vehicle controls represent the mean ± SD from three independent experiments with * ($p < 0.05$), ** ($p < 0.01$) and *** ($p < 0.001$) respectively.

Acetylation of the H4K16 mark increased in NHEKs treated with either EX-527 or arsenic, despite the fact that SIRT1 occupancy increased at gene loci during arsenic exposure. Taken together, these results demonstrate that arsenic increases H4K16 acetylation by altering SIRT1 activity and not by suppressing recruitment.

Interestingly, these changes were associated with chromatin remodelling of the *miR-34a* gene promoter, but not for the *SIRT1* gene promoter.

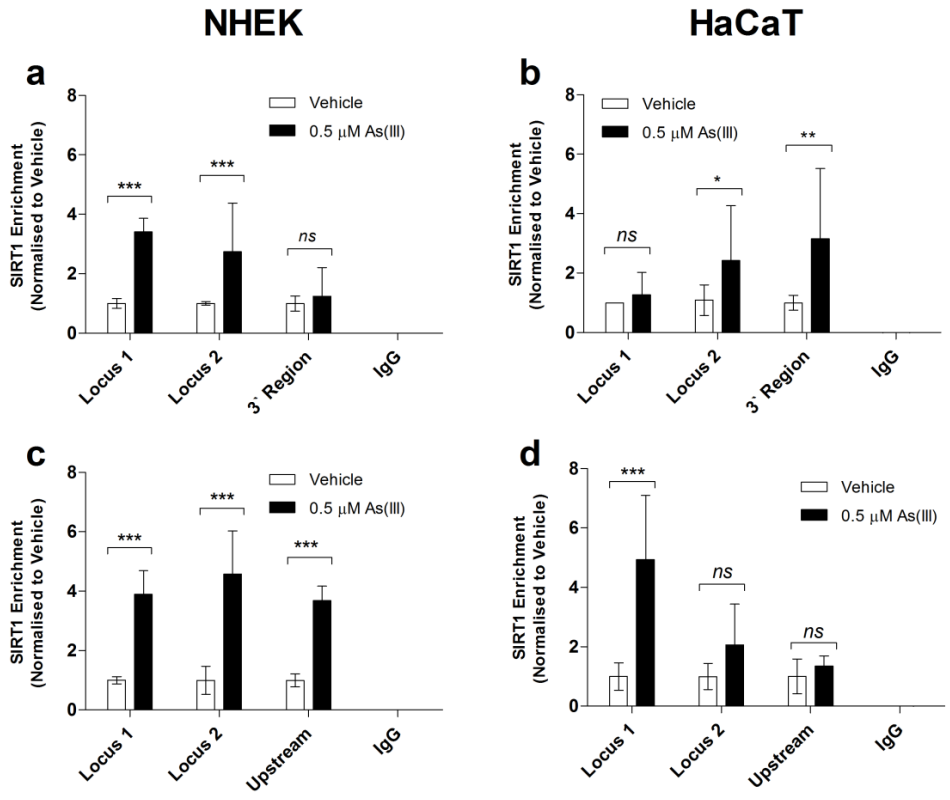


*Figure 6:11 SIRT1 ChIP*

Crosslinked chromatin was isolated from normal (NHEK) keratinocytes treated with As(III) for 24 hrs and chromatin associated with SIRT1 was captured with antibody-bound magnetic beads. Occupancy at *SIRT1* (Panels a amd c) and *pri-miR-34a* (Panels b and d) promoter regions were analysed by quantitative PCR relative to input DNA. Isotype matched IgG-bound beads were used as a control for immunoprecipitation, and 3' or upstream primers were used as PCR controls.

All data represents the mean ± SD from three independent experiments with * ($p < 0.05$), ** ($p < 0.01$) and *** ($p < 0.001$) respectively.

Additionally, the pattern of chromatin regulation was altered in HaCaT keratinocytes when compared to NHEKs, such that this cell line responded differently to arsenic-induced changes in SIRT1 activity. To investigate the nature of chromatin remodelling in arsenic-exposed HaCaTs, the level of chromatin condensation at pri-miR-34a and SIRT1 gene promoters was compared in untreated NHEK and HaCaT

cells [Figure 6:12]. Interestingly, the HaCaT genome was more sensitive to MNase digestion than that of the primary keratinocyte cell strain, indicating that HaCaT cells have a constitutively lower level of chromatin condensation at the miR-34a and SIRT1 gene promoters [Figure 6:12]. This is particularly evident for the miR-34a promoter, which measured 2.5-fold higher MNase accessibility in HaCaT cells when compared to NHEKs.

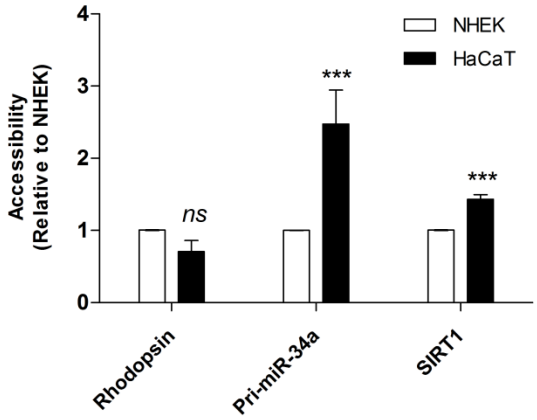


*Figure 6:12 Chromatin repatterning in HaCaT keratinocytes*

Primary human (NHEK, white bars) and p53-mutated (HaCaT, black bars) keratinocytes were grown in 100 $cm^2$ culture plates at a cell density of 75%. Chromatin was extracted and MNase-digested DNA fragments were assayed for accessibility at *SIRT1*, *pri-miR-34a* and *Rhodopsin* gene promoters. Results were normalised using undigested input DNA. HaCaT MNase accessibility data were analysed relative to accessibility in NHEKs by pairwise t-test and represent the mean ± SD from three culture populations with *ns* (not significant); and *** ($p < 0.001$).

Results from this analysis indicate that the chromosomal landscape in the HaCaT cell line is significantly different than primary keratinocytes, and therefore the impact of epigenetic modifiers on the genes tested is altered. Thus in contrast to the increase in chromatin accessibility measured in NHEK cells [Figure 6:9 (a)], arsenic treatment causes chromatin to be condensed in the HaCaT cell line [Figure 6:9 (b, d)].

## 6.4 DISCUSSION

In this study, we show that arsenic modulates SIRT1 and miR-34a expression in a dose-dependent manner, and influences chromatin condensation at the miR-34a promoter by altering histone H4 acetylation at lysine 16 (H4K16). When primary keratinocytes are exposed to arsenic, a genomewide increase in acetylation of H4K16 occurs, causing chromosomal loosening at the *pri-miR-34a* promoter, however this observation was not recorded for the p53 mutated HaCaT cell line.

For NHEK and HaCaT cells, arsenic increased metabolic activity at sublethal doses after 24 hrs, and this response was more pronounced for HaCaT cells than for NHEKs. Arsenic exposure disrupts mitochondrial membrane integrity (559, 560), increases cellular ROS (550, 551), causes chromosomal instability (559, 561), and oxidative DNA damage (562). Redox-regulating genes are induced in response to short-term arsenic exposures (548, 563), and conceivably, this enhances cellular reducing capacity and is responsible for increasing resozurin reduction in keratinocytes exposed to submicromolar doses of arsenic. Arsenic exposure causes extensive mutational damage to the mitochondrial genome (564) and increases glucose usage by inducing glycolysis (315). Changes attributed to mitochondrial damage are features of arsenic-induced Bowen's disease (565), and this mechanism is thought to trigger a metabolic switch from oxidative to glycolytic energy pathways (the 'Warburg effect') which provides a selective growth advantage for precarcinogenic cells during transformation (12, 352).

This investigation demonstrates that arsenic exposure suppresses SIRT1-mediated deacetylation of target substrates (p53 and histone H4) in human keratinocytes. SIRT1 activity is inhibited by numerous mechanisms, including microRNA inhibition, NAD depletion and oxidative posttranslational modifications (566), and bears cysteine residues which are particularly sensitive to oxidants and aldehydes (567). Arsenic is well known for its affinity for sulfhydryl groups in cysteine residues (568, 569); therefore SIRT1 is likely candidate for modification during arsenic exposure.

SIRT1 maintains mitochondrial biogenesis and control over cellular energy metabolism by regulating AMP-activated protein kinase (AMPK) and PCG-1α expression (570-572). Consequently, decreased SIRT1 expression is associated with loss of mitochondrial function and increased oxidative stress (566).

During genotoxic stress, SIRT1 is recruited to DNA strand breaks during the DNA damage response and plays a key role in regulating accessibility of DNA repair enzymes to the DNA by coordinating the process of chromatin remodeling (219). Consistent with the findings of other groups, (573, 574) our results demonstrate that arsenic exposure disturbs the structural arrangement of chromatin by interfering with histone deacetylase activity in exposed keratinocytes. The process of DNA repair is a complex one, and evidence indicates that histone deacetylases function late in the DNA damage response, presumably to reestablish the more condensed structure of facultative heterochromatin (575-577). Thus disruption of SIRT1 activity at sites of arsenic-induced DNA damage has the capacity to prevent chromatin from condensing following DNA repair. Results from this investigation suggest that arsenic toxicity has the potential to promote mutational damage by suppressing SIRT1-mediated chromatin remodeling.

Regulation of the epigenetic landscape is a critical requirement for the maintenance of genomic integrity. Genomic instability is a well-established hallmark of cancer (11), however the relationship between aberrant regulation of chromatin structure and cancer promotion is currently a matter of some debate (578). Impaired chromosomal remodelling during cellular replication and/or DNA damage and repair processes are thought to promote tumorigenesis through the acquisition of a diverse set of spontaneous mutations which enable neoplastic cells to adapt to their environment (578-580). As a carcinogen, arsenic appears to act in a manner consistent with this hypothesis. Arsenic does not interact directly with the DNA in a manner such as direct carcinogens, although it can introduce intranuclear conditions by which mutagenesis is more likely. These include induction of oxidative

DNA damage (288, 289), impaired DNA repair activity, disruption of mitotic spindle formation during replication (581-584), aneuploidy (290), and microsatellite formation.

During this investigation we have provided evidence showing that arsenic produces changes which are consistent with modulation of a key epigenetic regulator (SIRT1), and which alters the pattern of histone marks and chromatin condensation at the miR-34a promoter such that the gene is transcriptionally ready. Consistent with our results, Somji et al. have shown that arsenic transformation modifies the metal response element of the metallothionein 3 gene promoter such that the chromatin displays a poised pattern of histone marks (585). Whether these changes persist with extended exposure, and whether SIRT1 inactivation by arsenic plays a role in the promotion of keratinocyte transformation is unclear.

We also found here that p53-mutated keratinocytes (HaCaT cells) are resistant to arsenic-induced cell death, and acetylation of the H4K16 mark does not increase at gene promoters with arsenic exposure. This finding appears to contradict conclusions made regarding the effect of arsenic as an inhibitor of SIRT1 activity in NHEK cells. However, differences in the epigenetic regulatory machinery of HaCaTs may account for altered responses to arsenic when compared to NHEKs. Expression of SIRT1 is 3-fold higher in the HaCaT cell line, and the chromosomal architecture at gene promoters is more sensitive to MNase digestion. Moreover, stress-related gene expression in the HaCaT cell line appears to be higher than primary keratinocytes during arsenic-induced or UV-induced toxicity (548, 586). However it must be noted that these studies compared cells which were cultured in different growth media [keratinocyte growth media for NHEKs; RPMI or DMEM for HaCaT cells]. As we have shown in Chapter 3, physiological responses of HaCaT cells are sensitive to growth media, and HaCaT phenotype is more comparable to NHEKs when cultured in keratinocyte growth medium.

In Chapter 5, we demonstrated that HaCaTs are resistant to camptothecin-induced apoptosis and this appears to be augmented by SIRT1. Thus the effect of arsenic as an inhibitor of SIRT1 activity (as observed in NHEK cells) is less potent in the HaCaT cell line as a result of its greater intracellular SIRT1 protein level and antioxidant defense capacity. In the next chapter, , an extended treatment period was used to measure changes in the pattern of gene expression and DNA methylation with low-dose arsenic exposure to test whether arsenic-induced modifications to SIRT1 and miR-34a genes were sustained in NHEK cells over time.

# Chapter 7 -
# Progressive repatterning of DNA methylation in arsenic-exposed keratinocytes

## 7.1 ABSTRACT

Arsenic is an environmental contaminant which generates significant health issues for populations with chronic exposure. Human populations exposed to arsenic through drinking water are at risk of developing numerous pathologies of the skin, including hyperkeratosis, hyperpigmentation and carcinoma. Recent investigations show that histone deacetylase and DNA methyltransferase activity are altered by arsenic exposure and this appears to promote cellular transformation. The purpose of this investigation was to investigate the epimutagenic properties of arsenic in keratinocytes using an *in vitro* cell culture model. Acetylation of histone H4 progressively increased over 70 days in arsenic-exposed populations, whilst a loss of promoter methylation was observed across the miR-34a gene promoter during this timeframe. Experiments conducted in the previous chapter demonstrated that SIRT1 expression is up-regulated in keratinocytes which are exposed to 0.5 µM arsenic over short-term time frames. Results presented in this chapter further reveal that enhanced expression of SIRT1 in arsenic-treated keratinocytes is reversed during extended exposure by widespread epigenetic remodelling to *SIRT1* and *miR-34a* gene promoters, which up-regulates miR-34a expression, enhances feedback regulation of SIRT1, and suppresses transactivation of the SIRT1 promoter.

Primary human keratinocytes did not escape replicative senescence during the course of this experiment, although keratinocyte cell lines with impaired functional p53 have been successfully transformed by others using the same arsenic concentration within a 10 week period. We show here that hyperacetylation of histone proteins and reorganisation of promoter methylation are associated with a dysregulated pattern of SIRT1 and miR-34a expression, and these features are part of a wider landscape of altered epigenetic regulation in arsenic-exposed keratinocytes.

## 7.2 INTRODUCTION

Of all the organ systems, the skin is particularly sensitive to arsenic toxicity, either from systemic or topical exposures (587). Arsenite binds proteins bearing sulfhydryl moieties in thiol-rich proteins such as keratins (588, 589), and consequently, has a tendency to accumulate in keratinocytes of the epidermal layer of the skin (590). Arsenic toxicity produces a pathological profile which is characterised by hyperproliferation, dysplasia, presence of apoptotic cells and hyperpigmentation. Unlike UV-induced skin lesions, arsenic-induced hyperkeratotic skin lesions affect multiple sites across the epidermis and develop into non-melanoma skin cancers (NMSC) which are more aggressive than those triggered by sun exposure alone (287). Consequently, uncovering the mechanisms driving arsenic-induced carcinogenesis is a priority for development of strategies to reduce disease risk for exposed populations.

So far, most evidence indicates that arsenic does not directly interact with DNA and this contributes to a classification of arsenic as an indirect carcinogen in humans (283). The mutagenic potential of arsenic is thought to derive from oxidative DNA damage, clastogenic damage, and mitogenic stress (316, 562, 591, 592). In addition, arsenic exposure interferes with numerous regulatory processes which maintain genomic fidelity, including the DNA repair machinery and those responsible for epigenetic imprinting (582, 583, 593-596). As our understanding of carcinogenesis has evolved, cancer has been redefined as a disease of impaired epigenetic gene regulation in addition to DNA sequence mutations (178). The DNA methylome is maintained by DNA methyltransferases (DNMTs), which target position 5 of cytosine bases in CpG dinucleotides (597, 598). Cytosine methylation influences chromatin condensation and accessibility of regulatory elements to gene promoters, thus providing an additional layer of control over gene expression (599). In healthy cells, the majority of methylated CpG dinucleotides in the genome are part of non-coding tandem repeat sequences (LINEs, SINEs and LTRs) (100). In contrast, concentrated CpG regions associated with gene-regulatory domains (CpG

islands) are predominantly unmethylated (600). This pattern of DNA methylation shifts during carcinogenesis such that cancer cells develop genomewide DNA methylation abnormalities (601, 602), and these changes alter patterns of gene expression, increase mutational rates (603) and contribute to chromosomal instability (170, 604).

Arsenic exposure induces well-documented genomewide methylation changes in exposed individuals (376, 605), and is also known to alter the methylation status of cultured cells *in vitro* (396). Consistent with methylation patterns from cancer genomes, these studies show that arsenic exposure causes gene-associated hypermethylation of CpG islands and genomewide hypomethylation of repetitive sequences (357). A loss of methylation at non-CpG sites during cancer progression appears to be linked to redistribution of the epigenetic regulatory machinery and a concomitant increase in *de novo* methylation at promoter-associated CpG islands (170, 174, 606). Although a causative link has not been conclusively demonstrated, it is widely understood that this hypomethylation/hypermethylation process occurs concurrently during chemical carcinogenesis, as a consequence of alterations in the distribution of polycomb repressive group complexes across the chromatin and impaired DNA methyltransferase activity (607).This global loss of 5-methylcytosine in the genome also increases the rate of mutational damage (9, 13) and increases microsatellite instability (608). Along with alterations to microRNA expression (389), these studies provide growing evidence for a relationship between arsenic-induced epigenetic dysregulation and cancer. Whether these changes are derived from, or drive the process of arsenic-induced carcinogenic transformation is unclear.

SIRT1 is a lysine deacetylase which has a key role in regulating cellular responses to chronic stress. In addition to its role in modulating histone acetylation, SIRT1 facilitates CpG methylation during DNA damage, by recruiting DNMT3B to sites of DNA base oxidation and strand breaks (609, 610), and by modulating DNMT1 activity (611). SIRT1 expression is controlled by the microRNA miR-34a (479);

however miR-34a expression is frequently suppressed in cancer (478). Inactivation of the region of Chromosome 1 coding for the miR-34 gene (1p36.22) is associated with CpG hypermethylation in many cancers (612-616). Additionally, SIRT1 is overexpressed in cancer subtypes, including acute myeloid leukemia (617), hepatocellular carcinoma (618), prostate cancer (619), and non-melanoma skin cancer (522). SIRT1 regulates differentiation and senescence in normal keratinocytes (620-622), and suppresses epithelial-to-mesenchymal transition in breast cancer (623, 624); however the role of SIRT1 in arsenic-induced skin cancer has not previously been investigated.

Here, primary human keratinocytes were exposed to a sub-lethal concentration of arsenic continuously over a period of 10 weeks in order to generate epigenetic changes associated with carcinogenesis. DNA methylation analysis demonstrated arsenic-induced hypomethylation of the miR-34a promoter associated with up-regulation of its coding microRNA.

## 7.3 RESULTS

*Human keratinocytes enter senescence after 10 weeks in culture*

Normal human epidermal (NHEK) keratinocytes at passage 2 were grown in 75 $cm^2$ flasks from an initial population of 5 × $10^5$ cells and allowing an overnight settle prior to addition of the treatment medium. When the flasks had reached 75-85% confluence (approximately once per week), the cells were detached using TrypLE dissociation reagent (Invitrogen, Carlsbad, CA, USA), rinsed in Epilife and counted using a Haemocytometer. Harvested cells were seeded at a standard density of 5 × $10^3$ cells per square centimetre into a new 75 $cm^2$ culture flask, and the remaining harvested cells washed in PBS. Seeding medium was replaced with EpiLife growth medium containing 0.5 µM arsenic the following day. Untreated NHEK cells grown in EpiLife were harvested concurrently as passage matched controls.

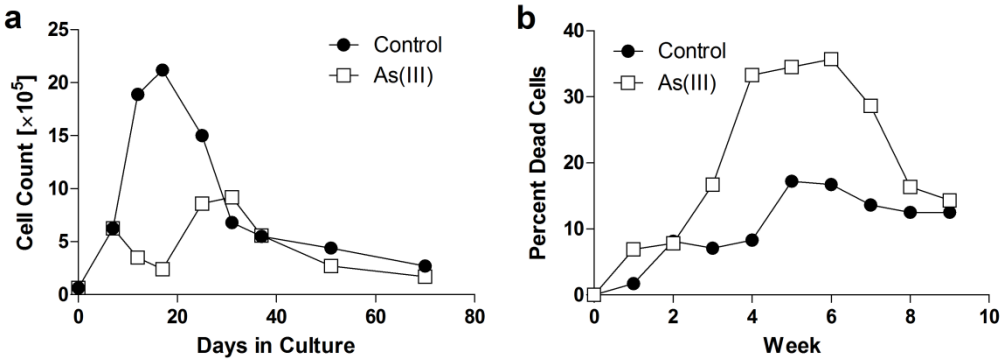


*Figure 7:1 Effect of arsenic on keratinocyte growth in culture*

Primary human keratinocytes (NHEK) were cultured for 10 weeks in EpiLife Keratinocyte growth medium into which had been added arsenite [As(III)] to a final concentration of 0.5 µM. The effect of arsenic on growth characteristics of keratinocytes in culture was determined using a cell count of cells stained with the vital dye, Trypan Blue performed at each passage. An untreated passage-matched population of NHEKs grown under identical conditions was used as a reference. Panel **a**: Total cells (× $10^5$); Panel **b**: Percentage non-viable cells.

The harvested NHEKs were pelleted in aliquots of 1 × $10^6$ cells and stored at −80°C until use. This experiment was repeated twice, for at least 10 weeks on each occasion, and similar results were obtained with each population

Primary keratinocytes reached a peak replicative capacity in culture at 20 days, declining rapidly thereafter. These data correlate with the growth characteristics of keratinocytes documented by others (450, 625). Arsenic suppressed growth of cultured keratinocytes during the initial 20 days of culture, after which a subpopulation continued to divide in a manner consistent with untreated keratinocytes [Figure 7:1 (a)]. Total cell yield was reduced by arsenic exposure, with the arsenic-treated population generating approximately $20 \times 10^6$ cells from the initial 500000 cell sample at the conclusion of the 70 day experiment, whereas keratinocytes growth in culture without arsenic generated approximately $27 \times 10^6$ cells in total. This observation was mirrored by the percentage of non-viable cells counted each week, with 30-35% dead cells measured during weeks 4-6 in the arsenic-exposed population, compared with a background yield of 10-15% dead cells in the non-exposed population [Figure 7:1 (b)].

*Analysis of promoter methylation in arsenic-exposed keratinocytes*

Until this study, the arsenic-induced modulation of SIRT1 and pri-miR-34a gene regulation has not been documented in depth, and so whether their promoter regions would be influenced by arsenic was unknown. Considering the effect of arsenic on mitochondrial function and energy metabolism, SIRT1 expression and activity was expected to change with extended exposure to arsenic. Based on results obtained from Chapter 6 experiments, we concluded that arsenic exposure suppresses SIRT1 deacetylase activity, and de-condenses chromatin in the *miR-34a* gene promoter, leaving the region susceptible to posttranscriptional remodeling factors. Here, primary human keratinocytes were exposed to arsenic for 60 days to induce arsenic-induced methylation changes at the target loci. A short region (190 bp) of the SIRT1 promoter between the p53 response element and the transcription start site (TSS) was targeted for analysis [Figure 7:2(a)]. Likewise, the regulatory domain of the *pri-miR-34a* promoter directly upstream of the p53 response element

was analysed by bisulfite sequencing [Figure 7:2(b)]. Potential regions for methylation analysis were identified using parameters outlined in Chapter 2.

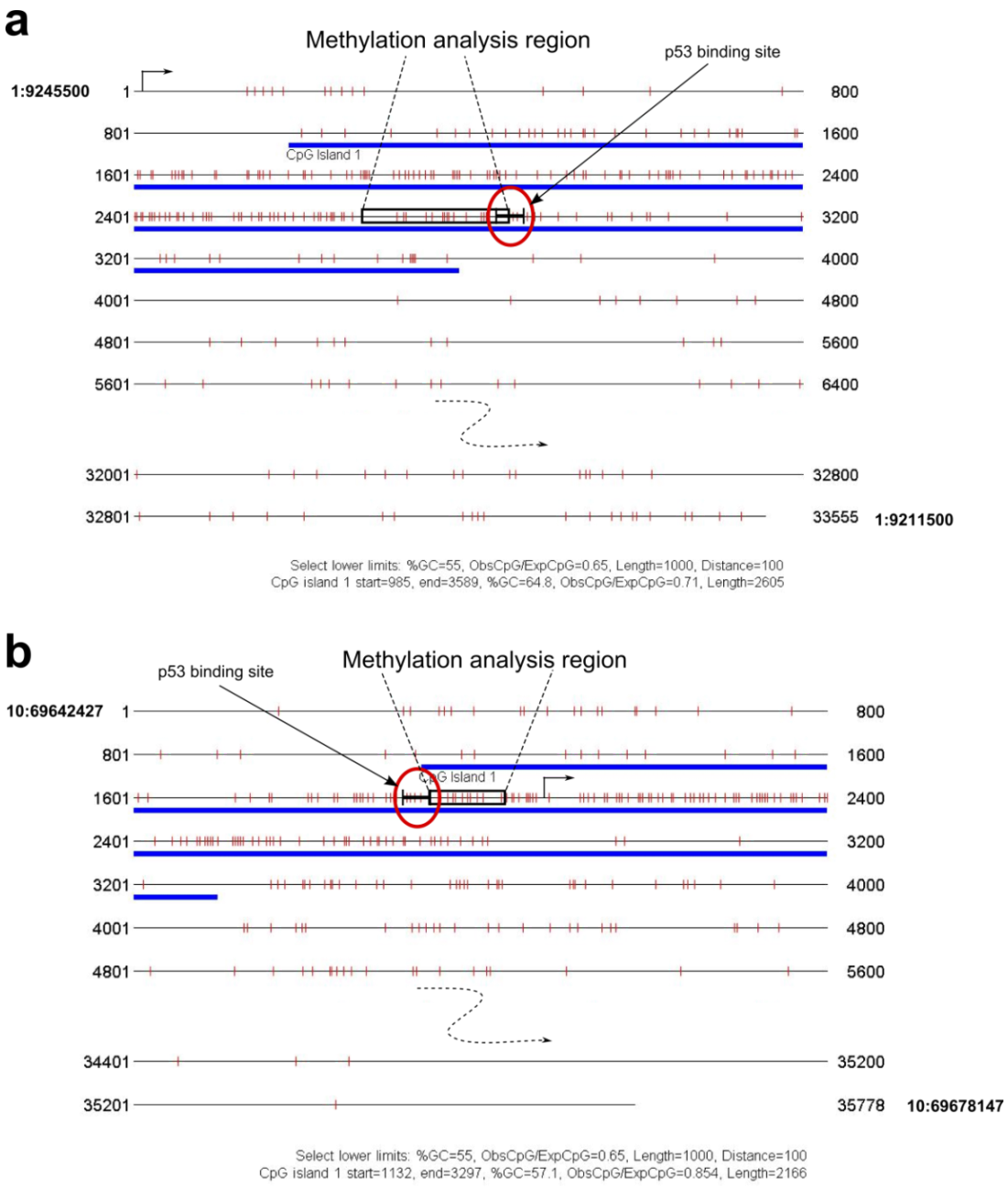


*Figure 7:2 Targets for Methylation Analysis*

Diagrammatic representation of regulatory domains for miR-34a (Panel a) and SIRT1 (Panel b) gene sequences with regions targeted for methylation analysis are annotated. Ticks indicate CpG dinucleotides, CpG islands are marked as blue, p53 binding sites are circled. The downstream region of each gene sequence has been omitted for clarity.

High Resolution Melt Curve Analysis (HRM) was used to screen arsenic-exposed NHEKs for methylation changes in the *SIRT1* and *pri-miR-34a* promoter regions to indicate if further analysis by sequencing was warranted. HRM is a technique which screens for variations in sample gene sequences by identifying differences in the melting properties of heterogeneous DNA sequences. Here, methylated and unmethylated cytosine residues were differentiated by bisulfite conversion and identified using difference plots derived from melt curves. Relative methylation of sample DNA was assessed by comparison with standards of known percentage methylation.

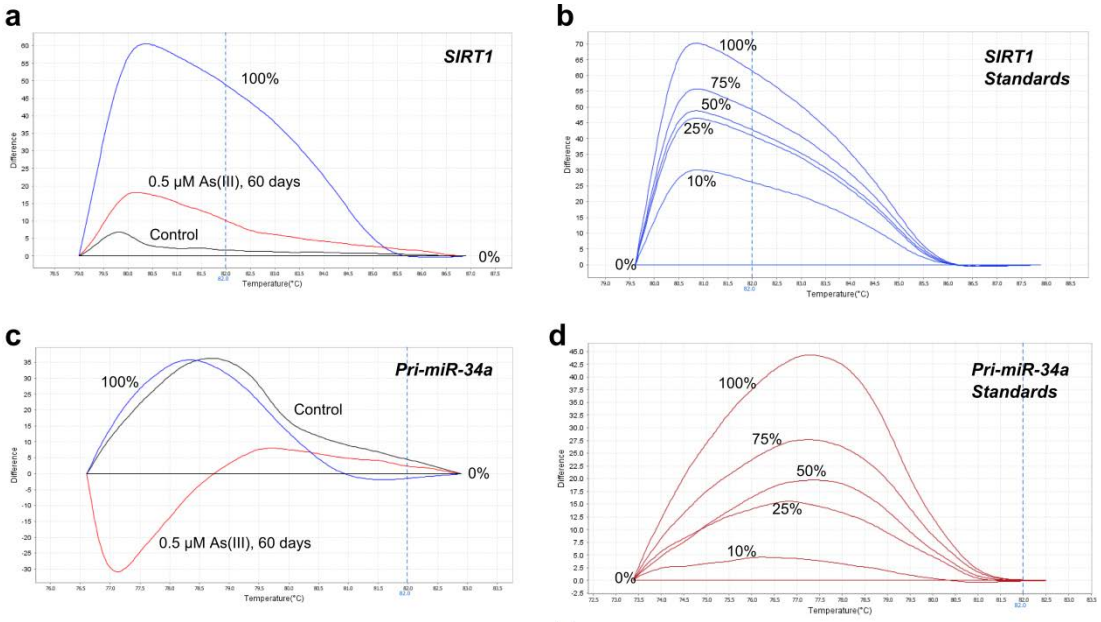


*Figure 7:3 Melt Curve Analysis, 60 day arsenic exposure in keratinocytes*

Bisulfite-converted DNA from arsenic-exposed keratinocytes was amplified using SIRT1 and pri-miR-34a bisulfite primers (Panels a & c), and high resolution melting was performed with MeltDoctor HRM Reagents. Melt curves were analysed and difference plots generated from the data using High Resolution Melt Software v3.0 (Applied Biosystems, Foster City, CA, USA). Standard curves generated from fully methylated and unmethylated control gDNA are included for reference (Panels b & d).

After 70 days of arsenic exposure, the SIRT1 difference plot from untreated NHEK control cells correlated with the 2.5% methylation standard, and the plot from

arsenic treated cells showed a further 5-6% increase in methylation status compared to untreated control [Figure 7:3 (a, b)]. For the *pri-miR-34a* locus, arsenic treatment produced a more marked change in percent methylation, with ~100% methylation in untreated keratinocytes, and >10% methylation in arsenic-treated keratinocytes at the target region [Figure 7:3 (c, d)]. These results support our hypothesis that arsenic alters methylation of the *pri-miR-34a* upstream regulatory region, and show that methylation changes at this locus can be detected by a relatively simple technique (HRM) within a 9-10 week experimental time frame.

### *Arsenic alters SIRT1 and pri-miR-34a gene expression in keratinocytes by repatterning promoter methylation*

Cytosine methylation in the promoter regions of *SIRT1* and *pri-miR-34a* genes was measured in NHEK cells which were cultured for 10 weeks in EpiLife Keratinocyte growth medium into which had been added arsenite [As(III)] to a final concentration of 0.5 µM. Methylation was analysed from the DNA of population samples extracted at weeks 1, 5, 9 and 10 by direct sequencing of bisulfite-modified target genes. Percentage cytosine methylation was determined manually for each CpG within the region from the sequencing trace, and results analysed using a BiQ Analyser software program (413). The effect of As(III)-mediated epigenetic repatterning of the *SIRT1* and *pri-miR-34a* promoter on expression of target genes was analysed using qRT-PCR. For this experiment, only one replicate was obtainable, and so results are presented without statistical analysis due to time constraints.

When compared to untreated, passage matched controls, arsenic increased CpG dinucleotide methylation in the SIRT1 promoter at 2 CpG sites in the first 5 weeks, and at two more CpG sites after a further 4-5 weeks of treatment [Figure 7:4 (a)]. Across the *pri-miR-34a* promoter region tested, CpG dinucleotides were predominantly methylated in untreated control keratinocytes, and methylation status remained constant during the 10 week exposure period [Figure 7:4(b)]. In

arsenic-treated keratinocytes, methylation progressively decreased, with distal changes occurring within the first week of treatment and proximal CpGs being affected after 9-10 weeks [Figure 7:4(b)].

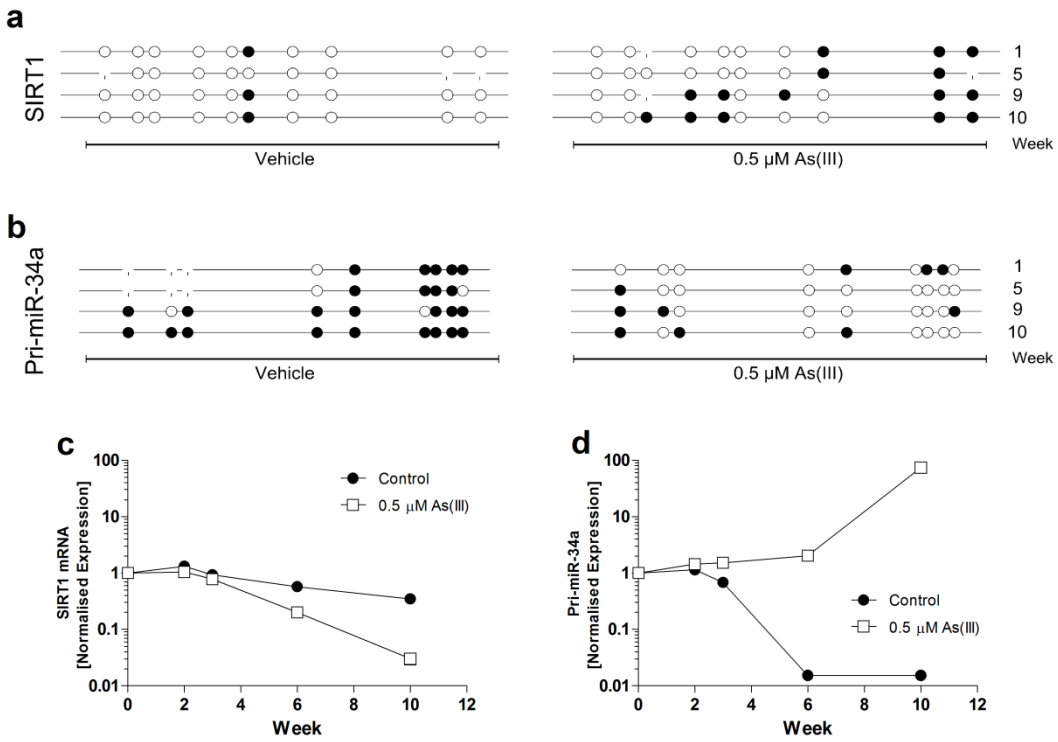


*Figure 7:4 Aberrant DNA methylation of specific loci is associated with altered gene expression during extended arsenic exposure*

Primary human keratinocytes were cultured in medium containing 0.5 µM As(III) continuously for a period of 10 weeks. Genomic DNA was extracted each week for bisulfite conversion and sequencing of SIRT1 (Panel **a**) and pri-miR-34a (Panel **b**) PCR fragments. Sequences were analysed for changes in cytosine methylation using BiQ Analyser v2.00 (413) using the ClustalW (626) algorithm, and the dataset converted into a graphical format (black circles > 50% methylated; white circles < 50% methylated).qRT-PCR was performed from single RNA extracts using primers for SIRT1 (Panel **c**) and pri-miR-34a (Panel **d**).

Promoter methylation repatterning in arsenic-treated NHEKs correlated with duration-dependent shifts in SIRT1 and miR-34a expression. For untreated NHEKs, SIRT1 mRNA expression did not alter dramatically during the 10 week timeframe, whereas SIRT1 expression was suppressed more than 10-fold with exposure to arsenic [Figure 7:4 (c)]. Conversely, pri-miR-34a increased almost 100-fold after 10

weeks of arsenic exposure and was down-regulated in untreated controls [Figure 7:4 (d)].

These data demonstrate a relationship between arsenic-induced changes in promoter methylation and altered expression of SIRT1 and miR-34a in keratinocytes. Considering that the NHEK cell strain consists of a heterogenous population of keratinocytes, it is most likely that the results presented in Figure 7.4 are a consequence of arsenic-mediated selection pressure. Thus the result is a generalized representation of methylation changes which may indicate that cells with certain methylation states have preferentially survived throughout the course of the experiment, rather than indicating that arsenic is directly responsible. Nonetheless, many investigators have demonstrated a causal relationship between arsenic exposure and alterations in the DNA methylation profile during *in vitro* experiments and in population studies. A more detailed method of methylation analysis using clonal sequencing would be able to detect population-based changes in the sample; however this technique was beyond the scope of this investigation.

To further ascertain the relationship between promoter hypermethylation, altered SIRT1 expression and chromatin remodelling, p53 expression and acetylation of histone H4 at lysine 16 was measured in arsenic-exposed keratinocytes.

### *Arsenic-mediated hyperacetylation of histone H4 in human keratinocytes*

Although SIRT1 expression was up-regulated in arsenic-treated NHEKs when compared to untreated controls for the initial 24 days of the treatment period, relative expression of SIRT1 protein decreased over time after the initial up-regulation observed with 1 day exposure to As(III) [Figure 7:5(a)].

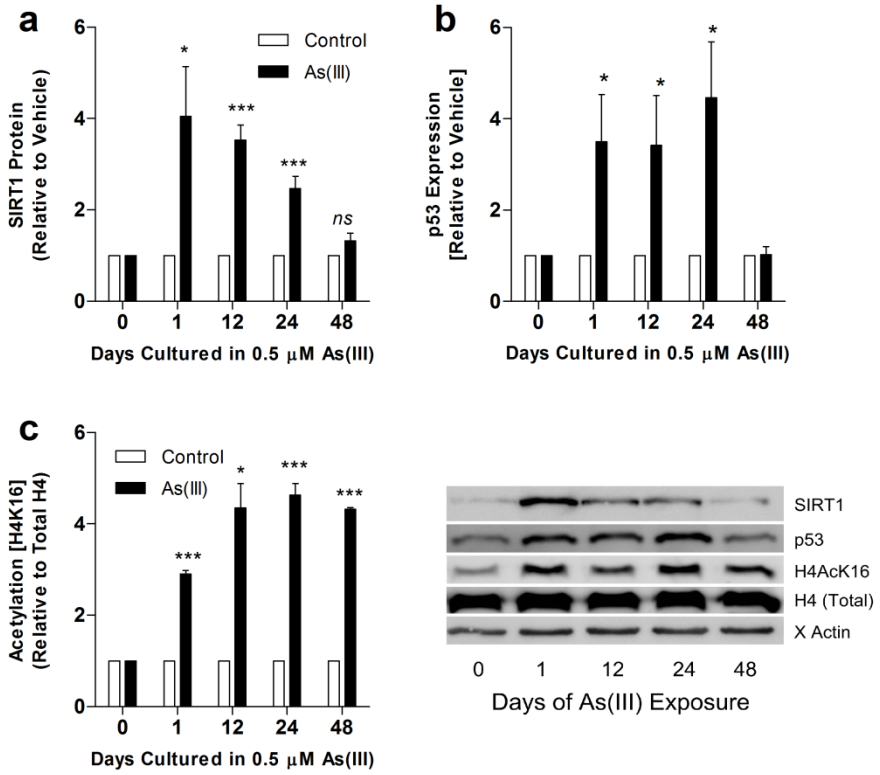


*Figure 7:5 Arsenic alters SIRT1/miR-34a axis regulation during prolonged exposure in keratinocytes*

Normal keratinocytes were continuously cultured in media containing 0.5 μM As(III) over a period of 10 weeks. Protein and RNA were extracted during the 10 weeks of treatment (*n*=2). SIRT1 protein (Panel **a**), p53 protein (Panel **b**) and acetylation of histone H4 at lysine 16 (H4AcK16; Panel **c**) was measured by immunoblotting. Protein loading was normalised using actin, and qRT-PCR data was normalised using 5S rRNA as an internal control gene. Acetylation was calculated relative to expression of histone H4.

Consistent with this observation, arsenic-mediated up-regulation of p53 expression was only sustained during the first 3 weeks of the experiment [Figure 7:5(b)]. Furthermore, relative acetylation of H4K16 progressively increased to become 5-fold higher in NHEKs after 24 days when compared to cells cultured in arsenic-free media over the same time period [Figure 7:5(c)]

## 7.4 DISCUSSION

SIRT1 is a critical mediator of physiological processes which regulate lifespan and ageing, predominantly by maintaining epigenetic control over gene expression (220, 627). In keratinocytes, up-regulation of SIRT1 redirects cellular signalling programs towards differentiation, and down-regulation of SIRT1 promotes senescence (620, 621). Additionally, miR-34a expression is known to increase during senescence, and this is associated with a down-regulation of SIRT1 protein (482).. Sirtuin expression is down-regulated in hyperkeratotic lesions from arsenic exposed individuals (628) - a result which is consistent with our findings in keratinocytes exposed to arsenic over 10 weeks. Paradoxically, other groups have shown that SIRT1 is overexpressed in skin cancer (522, 629), and when taken with our results, this disparity in the SIRT1 expression profile indicates that arsenic induces carcinogenic transformation in keratinocytes via a mechanism which differs from UV-induced skin cancer.

Regulation of the histone code and patterns of DNA methylation are inextricably linked, and cooperate to dynamically manage chromatin condensation. When keratinocytes were exposed to arsenic in our experiments, histone H4 was hyperacetylated at lysine 16 and CpG dinucleotides were demethylated at the pri-miR-34a promoter, resulting in a reorganisation of the chromatin structure and an increase in miR-34a expression. In recent years, clinical trials and *in vitro* studies have shown that arsenic transformed cells develop widespread histone modifications which are associated with changes to the DNA methylation profile (373, 535). For the most part, cells exposed to arsenic over extended time periods have hypermethylated and phosphoacetylated histone residues (355, 382, 630, 631), and methylation of CpG dinucleotides decreases (360, 396).

Histone modifications precede DNA methylation in the initiation and consolidation of tumour suppressor silencing (130). Our data show that as exposure time progresses, As(III)-induced histone modifications are replaced by a DNA methylation pattern which reinforces epigenetic regulation of gene expression in

keratinocytes. Specifically, keratinocytes exposed to arsenic underwent progressive shifts in the pattern of *SIRT1* and *pri-miR-34a* promoter methylation which were associated with concurrent changes in SIRT1 and miR-34a gene expression.

Further to our findings that epimutagenic properties of arsenic are related to impaired regulatory function of epigenetic modifiers such as SIRT1, arsenic exposure increases oxidative stress and alters cellular availability of redox cycling intermediates such as glutathione (549, 632). The epigenome is significantly modified when cells are exposed to oxidative stress (633, 634), a process which directly inhibits SIRT1 (567), and also indirectly suppresses activity by limiting cofactor availability. Here, functional activity of epigenetic modifying enzymes is influenced by reduced abundance of NAD+, which supplies PARP and SIRT1, Acetyl CoA, which supplies histone acetyltransferases, and *S*-adenosyl methionine (SAM) which supplies DNA methyltransferases (DNMTs) (221, 384, 635).

Mechanistically, DNA methylation changes associated with arsenic exposure have been attributed to competition for methyl group donors by methyltransferases (369, 535). This hypothesis is supported by *in vitro* studies demonstrating concurrent SAM insufficiency and inhibition of DNMT activity in cells treated with arsenic (360). This theory has been questioned as arsenic biotransformation by methylation is minimal in most tissues with the exception of the liver (636). An alternative mechanism proposes that glutathione synthesis during oxidative stress redirects cellular stores of homocysteine from pathways which recycle DNMT cofactors, such as SAM (373, 374). However, inhibition of DNMT in arsenic exposed cells has been shown to occur independently of SAM concentration (360). Nonetheless, arsenic exposure disrupts DNMT activity and expression (637), and causes a generalised loss of DNA methylation in arsenic-exposed keratinocytes (396).

Impairments to DNA methyltransferase activity cause disruptions to maintenance methylation during cell division (171, 638, 639), and increases cancer susceptibility

by destabilizing the genome (290). Furthermore, altering the activity of Polycomb Repressive Group (PRG) complexes enables *de novo* DNA methyltransferases DNMT3a and DNMT3b to methylate exposed gene promoters (126). Consequently, inhibition of PRG protein expression and DNMT activity by arsenic causes shifts in the pattern of DNA methylation (360, 371, 396). In accordance with this model, others have found that transformation of BALB/c 3T3 cells by extended exposure to 0.5 µM As(III) activates PRG proteins BMI1 and Suz12, and these changes were associated with suppression of $p16^{INK4A}$ and $p19^{ARF}$ expression (640). Our results support a model in which arsenic suppresses PRG-mediated gene repression and disrupts established patterns of histone acetylation by disrupting SIRT1 activity [Figure 7:6].

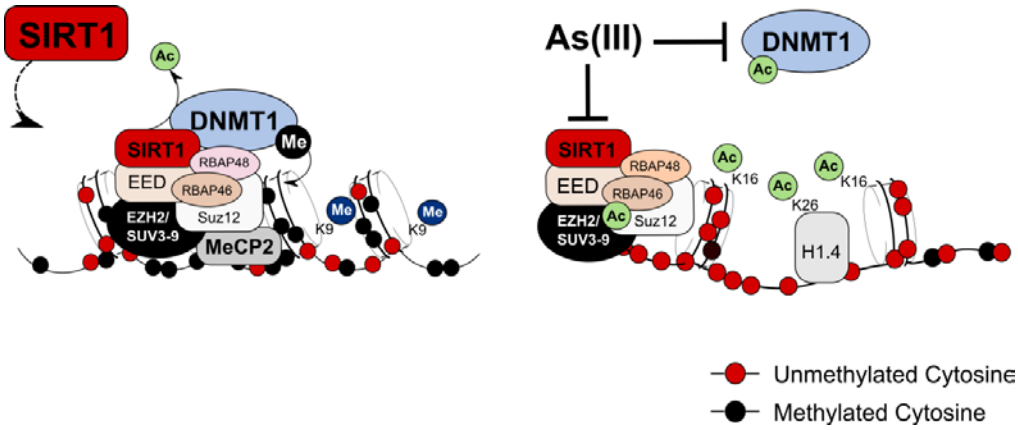


*Figure 7:6 Arsenic alters patterns of DNA methylation by blocking SIRT1 activity.*

SIRT1 is recruited to methylation sites as part of polycomb repressive group (PRG) complexes 2 and 4 where it associates with and regulates EZH2, EED, Suz12 and DNMT1 (180). As part of this gene repressive complex, SIRT1 induces chromatin condensation by deacetylating histone H4 at lysine 16 (H4K16) and maintains DNA methylation patterns by recruiting and activating DNA methyltransferase 1 (DNMT1).

Key: As(III) – arsenite; DNMT1 - DNA methyltransferase 1; EED – embryonic ectoderm development protein; EZH2/SUV3-9 – Enhancer of Zeste Homologue 2; MeCP2 – Methyl CpG binding protein 2; Suz12 – suppressor of zeste 12; RbAp46 & 48 – retinoblastoma binding proteins 46 & 48.

Moreover, our experimental findings provide evidence that arsenic is causing significant disruptions to the epigenetic machinery in a manner which is independent of p53 inactivation. In accordance with our investigations in Chapter 5, p53 must not only be expressed, but also be activated by an external (or internal) stressor for p53-dependent cellular processes (such as cell cycle arrest or survival signaling) to occur (641). It is no coincidence, then, that genes with aberrant DNA methylation in arsenic-exposed individuals are predominantly part of the p53 tumour suppressor network (605). However, cultured cells are responding to numerous stress signals which compound the effect of any carcinogenic insult (such as arsenic, as in our study), and which promote a low-level transactivation of p53 (642). Wild-type p53 expression is required for cells to enter mitotic arrest and apoptosis during arsenic exposure (643, 644).

In vitro models of oncogenic transformation are difficult to interpret for a variety of reasons – amongst which is the confounding influence of the cellular growth environment in culture. Our results indicate that cellular replication is suppressed by arsenic in culture, and that exposure to arsenic alone is not sufficient to induce cancerous change in primary keratinocytes. Whilst other groups have performed extended arsenic treatment experiments in culture, the cell lines used in these studies are derived from immortalized or pre-malignant sources (HaCaT (645, 646)), are transformed with hTERT (SAEC (647)), adenovirus-12 SV40 (BEAS-2B (648), UROtsa (649)) or HPV 18 (RWPE-1 (650, 651)), which, although enabling long-term growth in culture, may produce results that are non-representative of arsenic-induced carcinogenesis in vivo. Genes regulating G1 to S phase transition are down-regulated and genes promoting cell cycle arrest are up-regulated in NHEKs exposed to arsenic for 24 hour periods (547). However this expression profile does not persist in hyperkeratotic skin lesions, which show enhanced expression of genes promoting G1/S and G2-M phase transition (628). In general, SIRT1 expression decreases and acetylation of the SIRT1 histone substrate, histone H4 at lysine 16 (H4K16) increases with age (111), and is associated with higher-order remodelling

of the genome (544). Genomewide remodelling of higher-order chromatin structure occurs during keratinocyte differentiation (652), however H4K16 is hypoacetylated in senescent cells (621, 653, 654).

Since we found that primary keratinocytes were not transformed by extended arsenic treatment, it would be useful to determine if the epigenetic remodelling we measured during this experiment had altered keratinocyte susceptibility to transformation by other carcinogens such as UV exposure. The nature of arsenic-mediated transformation has not been fully defined, despite its classification as a known carcinogen by the International Agency for Research on Cancer (IARC) (283). Inorganic arsenic has been variously described as a non-genotoxic carcinogen, an indirect carcinogen or a co-carcinogen, and although exposure induces oxidative DNA lesions and alters oncogene expression (288, 289, 655), to our knowledge arsenic-mediated transformation has only been achieved in immortalised cell lines.

Acquisition of transformational changes by keratinocytes treated with arsenic was difficult to detect from our results, as data from this study represents population-wide outcomes rather than an analysis of isolated colonies. Primary keratinocytes rapidly enter mitotic senescence when cultured on plastic; however when exposed to an initiating carcinogen, individual cells may acquire changes which confer resistance to replicative senescence. As part of a wider population in culture, the population phenotype is only affected if clonal expansion of transformed cells is more rapid than their untransformed counterparts. This had not occurred at the end of the 70 day exposure period in our investigation. HaCaT keratinocytes have been successfully transformed within this time frame by other investigators (646, 656), and based on these in vitro transformation studies, we anticipated that extended growth in the presence of arsenic would alter the growth pattern of primary keratinocytes, and that arsenic would generate epigenetic changes which enabled cells to overcome senescence during the course of the experiment. As this did not appear to be the case for arsenic-exposed NHEKs, our interpretation is that

co-carcinogens such as UV produce the initiating event (such as inactivation of p53) which is necessary for arsenic-mediated oncogenic transformation in keratinocytes.

# General Discussion

SIRT1 is a novel pharmaceutical target which mediates the cell's adaptive responses to chronic stress. Current research suggests that SIRT1 activation is protective for individuals who are under biological stress or lack adequate homeostatic regulatory capacity but does not alter the health of already healthy individuals. On a cellular level, SIRT1 differentially targets diseased cells within a mixed population (such as found in tumour tissue) by enhancing redox and metabolic homeostasis, suppressing inflammatory signalling and improving responses to genotoxic damage and DNA repair. Consequently, SIRT1 protects against age-associated diseases and mediates cellular responses to genotoxins.

Arsenic toxicity causes numerous cellular defects and triggers carcinogenesis through a non-genotoxic mechanism which is poorly defined. Dysregulated maintenance of epigenetic imprinting promotes shifts in gene expression patterns which are associated with tumour development. This thesis explored a primary hypothesis that aberrant SIRT1 activity mediates the epigenetic events which initiate and promote arsenic-induced skin cancer. Additionally, since mutations to p53 are associated with overexpression of SIRT1 in skin cancer, this study also investigated the role of the p53/SIRT1/miR-34a axis during cell death signalling.

***The main experimental findings in this thesis are summarised below:***

Firstly, we established that p53 mutations in HaCaT keratinocytes increase SIRT1 expression by suppressing miR-34a-mediated regulatory control. These properties formed the basis for an *in vitro* model of dysregulated p53/SIRT1/miR-34a axis activity which is consistent with precarcinogenic changes observed in squamous cell carcinoma.

By transiently manipulating p53 and SIRT1 expression, we demonstrated that SIRT1 functions in combination with p53 to establish microRNA expression patterns in

human keratinocytes. Characteristic UV-induced TP53 mutations in HaCaT cells interfere with efficient biogenesis and maturation of a select group of microRNAs which regulate responses to genotoxic stress. As a result, expression of downstream microRNA-targeted mRNAs is poorly controlled in HaCaTs, causing overexpression of pro-survival proteins such as SIRT1. Up-regulation of cellular SIRT1 expression and inhibition of miR-34a processing suppresses p53 activation and contributes to apoptotic resistance in p53-mutated keratinocytes. Most importantly, by treating HaCaT keratinocytes with a pharmaceutical SIRT1 inhibitor, EX-527, we were able to enhance apoptotic sensitivity in this cell line by improving relative p53 acetylation.

Having characterised the role of p53/SIRT1/miR-34a axis activity in wild-type and pre-carcinogenic keratinocytes, we then tested the effect of arsenic on epigenetic regulation of SIRT1 and miR-34a gene promoters. Arsenic exposure over a 24 hr time frame alters the pattern of chromatin condensation by increasing histone H4 acetylation at lysine 16. These changes are consistent with inhibition of a key epigenetic regulator (SIRT1). Culture in arsenic-containing media for > 10 weeks did not induce sufficient phenotypic change to cause measureable transformation of cultured primary keratinocytes in this study; however the pattern of DNA methylation shifted in the regulatory promoter regions of SIRT1 and miR-34a genes and was associated with altered mRNA and protein expression. These data support our primary hypothesis, and correlate with evidence that PRG proteins (such as SIRT1) play a key role in arsenic-mediated transformation (640).

## *Future Directions*

SIRT1 inhibition has wide chemotherapeutic potential as a treatment strategy in skin cancer. Our investigations into p53/SIRT1/miR-34a axis activity were performed using HaCaT keratinocytes, and therefore conclusions about the effect of SIRT1 inhibition on apoptotic sensitivity in keratinocytes presented in Chapters 4

& 5 are only relevant in the context of the p53 mutations found in this cell line. Since TP53 alleles in the HaCaT cell line bear characteristic UV-induced mutations at commonly altered codons, it may be possible to expand the interpretation of our results in the context of other cancers with p53 mutations. Suppression of oncogenic proliferation by the SIRT1 inhibitor Tenovin-1 has recently been demonstrated in melanoma cell lines (629), and so to confirm the efficacy of EX-527 as an adjuvant for skin cancer therapy it would be useful to repeat our experiments using keratinocyte cell lines derived from epidermal squamous cell carcinomas. Further investigation is needed to explore the value of SIRT1 inhibitors in the design of targeted chemotherapeutic regimens for tumours with p53-mutated genotypes.

Future work in this area would be to track epigenetic changes in other key oncogenes/tumour suppressors using arsenic exposure in vitro as a model for carcinogenic transformation. Additionally, measurement of serum miRNA may be an alternative biomarker of arsenic toxicity in exposed populations. Ultimately, if we determine the significance of an epigenetic mode of action for arsenic-induced cancer, we could unlock the potential to block the transition of transformed cells between stages (particularly at the promotion stage, during which carcinogenesis is reversible) with epigenetic modulators or RNA interference therapy. This not only has implications for the prevention of cancer in arsenic-exposed populations, but also for our understanding and treatment of carcinogenesis as a multi-faceted disease.

## *Limiting Factors*

A major limiting factor during this investigation was the lack of a high-throughput technique for measuring SIRT1 activity. Although a number of multiplate assays designed to quantitate SIRT1 deacetylase activity are commercially available at present [ENZO Life Sciences, Catalogue # BML-AK555; Sigma-Aldrich, Catalogue # CS1040; Cayman Chemical Company, Catalogue # 10010991; Upstate (Millipore),

Catalogue # 17-10090; AbCam, Catalogue # ab156065], the accuracy of these assays was a matter of debate when this study commenced. As a rule, SIRT1 activity assays use a fluorescent probe attached to a modified peptide containing an acetylated lysine residue as an indicator. Several groups had revealed that these fluorescent probes acting as assay substrates were influencing SIRT1 activity (657). Since then, SIRT1 activity assays have been redesigned with luminescent indicators and are less prone to interference [Perkin-Elmer, Promega]. Retesting of SIRT1 activity in treated keratinocytes would be useful to confirm the inhibitory effect of arsenic in Chapter 6. Nonetheless, as the luciferase-bound substrate used in commercially available SIRT1 activity assays is a modified p53 peptide sequence containing an acetylated lysine residue, our results are still valid as we have used a comparable marker for SIRT1 activity (relative acetylation of p53 at lysine 382) to base our experimental conclusions - albeit using a semi-quantitative detection technique (immunoblotting).

As discussed in Chapter 1 [Table 1.6], the $K_m$ for lysine deacetylation by SIRT1 is substrate-specific; therefore assays which use a p53 peptide sequence as a marker may not provide an accurate representation of SIRT1 activity throughout the cell. Future enzymatic assays would be more sensitive and specific if they used an alternative marker [i.e. measure the formation of 2'-O-Acetyl-ADP-Ribose from NAD by nicotinamide cleavage and ADP-ribose transfer to acetate (212, 232, 233) to measure SIRT1 activity.

## *Conclusion*

In conclusion, this thesis has demonstrated the importance of efficient p53/SIRT1/miR-34a axis activity for protection of the skin from genotoxic insults, and that prolonged arsenic exposure impairs epigenetic regulation of SIRT1 and miR-34a gene expression in a duration-dependent manner. Aberrant miR-34a-mediated regulation of SIRT1 expression promotes carcinogenic transformation in

human keratinocytes, and consequently we demonstrated that manipulation of SIRT1 activity is sufficient to overcome apoptotic resistance with the p53-mutated HaCaT cell line. Finally, these data reveal novel insights into mechanisms which distinguish cells with p53 mutations from their healthy counterparts, and provides evidence which supports the use of SIRT1 inhibitors as a strategy for selective targeting of malignant cells during cancer therapy.

# Supplementary Material

# LIST OF BUFFER STOCK SOLUTIONS

## *Cell Culture*

| Dulbecco's Phosphate Buffered Saline [Calcium/Magnesium Free] | | |
|---|---|---|
| Components | g/L (10X) | Molarity (1X) |
| KCl | 2 | 2.7 mM |
| KH2PO4 (anhydrous) | 2 | 1.5 mM |
| NaCl | 80 | 136.9 mM |
| Na2HPO4 (anhydrous) | 11.5 | 8.9 mM |

| Hank's Balanced Salt Solution [Calcium/Magnesium Free] | | |
|---|---|---|
| Components | g/L (10X) | Molarity (1X) |
| KCl | 4 | 5.33 mM |
| KH2PO4 (anhydrous) | 0.6 | 0.44 mM |
| NaCl | 80 | 138 mM |
| Na2HPO4 (anhydrous) | 0.4788 | 0.3 mM |
| D-glucose | 10 | 5.6 mM |
| Phenol red (sodium salt) | 0.11 | 0.03 mM |
| NaHCO3 (add to 1X solution) | 0.35 (1X) | 4 mM |

## *Immunoprecipitation*

| Immunoprecipitation Lysis Buffer | |
|---|---|
| Tris-HCl (pH 7.5) | 50 mM |
| EDTA | 1 mM |
| Na3VO4 | 0.5 mM |
| β-mercaptoethanol | 0.10% |
| Triton X-100 | 1% |
| NaF | 50 mM |
| Sodium pyrophosphate | 5 mM |
| β-glycerophosphate | 10 mM |
| PMSF | 0.1 mM |
| Add Protease Inhibitor Cocktail before use | |

*Immunoblotting*

| Tris Buffered Saline Tween-20 [TBST] | |
|---|---|
| Components | Quantity (1×) |
| Tris HCl (7.6) | 20 mM |
| NaCl | 150 mM |
| Tween-20 | 0.10% |

| SDS-PAGE Running Buffer | |
|---|---|
| Components | Quantity (1×) |
| Tris HCl (8.3) | 25 mM |
| Glycine | 190 mM |
| SDS | 0.10% |

| SDS-PAGE Transfer Buffer [Towbins Buffer] | |
|---|---|
| Components | Quantity (1×) |
| Tris HCl (8.5) | 25 mM |
| Glycine | 0.2 M |
| Add 10% methanol to 1X solution prior to use | |

| RadioImmunoPrecipitation Assay [RIPA] Cell Lysis Buffer | |
|---|---|
| Components | Quantity (1×) |
| Tris-HCl (pH 8.0) | 50 mM |
| NaCl | 150 mM |
| NP-40 | 1% (v/v) |
| Sodium deoxycholate | 0.5% (w/v) |
| SDS | 0.1% (w/v) |
| Glycerol | 10% (v/v) |
| Add Protease and Phosphatase Inhibitors at time of use | |

| Laemmli Sample Buffer | |
|---|---|
| Components | Quantity (1×) |
| Tris HCl (6.8) | 62.5 mM |
| SDS | 2% (w/v) |
| Glycerol | 10% (v/v) |
| *DTT or BME | 50 mM |
| Bromophenol Blue | 0.01% (w/v) |
| *Add at time of use | |

*ChIP*

Nuclear Lysis Buffer (ChIP)

| Component | Concentration | |
|---|---|---|
| Tris.HCl (pH 8.0) | 50 mM | |
| EDTA | 10 mM | Add Protease Inhibitor Cocktail before use |
| SDS | 1% | |

Dilution Buffer (ChIP)

| Component | Concentration | |
|---|---|---|
| Tris.HCl (pH 8.0) | 16.7 mM | |
| NaCl | 167 mM | Add Protease Inhibitor Cocktail before use |
| EDTA | 1.2 mM | |
| Triton X-100 | 1% | |

Low Salt Buffer (ChIP)

| Component | Concentration |
|---|---|
| Tris.HCl (pH 8.0) | 20 mM |
| SDS | 0.10% |
| NaCl | 150 mM |
| EDTA | 2 mM |
| Triton X-100 | 1% |

High Salt Buffer (ChIP)

| Component | Concentration |
|---|---|
| Tris.HCl (pH 8.0) | 20 mM |
| SDS | 0.10% |
| NaCl | 500 mM |
| EDTA | 2 mM |
| Triton X-100 | 1% |

LiCl Buffer (ChIP)

| Component | Concentration |
|---|---|
| Tris.HCl (pH 8.0) | 10 mM |
| Igepal | 1% |
| LiCl | 250 mM |
| EDTA | 1 mM |
| Sodium Deoxycholate | 1% |

Elution Buffer (ChIP)

| Component | Concentration |
|---|---|
| SDS | 1% |
| NaHCO3 | 100 mM |

*PARP Sample Buffer*

| PARP Sample Buffer | |
|---|---|
| Component | Quantity (1×) |
| Tris HCl (6.8) | 62.5 mM |
| Urea | 6 M |
| Glycerol | 10% |
| SDS | 2% |
| Bromophenol Blue | 0.00% |
| B-mercaptoethanol | 5% |

*Staining*

| Coomassie Blue Gel Stain | Destaining Solution |
|---|---|
| 0.05% (w/v) Coomassie blue R-250 | 20% (v/v) ethanol |
| 40% (v/v) ethanol | 0.5% (v/v) acetic acid |
| 5% (v/v) acetic acid | |

## RANGE FINDING AND TOXICITY

Measuring and comparing the effect of p53 mutations on apoptotic sensitivity is complicated by many factors, including 1) method of induction; 2) duration of exposure; 3) endpoint targets; and 4) assay parameters.

Initial screening tests were designed to determine conditions of dose and duration which induce measurable apoptotic changes, and which are able to discriminate differences in apoptotic sensitivity between NHEK and HaCaT cells.

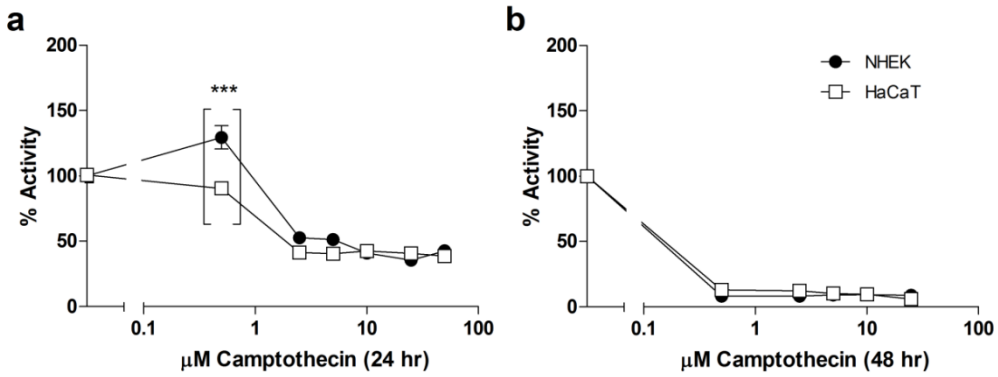


*Figure vii Range Finding - Apoptosis Inducers*

Primary (NHEK) (●) and p53-mutated (HaCaT) (□) keratinocytes were seeded into 96 well microplates at 5000 cells/well and allowed to recover overnight prior to camptothecin (CPT) treatment. Cellular activity was assayed by measuring resozurin reduction after 24 (Panel **a**), or 48 (Panel **b**) hours of exposure. The fluorimetric signal was normalised to unseeded media-only control wells, and results were analysed as a percentage of the signal from the untreated control population.
All data represent mean ± SEM of 4 independent experiments. Significant differences between cell lines are represented as *** ($p < 0.001$).

After 24 hrs, metabolic activity increased by 20% in NHEKs exposed to submicromolar CPT, however metabolic activity was not altered by CPT in HaCaTs under the same conditions [Figure i]. CPT-induced genotoxic damage induces mitochondrial reducing proteins – hence metabolic activity increases. An altered metabolic response to stress indicates that the HaCaT cell line has undergone a partial shift in its cellular respiration. Additionally, duration of exposure to CPT

influences its toxicity in both cell lines as the DNA damaging effect of Topoisomerase I inhibition is S-phase specific (658, 659); therefore greater cytotoxicity is measured after 48 hr [Figure i].

In order to discriminate between live, apoptotic and necrotic cells using the caspase 3/7 assay, the signal was normalised using results from co-treated cell proliferation assays. As keratinocytes are prone to detachment with cytotoxicity, some signal loss occurred using the CyQUANT assay due to the removal of detached cells with the treatment medium as part of the protocol. Thus this assay could not be reliably used to discriminate between healthy and apoptotic cells after CPT treatment [Figure ii (a)]. The ATPLite protocol did not require any removal of medium, and so was a better prospect for normalisation of the Apo-ONE assay [Figure ii(b)].

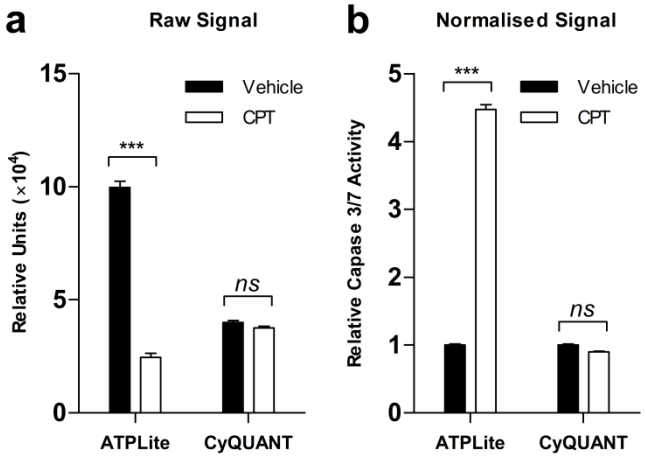


*Figure viii Normalisation of Caspase 3/7 activity by ATPLite and CyQUANT viability assays*

Primary keratinocytes (NHEKs) were seeded into microplate wells at 5,000 cells/well and treated with 5 μM CPT for 24 hr. Cell number was determined using CyQUANT and ATPLite viability assays (Panel **a**), and analysed using pairwise *t*-tests. Apoptosis was detected using the Apo-ONE caspase 3/7 activity assay (Panel **b**) according to the manufacturer's instructions, and normalised to cell number using both viability assays. The effect of CPT on caspase 3/7 activity in NHEKs was analysed from 4 independent populations relative to untreated vehicle controls using pairwise *t*-tests. Significant differences are represented as $p<0.001$; ***; or *ns*, not significant.

## TRANSIENT TRANSFECTION OF PRIMARY KERATINOCYTES

RNA interference (RNAi) is a posttranscriptional regulatory mechanism which uses complementary base pairing of ~21 nucleotide length small interfering RNAs (siRNA) to a target mRNA sequence. RNA oligonucleotides are processed by DICER into smaller fragments before the siRNA antisense strand is then loaded into an RNA-induced silencing complex (RISC) for recognition and degradation of the target mRNA sequence. Synthetic siRNAs utilise the endogenous cellular RNAi machinery to specifically act upon a target mRNA sequence for degradation.

RNAi experiments use cationic lipid, viral vector or electroporation techniques to deliver siRNAs across cell membranes, and most typically achieve a transient reduction in gene expression – however the production of stable transfectants is also possible (660). As an investigative technique, RNAi experiments are complex to interpret due to problems with cellular toxicity, interferon-mediated responses and off-target phenotypic effects (661-664). Knockdown of a gene with a targeting siRNA depends on both transfection efficiency (siRNA complex uptake) and reduction in gene expression/target protein activity. As these are highly variable between tissues, each RNAi experiment requires that the transfection conditions are optimised specifically to cater for specific cell lines (665). In order to determine the impact of arsenic on the SIRT1-p53-miR-34a axis, we first developed a model to characterise the axis in our cell cultures.

Cultured primary human keratinocytes are difficult to transfect with high efficiency (666). Transfection efficiency can be improved with removal of hormonal supplements from the transfection medium (667) or with nucleofection (668). Opti-MEM medium is normally recommended as a transfection diluent by the Lipofectamine2000 manufacturer (Invitrogen, Life Technologies); however this product induces senescence in keratinocytes as a consequence of its calcium content (1.8 mM). For this study, siRNA-Lipofectamine2000 complexes were prepared in unsupplemented EpiLife growth medium without added antibiotics and

added directly to the culture plates. Transfection was carried out at 37°C and 5% CO2 in a humidified incubator. After 3 hours, keratinocyte supplement solution was added to each well and the plates returned to the incubator.

For each cell culture, a range of doses was tested according to the manufacturer's instructions to determine tolerance to the cationic lipid in transfection solution. Relative toxicity was measured using AlamarBlue reagent and the dose which generated >80% viability was chosen as optimal for transfection. OnTARGET pool siRNA pellets were resuspended in 1X siRNA buffer [20 mM KCl, 6 mM HEPES (pH 7.5), 0.2 mM $MgCl_2$] to generate 20 µM stock solutions which were stored at −80°C. Prior to use, stock solutions were diluted to 5 µM in siRNA buffer, and then dissolved in the appropriate volume of transfection medium. A matrix of controls and a range of siRNA doses were tested using the transfection protocol outlined below. After 24 hours, mRNA was extracted and tested for knockdown of the target by RT-PCR. Knockdown of mRNA >80% represented optimal transfection.

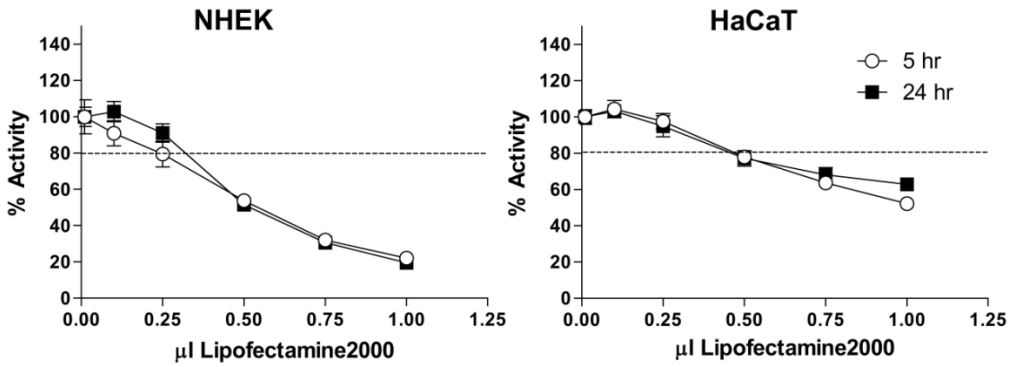


*Figure ix Lipofectamine2000 toxicity in primary and p53-mutated keratinocytes*

Primary (NHEK) and p53-mutated (HaCaT) keratinocytes were seeded into 96 well microplates at 5000 cells/well and allowed to recover overnight prior to Lipofectamine treatment. Cellular activity was assayed by measuring resozurin reduction after 5 (○), or 24 (■) hours of exposure. The fluorimetric signal was normalised to unseeded media-only control wells, and results were analysed as a percentage of the signal from the untreated control population.
All data represent mean ± SEM of 4 independent experiments.

First, to optimise the volume of Lipofectamine2000, toxicity was assayed in NHEK and HaCaT cells by introducing Lipofectamine2000 (0-1.25 µl/well) to the culture medium of cells growing in 96 well culture plates and testing cell viability by AlamarBlue assay after 5 hr and 24 hr of incubation. Exposure to Lipofectamine2000 was more toxic for NHEKs than for HaCaT keratinocytes, reducing cell viability to 80% at volumes >0.25 µl/well, and viability did not significantly decrease over time for either cell culture [Figure iii]. Using these results and scaling up the volume for transfection in 6 well culture plates, 5 µl/well was determined to be optimal for effective siRNA delivery with minimal toxicity.

siRNA concentration was titrated to find the optimal concentration for knockdown by treating NHEK and HaCaT keratinocytes with 5, 25 and 50 nM of ON-TARGET siRNA mix and measuring expression of the targeted mRNAs at 48hr and measuring protein expression at 72 hr incubation. Ablation of target mRNAs improved for both cell cultures when siRNA concentration increased. HaCaT keratinocytes had a higher knockdown efficiency than NHEK cells [Figure iv].

For the NHEK cell strain, SIRT1 mRNA was reduced from 55% (5 nM) to 35% (50 nM) and p53 mRNA from 60% (5 nM) to 39%. In HaCaTs, SIRT1 mRNA decreased from 52% (5 nM) to 14% (50 nM), and p53 mRNA decreased from 15% (5 nM) to 5% (50nM) when compared to expression in cells transfected with equivalent concentrations of a non-targeting siRNA pool [Figure iv]. Whilst knockdown by 50 nM of siRNA in HaCaTs was >80%, depletion of SIRT1 and p53 was unsatisfactory with this concentration of siRNAs in NHEK cells.

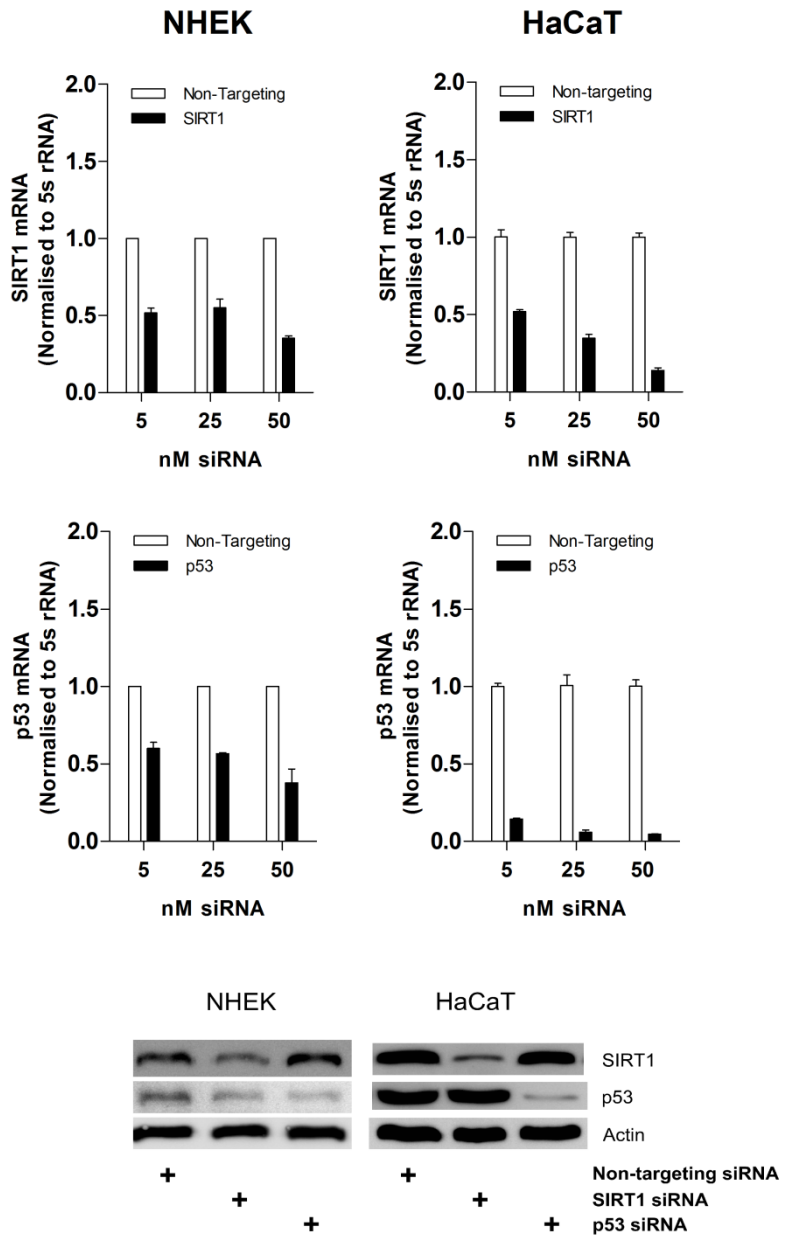


*Figure x SIRT1 and p53 siRNA transfection optimisation in human keratinocytes*

Primary (NHEK) and p53-mutated (HaCaT) human keratinocytes were transfected with 5, 25 or 50 nM of SIRT1 or p53 siRNA oligonucleotide pools. SIRT1 mRNA and p53 mRNA expression was measured by RT-PCR after 48 hrs, and SIRT1 or p53 ablation was analysed relative to transfection with equal concentrations of a non-targeting oligonucleotide pool. Values were normalised using 5S rRNA as a control gene.

Next, the siRNA concentration was increased to 100 nM in the NHEK cell strain in an attempt to improve knockdown efficacy. Although SIRT1 further decreased [35% →

18%; Figure v] with the increase in siRNA concentration, suppression of p53 only improved by 10% at 100 nM siRNA [39% → 29%; Figure v].

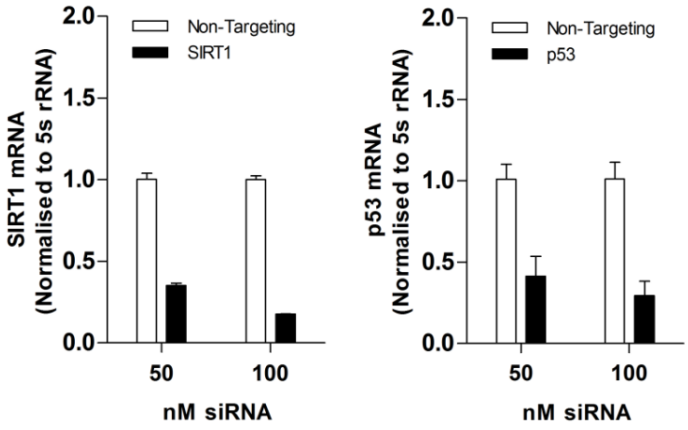


*Figure xi Transient knockdown of SIRT1 and p53 with 100 nM siRNA targeting pools in primary human keratinocytes*

Primary human keratinocytes (NHEK) were transfected with 50 or 100 nM of SIRT1 or p53 siRNA oligonucleotide pools. SIRT1 mRNA and p53 mRNA expression was measured by RT-PCR after 48 hrs, and SIRT1 or p53 ablation was analysed relative to transfection with equal concentrations of a non-targeting oligonucleotide pool. Values were normalised using 5S rRNA as a control gene.

For our study, Lipofectamine2000 (Invitrogen, Life Technologies) was initially used as an siRNA delivery system; however NHEKs transfected using Lipofectamine2000 demonstrated morphological changes consistent with an increase in toxicity. Based on this observation, an alternative cationic delivery system, RNAiMAX (Invitrogen, Life Technologies), was used to decrease the risk of stress-induced off-target interference in NHEK cells. RNAiMAX reduced toxicity during transfection and improved siRNA delivery, enabling transfection with 10 nM siRNA and achieving a percentage reduction in target gene expression which was comparable to that achieved with 100 nM siRNA using Lipofectamine2000 as a delivery system.

## TARGET SITE MASKING BY LNA-MODIFIED OLIGONUCLEOTIDES

Overexpression vectors (either plasmid or viral) are classically used to manipulate gene expression by increasing copy number. However insertion of these vectors into a proliferating cell line is fraught with similar issues as for RNAi – i.e. off-target expression changes, toxicity, and inconsistent stability. Considering the sensitivity of NHEKs to transfection during knockdown experiments, alternative approaches for up-regulating gene expression were adopted.

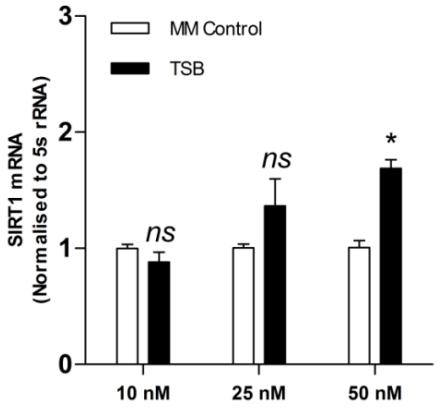


*Figure xii Titration of delivery dose for effective miR-34a:SIRT1 target site masking*

Primary human keratinocytes (NHEK) were transfected with 10 nM, 25 nM or 50 nM of a directed miR-34a:SIRT1 target site blocking (TSB) or mismatched control (MM Control) LNA-modified oligonucleotide pool. SIRT1 mRNA, was measured by qRT-PCR, and the effect of target site masking analysed relative to the mismatched control treatment. Values were normalised using 5S rRNA as a control gene. Results were analysed by paired *t* test; with * ($p$<0.05; $n$=3).

SIRT1 expression is modulated by a suite of posttranscriptional and posttranslational regulatory mechanisms, including those directed by non-coding RNAs. The consensus opinion is that miR-34a binding to the SIRT1 3'UTR promotes mRNA degradation and blocks protein translation (479). In addition to SIRT1, miR-34a regulates numerous targets within the cell. Although others have used siRNA-based techniques to investigate miR-34a-mediated gene regulation, miR-34a inhibitors potentially impact numerous cellular processes and therefore this

technique is non-specific from a mechanistic point of view. With this in mind, we designed oligonucleotides to competitively inhibit the SIRT1 mRNA binding site targeted by miR-34a. This approach allowed us to determine the role of the SIRT1/miR-34a regulatory axis during genotoxic stress in a more specific manner.

The efficacy of miR-34a:SIRT1 target site masking was confirmed by assaying SIRT1 expression following introduction of the miR-34a:SIRT1 target site blocking oligonucleotides. During a 48 hour treatment period, effective miR-34a:SIRT1 binding site masking was achieved with 50 nM of LNA-modified oligonucleotides [Figure vi]. This concentration was chosen for use in future experiments, and a total exposure time of 72 hours was used to enable detection of accumulated SIRT1 protein in NHEK cells.

## IMMUNOPRECIPITATION

To perform these experiments, two methodologies were used – first, immunocomplexes were captured using SIRT1 antibodies, prior to western blotting with p53-targeting antibodies; and alternatively, p53 antibodies were used for immunoprecipitation, with associated SIRT1 in the precipitate detected by immunoblotting. Both approaches were used to ensure that results were not affected by differences in antibody-antigen binding kinetics between the p53 and SIRT1 antibodies used for the experiment. Initially, immunoprecipitation was successful using a SIRT1 antibody [#2496, Cell Signalling Technology], however a p53 antibody solution [sc-98, Santa Cruz Biotechnology] failed to capture p53:SIRT1 immunocomplexes [Figure vii]. In later experiments, an alternative p53 antibody [#9282, Cell Signalling Technology] was used for antigen capture, and associations between p53 and SIRT1 detected by Western blotting with the anti-SIRT1 antibody.

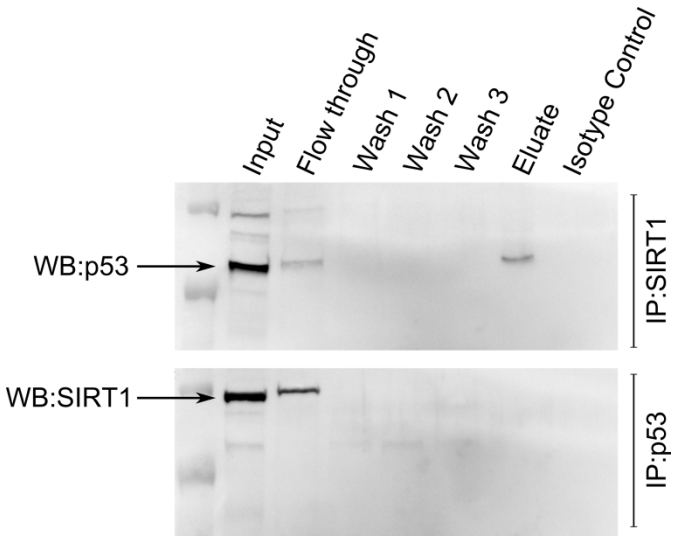


*Figure xiii Optimisation of immunoprecipitation methodology*

## ANALYSIS OF CpG METHYLATION

To test whether arsenic treatment influences DNA methylation patterns, 5 × 105 cells were harvested after 10 weeks of arsenic exposure, washed in PBS and the DNA prepared for methylation analysis with a Cells-to-CpG Bisulfite Conversion Kit (Applied Biosystems, Foster City, CA, USA) according to the manufacturer's instructions.

### *High Resolution Melt Curve Analysis*

Genomic DNA from treated cells was amplified with MeltDoctor high resolution melt (HRM) reagents (Applied Biosystems, Foster City, CA, USA) using cycling conditions optimized for each individual primer set used, and then subjected to melt curve analysis. Methylation standards were included in each experiment and bisulfite converted gDNA from an immortal human keratinocyte cell line grown in EpiLife (HaCaT) was included for comparison. Melt curve data was analysed using High Resolution Melt Software v3.0 (Applied Biosystems, Foster City, CA, USA).

HRM analysis represents an average of methylation information across the amplified region, and so results should be interpreted as such. Additionally, data are shown as a range of values rather than an absolute figure as these are generated from pooled sample populations. Difference plots were analysed by comparing percentage methylation relative to melt curve standards across each target region, and this information was used to predict the outcome of sequencing analysis. Here CpG methylation in the SIRT1 promoter progressively increased, whilst pri-miR-34a promoter methylation decreased with arsenic treatment [Figure viii].

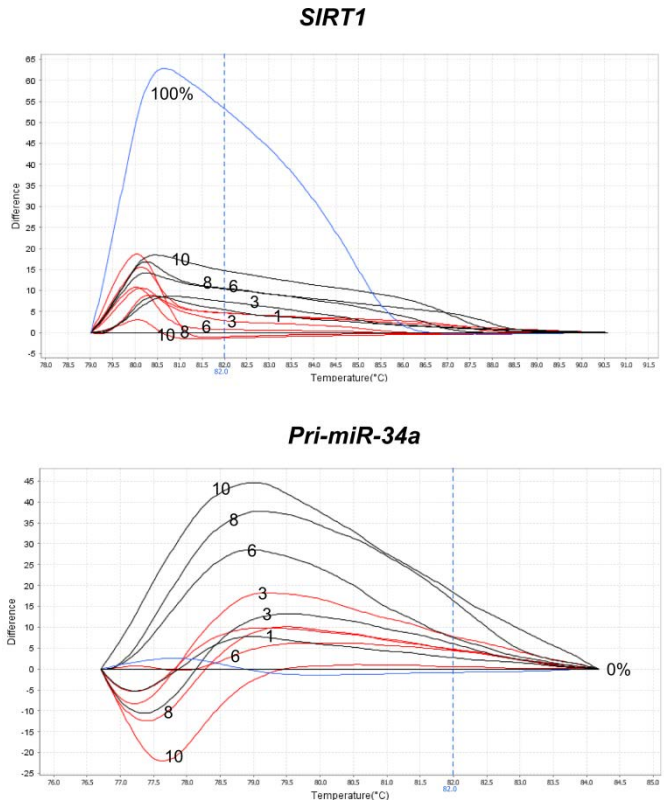


*Figure xiv Melt Curve Analysis – 10 week (70 day) treatments*

Bisulfite-converted DNA from arsenic-exposed keratinocytes was amplified using SIRT1 and pri-miR-34a bisulfite primers and high resolution melting performed with MeltDoctor HRM Reagents. Melt curves were analysed using High Resolution Melt Software v3.0 (Applied Biosystems, Foster City, CA, USA). Difference plots are represented by week (1-10).

Control samples are represented in black, and As(III) treated samples are red. Curves generated from methylated and unmethylated control DNA are included for reference.

*Analysis of Partial Methylation*

The DNA sequences of bisulfite converted samples were assayed after PCR amplification by Sanger sequencing using an ABI Prism 310 Genetic Analyser. As these samples were obtained from heterogeneous cell populations rather than from individual clones, the signal trace represented a mixture of methylation states at each CpG locus. The ratio of mixed bases [methylated:non-methylated cytosines] on sequencing traces was analysed using the schematic in Figure ix.

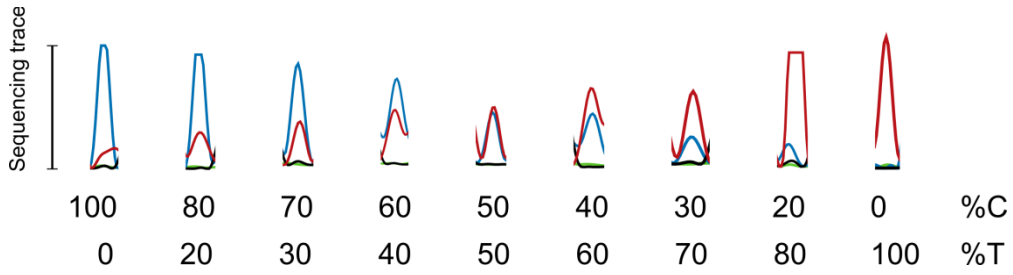


*Figure xv Assessment of partial methylation in heterogeneous populations*

Schematic demonstrating sequencing traces obtained from populations with heterogeneous methylation states at CpG loci. Blue chromatogram trace represents the signal measured from cytosine bases, red trace represents thymine bases

The effect of arsenic on CpG methylation in the treated population was represented graphically using the CLC Main Workbench application (Version 6.7.1). [Figure x; Figure xi]. These histograms were used to confirm the methylation output from BiQ Analysis of the derived sequences. Note – the data produced by BiQ analysis represents either non-methylation or full methylation of CpG loci. For homogeneous sequencing data derived from cloned samples, the cytosine of each locus is either 0% or 100% methylated, however the CpG loci of heterogeneous samples analysed here have been assigned methylation status based on <50% (unmethylated) or >50% (methylated) methylation of the cytosine signal.

At the SIRT1 promoter, methylation increased for loci **c**, **d**, **e**, **i** & **j**; and decreased at locus **h** in arsenic-exposed keratinocytes. Moreover, specific loci (**d**, **e**, **f**) responded

to arsenic exposure in a duration-dependent manner, however loci **i** & **j** were consistently methylated by arsenic treatment [Figure x].

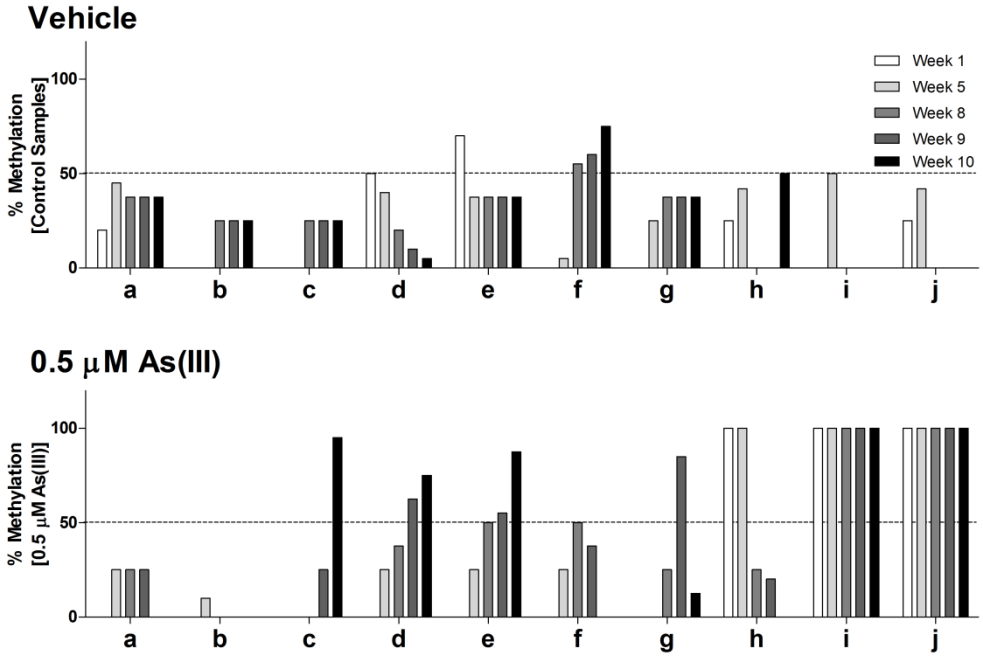


*Figure xvi Percentage methylation of SIRT1 promoter CpG loci in vehicle and arsenic-exposed keratinocytes*

Normal human keratinocytes were cultured in media containing 0.5 µM As(III) for a period of 10 weeks. Genomic DNA was extracted at weeks 1, 5, 9 & 10 for bisulfite conversion and sequencing of SIRT1 PCR fragments. The sequencing trace was assessed for percentage methylation of each CpG dinucleotide (a-j) and represented histogrammatically.

Methylation analysis at the miR-34a promoter was more complicated, as the sequence was particularly unstable during bisulfite conversion. Consequently, our analysis of cytosine methylation was not conclusive for all samples, and so paired results are presented for weeks 5, 9 & 10 only [Figure xi]. Overall, arsenic-treated samples had a lower percent methylation at miR-34a promoter CpG dinucleotides than their passage-matched controls.

Analysis of the sequencing traces correlated with BiQ analysis of the raw data presented in Chapter 7.

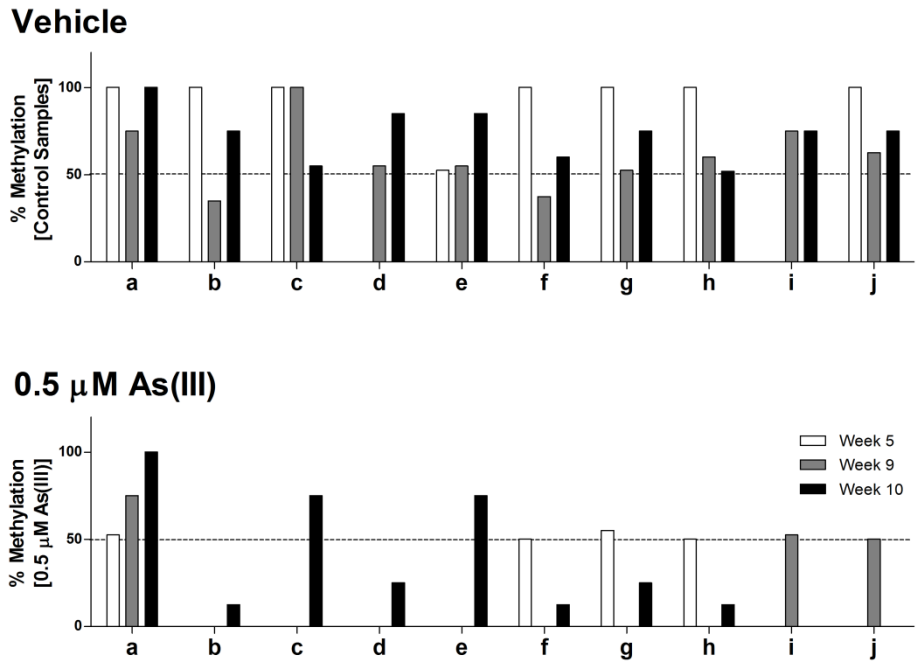


*Figure xvii Percentage methylation of miR-34a promoter CpG loci in vehicle and arsenic-exposed keratinocytes*

Normal human keratinocytes were cultured in keratinocyte growth media (Vehicle) or media containing arsenic (0.5 μM As(III)) for a period of 10 weeks. Genomic DNA was extracted at weeks 5, 9 & 10 for bisulfite conversion and sequencing of pri-miR-34a PCR fragments. The sequencing trace was assessed for percentage methylation of each CpG dinucleotide (a-j) and represented histogrammatically.

## MICROCOCCAL NUCLEASE DIGEST

Micrococcal nuclease is a non-specific endonuclease that preferentially cleaves internucleosomal regions of DNA, limiting PCR amplification of digested templates by nucleosome-spanning primers. The principle of the micrococcal nuclease (MNase) assay is that silent 'closed' heterochromatin is more compacted than 'open' euchromatin, and thus a ≥10-fold differences in enzyme activity is required to cleave a specific genomic sequence to the same extent (669). These differences in MNase accessibility can be used to assay chromosomal structure by PCR amplification of a target region.

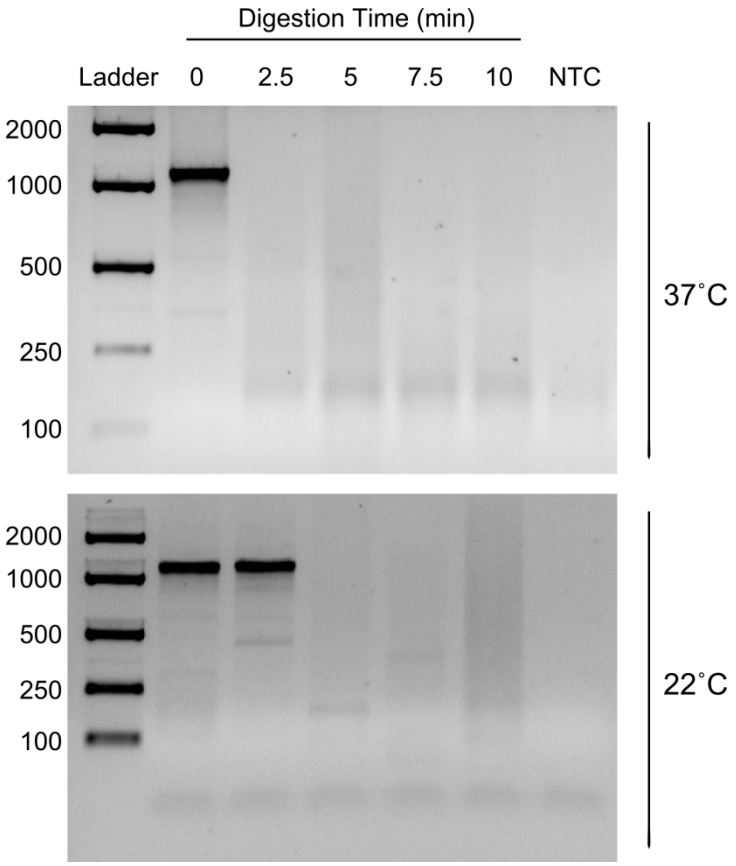


*Figure xviii Optimisation of MNase Digestion Temperature*

Nuclei were isolated from NHEK cells and incubated with micrococcal nuclease at 37°C or 22°C for increasing digestion times. DNA was extracted according to the ChART protocol outlined in Chapter 2, and equal concentrations were amplified for 40 PCR cycles using *pri-miR-34a* ChART primers. PCR product was run on 2% agarose gel and visualised with SYBR Safe DNA stain.

To discriminate between loose and compact chromatin states, MNase activity was limited to enhance the assay's specificity, and it was therefore necessary to empirically determine the appropriate MNase reaction conditions necessary to differentially analyse chromatin structure over the genomic locus of interest. This was achieved by using short incubation times and suboptimal reaction temperatures. Micrococcal nuclease activity is optimal at 37°C and DNA cutting most efficient with an incubation time of 20 min. By reducing reaction temperature to 22°C (room temperature) MNase activity was limited, allowing PCR product to be amplified with a digestion time of 2.5 min [Figure xii].

Although cleavage was limited for the miR-34a target at the lower temperature, this result was only evident at the minimal digestion time used in the experiment. Next, the ability of MNase digestion to discriminate between chromatin condensation states of different genes was assessed by comparison with the amplification profile of the control gene (*Rhodopsin*), which was assumed to be inactive (and therefore condensed) in keratinocytes.

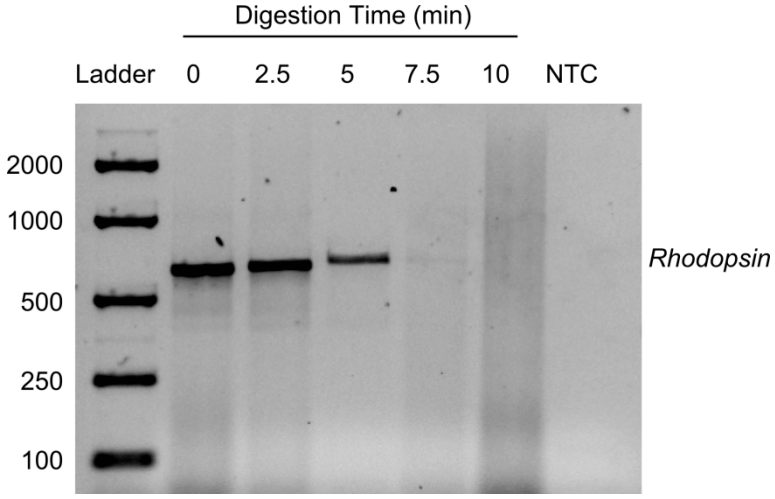


*Figure xix Optimisation of MNase Incubation Time*

Nuclei were isolated from NHEK cells and incubated with micrococcal nuclease at 22°C for increasing digestion times. DNA was extracted according to the ChART protocol outlined in Chapter 2, and equal concentrations were amplified for 40 PCR cycles using ChART primers targeting *Rhodopsin*. PCR product was run on 2% agarose gel and visualised with SYBR Safe DNA stain.

Using the previously outlined incubation conditions, a drop-off in PCR product after end-point amplification demonstrates that MNase digestion has increased in a time-dependent manner [Figure xiii], with the target region completely cleaved after 10 minutes of enzyme activity at 22°C. When compared with results obtained for the miR-34a target region, which was completely cleaved after 5 min [Figure xii], it appears that *Rhodopsin* is more MNase resistant than the *pri-miR-34a* promoter region. These results indicate that the chromatin containing the region of DNA amplified by the *Rhodopsin* primers is more compacted (and less MNase-accessible) than the corresponding chromatin/DNA amplified by *pri-miR-34a*-targeting primers. From these data, 5 minutes of MNase digestion at 22°C proved optimal for differential detection of variability in chromatin structure in this study.

## SAMPLE PREPARATION FOR ChIP

### *Sample Preclearing*

Unlike protocols for immunoprecipitation with agarose beads, when using magnetic beads for immunoprecipitation, sample preclearing is not required and blocking the beads with salmon sperm DNA is not recommended (according to manufacturers' protocols). Sodium butyrate is a general histone deacetylase inhibitor and is included in buffer solutions used for analysis of histone posttranslational modifications (670, 671). When samples were processed with 5 µM sodium butyrate in lysis buffer solutions, the isotype/IgG control templates amplified more strongly than the 5% input templates [Figure xiv].

Sodium butyrate appears to enhance binding of free DNA to the magnetic beads when included in buffer solutions. Background was reduced by preclearing these samples in the same volume of magnetic beads, however this was only partially

effective [Figure xiv]. Consequently, sodium butyrate was removed from lysis buffers to prevent background DNA from sticking to the beads.

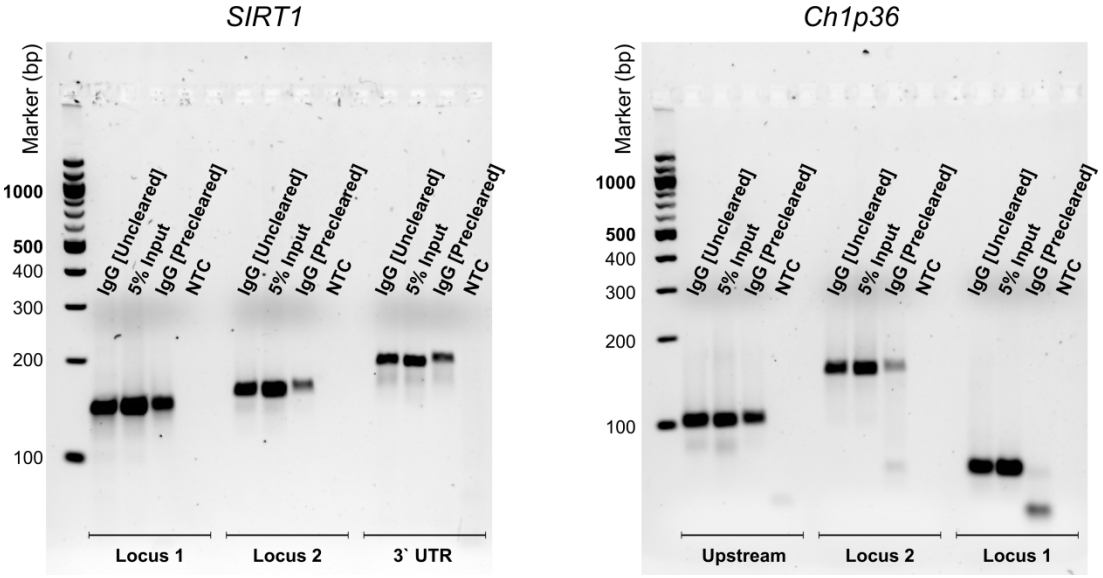


*Figure xx Sample preclearing decreases ChIP background signal*

Crosslinked chromatin was prepared from NHEK cells isolated in buffer solutions containing 5µM sodium butyrate. Samples were precleared by incubation with Protein G Magnetic beads for 1 hr at 4°C on a roller, and then incubated in IgG-bound Protein G Magnetic beads overnight at 4°C on a roller. Captured DNA was extracted according to the ChIP protocol outlined in Chapter 2, and amplified *with SIRT1* and *pri-miR-34a* targeting primer sets for 40 PCR cycles. Equal volumes of PCR product were run on 2% agarose gel and visualised with SYBR Safe DNA stain.
Input (5%) and non-cleared, IgG-incubated sample DNA was amplified for comparison.

## *Analysis of Results*

To ensure that the experimental results were consistent and representative of arsenic-induced effects, each ChIP experiment was controlled by the following methods:

- An isotype matched immunoglobulin (Ig) was used as a non-targeting immunoprecipitation control in all experiments.
- Anti-Histone H3 ChIP was used as a positive control for enrichment [Figure xv]

- A non-template control was included in each PCR reaction
- *RPL30* (Ribosomal Protein L30, Exon 3) was used as a constitutive gene control. It is assumed that occupancy at the RPL30 locus is invariant between treated samples.
- Positive (region of the gene target containing suspected locus of interest) and negative (region of the gene target distant to locus of interest) control loci were targeted for amplification by RT-PCR. The 3'UTR was the negative control locus for *SIRT1*, and for *pri-miR-34a*, a region of the gene upstream from the CpG island was used.

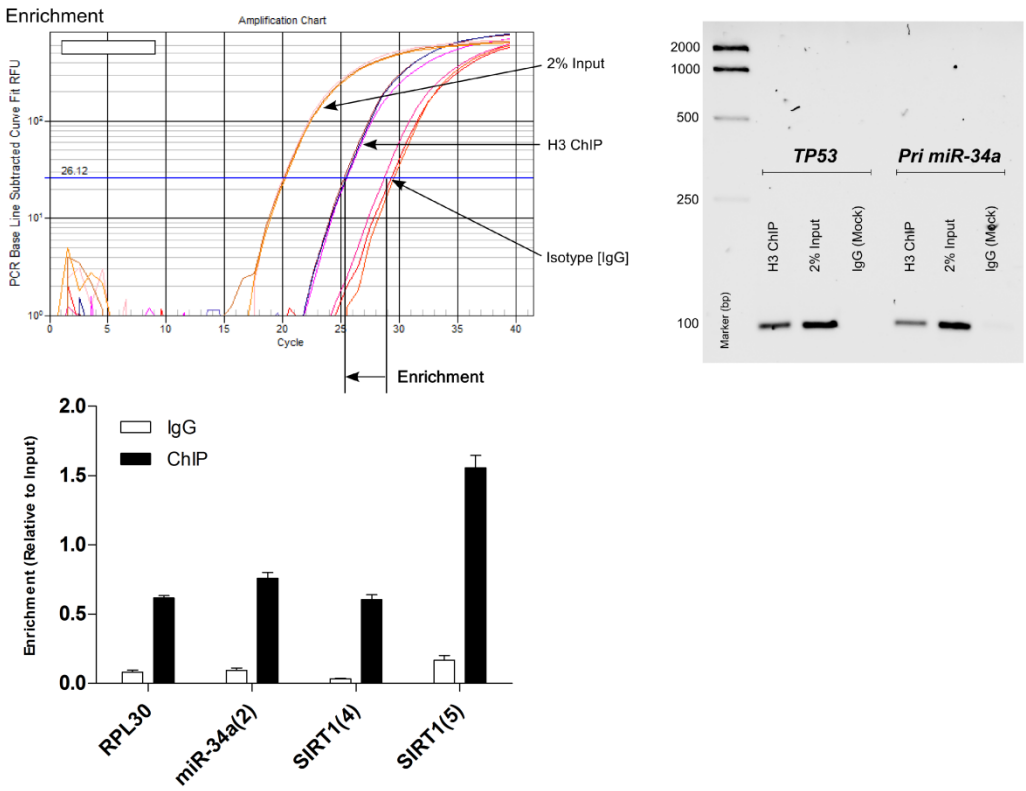


*Figure xxi ChIP enrichment with H3(Total) antibody*

Crosslinked chromatin was prepared from NHEK cells and incubated in H3 antibody-bound Protein G Magnetic beads overnight at 4°C on a roller. Captured DNA was extracted according to the ChIP protocol outlined in Chapter 2, and amplified *with TP53* and *pri-miR-34a* targeting primer sets for 40 PCR cycles. Equal volumes of PCR product were run on 2% agarose gel and visualised with SYBR Safe DNA stain. Input (2%) and IgG-incubated sample DNA was amplified for comparison.

Amplification of the captured target ChIP at the non-targeting negative control locus was not substantially different from amplification by sample incubated with isotype control IgG [Figure xvi(a)], and the positive control primer set amplified the ChIP target sample more strongly relative to the total input samples than the negative control primer set [Figure xvi(b)]. This represented the occupancy at target promoters for the ChIP sample.

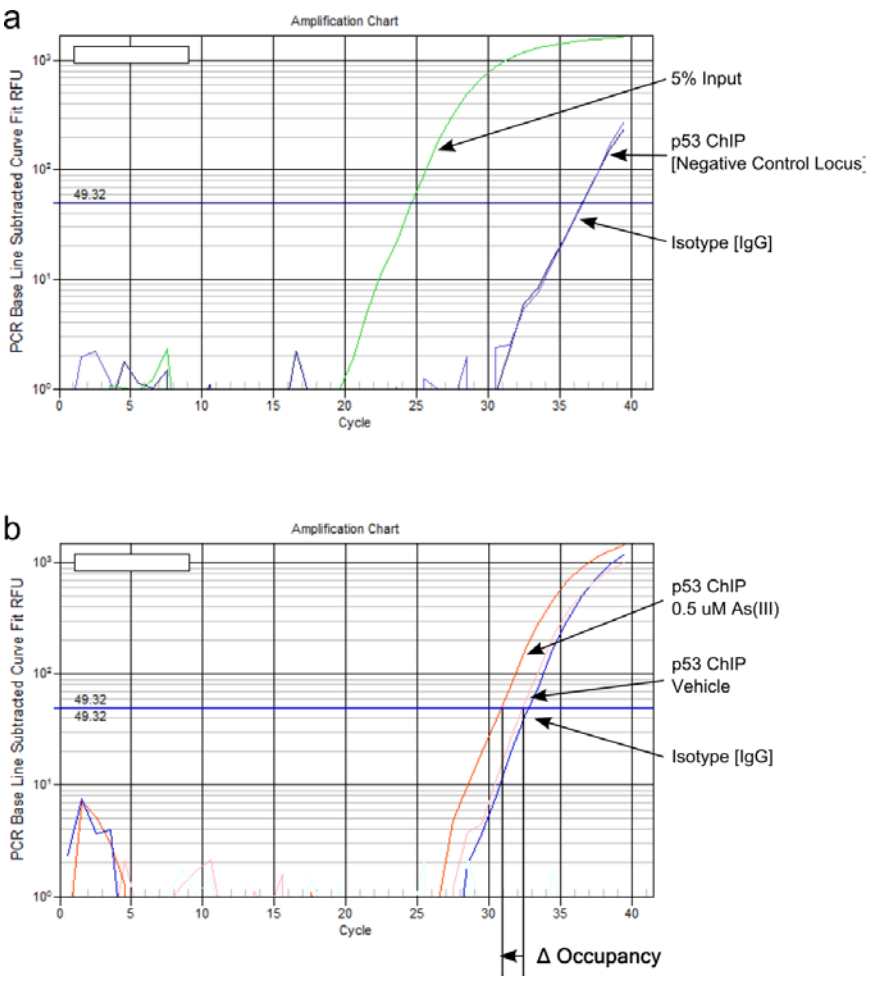


*Figure xxii Gene Target Controls for ChIP*

PCR amplification traces from As(III)-treated NHEK samples following incubation with p53 antibody-bound Protein G Magnetic beads. Panel a: Negative control gene locus (*pri-miR-34a*); Panel b: Positive control gene locus (*pri-miR-34a*).

*Endpoint ChIP-PCR*

Endpoint ChIP-PCR was performed to verify the ability of quantitative ChIP-PCR to differentiate between arsenic-treated samples. Equal template volumes from Vehicle, As(III)-treated, IgG isotype control, and 5% Input DNA were amplified for 40 PCR cycles using *Pri-miR-34a* and *SIRT1* ChIP primers according to the protocol outlined in Chapter 2 and PCR products were visualised by agarose gel electrophoresis.

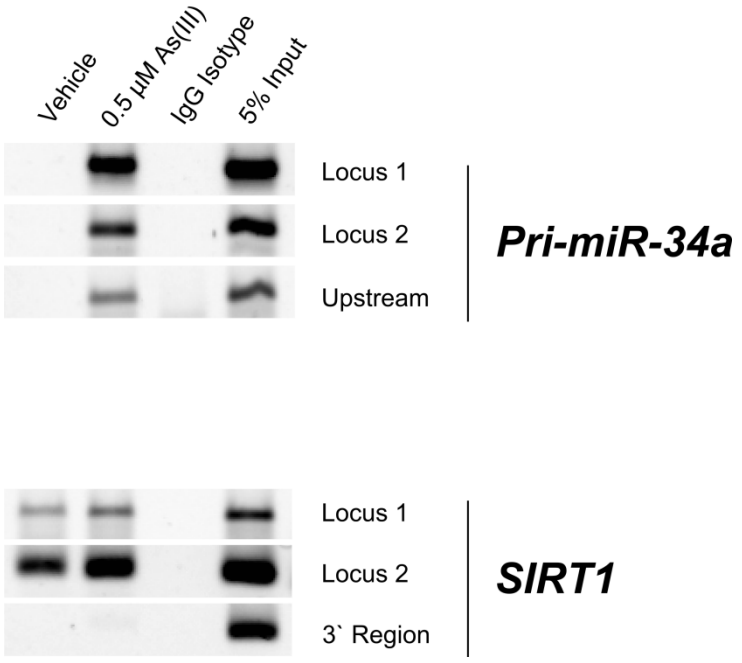


*Figure xxiii Endpoint PCR in Arsenic-Treated Keratinocytes*

ChIP was performed on crosslinked chromatin from As(III)-treated NHEK samples using Histone H4 acetyl K16 antibody-bound Protein G Magnetic beads. Samples were amplified for 40 cycles using *SIRT1* and *pri-miR-34a* ChIP-PCR primers, and 8 µl PCR product was separated on 2% agarose electrophoresis gels and bands visualised by SYBR Safe staining.

Here, visualised endpoint PCR products correlated with results calculated by quantitative PCR [Figure xvii].

# Publications and Conference Abstracts

Herbert, K. J., Snow, E. T., 2012, Modulation of arsenic-induced epidermal growth factor receptor pathway signalling by resveratrol, *Chem Biol Interact* **198** (38-48)

Arsenic (As) is both a human carcinogen and an effective anticancer drug. These aspects of arsenic toxicity develop as a consequence of arsenic-induced oxidative stress and modifications to signal pathway activity which alter gene expression. Resveratrol (RVL) a food antioxidant found in grapes and other fruits, exhibits anti-carcinogenic properties by reducing oxidative stress and restoring signal pathway control. This study investigated the impact of RVL on arsenite [As(III)]-induced cell signalling in HaCaT keratinocytes by assaying phosphorylation status of epidermal growth factor receptor (EGFR) signalling intermediates and measuring changes in expression of Phase II and DNA repair biomarkers.

As(III) exposure produced dose-dependent toxicity which was associated with increased activation of EGFR pathway intermediates, cSrc, Rac1 and extracellular signal-regulated kinases 1 & 2 (ERK1/2). Arsenic-mediated ERK1/2 activation negatively regulated DNA polymerase beta expression and up regulated heme-oxygenase-1 at toxic concentrations. RVL treatment modulated As(III)-mediated ERK1/2 activation by shifting the balance of cSrc regulatory domain phosphorylation. These effects significantly altered the response of the EGFR pathway to growth factor-induced stimulation.

Our research provides evidence that treatment with pharmacologically relevant doses of RVL influences cellular responses to As(III), largely due to RVL-mediated changes to Src and ERK1/2 activation.

Herbert, K. J., Cook, A. L., Snow, E. T., 2014, SIRT1 Modulates miRNA Processing Defects in p53-Mutated Human Keratinocytes, *J Dermatol Sci*, **74**(2): 142-149. [Impact Factor: 3.520]

Background: Together with p53, the NAD-dependent lysine deacetylase SIRT1 and the microRNA miR-34a form a feedback loop which self-regulates SIRT1 expression and modulates p53-dependent responses. In addition to its well-described role in mediating transcriptional responses to genotoxic stress, p53 may also regulate microRNA processing and maturation. Objective: This study explored the functional relationship between p53, SIRT1 and miR-34a, and the influence of p53 and SIRT1 on microRNA biogenesis and maturation in primary (NHEK) and p53-mutated (HaCaT) keratinocyte cell lines.

Methods: RNAi, miRNA target site blocking oligonucleotides and small molecule inhibitors were used to modulate activity and expression of SIRT1 and p53. Changes in microRNA and mRNA were analysed by qRT-PCR and protein expression was determined by immunoblotting.

Results: Mature miR-34a decreased in p53-suppressed NHEK cells, whereas ablation of SIRT1 reduced the primary transcript (pri-miR-34a). When either SIRT1 expression or activity was inhibited in combination with p53 ablation, pri-miR-34a levels increased and mature miR-34a levels decreased. Under these same conditions, additional p53-regulated microRNAs (miRs 16-1/15, 145 and 107) also failed to mature. In HaCaT cells, primary microRNA transcripts for miR-16-1/15, miR-145 miR200c/141 and miRNA-107, but not miR-34a, were approximately 8-fold higher than in NHEK cells. However, the levels of mature microRNA sequences in HaCaT cells were only 1.5-2 fold higher (miR-16-1, miR-145), unchanged (miR-107) or decreased (miR-200c/141, miR-34a) compared to NHEK cells.

Conclusions: Our results suggest that p53 mutations interfere with efficient microRNA biogenesis in keratinocytes, and that SIRT1 functions in combination with p53 in this process.

Herbert, K. J., Cook, A. L., Snow, E. T., 2014, SIRT1 Inhibition Restores Apoptotic Sensitivity in p53-Mutated Human Keratinocytes, *Toxicol Appl Pharmacol*, (in press, available online: 12 April 2014) [Impact Factor: TAAP = 3.975]

Mutations to the p53 gene are common in UV-exposed keratinocytes and contribute to apoptotic resistance in skin cancer. P53-dependent activity is modulated, in part, by a complex, self-limiting feedback loop imposed by miR-34a-mediated regulation of the lysine deacetylase, SIRT1. Expression of numerous microRNAs is dysregulated in squamous and basal cell carcinomas; however the contribution of specific microRNAs to the pathogenesis of skin cancer remains untested. Through use of RNAi, miRNA target site blocking oligonucleotides and small molecule inhibitors, this study explored the influence of p53 mutational status, SIRT1 activity and miR-34a levels on apoptotic sensitivity in primary (NHEK) and p53-mutated (HaCaT) keratinocyte cell lines. SIRT1 and p53 are overexpressed in p53-mutated keratinocytes, whilst miR-34a levels are 90% less in HaCaT cells. HaCaTs have impaired responses to p53/SIRT1/miR-34a axis manipulation which enhanced survival during exposure to the chemotherapeutic agent, camptothecin. Inhibition of SIRT1 activity in this cell line increased p53 acetylation and doubled camptothecin-induced cell death. Our results demonstrate that p53 mutations increase apoptotic resistance in keratinocytes by interfering with miR-34a-mediated regulation of SIRT1 expression. Thus, SIRT1 inhibitors may have therapeutic potential for overcoming apoptotic resistance during skin cancer treatment.

Herbert, K. J., Holloway, A. F., Cook, A. L., Chin, S. P., Snow, E. T., 2014, Arsenic Exposure Disrupts Epigenetic Regulation of SIRT1 in Human Keratinocytes, (Manuscript in Preparation)

Herbert K. J., Snow E. T., *Modulation of Arsenic-Induced Toxicity by Resveratrol*; AH & MRC Congress, Melbourne 2010

Inorganic arsenic (As) is a human carcinogen; yet arsenic trioxide [As(III)] is also an effective anticancer drug with particular efficacy against acute promyelocytic leukemia. Evidence suggests induction of oxidative stress, disruption of redox homeostasis and activation of signal transduction pathways are responsible for arsenic toxicity and its anticancer activity. Resveratrol (RVL), a polyphenol found in red wine, has anti-carcinogenic properties that may provide chemotherapeutic benefits by reducing oxidative stress and restoring signal pathway control. This study investigated the impact of RVL on As(III)-induced toxicity by assaying activation of extracellular signal-regulated kinase (ERK1/2) signaling intermediates cSrc and Rac1; and by measuring mRNA and protein expression for heme-oxygenase-1 (HO-1) and DNA polymerase beta (Polβ) in cultured HaCaT keratinocytes. Twenty hours of As(III) exposure produced dose-dependent toxicity which was associated with increased activation of ERK1/2 and its intermediates. Upstream from ERK1/2, RVL treatment modulated As(III)-mediated ERK pathway control by shifting the balance of cSrc regulatory domain phosphorylation, but did not significantly influence Rac1 activation. Arsenic-mediated ERK pathway activation negatively regulated Polβ mRNA expression and increased expression of HO-1, a Phase II xenobiotic response gene, at toxic concentrations. ERK1/2 inhibition increased mRNA levels for both HO-1 and Polβ, while low doses of As(III) significantly enhanced Polβ protein expression when ERK1/2 was inhibited. Our research indicates that pretreatment with pharmacologically relevant doses of RVL induces changes to Src and ERK pathway interactions in the presence of arsenic. This study supports growing evidence of RVL's properties as an anti-transforming agent by demonstrating its ability to influence cellular growth and survival responses to As(III)-induced toxicity.

Herbert K. J., Cook, A.L., Snow E. T., *Regulation of the SIRT1/p53/miR-34a axis in Human Keratinocytes*; AH & MRC Congress, Adelaide 2012

SIRT1 is an NAD-dependent deacetylase which influences the outcome of cellular stress by regulating histone-mediated chromatin remodelling and the p53-dependent DNA damage response. As such, SIRT1 modulates key signalling pathways which influence carcinogenesis. SIRT1 expression is regulated by p53 activity at the transcriptional level, and by the microRNA miR-34a at the translational level. Together SIRT1, p53 and miR-34a form a feedback loop which self-regulates p53 activation.The tumour suppressor p53 is mutated in >60% of all cancers, including those affecting the skin. Thus the development of pharmaceutical agents which differentially target cells on the basis of p53 mutational status is of interest in the prevention and treatment of skin cancer. In this study, we used primary keratinocytes (neonatal human epidermal keratinocytes - NHEKs) and p53-mutated keratinocytes (HaCaTs) cultured in identical serum-free conditions to investigate the relationship between p53 mutational status, SIRT1 activity and miR-34a processing in human keratinocytes.

Expression of miR-34a was up-regulated by transient ablation of SIRT1 in NHEKs; but was suppressed by dual knockdown of SIRT1 and p53. In contrast, SIRT1 knockdown reduced miR-34a in HaCaTs keratinocytes whilst concomitantly up-regulating expression of its precursor transcript. This discrepancy between mature and precursor transcript levels was also observed after pharmaceutical SIRT1 inhibition in both p53-ablated and HaCaT keratinocytes. Additionally, differences in the level of p53 expression and acetylation observed between the NHEK and HaCaT cell lines was partially restored by inhibiting SIRT1 in the p53-mutated cell line.

Our results indicate that p53 haploinsufficiency impairs regulatory control of the SIRT1-miR-34a axis. SIRT1 inhibitors enable keratinocytes with p53 mutations to regulate p53 expression and relative acetylation and may therefore have therapeutic potential for the treatment and prevention of skin cancer.

Herbert K. J., Cook, A.L., Snow E. T., *SIRT1 Inhibition Promotes Apoptotic Sensitivity in p53-Mutated Keratinocytes*; Breakfast SIG (Epigenetic Drugs and Toxicity), 44th EMGS Annual Meeting 2013, Sept 21rd-25th, Monterey – CA

Mutations to the p53 gene are common in UV-exposed keratinocytes and contribute to apoptotic resistance in skin cancer. Together with p53, SIRT1 and miR-34a form a feedback loop which self-regulates SIRT1 and modulates p53-dependent apoptosis. Through use of RNAi, miRNA target site blocking oligonucleotides and small molecular inhibitors, we explored the influence of p53 status, SIRT1 activity and miR-34a levels on apoptotic sensitivity in primary (NHEK) and p53-mutated (HaCaT) keratinocyte cell lines. This study found that mutations to p53 impair SIRT1/miR-34a feedback responses in keratinocytes by interfering with miR-34a biogenesis. When compared with NHEKs, HaCaTs had 4-fold higher SIRT1 and p53 protein expression, and 80% lower miR-34a. Inhibition of SIRT1 with EX-527 induced miR-34a expression in NHEKs; however in HaCaTs, the primary transcript, but not mature miR-34a was up-regulated by EX-527. Additionally, EX-527 treatment caused SIRT1 protein to accumulate in HaCaTs, increasing relative p53 acetylation. This result mirrored the effect of a targeted miR-34a-binding site block to the SIRT1 3'UTR in NHEKs, which induced the miR-34a primary transcript and increased SIRT1 expression.

Here we provide mechanistic data which demonstrates that miR-34a-mediated control of SIRT1 expression regulates apoptotic sensitivity in a p53-dependent manner. When compared to NHEKs, HaCaTs were resistant to camptothecin-induced apoptosis, however apoptotic sensitivity was restored by inhibiting SIRT1 in the p53-mutated cell line. These results indicate that using SIRT1 inhibition to overcome chemotherapeutic resistance in p53-mutated keratinocytes is an attractive adjuvant strategy for skin cancer treatment.

Herbert K. J., Cook, A.L., Snow E. T., *Arsenic-Induced Epigenetic Repatterning in Human Keratinocytes*; 6th AOCP Conference/MEPSA Annual Scientific Meeting, November 10rd-14th, Sydney 2013

Arsenic is an environmental toxin which increases skin cancer risk for exposed populations worldwide, however the biomolecular mechanism remains unclear. Recent investigations show that histone deacetylase and DNA methyltransferase activity is altered by arsenic exposure and this appears to promote cellular transformation. Expression of the lysine deacetylase SIRT1 is altered in solid tumours and haematological malignancy; however its role in arsenic-induced pathology is unknown. In this study we investigated the effect of arsenic on epigenetic regulation of SIRT1 and its targeting microRNA, miR-34a in human keratinocytes exposed to arsenic continuously for 10 weeks.

In whole cell lysates, acetylation of the permissive mark, histone H4 at lysine 16 (H4K16), increased over the initial 12 days' exposure to arsenic. Arsenic increased H4K16 acetylation for the SIRT1 gene promoter and decreased H4K16 acetylation at the miR-34a promoter. Moreover, although SIRT1 expression was induced by arsenic within the first 24 hrs, after 24 days SIRT1 protein was not significantly different in arsenic-exposed cells. With extended treatment (> 5 weeks) these cells showed altered sensitivity to induction by arsenic, with significant shifts in DNA methylation of the SIRT1 and miR-34a promoters associated with altered expression patterns for both genes. We have found that arsenic exposure generates complex temporal effects on the cellular epigenetic machinery in keratinocytes. Arsenic appears to alter regulation of SIRT1 expression via chromatin-mediated modulation of SIRT1 and miR-34a p53 promoter binding in the initial 24 hours and through shifts in promoter DNA methylation with extended exposure times.

Herbert K. J., *Modeling Epigenetic Factors in Disease – A Case for Arsenic Toxicity*; AH & MRC Congress, Melbourne 2010

Epigenetics is an emerging field in the study of disease etiology. Chronic diseases are strongly associated with extensive epigenetic reprogramming, with many exhibiting specific histone and DNA methylation patterns, chromatin condensation and microRNA profiles. Epigenetic modification is thought to be stimulated by self-maintenance and repair responses which promote cellular adaptation and protection in conditions of environmental stress. Unlike mutagenic change, epigenetic remodeling is potentially reversible. However, loss of primary imprinting and induction of secondary imprinting during sustained exposure to epigenetic modifiers is heritable in clonal cell lines. Thus, the window of opportunity for therapeutically reestablishing basal epigenetic profiles appears to be limited.

Long-term arsenic exposure produces aberrant gene expression which is associated with global genomewide hypomethylation and focal CpG hypermethylation. Additionally, arsenic treatment alters the activity and expression of numerous proteins which are vital for epigenetic remodeling. Arsenic itself is not a direct mutagen, however destabilization of genomic fidelity as a result of epigenetic modifications may account for arsenic-induced pathogenic changes.

Many questions about the origins and development of disease remain to be answered. Unfortunately, disease-related phenotypic changes are measureable only after their 'silent' genotypic onset has occurred. By monitoring arsenic-induced epigenetic changes as they manifest, we gain insights into the modality of environmental stress-induced adaptive mechanisms and how they progress to pathogenic responses over time.

Herbert K. J., Cook, A.L., Snow E. T., *Characterisation of the SIRT1:p53 Axis in Cultured Human Keratinocyte Cell Lines*; MEPSA Scientific Meeting, Brisbane 2011.

In healthy cells the tumour suppressor protein p53 coordinates cellular responses to genotoxic damage, and as such is considered to be the 'guardian of the genome'. Consequently, functional alterations to the p53 gene and its expressional profile are common features in the etiology of cancer. The role of SIRT1 as a cellular stress response protein has recently gained interest due to its association with disease prevention and control of organismal ageing. Although its mode of action is incompletely understood, SIRT1 is thought to influence cellular growth and survival by modulating p53 activity. SIRT1:p53 axis responses were characterised by comparing p53 acetylation, relative gene expression, and cellular metabolic activity in wild-type and p53-mutated human keratinocyte cell lines.Basal p53 and SIRT1 expression was elevated in p53-mutated ($p53^{m1/m2}$) when compared to wild-type ($p53^{+/+}$) keratinocytes. SIRT1 inhibition increased relative p53 acetylation 3-fold for both cell lines, and decreased relative association of SIRT1 with p53 by a factor of 10. Overnight SIRT1 inhibition down-regulated p53 and SIRT1 transcription in $p53^{m1/m2}$ and increased relative premiR-34a. However, although SIRT1 inhibition induced p53 and SIRT1 transcription in $p53^{+/+}$, p53 protein was significantly reduced, indicating increased protein cycling. PARP1 expression increased, and relative PARP1 cleavage decreased for both cell lines, although the effect of SIRT1 inhibition was more pronounced for cells with mutated p53. Additionally, SIRT1 inhibition decreased metabolic activity in $p53^{m1/m2}$ keratinocytes, restricting cellular growth and proliferation in the mutated cell line.This study provides evidence that SIRT1 contributes to the DNA damage response by modulating p53-regulated gene expression. SIRT1 negatively regulates p53 activity in normally functioning keratinocytes; however p53 mutations influence the nature of gene expression, metabolic activity and SIRT1-mediated stress responses. Taken together, these results demonstrate the impact of p53 haploinsufficiency on the SIRT1:p53 axis in human skin cells.

Herbert K. J., Cook, A.L., Snow E. T., *Characterisation of the SIRT1:p53 Axis in Cultured Human Keratinocyte Cell Lines*; UTAS Graduate Research Conference, 2011: Sharing Excellence in Research (SEiR), Sept 1-2, Hobart, TAS

In healthy cells the tumour suppressor protein p53 coordinates cellular responses to genotoxic damage, and as such is considered to be the 'guardian of the genome'. Consequently, functional alterations to the p53 gene and its expressional profile are common features in the etiology of cancer. The role of SIRT1 as a cellular stress response protein has recently gained interest due to its association with disease prevention and control of organismal ageing. Although its mode of action is incompletely understood, SIRT1 is thought to influence cellular growth and survival by modulating p53 activity.

The SIRT1:p53 axis in cultured keratinocytes was characterised by assaying p53 acetylation, relative gene expression, and cellular metabolic activity. Overnight SIRT1 inhibition increased relative p53 acetylation, however downstream responses differed in p53-mutated (HaCaT) and wild-type (NHEK) keratinocyte cell lines. P53 and SIRT1 protein expression was down-regulated in SIRT1-inhibited NHEKs; whilst relative cellular p53 and SIRT1 mRNA levels remained steady. Paradoxically, p53 and SIRT1 mRNA levels were significantly reduced in HaCaTs, but protein expression was unchanged by SIRT1 inhibition. Cellular growth and proliferation was also influenced by p53 status, with NHEKs showing a relative increase, and HaCaTs showing a relative decrease in metabolic activity with SIRT1 inhibition.

This study provides evidence that SIRT1 contributes to the DNA damage response by modulating p53-regulated gene expression. SIRT1 negatively regulates p53 activity in normally functioning keratinocytes; however SIRT1-mediated responses differ in p53-mutated keratinocytes, which produce altered gene expression, metabolic activity and regulatory responses with SIRT1 inhibition. Taken together, these results demonstrate the critical nature of cellular p53 status in the outcome of SIRT1:p53 axis responses in human skin cells.

Herbert K. J., Cook, A.L., Snow E. T., *SIRT1 Inhibition Promotes Apoptotic Sensitivity in p53-Mutated Keratinocytes*; 44th EMGS Annual Meeting 2013, Sept 21rd-25th, Monterey – CA

Mutations to the p53 gene are common in UV-exposed keratinocytes and contribute to apoptotic resistance in skin cancer. Together with p53, SIRT1 and miR-34a form a feedback loop which self-regulates SIRT1 and modulates p53-dependent apoptosis. Through use of RNAi, miRNA target site blocking oligonucleotides and small molecular inhibitors, we explored the influence of p53 status, SIRT1 activity and miR-34a levels on apoptotic sensitivity in primary (NHEK) and p53-mutated (HaCaT) keratinocyte cell lines. This study found that mutations to p53 impair SIRT1/miR-34a feedback responses in keratinocytes by interfering with miR-34a biogenesis. When compared with NHEKs, HaCaTs had 4-fold higher SIRT1 and p53 protein expression, and 80% lower miR-34a. Inhibition of SIRT1 with EX-527 induced miR-34a expression in NHEKs; however in HaCaTs, the primary transcript, but not mature miR-34a was up-regulated by EX-527. Additionally, EX-527 treatment caused SIRT1 protein to accumulate in HaCaTs, increasing relative p53 acetylation. This result mirrored the effect of a targeted miR-34a-binding site block to the SIRT1 3'UTR in NHEKs, which induced the miR-34a primary transcript and increased SIRT1 expression.

Here we provide mechanistic data which demonstrates that miR-34a-mediated control of SIRT1 expression regulates apoptotic sensitivity in a p53-dependent manner. When compared to NHEKs, HaCaTs were resistant to camptothecin-induced apoptosis, however apoptotic sensitivity was restored by inhibiting SIRT1 in the p53-mutated cell line. These results indicate that using SIRT1 inhibition to overcome chemotherapeutic resistance in p53-mutated keratinocytes is an attractive adjuvant strategy for skin cancer treatment.

Herbert K. J., Cook, A.L., Snow E. T., *SIRT1 Inhibition Promotes Apoptotic Sensitivity in p53-Mutated Keratinocytes*; 11th ICEM 2013, November 3rd-8th, Foz do Iguassu – Brazil

Mutations to the p53 gene are common in UV-exposed keratinocytes and contribute to apoptotic resistance in skin cancer. Together with p53, SIRT1 and miR-34a form a feedback loop which self-regulates SIRT1 and modulates p53-dependent apoptosis. Through use of RNAi, miRNA target site blocking oligonucleotides and small molecular inhibitors, we explored the influence of p53 status, SIRT1 activity and miR-34a levels on apoptotic sensitivity in primary (NHEK) and p53-mutated (HaCaT) keratinocyte cell lines. This study found that mutations to p53 impair SIRT1/miR-34a feedback responses in keratinocytes by interfering with miR-34a biogenesis. When compared with NHEKs, HaCaTs had 4-fold higher SIRT1 and p53 protein expression, and 80% lower miR-34a. Inhibition of SIRT1 with EX-527 induced miR-34a expression in NHEKs; however in HaCaTs, the primary transcript, but not mature miR-34a was up-regulated by EX-527. Additionally, EX-527 treatment caused SIRT1 protein to accumulate in HaCaTs, increasing relative p53 acetylation. This result mirrored the effect of a targeted miR-34a-binding site block to the SIRT1 3'UTR in NHEKs, which induced the miR-34a primary transcript and increased SIRT1 expression.

Here we provide mechanistic data which demonstrates that miR-34a-mediated control of SIRT1 expression regulates apoptotic sensitivity in a p53-dependent manner. When compared to NHEKs, HaCaTs were resistant to camptothecin-induced apoptosis, however apoptotic sensitivity was restored by inhibiting SIRT1 in the p53-mutated cell line. These results indicate that using SIRT1 inhibition to overcome chemotherapeutic resistance in p53-mutated keratinocytes is an attractive adjuvant strategy for skin cancer treatment.

Herbert K. J., Cook, A.L., Snow E. T., *Keratinocyte Phenotype is Dictated by Culture Medium*; 6th AOCP Conference/MEPSA Annual Scientific Meeting, November 10rd-14th, Sydney 2013

Growth of cells in culture is an efficient means for analysis and modelling of cellular responses in vitro. Findings from these investigations inform animal studies and human clinical trials and influence our understanding of disease processes. Biological activity is a product of intrinsic cellular potential and the external environment, whether the cell exists *in vivo* or *in vitro*.

Extracellular environment directly influences established patterns of epigenetic regulation in cultured keratinocytes. In this investigation, we found that histone acetylation and microRNA expression were media-dependent. HaCaT keratinocytes cultured in a serum-free, low-calcium medium (Epilife®) displayed a less differentiated morphology and were more sensitive to genotoxins than those grown in undefined (DMEM-F12) media with added serum. In fact, HaCaT cells grown in Epilife® medium exhibited a phenotype much more similar to normal keratinocytes than those grown in DMEM-F12. Here we show that choice of culture media not only affects keratinocyte phenotype, but also directly influences stress responses by altering patterns of epigenetic regulation. Therefore growth conditions including choice of growth medium should be carefully considered prior to conducting any *in vitro* investigation which utilises keratinocyte cell lines.

# REFERENCES


1. AIHW, AACR. Cancer in Australia: an overview, 2012. In. Canberra: AIHW, 2012.

2. AIHW, AACR. Non-melanoma skin cancer: general practice consultations, hospitalisation and mortality. In: AIHW, ed. Canberra: AIHW, 2008.

3. Chen A C, Halliday G M, Damian D L. Non-melanoma skin cancer: carcinogenesis and chemoprevention. Pathology 2013: 45: 331-341.

4. Staples M P, Elwood M, Burton R C, Williams J L, Marks R, Giles G G. Non-melanoma skin cancer in Australia: the 2002 national survey and trends since 1985. Med J Aust 2006: 184: 6-10.

5. Fransen M, Karahalios A, Sharma N, English D R, Giles G G, Sinclair R D. Non-melanoma skin cancer in Australia. Med J Aust 2012: 197: 565-568.

6. Lee J, Moon C. Current status of experimental therapeutics for head and neck cancer. Experimental Biology and Medicine 2011: 236: 375-389.

7. Mareel M, Leroy A. Clinical, cellular, and molecular aspects of cancer invasion. Physiol Rev 2003: 83: 337-376.

8. Dhillon A S, Hagan S, Rath O, Kolch W. MAP kinase signalling pathways in cancer. Oncogene 2007: 26: 3279-3290.

9. Jones P A, Baylin S B. The fundamental role of epigenetic events in cancer. Nat Rev Genet 2002: 3: 415-428.

10. Weinberg R A. Mechanisms of malignant progression. Carcinogenesis 2008: 29: 1092-1095.

11. Hanahan D, Weinberg R A. The hallmarks of cancer. Cell 2000: 100: 57-70.

12. Hanahan D, Weinberg R A. Hallmarks of cancer: the next generation. Cell 2011: 144: 646-674.

13. Negrini S, Gorgoulis V G, Halazonetis T D. Genomic instability--an evolving hallmark of cancer. Nat Rev Mol Cell Biol 2010: 11: 220-228.

14. Colotta F, Allavena P, Sica A, Garlanda C, Mantovani A. Cancer-related inflammation, the seventh hallmark of cancer: links to genetic instability. Carcinogenesis 2009: 30: 1073-1081.

15. Hsu P P, Sabatini D M. Cancer cell metabolism: Warburg and beyond. Cell 2008: 134: 703-707.

16. Luo J, Solimini N L, Elledge S J. Principles of cancer therapy: oncogene and non-oncogene addiction. Cell 2009: 136: 823-837.

17. Shen H, Laird P W. Interplay between the cancer genome and epigenome. Cell 2013: 153: 38-55.

18. Feinberg A P, Ohlsson R, Henikoff S. The epigenetic progenitor origin of human cancer. Nat Rev Genet 2006: 7: 21-33.

19. De Craene B, Berx G. Regulatory networks defining EMT during cancer initiation and progression. Nat Rev Cancer 2013: 13: 97-110.

20. Timp W, Feinberg A P. Cancer as a dysregulated epigenome allowing cellular growth advantage at the expense of the host. Nat Rev Cancer 2013: 13: 497-510.

21. Liu W F, Yu S S, Chen G J, Li Y Z. DNA damage checkpoint, damage repair, and genome stability. Yi Chuan Xue Bao 2006: 33: 381-390.

22. Norbury C J, Zhivotovsky B. DNA damage-induced apoptosis. Oncogene 2004: 23: 2797-2808.

23. Niida H, Nakanishi M. DNA damage checkpoints in mammals. Mutagenesis 2006: 21: 3-9.

24. Zhou B B, Elledge S J. The DNA damage response: putting checkpoints in perspective. Nature 2000: 408: 433-439.

25. Bartek J, Bartkova J, Lukas J. DNA damage signalling guards against activated oncogenes and tumour progression. Oncogene 2007: 26: 7773-7779.

26. Bartek J, Lukas J, Bartkova J. DNA damage response as an anti-cancer barrier: damage threshold and the concept of 'conditional haploinsufficiency'. Cell Cycle 2007: 6: 2344-2347.

27. Bartkova J, Horejsi Z, Koed K, et al. DNA damage response as a candidate anti-cancer barrier in early human tumorigenesis. Nature 2005: 434: 864-870.

28. Ishikawa K, Ishii H, Saito T. DNA damage-dependent cell cycle checkpoints and genomic stability. DNA Cell Biol 2006: 25: 406-411.

29. Carrier F, Georgel P T, Pourquier P, et al. Gadd45, a p53-responsive stress protein, modifies DNA accessibility on damaged chromatin. Mol Cell Biol 1999: 19: 1673-1685.

30. Peng A, Maller J L. Serine/threonine phosphatases in the DNA damage response and cancer. Oncogene 2010: 29: 5977-5988.

31. Polo S E, Kaidi A, Baskcomb L, Galanty Y, Jackson S P. Regulation of DNA-damage responses and cell-cycle progression by the chromatin remodelling factor CHD4. EMBO J 2010: 29: 3130-3139.

32. Sakaguchi K, Herrera J E, Saito S, et al. DNA damage activates p53 through a phosphorylation-acetylation cascade. Genes Dev 1998: 12: 2831-2841.

33. Lukas C, Falck J, Bartkova J, Bartek J, Lukas J. Distinct spatiotemporal dynamics of mammalian checkpoint regulators induced by DNA damage. Nat Cell Biol 2003: 5: 255-260.

34. Vogelstein B, Lane D, Levine A J. Surfing the p53 network. Nature 2000: 408: 307-310.

35. Vousden K H, Lu X. Live or let die: the cell's response to p53. Nat Rev Cancer 2002: 2: 594-604.

36. Giaccia A J, Kastan M B. The complexity of p53 modulation: emerging patterns from divergent signals. Genes Dev 1998: 12: 2973-2983.

37. Lakin N D, Jackson S P. Regulation of p53 in response to DNA damage. Oncogene 1999: 18: 7644-7655.

38. Siafakas R A, Richardson D R. Growth arrest and DNA damage-45 alpha (GADD45alpha). Int J Biochem Cell Biol 2009: 41: 986-989.

39. Bieging K T, Mello S S, Attardi L D. Unravelling mechanisms of p53-mediated tumour suppression. Nat Rev Cancer 2014: 14: 359-370.

40. Wang Y, Schwedes J F, Parks D, Mann K, Tegtmeyer P. Interaction of p53 with its consensus DNA-binding site. Mol Cell Biol 1995: 15: 2157-2165.

41. el-Deiry W S, Kern S E, Pietenpol J A, Kinzler K W, Vogelstein B. Definition of a consensus binding site for p53. Nat Genet 1992: 1: 45-49.

42. Gaglia G, Guan Y, Shah J V, Lahav G. Activation and control of p53 tetramerization in individual living cells. Proc Natl Acad Sci U S A 2013: 110: 15497-15501.

43. Weinberg R L, Veprintsev D B, Bycroft M, Fersht A R. Comparative binding of p53 to its promoter and DNA recognition elements. J Mol Biol 2005: 348: 589-596.

44. Wang B, Xiao Z, Ko H L, Ren E-C. The p53 response element and transcriptional repression. Cell Cycle 2010: 9: 870-879.

45. Wang B, Xiao Z, Ren E C. Redefining the p53 response element. Proc Natl Acad Sci U S A 2009: 106: 14373-14378.

46. Brooks C L, Gu W. Ubiquitination, phosphorylation and acetylation: the molecular basis for p53 regulation. Curr Opin Cell Biol 2003: 15: 164-171.

47. Brooks C L, Gu W. New insights into p53 activation. Cell Res 2010: 20: 614-621.

48. Bode A M, Dong Z. Post-translational modification of p53 in tumorigenesis. Nat Rev Cancer 2004: 4: 793-805.

49. Leng R P, Lin Y, Ma W, et al. Pirh2, a p53-induced ubiquitin-protein ligase, promotes p53 degradation. Cell 2003: 112: 779-791.

50. Li M, Luo J, Brooks C L, Gu W. Acetylation of p53 inhibits its ubiquitination by Mdm2. J Biol Chem 2002: 277: 50607-50611.

51. Luo J, Li M, Tang Y, Laszkowska M, Roeder R G, Gu W. Acetylation of p53 augments its site-specific DNA binding both in vitro and in vivo. Proc Natl Acad Sci U S A 2004: 101: 2259-2264.

52. Carter S, Vousden K H. Modifications of p53: competing for the lysines. Curr Opin Genet Dev 2009: 19: 18-24.

53. Glozak M A, Sengupta N, Zhang X, Seto E. Acetylation and deacetylation of non-histone proteins. Gene 2005: 363: 15-23.

54. Kruse J P, Gu W. Modes of p53 regulation. Cell 2009: 137: 609-622.

55. Juan L J, Shia W J, Chen M H, et al. Histone deacetylases specifically down-regulate p53-dependent gene activation. J Biol Chem 2000: 275: 20436-20443.

56. Chuikov S, Kurash J K, Wilson J R, et al. Regulation of p53 activity through lysine methylation. Nature 2004: 432: 353-360.

57. Huang J, Perez-Burgos L, Placek B J, et al. Repression of p53 activity by Smyd2-mediated methylation. Nature 2006: 444: 629-632.

58. Ivanov G S, Ivanova T, Kurash J, et al. Methylation-acetylation interplay activates p53 in response to DNA damage. Mol Cell Biol 2007: 27: 6756-6769.

59. Choudhary C, Kumar C, Gnad F, et al. Lysine acetylation targets protein complexes and co-regulates major cellular functions. Science 2009: 325: 834-840.

60. Yang X J, Seto E. Lysine acetylation: codified crosstalk with other posttranslational modifications. Mol Cell 2008: 31: 449-461.

61. Brooks C L, Gu W. The impact of acetylation and deacetylation on the p53 pathway. Protein & cell 2011: 2: 456-462.

62. Luo J, Su F, Chen D, Shiloh A, Gu W. Deacetylation of p53 modulates its effect on cell growth and apoptosis. Nature 2000: 408: 377-381.

63. Purvis J E, Karhohs K W, Mock C, Batchelor E, Loewer A, Lahav G. p53 dynamics control cell fate. Science 2012: 336: 1440-1444.

64. Haupt S, Berger M, Goldberg Z, Haupt Y. Apoptosis - the p53 network. J Cell Sci 2003: 116: 4077-4085.

65. Ito A, Lai C H, Zhao X, et al. p300/CBP-mediated p53 acetylation is commonly induced by p53-activating agents and inhibited by MDM2. EMBO J 2001: 20: 1331-1340.

66. Lill N L, Grossman S R, Ginsberg D, DeCaprio J, Livingston D M. Binding and modulation of p53 by p300/CBP coactivators. Nature 1997: 387: 823-827.

67. Tang Y, Luo J, Zhang W, Gu W. Tip60-dependent acetylation of p53 modulates the decision between cell-cycle arrest and apoptosis. Mol Cell 2006: 24: 827-839.

68. Halazonetis T D, Gorgoulis V G, Bartek J. An oncogene-induced DNA damage model for cancer development. Science 2008: 319: 1352-1355.

69. Joerger A C, Fersht A R. Structure-function-rescue: the diverse nature of common p53 cancer mutants. Oncogene 2007: 26: 2226-2242.

70. Joerger A C, Fersht A R. Structural biology of the tumor suppressor p53. Annu Rev Biochem 2008: 77: 557-582.

71. Kamada R, Nomura T, Anderson C W, Sakaguchi K. Cancer-associated p53 tetramerization domain mutants: quantitative analysis reveals a low threshold for tumor suppressor inactivation. J Biol Chem 2011: 286: 252-258.

72. Pfeifer G P. p53 mutational spectra and the role of methylated CpG sequences. Mutat Res 2000: 450: 155-166.

73. Lynch C J, Milner J. Loss of one p53 allele results in four-fold reduction of p53 mRNA and protein: a basis for p53 haplo-insufficiency. Oncogene 2006: 25: 3463-3470.

74. Liu D P, Song H, Xu Y. A common gain of function of p53 cancer mutants in inducing genetic instability. Oncogene 2010: 29: 949-956.

75. van Oijen M G, Slootweg P J. Gain-of-function mutations in the tumor suppressor gene p53. Clin Cancer Res 2000: 6: 2138-2145.

76. Zambetti G P, Levine A J. A comparison of the biological activities of wild-type and mutant p53. FASEB J 1993: 7: 855-865.

77. Zambetti G P. The p53 mutation "gradient effect" and its clinical implications. J Cell Physiol 2007: 213: 370-373.

78. Cadwell C, Zambetti G P. The effects of wild-type p53 tumor suppressor activity and mutant p53 gain-of-function on cell growth. Gene 2001: 277: 15-30.

79. Xu Y. Induction of genetic instability by gain-of-function p53 cancer mutants. Oncogene 2008: 27: 3501-3507.

80. Goh A M, Coffill C R, Lane D P. The role of mutant p53 in human cancer. J Pathol 2011: 223: 116-126.

81. Willis A, Jung E J, Wakefield T, Chen X. Mutant p53 exerts a dominant negative effect by preventing wild-type p53 from binding to the promoter of its target genes. Oncogene 2004: 23: 2330-2338.

82. Rangel L P, Costa D C, Vieira T C, Silva J L. The aggregation of mutant p53 produces prion-like properties in cancer. Prion 2014: 8.

83. Sigal A, Rotter V. Oncogenic mutations of the p53 tumor suppressor: the demons of the guardian of the genome. Cancer Res 2000: 60: 6788-6793.

84. Wade M, Li Y-C, Wahl G M. MDM2, MDMX and p53 in oncogenesis and cancer therapy. Nat Rev Cancer 2013: 13: 83-96.

85. Vazquez A, Bond E E, Levine A J, Bond G L. The genetics of the p53 pathway, apoptosis and cancer therapy. Nat Rev Drug Discov 2008: 7: 979-987.

86. Wang Z, Sun Y. Targeting p53 for novel anticancer therapy. Trans Oncol 2010: 3: 1-12.

87. Lane D P, Cheok C F, Lain S. p53-based cancer therapy. Cold Spring Harb Perspect Biol 2010: 2: a001222.

88. Selivanova G. Wild type p53 reactivation: from lab bench to clinic. FEBS Lett 2014.

89. Brown C J, Lain S, Verma C S, Fersht A R, Lane D P. Awakening guardian angels: drugging the p53 pathway. Nat Rev Cancer 2009: 9: 862-873.

90. Chen F, Wang W, El-Deiry W S. Current strategies to target p53 in cancer. Biochem Pharmacol 2010: 80: 724-730.

91. Li Y, Prives C. Are interactions with p63 and p73 involved in mutant p53 gain of oncogenic function? Oncogene 2007: 26: 2220-2225.

92. Hong B, Prabhu V V, Zhang S, et al. Prodigiosin Rescues Deficient p53 Signaling and Antitumor Effects via Upregulating p73 and Disrupting Its Interaction with Mutant p53. Cancer Res 2014: 74: 1153-1165.

93. Chan W M, Siu W Y, Lau A, Poon R Y. How many mutant p53 molecules are needed to inactivate a tetramer? Mol Cell Biol 2004: 24: 3536-3551.

94. Muller P A, Vousden K H. Mutant p53 in cancer: new functions and therapeutic opportunities. Cancer Cell 2014: 25: 304-317.

95. Rao B, Lain S, Thompson A M. p53-Based cyclotherapy: exploiting the 'guardian of the genome' to protect normal cells from cytotoxic therapy. Br J Cancer 2013: 109: 2954-2958.

96. Hoe K K, Verma C S, Lane D P. Drugging the p53 pathway: understanding the route to clinical efficacy. Nat Rev Drug Discov 2014: 13: 217-236.

97. Bird A. Perceptions of epigenetics. Nature 2007: 447: 396-398.

98. Jaenisch R, Bird A. Epigenetic regulation of gene expression: how the genome integrates intrinsic and environmental signals. Nat Genet 2003: 33 Suppl: 245-254.

99. Razin A, Cedar H. DNA methylation and gene expression. Microbiological reviews 1991: 55: 451-458.

100. Rollins R A, Haghighi F, Edwards J R, et al. Large-scale structure of genomic methylation patterns. Genome Res 2006: 16: 157-163.

101. van Eijk K R, de Jong S, Boks M P, et al. Genetic analysis of DNA methylation and gene expression levels in whole blood of healthy human subjects. BMC Genomics 2012: 13: 636.

102. Campos E I, Reinberg D. Histones: annotating chromatin. Annu Rev Genet 2009: 43: 559-599.

103. Shahbazian M D, Grunstein M. Functions of site-specific histone acetylation and deacetylation. Annu Rev Biochem 2007: 76: 75-100.

104. Kouzarides T. Chromatin modifications and their function. Cell 2007: 128: 693-705.

105. Li B, Carey M, Workman J L. The role of chromatin during transcription. Cell 2007: 128: 707-719.

106. Berger S L. Histone modifications in transcriptional regulation. Curr Opin Genet Dev 2002: 12: 142-148.

107. Guillemette B, Drogaris P, Lin H H, et al. H3 lysine 4 is acetylated at active gene promoters and is regulated by H3 lysine 4 methylation. PLoS Genet 2011: 7: e1001354.

108. Zhu Q, Wani A A. Histone modifications: crucial elements for damage response and chromatin restoration. J Cell Physiol 2010: 223: 283-288.

109. Lennartsson A, Ekwall K. Histone modification patterns and epigenetic codes. Biochim Biophys Acta 2009: 1790: 863-868.

110. Ciccone D N, Chen T. Histone lysine methylation in genomic imprinting. Epigenetics 2009: 4: 216-220.

111. Dang W, Steffen K K, Perry R, et al. Histone H4 lysine 16 acetylation regulates cellular lifespan. Nature 2009: 459: 802-807.

112. Zhang Y, Griffin K, Mondal N, Parvin J D. Phosphorylation of histone H2A inhibits transcription on chromatin templates. J Biol Chem 2004: 279: 21866-21872.

113. Wyrick J J, Parra M A. The role of histone H2A and H2B post-translational modifications in transcription: a genomic perspective. Biochim Biophys Acta 2009: 1789: 37-44.

114. Nozaki T, Yachie N, Ogawa R, Kratz A, Saito R, Tomita M. Tight associations between transcription promoter type and epigenetic variation in histone positioning and modification. BMC Genomics 2011: 12: 416.

115. Nakayama J, Rice J C, Strahl B D, Allis C D, Grewal S I. Role of histone H3 lysine 9 methylation in epigenetic control of heterochromatin assembly. Science 2001: 292: 110-113.

116. Lachner M, O'Carroll D, Rea S, Mechtler K, Jenuwein T. Methylation of histone H3 lysine 9 creates a binding site for HP1 proteins. Nature 2001: 410: 116-120.

117. Yun M, Wu J, Workman J L, Li B. Readers of histone modifications. Cell Res 2011: 21: 564-578.

118. Suganuma T, Workman J L. Signals and combinatorial functions of histone modifications. Annu Rev Biochem 2011: 80: 473-499.

119. Mujtaba S, Zeng L, Zhou M M. Structure and acetyl-lysine recognition of the bromodomain. Oncogene 2007: 26: 5521-5527.

120. de la Cruz X, Lois S, Sanchez-Molina S, Martinez-Balbas M A. Do protein motifs read the histone code? Bioessays 2005: 27: 164-175.

121. Musselman C A, Lalonde M E, Cote J, Kutateladze T G. Perceiving the epigenetic landscape through histone readers. Nat Struct Mol Biol 2012: 19: 1218-1227.

122. Eissenberg J C. Structural biology of the chromodomain: form and function. Gene 2012: 496: 69-78.

123. Daniel J A, Pray-Grant M G, Grant P A. Effector proteins for methylated histones: an expanding family. Cell Cycle 2005: 4: 919-926.

124. Zeng L, Zhou M M. Bromodomain: an acetyl-lysine binding domain. FEBS Lett 2002: 513: 124-128.

125. Schwartz Y B, Pirrotta V. A new world of Polycombs: unexpected partnerships and emerging functions. Nat Rev Genet 2013: 14: 853-864.

126. Cedar H, Bergman Y. Linking DNA methylation and histone modification: patterns and paradigms. Nat Rev Genet 2009: 10: 295-304.

127. Guil S, Esteller M. DNA methylomes, histone codes and miRNAs: tying it all together. Int J Biochem Cell Biol 2009: 41: 87-95.

128. Vaissiere T, Sawan C, Herceg Z. Epigenetic interplay between histone modifications and DNA methylation in gene silencing. Mutat Res 2008: 659: 40-48.

129. Fuks F, Burgers W A, Brehm A, Hughes-Davies L, Kouzarides T. DNA methyltransferase Dnmt1 associates with histone deacetylase activity. Nat Genet 2000: 24: 88-91.

130. Bachman K E, Park B H, Rhee I, et al. Histone modifications and silencing prior to DNA methylation of a tumor suppressor gene. Cancer Cell 2003: 3: 89-95.

131. Becker P B, Horz W. ATP-dependent nucleosome remodeling. Annu Rev Biochem 2002: 71: 247-273.

132. Clapier C R, Cairns B R. The biology of chromatin remodeling complexes. Annu Rev Biochem 2009: 78: 273-304.

133. Goren A, Cedar H. Replicating by the clock. Nat Rev Mol Cell Biol 2003: 4: 25-32.

134. Rountree M R, Bachman K E, Baylin S B. DNMT1 binds HDAC2 and a new co-repressor, DMAP1, to form a complex at replication foci. Nat Genet 2000: 25: 269-277.

135. Lande-Diner L, Cedar H. Silence of the genes--mechanisms of long-term repression. Nat Rev Genet 2005: 6: 648-654.

136. Rountree M R, Bachman K E, Herman J G, Baylin S B. DNA methylation, chromatin inheritance, and cancer. Oncogene 2001: 20: 3156-3165.

137. Erson A E, Petty E M. MicroRNAs in development and disease. Clin Genet 2008: 74: 296-306.

138. Schmittgen T D. Regulation of microRNA processing in development, differentiation and cancer. J Cell Mol Med 2008: 12: 1811-1819.

139. Lee Y, Kim M, Han J, et al. MicroRNA genes are transcribed by RNA polymerase II. EMBO J 2004: 23: 4051-4060.

140. Lee Y, Ahn C, Han J, et al. The nuclear RNase III Drosha initiates microRNA processing. Nature 2003: 425: 415-419.

141. Yi R, Qin Y, Macara I G, Cullen B R. Exportin-5 mediates the nuclear export of pre-microRNAs and short hairpin RNAs. Genes Dev 2003: 17: 3011-3016.

142. Lund E, Guttinger S, Calado A, Dahlberg J E, Kutay U. Nuclear export of microRNA precursors. Science 2004: 303: 95-98.

143. Zhang X, Zeng Y. The terminal loop region controls microRNA processing by Drosha and Dicer. Nucleic Acids Res 2010: 38: 7689-7697.

144. Gregory R I, Chendrimada T P, Cooch N, Shiekhattar R. Human RISC couples microRNA biogenesis and posttranscriptional gene silencing. Cell 2005: 123: 631-640.

145. Chendrimada T P, Gregory R I, Kumaraswamy E, et al. TRBP recruits the Dicer complex to Ago2 for microRNA processing and gene silencing. Nature 2005: 436: 740-744.

146. Kai Z S, Pasquinelli A E. MicroRNA assassins: factors that regulate the disappearance of miRNAs. Nat Struct Mol Biol 2010: 17: 5-10.

147. Iorio M V, Piovan C, Croce C M. Interplay between microRNAs and the epigenetic machinery: An intricate network. Biochim Biophys Acta 2010.

148. Siomi H, Siomi M C. Posttranscriptional regulation of microRNA biogenesis in animals. Mol Cell 2010: 38: 323-332.

149. Hermeking H. MicroRNAs in the p53 network: micromanagement of tumour suppression. Nat Rev Cancer 2012: 12: 613-626.

150. Suzuki H I, Yamagata K, Sugimoto K, Iwamoto T, Kato S, Miyazono K. Modulation of microRNA processing by p53. Nature 2009: 460: 529-533.

151. Shi M, Liu D, Shen B, Guo N. Helpers of the cellular gatekeeper-miRNAs dance in P53 network. Biochim Biophys Acta 2010: 1805: 218-225.

152. Chang J, Davis-Dusenbery B N, Kashima R, et al. Acetylation of p53 stimulates miRNA processing and determines cell survival following genotoxic stress. EMBO J 2013: 32: 3192-3205.

153. Chowdhury R, Chowdhury S, Roychoudhury P, Mandal C, Chaudhuri K. Arsenic induced apoptosis in malignant melanoma cells is enhanced by menadione through ROS generation, p38 signaling and p53 activation. Apoptosis 2009: 14: 108-123.

154. Hu H, Gatti R A. MicroRNAs: new players in the DNA damage response. J Mol Cell Biol 2010.

155. Esteller M. Non-coding RNAs in human disease. Nat Rev Genet 2011: 12: 861-874.

156. Moss T J, Wallrath L L. Connections between epigenetic gene silencing and human disease. Mutat Res 2007: 618: 163-174.

157. Gopalakrishnan S, Van Emburgh B O, Robertson K D. DNA methylation in development and human disease. Mutat Res 2008: 647: 30-38.

158. Wilson A S, Power B E, Molloy P L. DNA hypomethylation and human diseases. Biochim Biophys Acta 2007: 1775: 138-162.

159. Esteller M. Cancer epigenomics: DNA methylomes and histone-modification maps. Nat Rev Genet 2007: 8: 286-298.

160. Plass C, Pfister S M, Lindroth A M, Bogatyrova O, Claus R, Lichter P. Mutations in regulators of the epigenome and their connections to global chromatin patterns in cancer. Nat Rev Genet 2013: 14: 765-780.

161. Miremadi A, Oestergaard M Z, Pharoah P D, Caldas C. Cancer genetics of epigenetic genes. Hum Mol Genet 2007: 16 Spec No 1: R28-49.

162. Calin G A, Croce C M. MicroRNA signatures in human cancers. Nat Rev Cancer 2006: 6: 857-866.

163. Claes B, Buysschaert I, Lambrechts D. Pharmaco-epigenomics: discovering therapeutic approaches and biomarkers for cancer therapy. Heredity 2010: 105: 152-160.

164. Feinberg A P, Tycko B. The history of cancer epigenetics. Nat Rev Cancer 2004: 4: 143-153.

165. Pfeifer G P, Besaratinia A. Mutational spectra of human cancer. Hum Genet 2009: 125: 493-506.

166. Jones P A, Laird P W. Cancer epigenetics comes of age. Nat Genet 1999: 21: 163-167.

167. Jelinic P, Shaw P. Loss of imprinting and cancer. J Pathol 2007: 211: 261-268.

168. Tost J. DNA methylation: an introduction to the biology and the disease-associated changes of a promising biomarker. Mol Biotechnol 2010: 44: 71-81.

169. Imai K, Yamamoto H. Carcinogenesis and microsatellite instability: the interrelationship between genetics and epigenetics. Carcinogenesis 2008: 29: 673-680.

170. Esteller M. Aberrant DNA methylation as a cancer-inducing mechanism. Annu Rev Pharmacol Toxicol 2005: 45: 629-656.

171. Robertson K D. DNA methylation and human disease. Nat Rev Genet 2005: 6: 597-610.

172. Toyota M, Suzuki H. Epigenetic drivers of genetic alterations. Adv Genet 2010: 70: 309-323.

173. You J S, Jones P A. Cancer genetics and epigenetics: two sides of the same coin? Cancer Cell 2012: 22: 9-20.

174. Ehrlich M. DNA methylation in cancer: too much, but also too little. Oncogene 2002: 21: 5400-5413.

175. Wagner J M, Hackanson B, Lubbert M, Jung M. Histone deacetylase (HDAC) inhibitors in recent clinical trials for cancer therapy. Clin Epigenetics 2010: 1: 117-136.

176. Ropero S, Esteller M. The role of histone deacetylases (HDACs) in human cancer. Mol Oncol 2007: 1: 19-25.

177. Sawan C, Herceg Z. Histone modifications and cancer. Adv Genet 2010: 70: 57-85.

178. Iacobuzio-Donahue C A. Epigenetic changes in cancer. Annu Rev Pathol 2009: 4: 229-249.

179. Fraga M F, Ballestar E, Villar-Garea A, et al. Loss of acetylation at Lys16 and trimethylation at Lys20 of histone H4 is a common hallmark of human cancer. Nat Genet 2005: 37: 391-400.

180. Kuzmichev A, Margueron R, Vaquero A, et al. Composition and histone substrates of polycomb repressive group complexes change during cellular differentiation. Proc Natl Acad Sci U S A 2005: 102: 1859-1864.

181. Kleer C G, Cao Q, Varambally S, et al. EZH2 is a marker of aggressive breast cancer and promotes neoplastic transformation of breast epithelial cells. Proc Natl Acad Sci U S A 2003: 100: 11606-11611.

182. Tonini T, D'Andrilli G, Fucito A, Gaspa L, Bagella L. Importance of Ezh2 polycomb protein in tumorigenesis process interfering with the pathway of growth suppressive key elements. J Cell Physiol 2008: 214: 295-300.

183. Ruan K, Fang X, Ouyang G. MicroRNAs: novel regulators in the hallmarks of human cancer. Cancer Lett 2009: 285: 116-126.

184. Croce C M. Causes and consequences of microRNA dysregulation in cancer. Nat Rev Genet 2009: 10: 704-714.

185. Garzon R, Calin G A, Croce C M. MicroRNAs in Cancer. Annu Rev Med 2009: 60: 167-179.

186. Suzuki H, Maruyama R, Yamamoto E, Kai M. DNA methylation and microRNA dysregulation in cancer. Mol Oncol 2012: 6: 567-578.

187. Suzuki H, Maruyama R, Yamamoto E, Kai M. Epigenetic alteration and microRNA dysregulation in cancer. Frontiers in genetics 2013: 4: 258.

188. Brase J C, Wuttig D, Kuner R, Sultmann H. Serum microRNAs as non-invasive biomarkers for cancer. Mol Cancer 2010: 9: 306.

189. Wittmann J, Jack H M. Serum microRNAs as powerful cancer biomarkers. Biochim Biophys Acta 2010: 1806: 200-207.

190. Kumar M S, Pester R E, Chen C Y, et al. Dicer1 functions as a haploinsufficient tumor suppressor. Genes Dev 2009: 23: 2700-2704.

191. Lambertz I, Nittner D, Mestdagh P, et al. Monoallelic but not biallelic loss of Dicer1 promotes tumorigenesis in vivo. Cell Death Differ 2010: 17: 633-641.

192. Karube Y, Tanaka H, Osada H, et al. Reduced expression of Dicer associated with poor prognosis in lung cancer patients. Cancer Sci 2005: 96: 111-115.

193. Merritt W M, Lin Y G, Han L Y, et al. Dicer, Drosha, and outcomes in patients with ovarian cancer. N Engl J Med 2008: 359: 2641-2650.

194. Guo X, Liao Q, Chen P, et al. The microRNA-processing enzymes: Drosha and Dicer can predict prognosis of nasopharyngeal carcinoma. J Cancer Res Clin Oncol 2012: 138: 49-56.

195. Grelier G, Voirin N, Ay A S, et al. Prognostic value of Dicer expression in human breast cancers and association with the mesenchymal phenotype. Br J Cancer 2009: 101: 673-683.

196. Lee E J, Baek M, Gusev Y, Brackett D J, Nuovo G J, Schmittgen T D. Systematic evaluation of microRNA processing patterns in tissues, cell lines, and tumors. RNA 2008: 14: 35-42.

197. Lee Y S, Dutta A. MicroRNAs in cancer. Annu Rev Pathol 2009: 4: 199-227.

198. Kelly T K, De Carvalho D D, Jones P A. Epigenetic modifications as therapeutic targets. Nat Biotechnol 2010: 28: 1069-1078.

199. Glozak M A, Seto E. Histone deacetylases and cancer. Oncogene 2007: 26: 5420-5432.

200. Michishita E, Park J Y, Burneskis J M, Barrett J C, Horikawa I. Evolutionarily conserved and nonconserved cellular localizations and functions of human SIRT proteins. Mol Biol Cell 2005: 16: 4623-4635.

201. Vaziri H, Dessain S K, Ng Eaton E, et al. hSIR2(SIRT1) functions as an NAD-dependent p53 deacetylase. Cell 2001: 107: 149-159.

202. Luo J, Nikolaev A Y, Imai S, et al. Negative control of p53 by Sir2alpha promotes cell survival under stress. Cell 2001: 107: 137-148.

203. Han M K, Song E K, Guo Y, Ou X, Mantel C, Broxmeyer H E. SIRT1 regulates apoptosis and Nanog expression in mouse embryonic stem cells by controlling p53 subcellular localization. Cell Stem Cell 2008: 2: 241-251.

204. Sakamoto K. Silencing metabolic disorders by novel SIRT1 activators. Cell Metab 2008: 7: 3-4.

205. Hubbard B P, Sinclair D A. Small molecule SIRT1 activators for the treatment of aging and age-related diseases. Trends Pharmacol Sci 2014.

206. Wang Z, Chen W. Emerging Roles of SIRT1 in Cancer Drug Resistance. Genes Cancer 2013: 4: 82-90.

207. Sonnemann J, Marx C, Becker S, et al. p53-dependent and p53-independent anticancer effects of different histone deacetylase inhibitors. Br J Cancer 2014: 110: 656-667.

208. Gregoretti I V, Lee Y M, Goodson H V. Molecular evolution of the histone deacetylase family: functional implications of phylogenetic analysis. J Mol Biol 2004: 338: 17-31.

209. Haberland M, Montgomery R L, Olson E N. The many roles of histone deacetylases in development and physiology: implications for disease and therapy. Nat Rev Genet 2009: 10: 32-42.

210. Haigis M C, Guarente L P. Mammalian sirtuins--emerging roles in physiology, aging, and calorie restriction. Genes Dev 2006: 20: 2913-2921.

211. Tanner K G, Landry J, Sternglanz R, Denu J M. Silent information regulator 2 family of NAD- dependent histone/protein deacetylases generates a unique product, 1-O-acetyl-ADP-ribose. Proc Natl Acad Sci U S A 2000: 97: 14178-14182.

212. Marmorstein R. Structure and chemistry of the Sir2 family of NAD+-dependent histone/protein deactylases. Biochem Soc Trans 2004: 32: 904-909.

213. Cyr A R, Domann F E. The redox basis of epigenetic modifications: from mechanisms to functional consequences. Antioxid Redox Signal 2011: 15: 551-589.

214. Haigis M C, Sinclair D A. Mammalian sirtuins: biological insights and disease relevance. Annu Rev Pathol 2010: 5: 253-295.

215. Di Marcotullio L, Canettieri G, Infante P, Greco A, Gulino A. Protected from the inside: endogenous histone deacetylase inhibitors and the road to cancer. Biochim Biophys Acta 2011: 1815: 241-252.

216. McGuinness D, McGuinness D H, McCaul J A, Shiels P G. Sirtuins, bioageing, and cancer. J Aging Res 2011: 2011: 235754.

217. Li X, Kazgan N. Mammalian sirtuins and energy metabolism. Int J Biol Sci 2011: 7: 575-587.

218. Cen Y, Youn D Y, Sauve A A. Advances in characterization of human sirtuin isoforms: chemistries, targets and therapeutic applications. Curr Med Chem 2011: 18: 1919-1935.

219. Oberdoerffer P, Michan S, McVay M, et al. SIRT1 redistribution on chromatin promotes genomic stability but alters gene expression during aging. Cell 2008: 135: 907-918.

220. Kim E J, Um S J. SIRT1: roles in aging and cancer. BMB Rep 2008: 41: 751-756.

221. Braidy N, Guillemin G J, Mansour H, Chan-Ling T, Poljak A, Grant R. Age related changes in NAD+ metabolism oxidative stress and Sirt1 activity in wistar rats. PLoS One 2011: 6: e19194.

222. Hou X, Xu S, Maitland-Toolan K A, et al. SIRT1 regulates hepatocyte lipid metabolism through activating AMP-activated protein kinase. J Biol Chem 2008: 283: 20015-20026.

223. Imai S, Guarente L. Ten years of NAD-dependent SIR2 family deacetylases: implications for metabolic diseases. Trends Pharmacol Sci 2010: 31: 212-220.

224. Schug T T, Li X. Sirtuin 1 in lipid metabolism and obesity. Ann Med 2011: 43: 198-211.

225. Borra M T, Langer M R, Slama J T, Denu J M. Substrate specificity and kinetic mechanism of the Sir2 family of NAD+-dependent histone/protein deacetylases. Biochemistry 2004: 43: 9877-9887.

226. Cosgrove M S, Bever K, Avalos J L, Muhammad S, Zhang X, Wolberger C. The structural basis of sirtuin substrate affinity. Biochemistry 2006: 45: 7511-7521.

227. Moniot S, Schutkowski M, Steegborn C. Crystal structure analysis of human Sirt2 and its ADP-ribose complex. Journal of Structural Biology.

228. Davenport A M, Huber F M, Hoelz A. Structural and Functional Analysis of Human SIRT1. J Mol Biol 2013.

229. Zhao X, Allison D, Condon B, et al. The 2.5 A crystal structure of the SIRT1 catalytic domain bound to nicotinamide adenine dinucleotide (NAD+) and an indole (EX527 analogue) reveals a novel mechanism of histone deacetylase inhibition. J Med Chem 2013: 56: 963-969.

230. Madej T, Addess K J, Fong J H, et al. MMDB: 3D structures and macromolecular interactions. Nucleic Acids Res 2012: 40: D461-464.

231. Feldman J L, Dittenhafer-Reed K E, Denu J M. Sirtuin catalysis and regulation. J Biol Chem 2012: 287: 42419-42427.

232. Zhao K, Harshaw R, Chai X, Marmorstein R. Structural basis for nicotinamide cleavage and ADP-ribose transfer by NAD(+)-dependent Sir2 histone/protein deacetylases. Proc Natl Acad Sci U S A 2004: 101: 8563-8568.

233. Yuan H, Marmorstein R. Structural basis for sirtuin activity and inhibition. J Biol Chem 2012: 287: 42428-42435.

234. Solomon J M, Pasupuleti R, Xu L, et al. Inhibition of SIRT1 catalytic activity increases p53 acetylation but does not alter cell survival following DNA damage. Mol Cell Biol 2006: 26: 28-38.

235. Peck B, Chen C Y, Ho K K, et al. SIRT inhibitors induce cell death and p53 acetylation through targeting both SIRT1 and SIRT2. Mol Cancer Ther 2010: 9: 844-855.

236. Gertz M, Fischer F, Nguyen G T, et al. Ex-527 inhibits Sirtuins by exploiting their unique NAD+-dependent deacetylation mechanism. Proc Natl Acad Sci U S A 2013: 110: E2772-2781.

237. Baur J A. Biochemical effects of SIRT1 activators. Biochim Biophys Acta 2010: 1804: 1626-1634.

238. Zschoernig B, Mahlknecht U. SIRTUIN 1: regulating the regulator. Biochem Biophys Res Commun 2008: 376: 251-255.

239. Yang Y, Fu W, Chen J, et al. SIRT1 sumoylation regulates its deacetylase activity and cellular response to genotoxic stress. Nat Cell Biol 2007: 9: 1253-1262.

240. Chen L. Medicinal chemistry of sirtuin inhibitors. Curr Med Chem 2011: 18: 1936-1946.

241. Lawson M, Uciechowska U, Schemies J, Rumpf T, Jung M, Sippl W. Inhibitors to understand molecular mechanisms of NAD(+)-dependent deacetylases (sirtuins). Biochim Biophys Acta 2010: 1799: 726-739.

242. Zhang T, Berrocal J G, Frizzell K M, et al. Enzymes in the NAD+ salvage pathway regulate SIRT1 activity at target gene promoters. J Biol Chem 2009: 284: 20408-20417.

243. Zhang T, Kraus W L. SIRT1-dependent regulation of chromatin and transcription: linking NAD(+) metabolism and signaling to the control of cellular functions. Biochim Biophys Acta 2010: 1804: 1666-1675.

244. Imai S. A possibility of nutriceuticals as an anti-aging intervention: activation of sirtuins by promoting mammalian NAD biosynthesis. Pharmacol Res 2010: 62: 42-47.

245. Guo X, Williams J G, Schug T T, Li X. DYRK1A and DYRK3 promote cell survival through phosphorylation and activation of SIRT1. J Biol Chem 2010: 285: 13223-13232.

246. Kang H, Jung J W, Kim M K, Chung J H. CK2 is the regulator of SIRT1 substrate-binding affinity, deacetylase activity and cellular response to DNA-damage. PLoS One 2009: 4: e6611.

247. Ford J, Ahmed S, Allison S, Jiang M, Milner J. JNK2-dependent regulation of SIRT1 protein stability. Cell Cycle 2008: 7: 3091-3097.

248. Kim E J, Kho J H, Kang M R, Um S J. Active regulator of SIRT1 cooperates with SIRT1 and facilitates suppression of p53 activity. Mol Cell 2007: 28: 277-290.

249. Zhao W, Kruse J P, Tang Y, Jung S Y, Qin J, Gu W. Negative regulation of the deacetylase SIRT1 by DBC1. Nature 2008: 451: 587-590.

250. Chen W Y, Wang D H, Yen R C, Luo J, Gu W, Baylin S B. Tumor suppressor HIC1 directly regulates SIRT1 to modulate p53-dependent DNA-damage responses. Cell 2005: 123: 437-448.

251. Wang C, Chen L, Hou X, et al. Interactions between E2F1 and SirT1 regulate apoptotic response to DNA damage. Nat Cell Biol 2006: 8: 1025-1031.

252. Abdelmohsen K, Pullmann R, Jr., Lal A, et al. Phosphorylation of HuR by Chk2 regulates SIRT1 expression. Mol Cell 2007: 25: 543-557.

253. Eades G, Yao Y, Yang M, Zhang Y, Chumsri S, Zhou Q. miR-200a regulates SIRT1 expression and epithelial to mesenchymal transition (EMT)-like transformation in mammary epithelial cells. J Biol Chem 2011: 286: 25992-26002.

254. Ford J, Jiang M, Milner J. Cancer-specific functions of SIRT1 enable human epithelial cancer cell growth and survival. Cancer Res 2005: 65: 10457-10463.

255. Kume S, Haneda M, Kanasaki K, et al. SIRT1 inhibits transforming growth factor beta-induced apoptosis in glomerular mesangial cells via Smad7 deacetylation. J Biol Chem 2007: 282: 151-158.

256. Bouras T, Fu M, Sauve A A, et al. SIRT1 deacetylation and repression of p300 involves lysine residues 1020/1024 within the cell cycle regulatory domain 1. J Biol Chem 2005: 280: 10264-10276.

257. Back J H, Rezvani H R, Zhu Y, et al. Cancer cell survival following DNA damage-mediated premature senescence is regulated by mammalian target of rapamycin (mTOR)-dependent inhibition of sirtuin 1. J Biol Chem 2011.

258. Yeung F, Hoberg J E, Ramsey C S, et al. Modulation of NF-kappaB-dependent transcription and cell survival by the SIRT1 deacetylase. EMBO J 2004: 23: 2369-2380.

259. Bernier M, Paul R K, Martin-Montalvo A, et al. Negative regulation of STAT3-mediated cellular respiration by SirT1. J Biol Chem 2011.

260. Vaquero A, Scher M, Erdjument-Bromage H, Tempst P, Serrano L, Reinberg D. SIRT1 regulates the histone methyl-transferase SUV39H1 during heterochromatin formation. Nature 2007: 450: 440-444.

261. Vaquero A, Sternglanz R, Reinberg D. NAD+-dependent deacetylation of H4 lysine 16 by class III HDACs. Oncogene 2007: 26: 5505-5520.

262. Vaquero A, Scher M, Lee D, Erdjument-Bromage H, Tempst P, Reinberg D. Human SirT1 interacts with histone H1 and promotes formation of facultative heterochromatin. Mol Cell 2004: 16: 93-105.

263. Kashiwagi K, Nimura K, Ura K, Kaneda Y. DNA methyltransferase 3b preferentially associates with condensed chromatin. Nucleic Acids Res 2011: 39: 874-888.

264. Imai S. From heterochromatin islands to the NAD World: a hierarchical view of aging through the functions of mammalian Sirt1 and systemic NAD biosynthesis. Biochim Biophys Acta 2009: 1790: 997-1004.

265. Lee I H, Cao L, Mostoslavsky R, et al. A role for the NAD-dependent deacetylase Sirt1 in the regulation of autophagy. Proc Natl Acad Sci U S A 2008: 105: 3374-3379.

266. Wang R H, Sengupta K, Li C, et al. Impaired DNA damage response, genome instability, and tumorigenesis in SIRT1 mutant mice. Cancer Cell 2008: 14: 312-323.

267. El Ramy R, Magroun N, Messadecq N, et al. Functional interplay between Parp-1 and SirT1 in genome integrity and chromatin-based processes. Cell Mol Life Sci 2009: 66: 3219-3234.

268. Mulligan P, Yang F, Di Stefano L, et al. A SIRT1-LSD1 Corepressor Complex Regulates Notch Target Gene Expression and Development. Mol Cell 2011: 42: 689-699.

269. Yamamori T, DeRicco J, Naqvi A, et al. SIRT1 deacetylates APE1 and regulates cellular base excision repair. Nucleic Acids Res 2010: 38: 832-845.

270. Lombard D B, Schwer B, Alt F W, Mostoslavsky R. SIRT6 in DNA repair, metabolism and ageing. J Intern Med 2008: 263: 128-141.

271. Yuan Z, Seto E. A functional link between SIRT1 deacetylase and NBS1 in DNA damage response. Cell Cycle 2007: 6: 2869-2871.

272. Yuan Z, Zhang X, Sengupta N, Lane W S, Seto E. SIRT1 regulates the function of the Nijmegen breakage syndrome protein. Mol Cell 2007: 27: 149-162.

273. Yamagata K, Kitabayashi I. Sirt1 physically interacts with Tip60 and negatively regulates Tip60-mediated acetylation of H2AX. Biochemical and Biophysical Research Communications 2009: 390: 1355-1360.

274. Jeong J, Juhn K, Lee H, et al. SIRT1 promotes DNA repair activity and deacetylation of Ku70. Exp Mol Med 2007: 39: 8-13.

275. Fan W, Luo J. SIRT1 regulates UV-induced DNA repair through deacetylating XPA. Mol Cell 2010: 39: 247-258.

276. Uhl M, Csernok A, Aydin S, Kreienberg R, Wiesmuller L, Gatz S A. Role of SIRT1 in homologous recombination. DNA Repair (Amst) 2010: 9: 383-393.

277. Li K, Casta A, Wang R, et al. Regulation of WRN protein cellular localization and enzymatic activities by SIRT1-mediated deacetylation. J Biol Chem 2008: 283: 7590-7598.

278. Brunet A, Sweeney L B, Sturgill J F, et al. Stress-dependent regulation of FOXO transcription factors by the SIRT1 deacetylase. Science 2004: 303: 2011-2015.

279. Motta M C, Divecha N, Lemieux M, et al. Mammalian SIRT1 represses forkhead transcription factors. Cell 2004: 116: 551-563.

280. Dai J M, Wang Z Y, Sun D C, Lin R X, Wang S Q. SIRT1 interacts with p73 and suppresses p73-dependent transcriptional activity. J Cell Physiol 2007: 210: 161-166.

281. Wong S, Weber J D. Deacetylation of the retinoblastoma tumour suppressor protein by SIRT1. Biochem J 2007: 407: 451-460.

282. Yuan J, Minter-Dykhouse K, Lou Z. A c-Myc-SIRT1 feedback loop regulates cell growth and transformation. J Cell Biol 2009: 185: 203-211.

283. IARC. Arsenic and arsenic compounds. In: IARC Monographs on the evaluation of the carcinogenic risk of chemicals to humans. Lyon, 2011: 41-94.

284. IARC. Arsenic in Drinking Water. In: IARC Monographs Lyon, France: World Health Organisation, 2004: 41-267.

285. IARC. Preamble. In: Cancer W I A f R o, ed. IARC Monographs on the Evaluation of Carcinogenic Risks to Humans. Lyon, France, 2006.

286. Tchounwou P B, Patlolla A K, Centeno J A. Carcinogenic and systemic health effects associated with arsenic exposure--a critical review. Toxicol Pathol 2003: 31: 575-588.

287. Centeno J A, Mullick F G, Martinez L, et al. Pathology related to chronic arsenic exposure. Environ Health Perspect 2002: 110 Suppl 5: 883-886.

288. Hei T K, Filipic M. Role of oxidative damage in the genotoxicity of arsenic. Free Radic Biol Med 2004: 37: 574-581.

289. Hei T K, Liu S X, Waldren C. Mutagenicity of arsenic in mammalian cells: role of reactive oxygen species. Proc Natl Acad Sci U S A 1998: 95: 8103-8107.

290. Sciandrello G, Caradonna F, Mauro M, Barbata G. Arsenic-induced DNA hypomethylation affects chromosomal instability in mammalian cells. Carcinogenesis 2004: 25: 413-417.

291. Sun Y, Kojima C, Chignell C, Mason R, Waalkes M P. Arsenic transformation predisposes human skin keratinocytes to UV-induced DNA damage yet enhances their survival apparently by diminishing oxidant response. Toxicol Appl Pharmacol 2011: 255: 242-250.

292. Lee-Chen S F, Gurr J R, Lin I B, Jan K Y. Arsenite enhances DNA double-strand breaks and cell killing of methyl methanesulfonate-treated cells by inhibiting the excision of alkali-labile sites. Mutat Res 1993: 294: 21-28.

293. Lindberg A L, Sohel N, Rahman M, Persson L A, Vahter M. Impact of smoking and chewing tobacco on arsenic-induced skin lesions. Environ Health Perspect 2010: 118: 533-538.

294. McCarty K M, Houseman E A, Quamruzzaman Q, et al. The impact of diet and betel nut use on skin lesions associated with drinking-water arsenic in Pabna, Bangladesh. Environ Health Perspect 2006: 114: 334-340.

295. Chen Y, Graziano J H, Parvez F, et al. Modification of risk of arsenic-induced skin lesions by sunlight exposure, smoking, and occupational exposures in Bangladesh. Epidemiology 2006: 17: 459-467.

296. Chen Y C, Guo Y L, Su H J, et al. Arsenic methylation and skin cancer risk in southwestern Taiwan. J Occup Environ Med 2003: 45: 241-248.

297. Ahsan H, Chen Y, Kibriya M G, et al. Arsenic metabolism, genetic susceptibility, and risk of premalignant skin lesions in Bangladesh. Cancer Epidemiol Biomarkers Prev 2007: 16: 1270-1278.

298. Breton C V, Zhou W, Kile M L, et al. Susceptibility to arsenic-induced skin lesions from polymorphisms in base excision repair genes. Carcinogenesis 2007: 28: 1520-1525.

299. Argos M, Rathouz P J, Pierce B L, et al. Dietary B vitamin intakes and urinary total arsenic concentration in the Health Effects of Arsenic Longitudinal Study (HEALS) cohort, Bangladesh. Eur J Nutr 2010: 49: 473-481.

300. Zablotska L B, Chen Y, Graziano J H, et al. Protective effects of B vitamins and antioxidants on the risk of arsenic-related skin lesions in Bangladesh. Environ Health Perspect 2008: 116: 1056-1062.

301. Kile M L, Hoffman E, Rodrigues E G, et al. A pathway-based analysis of urinary arsenic metabolites and skin lesions. Am J Epidemiol 2011: 173: 778-786.

302. Yu H S, Liao W T, Chai C Y. Arsenic carcinogenesis in the skin. J Biomed Sci 2006: 13: 657-666.

303. Pilsner J R, Liu X, Ahsan H, et al. Folate deficiency, hyperhomocysteinemia, low urinary creatinine, and hypomethylation of leukocyte DNA are risk factors for arsenic-induced skin lesions. Environ Health Perspect 2009: 117: 254-260.

304. Huff J, Chan P, Nyska A. Is the human carcinogen arsenic carcinogenic to laboratory animals? Toxicol Sci 2000: 55: 17-23.

305. Maronpot R R, Flake G, Huff J. Relevance of animal carcinogenesis findings to human cancer predictions and prevention. Toxicol Pathol 2004: 32 Suppl 1: 40-48.

306. Cohen S M, Arnold L L, Eldan M, Lewis A S, Beck B D. Methylated arsenicals: the implications of metabolism and carcinogenicity studies in rodents to human risk assessment. Crit Rev Toxicol 2006: 36: 99-133.

307. Combes R, Balls M, Curren R, et al. Cell Transformation Assays as Predictors of Human Carcinogenicity. ATLA 1999: 27: 745-767.

308. Chanda S, Dasgupta U B, Guhamazumder D, et al. DNA hypermethylation of promoter of gene p53 and p16 in arsenic-exposed people with and without malignancy. Toxicol Sci 2006: 89: 431-437.

309. Mass M J, Wang L. Arsenic alters cytosine methylation patterns of the promoter of the tumor suppressor gene p53 in human lung cells: a model for a mechanism of carcinogenesis. Mutat Res 1997: 386: 263-277.

310. Ouyang W, Luo W, Zhang D, et al. PI-3K/Akt pathway-dependent cyclin D1 expression is responsible for arsenite-induced human keratinocyte transformation. Environ Health Perspect 2008: 116: 1-6.

311. Li G, Lee L S, Li M, Tsao S W, Chiu J F. Molecular changes during arsenic-induced cell transformation. J Cell Physiol 2011: 226: 3225-3232.

312. Chen H, Liu J, Zhao C Q, Diwan B A, Merrick B A, Waalkes M P. Association of c-myc overexpression and hyperproliferation with arsenite-induced malignant transformation. Toxicol Appl Pharmacol 2001: 175: 260-268.

313. Qu W, Bortner C D, Sakurai T, Hobson M J, Waalkes M P. Acquisition of apoptotic resistance in arsenic-induced malignant transformation: role of the JNK signal transduction pathway. Carcinogenesis 2002: 23: 151-159.

314. Benbrahim-Tallaa L, Webber M M, Waalkes M P. Acquisition of androgen independence by human prostate epithelial cells during arsenic-induced malignant transformation. Environ Health Perspect 2005: 113: 1134-1139.

315. Zhao F, Severson P, Pacheco S, Futscher B W, Klimecki W T. Arsenic exposure induces the Warburg effect in cultured human cells. Toxicol Appl Pharmacol 2013: 271: 72-77.

316. Klein C B, Leszczynska J, Hickey C, Rossman T G. Further evidence against a direct genotoxic mode of action for arsenic-induced cancer. Toxicol Appl Pharmacol 2007: 222: 289-297.

317. Rossman T G. Mechanism of arsenic carcinogenesis: an integrated approach. Mutat Res 2003: 533: 37-65.

318. Ouyang W, Li J, Ma Q, Huang C. Essential roles of PI-3K/Akt/IKKbeta/NFkappaB pathway in cyclin D1 induction by arsenite in JB6 Cl41 cells. Carcinogenesis 2006: 27: 864-873.

319. Qian Y, Liu K J, Chen Y, Flynn D C, Castranova V, Shi X. Cdc42 regulates arsenic-induced NADPH oxidase activation and cell migration through actin filament reorganization. J Biol Chem 2005: 280: 3875-3884.

320. Ludwig S, Hoffmeyer A, Goebeler M, et al. The stress inducer arsenite activates mitogen-activated protein kinases extracellular signal-regulated kinases 1 and 2 via a MAPK kinase 6/p38-dependent pathway. J Biol Chem 1998: 273: 1917-1922.

321. Park J W, Choi Y J, Jang M A, et al. Arsenic trioxide induces G2/M growth arrest and apoptosis after caspase-3 activation and bcl-2 phosphorylation in promonocytic U937 cells. Biochem Biophys Res Commun 2001: 286: 726-734.

322. Lau A T, Li M, Xie R, He Q Y, Chiu J F. Opposed arsenite-induced signaling pathways promote cell proliferation or apoptosis in cultured lung cells. Carcinogenesis 2004: 25: 21-28.

323. Lehmann G M, McCabe M J, Jr. Arsenite slows S phase progression via inhibition of cdc25A dual specificity phosphatase gene transcription. Toxicol Sci 2007: 99: 70-78.

324. Ivanov V N, Hei T K. Combined treatment with EGFR inhibitors and arsenite upregulated apoptosis in human EGFR-positive melanomas: a role of suppression of the PI3K-AKT pathway. Oncogene 2005: 24: 616-626.

325. Chen F, Zhang Z, Bower J, et al. Arsenite-induced Cdc25C degradation is through the KEN-box and ubiquitin-proteasome pathway. Proc Natl Acad Sci U S A 2002: 99: 1990-1995.

326. Chen H, Liu J, Merrick B A, Waalkes M P. Genetic events associated with arsenic-induced malignant transformation: applications of cDNA microarray technology. Mol Carcinog 2001: 30: 79-87.

327. Andrew A S, Burgess J L, Meza M M, et al. Arsenic exposure is associated with decreased DNA repair in vitro and in individuals exposed to drinking water arsenic. Environ Health Perspect 2006: 114: 1193-1198.

328. Zheng X H, Watts G S, Vaught S, Gandolfi A J. Low-level arsenite induced gene expression in HEK293 cells. Toxicology 2003: 187: 39-48.

329. Hamadeh H K, Vargas M, Lee E, Menzel D B. Arsenic disrupts cellular levels of p53 and mdm2: a potential mechanism of carcinogenesis. Biochem Biophys Res Commun 1999: 263: 446-449.

330. Ahn W S, Bae S M, Lee K H, et al. Comparison of effects of As2O3 and As4O6 on cell growth inhibition and gene expression profiles by cDNA microarray analysis in SiHa cells. Oncol Rep 2004: 12: 573-580.

331. Habib G M. p53 regulates Hsp90beta during arsenite-induced cytotoxicity in glutathione-deficient cells. Arch Biochem Biophys 2009: 481: 101-109.

332. Hwang B J, Utti C, Steinberg M. Induction of cyclin D1 by submicromolar concentrations of arsenite in human epidermal keratinocytes. Toxicol Appl Pharmacol 2006: 217: 161-167.

333. Giafis N, Katsoulidis E, Sassano A, et al. Role of the p38 mitogen-activated protein kinase pathway in the generation of arsenic trioxide-dependent cellular responses. Cancer Res 2006: 66: 6763-6771.

334. Andrew A S, Mason R A, Memoli V, Duell E J. Arsenic activates EGFR pathway signaling in the lung. Toxicol Sci 2009: 109: 350-357.

335. Olsen C E, Liguori A E, Zong Y, Lantz R C, Burgess J L, Boitano S. Arsenic upregulates MMP-9 and inhibits wound repair in human airway epithelial cells. Am J Physiol Lung Cell Mol Physiol 2008: 295: L293-302.

336. Josyula A B, Poplin G S, Kurzius-Spencer M, et al. Environmental arsenic exposure and sputum metalloproteinase concentrations. Environ Res 2006: 102: 283-290.

337. Soucy N V, Mayka D, Klei L R, Nemec A A, Bauer J A, Barchowsky A. Neovascularization and angiogenic gene expression following chronic arsenic exposure in mice. Cardiovasc Toxicol 2005: 5: 29-41.

338. Kamat C D, Green D E, Curilla S, et al. Role of HIF signaling on tumorigenesis in response to chronic low-dose arsenic administration. Toxicol Sci 2005: 86: 248-257.

339. Kao Y H, Yu C L, Chang L W, Yu H S. Low concentrations of arsenic induce vascular endothelial growth factor and nitric oxide release and stimulate angiogenesis in vitro. Chem Res Toxicol 2003: 16: 460-468.

340. Soucy N V, Ihnat M A, Kamat C D, et al. Arsenic stimulates angiogenesis and tumorigenesis in vivo. Toxicol Sci 2003: 76: 271-279.

341. Straub A C, Stolz D B, Vin H, et al. Low level arsenic promotes progressive inflammatory angiogenesis and liver blood vessel remodeling in mice. Toxicol Appl Pharmacol 2007: 222: 327-336.

342. Griffin R J, Lee S H, Rood K L, et al. Use of arsenic trioxide as an antivascular and thermosensitizing agent in solid tumors. Neoplasia 2000: 2: 555-560.

343. Pi J, He Y, Bortner C, et al. Low level, long-term inorganic arsenite exposure causes generalized resistance to apoptosis in cultured human keratinocytes: potential role in skin co-carcinogenesis. Int J Cancer 2005: 116: 20-26.

344. Cavigelli M, Li W, Lin A, Su B, Yoshioka K, Karin M. The tumor promoter arsenite stimulates AP-1 activity by inhibiting a JNK phosphatase. EMBO J 1996: 15: 6269-6279.

345. Simeonova P P, Wang S, Toriuma W, et al. Arsenic mediates cell proliferation and gene expression in the bladder epithelium: association with activating protein-1 transactivation. Cancer Res 2000: 60: 3445-3453.

346. Hu Y, Jin X, Snow E T. Effect of arsenic on transcription factor AP-1 and NF-kappaB DNA binding activity and related gene expression. Toxicol Lett 2002: 133: 33-45.

347. Barchowsky A, Dudek E J, Treadwell M D, Wetterhahn K E. Arsenic induces oxidant stress and NF-kappa B activation in cultured aortic endothelial cells. Free Radic Biol Med 1996: 21: 783-790.

348. Wijeweera J B, Gandolfi A J, Parrish A, Lantz R C. Sodium arsenite enhances AP-1 and NFkappaB DNA binding and induces stress protein expression in precision-cut rat lung slices. Toxicol Sci 2001: 61: 283-294.

349. Zhang T C, Schmitt M T, Mumford J L. Effects of arsenic on telomerase and telomeres in relation to cell proliferation and apoptosis in human keratinocytes and leukemia cells in vitro. Carcinogenesis 2003: 24: 1811-1817.

350. Chou W C, Hawkins A L, Barrett J F, Griffin C A, Dang C V. Arsenic inhibition of telomerase transcription leads to genetic instability. J Clin Invest 2001: 108: 1541-1547.

351. Ward P S, Thompson C B. Metabolic reprogramming: a cancer hallmark even warburg did not anticipate. Cancer Cell 2012: 21: 297-308.

352. Gatenby R A, Gillies R J. Why do cancers have high aerobic glycolysis? Nat Rev Cancer 2004: 4: 891-899.

353. Locasale J W. Serine, glycine and one-carbon units: cancer metabolism in full circle. Nat Rev Cancer 2013.

354. Li J, Chen P, Sinogeeva N, et al. Arsenic trioxide promotes histone H3 phosphoacetylation at the chromatin of CASPASE-10 in acute promyelocytic leukemia cells. J Biol Chem 2002: 277: 49504-49510.

355. Li J, Gorospe M, Barnes J, Liu Y. Tumor promoter arsenite stimulates histone H3 phosphoacetylation of proto-oncogenes c-fos and c-jun chromatin in human diploid fibroblasts. J Biol Chem 2003: 278: 13183-13191.

356. Jensen T J, Novak P, Eblin K E, Gandolfi A J, Futscher B W. Epigenetic remodeling during arsenical-induced malignant transformation. Carcinogenesis 2008: 29: 1500-1508.

357. Jensen T J, Novak P, Wnek S M, Gandolfi A J, Futscher B W. Arsenicals produce stable progressive changes in DNA methylation patterns that are linked to malignant transformation of immortalized urothelial cells. Toxicol Appl Pharmacol 2009: 241: 221-229.

358. Eblin K E, Bredfeldt T G, Gandolfi A J. Immortalized human urothelial cells as a model of arsenic-induced bladder cancer. Toxicology 2008: 248: 67-76.

359. Bredfeldt T G, Jagadish B, Eblin K E, Mash E A, Gandolfi A J. Monomethylarsonous acid induces transformation of human bladder cells. Toxicol Appl Pharmacol 2006: 216: 69-79.

360. Zhao C Q, Young M R, Diwan B A, Coogan T P, Waalkes M P. Association of arsenic-induced malignant transformation with DNA hypomethylation and aberrant gene expression. Proc Natl Acad Sci U S A 1997: 94: 10907-10912.

361. Boonchai W, Walsh M, Cummings M, Chenevix-Trench G. Expression of p53 in arsenic-related and sporadic basal cell carcinoma. Arch Dermatol 2000: 136: 195-198.

362. Chen H, Li S, Liu J, Diwan B A, Barrett J C, Waalkes M P. Chronic inorganic arsenic exposure induces hepatic global and individual gene hypomethylation: implications for arsenic hepatocarcinogenesis. Carcinogenesis 2004: 25: 1779-1786.

363. Hughes M F. Arsenic methylation, oxidative stress and cancer--is there a link? J Natl Cancer Inst 2009: 101: 1660-1661.

364. Hsu C H, Yang S A, Wang J Y, Yu H S, Lin S R. Mutational spectrum of p53 gene in arsenic-related skin cancers from the blackfoot disease endemic area of Taiwan. Br J Cancer 1999: 80: 1080-1086.

365. Brash D E, Rudolph J A, Simon J A, et al. A role for sunlight in skin cancer: UV-induced p53 mutations in squamous cell carcinoma. Proc Natl Acad Sci U S A 1991: 88: 10124-10128.

366. Ziegler A, Jonason A S, Leffell D J, et al. Sunburn and p53 in the onset of skin cancer. Nature 1994: 372: 773-776.

367. Ziegler A, Leffell D J, Kunala S, et al. Mutation hotspots due to sunlight in the p53 gene of nonmelanoma skin cancers. Proc Natl Acad Sci U S A 1993: 90: 4216-4220.

368. Burren R, Scaletta C, Frenk E, Panizzon R G, Applegate L A. Sunlight and carcinogenesis: expression of p53 and pyrimidine dimers in human skin following UVA I, UVA I + II and solar simulating radiations. Int J Cancer 1998: 76: 201-206.

369. Detich N, Hamm S, Just G, Knox J D, Szyf M. The methyl donor S-Adenosylmethionine inhibits active demethylation of DNA: a candidate novel mechanism for the pharmacological effects of S-Adenosylmethionine. J Biol Chem 2003: 278: 20812-20820.

370. Cui X, Wakai T, Shirai Y, Hatakeyama K, Hirano S. Chronic oral exposure to inorganic arsenate interferes with methylation status of p16INK4a and RASSF1A and induces lung cancer in A/J mice. Toxicol Sci 2006: 91: 372-381.

371. Cui X, Wakai T, Shirai Y, Yokoyama N, Hatakeyama K, Hirano S. Arsenic trioxide inhibits DNA methyltransferase and restores methylation-silenced genes in human liver cancer cells. Hum Pathol 2006: 37: 298-311.

372. Fu H Y, Shen J Z, Wu Y, Shen S F, Zhou H R, Fan L P. Arsenic trioxide inhibits DNA methyltransferase and restores expression of methylation-silenced CDKN2B/CDKN2A genes in human hematologic malignant cells. Oncol Rep 2010: 24: 335-343.

373. Reichard J F, Puga A. Effects of arsenic exposure on DNA methylation and epigenetic gene regulation. Epigenomics 2010: 2: 87-104.

374. Coppin J F, Qu W, Waalkes M P. Interplay between cellular methyl metabolism and adaptive efflux during oncogenic transformation from chronic arsenic exposure in human cells. J Biol Chem 2008: 283: 19342-19350.

375. Friso S, Choi S W. Gene-nutrient interactions and DNA methylation. J Nutr 2002: 132: 2382S-2387S.

376. Pilsner J R, Liu X, Ahsan H, et al. Genomic methylation of peripheral blood leukocyte DNA: influences of arsenic and folate in Bangladeshi adults. Am J Clin Nutr 2007: 86: 1179-1186.

377. Majumdar S, Maiti A, Karmakar S, et al. Antiapoptotic efficacy of folic acid and vitamin B(12) against arsenic-induced toxicity. Environ Toxicol 2010.

378. Wang K Y, James Shen C K. DNA methyltransferase Dnmt1 and mismatch repair. Oncogene 2004: 23: 7898-7902.

379. Barreto G, Schafer A, Marhold J, et al. Gadd45a promotes epigenetic gene activation by repair-mediated DNA demethylation. Nature 2007: 445: 671-675.

380. Gehring M, Reik W, Henikoff S. DNA demethylation by DNA repair. Trends Genet 2009: 25: 82-90.

381. Ma D K, Guo J U, Ming G L, Song H. DNA excision repair proteins and Gadd45 as molecular players for active DNA demethylation. Cell Cycle 2009: 8: 1526-1531.

382. Zhou X, Sun H, Ellen T P, Chen H, Costa M. Arsenite alters global histone H3 methylation. Carcinogenesis 2008: 29: 1831-1836.

383. Jensen T J, Wozniak R J, Eblin K E, Wnek S M, Gandolfi A J, Futscher B W. Epigenetic mediated transcriptional activation of WNT5A participates in arsenical-associated malignant transformation. Toxicol Appl Pharmacol 2009: 235: 39-46.

384. Wellen K E, Hatzivassiliou G, Sachdeva U M, Bui T V, Cross J R, Thompson C B. ATP-citrate lyase links cellular metabolism to histone acetylation. Science 2009: 324: 1076-1080.

385. Cai L, Sutter B M, Li B, Tu B P. Acetyl-CoA induces cell growth and proliferation by promoting the acetylation of histones at growth genes. Mol Cell 2011: 42: 426-437.

386. Rahman I, Marwick J, Kirkham P. Redox modulation of chromatin remodeling: impact on histone acetylation and deacetylation, NF-kappaB and pro-inflammatory gene expression. Biochem Pharmacol 2004: 68: 1255-1267.

387. Doyle K, Fitzpatrick F A. Redox signaling, alkylation (carbonylation) of conserved cysteines inactivates class I histone deacetylases 1, 2, and 3 and

antagonizes their transcriptional repressor function. J Biol Chem 2010: 285: 17417-17424.

388. Chiarugi A, Dolle C, Felici R, Ziegler M. The NAD metabolome - a key determinant of cancer cell biology. Nature reviews Cancer 2012: 12: 741-752.

389. Meng X Z, Zheng T S, Chen X, et al. microRNA expression alteration after arsenic trioxide treatment in HepG-2 cells. J Gastroenterol Hepatol 2011: 26: 186-193.

390. Cao Y, Yu S L, Wang Y, Guo G Y, Ding Q, An R H. MicroRNA-dependent regulation of PTEN after arsenic trioxide treatment in bladder cancer cell line T24. Tumour Biol 2011: 32: 179-188.

391. Wang Z, Zhao Y, Smith E, et al. Reversal and prevention of arsenic-induced human bronchial epithelial cell malignant transformation by microRNA-200b. Toxicol Sci 2011: 121: 110-122.

392. Ling M, Li Y, Xu Y, et al. Regulation of miRNA-21 by reactive oxygen species-activated ERK/NF-kappaB in arsenite-induced cell transformation. Free Radic Biol Med 2012.

393. Liang H, Li X, Wang L, et al. MicroRNAs contribute to promyelocyte apoptosis in As2O3-treated APL cells. Cell Physiol Biochem 2013: 32: 1818-1829.

394. Ngalame N N, Tokar E J, Person R J, Xu Y, Waalkes M P. Aberrant microRNA Expression Likely Controls RAS Oncogene Activation During Malignant Transformation of Human Prostate Epithelial and Stem Cells by Arsenic. Toxicol Sci 2014.

395. Boellmann F, Zhang L, Clewell H J, et al. Genome-wide analysis of DNA methylation and gene expression changes in the mouse lung following subchronic arsenate exposure. Toxicol Sci 2010: 117: 404-417.

396. Reichard J F, Schnekenburger M, Puga A. Long term low-dose arsenic exposure induces loss of DNA methylation. Biochem Biophys Res Commun 2007: 352: 188-192.

397. Zykova T A, Zhu F, Lu C, et al. Lymphokine-activated killer T-cell-originated protein kinase phosphorylation of histone H2AX prevents arsenite-induced apoptosis in RPMI7951 melanoma cells. Clin Cancer Res 2006: 12: 6884-6893.

398. Boukamp P, Petrussevska R T, Breitkreutz D, Hornung J, Markham A, Fusenig N E. Normal keratinization in a spontaneously immortalized aneuploid human keratinocyte cell line. J Cell Biol 1988: 106: 761-771.

399. Page B, Page M, Noel C. A new fluorometric assay for cytotoxicity measurements in-vitro. Int J Oncol 1993: 3: 473-476.

400. Nociari M M, Shalev A, Benias P, Russo C. A novel one-step, highly sensitive fluorometric assay to evaluate cell-mediated cytotoxicity. J Immunol Methods 1998: 213: 157-167.

401. Liu L F, Desai S D, Li T K, Mao Y, Sun M, Sim S P. Mechanism of action of camptothecin. Ann N Y Acad Sci 2000: 922: 1-10.

402. Garcia-Carbonero R, Supko J G. Current perspectives on the clinical experience, pharmacology, and continued development of the camptothecins. Clin Cancer Res 2002: 8: 641-661.

403. Livak K J, Schmittgen T D. Analysis of relative gene expression data using real-time quantitative PCR and the 2(-Delta Delta C(T)) Method. Methods 2001: 25: 402-408.

404. Schmittgen T D, Livak K J. Analyzing real-time PCR data by the comparative C(T) method. Nat Protoc 2008: 3: 1101-1108.

405. Sajan S A, Hawkins R D. Methods for identifying higher-order chromatin structure. Annu Rev Genomics Hum Genet 2012: 13: 59-82.

406. Rao S, Procko E, Shannon M F. Chromatin remodeling, measured by a novel real-time polymerase chain reaction assay, across the proximal promoter region of the IL-2 gene. J Immunol 2001: 167: 4494-4503.

407. Zaret K. Micrococcal nuclease analysis of chromatin structure. Curr Protoc Mol Biol 2005: Chapter 21: Unit 21 21.

408. Hayatsu H. The bisulfite genomic sequencing used in the analysis of epigenetic states, a technique in the emerging environmental genotoxicology research. Mutat Res 2008: 659: 77-82.

409. Fraga M F, Ferrero C, Esteller M. Methyl Primer Express. In: Applied Biosystems, 2006.

410. Li L C, Dahiya R. MethPrimer: designing primers for methylation PCRs. Bioinformatics 2002: 18: 1427-1431.

411. Wojdacz T K, Dobrovic A, Hansen L L. Methylation-sensitive high-resolution melting. Nat Protoc 2008: 3: 1903-1908.

412. Jensen M A, Fukushima M, Davis R W. DMSO and betaine greatly improve amplification of GC-rich constructs in de novo synthesis. PLoS One 2010: 5: e11024.

413. Bock C, Reither S, Mikeska T, Paulsen M, Walter J, Lengauer T. BiQ Analyzer: visualization and quality control for DNA methylation data from bisulfite sequencing. Bioinformatics 2005: 21: 4067-4068.

414. Chene P. The role of tetramerization in p53 function. Oncogene 2001: 20: 2611-2617.

415. Olivier M, Hollstein M, Hainaut P. TP53 mutations in human cancers: origins, consequences, and clinical use. Cold Spring Harb Perspect Biol 2010: 2: a001008.

416. Pfeifer G P, You Y H, Besaratinia A. Mutations induced by ultraviolet light. Mutat Res 2005: 571: 19-31.

417. Cadet J, Sage E, Douki T. Ultraviolet radiation-mediated damage to cellular DNA. Mutat Res 2005: 571: 3-17.

418. Matsumura Y, Ananthaswamy H N. Toxic effects of ultraviolet radiation on the skin. Toxicol Appl Pharmacol 2004: 195: 298-308.

419. Tommasi S, Denissenko M F, Pfeifer G P. Sunlight induces pyrimidine dimers preferentially at 5-methylcytosine bases. Cancer Research 1997: 57: 4727-4730.

420. Brash D E. Roles of the transcription factor p53 in keratinocyte carcinomas. Br J Dermatol 2006: 154 Suppl 1: 8-10.

421. Klein A M, Brash D E, Jones P H, Simons B D. Stochastic fate of p53-mutant epidermal progenitor cells is tilted toward proliferation by UV B during preneoplasia. Proc Natl Acad Sci U S A 2010: 107: 270-275.

422. Melnikova V O, Ananthaswamy H N. Cellular and molecular events leading to the development of skin cancer. Mutat Res 2005: 571: 91-106.

423. Stahl P L, Stranneheim H, Asplund A, Berglund L, Ponten F, Lundeberg J. Sun-induced nonsynonymous p53 mutations are extensively accumulated and tolerated in normal appearing human skin. J Invest Dermatol 2011: 131: 504-508.

424. Boyce S T, Ham R G. Calcium-regulated differentiation of normal human epidermal keratinocytes in chemically defined clonal culture and serum-free serial culture. J Invest Dermatol 1983: 81: 33s-40s.

425. Menon G K, Grayson S, Elias P M. Ionic calcium reservoirs in mammalian epidermis: ultrastructural localization by ion-capture cytochemistry. J Invest Dermatol 1985: 84: 508-512.

426. Bikle D D, Ratnam A, Mauro T, Harris J, Pillai S. Changes in calcium responsiveness and handling during keratinocyte differentiation. Potential role of the calcium receptor. J Clin Invest 1996: 97: 1085-1093.

427. Pillai S, Bikle D D, Mancianti M L, Cline P, Hincenbergs M. Calcium regulation of growth and differentiation of normal human keratinocytes: modulation of differentiation competence by stages of growth and extracellular calcium. J Cell Physiol 1990: 143: 294-302.

428. Pillai S, Bikle D D, Hincenbergs M, Elias P M. Biochemical and morphological characterization of growth and differentiation of normal human neonatal keratinocytes in a serum-free medium. J Cell Physiol 1988: 134: 229-237.

429. Gibson D F, Ratnam A V, Bikle D D. Evidence for separate control mechanisms at the message, protein, and enzyme activation levels for transglutaminase during calcium-induced differentiation of normal and transformed human keratinocytes. J Invest Dermatol 1996: 106: 154-161.

430. Lehman T A, Modali R, Boukamp P, et al. p53 mutations in human immortalized epithelial cell lines. Carcinogenesis 1993: 14: 833-839.

431. Martynova E, Pozzi S, Basile V, et al. Gain-of-function p53 mutants have widespread genomic locations partially overlapping with p63. Oncotarget 2012: 3: 132-143.

432. Boukamp P, Popp S, Altmeyer S, et al. Sustained nontumorigenic phenotype correlates with a largely stable chromosome content during long-term culture of the human keratinocyte line HaCaT. Genes, chromosomes & cancer 1997: 19: 201-214.

433. Schoop V M, Mirancea N, Fusenig N E. Epidermal organization and differentiation of HaCaT keratinocytes in organotypic coculture with human dermal fibroblasts. The Journal of investigative dermatology 1999: 112: 343-353.

434. Development Organization Workgroup Asn A T C C S. Cell line misidentification: the beginning of the end. Nat Rev Cancer 2010: 10.

435. Capes-Davis A, Theodosopoulos G, Atkin I, et al. Check your cultures! A list of cross-contaminated or misidentified cell lines. International Journal of Cancer 2010: 127: 1-8.

436. Clement V, Marino D, Cudalbu C, et al. Marker-independent identification of glioma-initiating cells. Nat Meth 2013: 10: 1035-1035.

437. Reid Y, Storts D, Riss T, Minor L. Authentication of Human Cell Lines by STR DNA Profiling Analysis. In: Sittampalam G S, Gal-Edd N, Arkin M, et al., eds. Assay Guidance Manual. Bethesda (MD), 2004.

438. Harle-Bachor C, Boukamp P. Telomerase activity in the regenerative basal layer of the epidermis inhuman skin and in immortal and carcinoma-derived skin keratinocytes. Proc Natl Acad Sci U S A 1996: 93: 6476-6481.

439. Cerezo A, Stark H J, Moshir S, Boukamp P. Constitutive overexpression of human telomerase reverse transcriptase but not c-myc blocks terminal differentiation in human HaCaT skin keratinocytes. J Invest Dermatol 2003: 121: 110-119.

440. Bi W, Stambrook P J. Detection of known mutation by proof-reading PCR. Nucleic Acids Res 1998: 26: 3073-3075.

441. Bourdon J C. p53 and its isoforms in cancer. Br J Cancer 2007: 97: 277-282.

442. Marcel V, Dichtel-Danjoy M L, Sagne C, et al. Biological functions of p53 isoforms through evolution: lessons from animal and cellular models. Cell Death Differ 2011: 18: 1815-1824.

443. Khoury M P, Bourdon J-C. The Isoforms of the p53 Protein. Cold Spring Harbor Perspectives in Biology 2010: 2.

444. Olivier M, Eeles R, Hollstein M, Khan M A, Harris C C, Hainaut P. The IARC TP53 database: new online mutation analysis and recommendations to users. Hum Mutat 2002: 19: 607-614.

445. Petitjean A, Mathe E, Kato S, et al. Impact of mutant p53 functional properties on TP53 mutation patterns and tumor phenotype: lessons from recent developments in the IARC TP53 database. Human Mutation 2007: 28: 622-629.

446. Dmitriev D A, Rakitov R A. Decoding of Superimposed Traces Produced by Direct Sequencing of Heterozygous Indels. PLoS Comput Biol 2008: 4: e1000113.

447. Tariq M A, Pourmand N. Template tailoring: Accurate determination of heterozygous alleles using peptide nucleic acid and dideoxyNTP. Electrophoresis 2010: 31: 1322-1329.

448. Poumay Y, Pittelkow M R. Cell density and culture factors regulate keratinocyte commitment to differentiation and expression of suprabasal K1/K10 keratins. J Invest Dermatol 1995: 104: 271-276.

449. Shipley G D, Pittelkow M R. Control of growth and differentiation in vitro of human keratinocytes cultured in serum-free medium. Arch Dermatol 1987: 123: 1541a-1544a.

450. Wille J J, Jr., Pittelkow M R, Shipley G D, Scott R E. Integrated control of growth and differentiation of normal human prokeratinocytes cultured in serum-free medium: clonal analyses, growth kinetics, and cell cycle studies. J Cell Physiol 1984: 121: 31-44.

451. Hawker N P, Pennypacker S D, Chang S M, Bikle D D. Regulation of human epidermal keratinocyte differentiation by the vitamin D receptor and its coactivators DRIP205, SRC2, and SRC3. The Journal of investigative dermatology 2007: 127: 874-880.

452. Micallef L, Belaubre F, Pinon A, et al. Effects of extracellular calcium on the growth-differentiation switch in immortalized keratinocyte HaCaT cells compared with normal human keratinocytes. Experimental dermatology 2009: 18: 143-151.

453. Sandilands A, Sutherland C, Irvine A D, McLean W H. Filaggrin in the frontline: role in skin barrier function and disease. J Cell Sci 2009: 122: 1285-1294.

454. Fleckman P, Dale B A, Holbrook K A. Profilaggrin, a high-molecular-weight precursor of filaggrin in human epidermis and cultured keratinocytes. J Invest Dermatol 1985: 85: 507-512.

455. Holbrook K A, Hennings H. Phenotypic expression of epidermal cells in vitro: a review. J Invest Dermatol 1983: 81: 11s-24s.

456. Eckert R L, Rorke E A. Molecular biology of keratinocyte differentiation. Environ Health Perspect 1989: 80: 109-116.

457. Hitomi K. Transglutaminases in skin epidermis. Eur J Dermatol 2005: 15: 313-319.

458. Eckert R L, Sturniolo M T, Broome A M, Ruse M, Rorke E A. Transglutaminase function in epidermis. J Invest Dermatol 2005: 124: 481-492.

459. Foo R S, Nam Y J, Ostreicher M J, et al. Regulation of p53 tetramerization and nuclear export by ARC. Proc Natl Acad Sci U S A 2007: 104: 20826-20831.

460. Frey L M, Houben R, Brocker E B. Pigmentation, Melanocyte Colonization, and p53 Status in Basal Cell Carcinoma. J Skin Cancer 2011: 2011: 349726.

461. Mirza A, McGuirk M, Hockenberry T N, et al. Human survivin is negatively regulated by wild-type p53 and participates in p53-dependent apoptotic pathway. Oncogene 2002: 21: 2613-2622.

462. Hemann M T, Lowe S W. The p53-Bcl-2 connection. Cell Death Differ 2006: 13: 1256-1259.

463. Hoffman W H, Biade S, Zilfou J T, Chen J, Murphy M. Transcriptional Repression of the Anti-apoptoticsurvivin Gene by Wild Type p53. Journal of Biological Chemistry 2002: 277: 3247-3257.

464. Dallaglio K, Petrachi T, Marconi A, et al. Expression of nuclear survivin in normal skin and squamous cell carcinoma: a possible role in tumour invasion. Br J Cancer 2013.

465. Cho Y, Gorina S, Jeffrey P D, Pavletich N P. Crystal structure of a p53 tumor suppressor-DNA complex: understanding tumorigenic mutations. Science 1994: 265: 346-355.

466. Herbert K J, Cook A L, Snow E T. SIRT1 modulates miRNA processing defects in p53-mutated human keratinocytes. J Dermatol Sci 2014: 74: 142-149.

467. Zilfou J T, Lowe S W. Tumor Suppressive Functions of p53. Cold Spring Harbor Perspectives in Biology 2009: 1.

468. Szak S T, Mays D, Pietenpol J A. Kinetics of p53 binding to promoter sites in vivo. Mol Cell Biol 2001: 21: 3375-3386.

469. Bohlig L, Rother K. One function--multiple mechanisms: the manifold activities of p53 as a transcriptional repressor. J Biomed Biotechnol 2011: 2011: 464916.

470. Knights C D, Catania J, Di Giovanni S, et al. Distinct p53 acetylation cassettes differentially influence gene-expression patterns and cell fate. J Cell Biol 2006: 173: 533-544.

471. Chen X, Ko L J, Jayaraman L, Prives C. p53 levels, functional domains, and DNA damage determine the extent of the apoptotic response of tumor cells. Genes Dev 1996: 10: 2438-2451.

472. Fridman J S, Lowe S W. Control of apoptosis by p53. Oncogene 2003: 22: 9030-9040.

473. Hermeking H. p53 Enters the MicroRNA World. Cancer Cell 2007: 12: 414-418.

474. Winter J, Jung S, Keller S, Gregory R I, Diederichs S. Many roads to maturity: microRNA biogenesis pathways and their regulation. Nat Cell Biol 2009: 11: 228-234.

475. Rivlin N, Brosh R, Oren M, Rotter V. Mutations in the p53 Tumor Suppressor Gene: Important Milestones at the Various Steps of Tumorigenesis. Genes Cancer 2011: 2: 466-474.

476. Hermeking H. The miR-34 family in cancer and apoptosis. Cell Death Differ 2010: 17: 193-199.

477. He L, He X, Lim L P, et al. A microRNA component of the p53 tumour suppressor network. Nature 2007: 447: 1130-1134.

478. He L, He X, Lowe S W, Hannon G J. microRNAs join the p53 network--another piece in the tumour-suppression puzzle. Nat Rev Cancer 2007: 7: 819-822.

479. Yamakuchi M, Ferlito M, Lowenstein C J. miR-34a repression of SIRT1 regulates apoptosis. Proc Natl Acad Sci U S A 2008: 105: 13421-13426.

480. Yamakuchi M, Lowenstein C J. MiR-34, SIRT1 and p53: the feedback loop. Cell Cycle 2009: 8: 712-715.

481. Aranha M M, Santos D M, Sola S, Steer C J, Rodrigues C M. miR-34a regulates mouse neural stem cell differentiation. PLoS One 2011: 6: e21396.

482. Ito T, Yagi S, Yamakuchi M. MicroRNA-34a regulation of endothelial senescence. Biochem Biophys Res Commun 2010: 398: 735-740.

483. Zhao T, Li J, Chen A F. MicroRNA-34a induces endothelial progenitor cell senescence and impedes its angiogenesis via suppressing silent information regulator 1. Am J Physiol Endocrinol Metab 2010: 299: E110-116.

484. Hubbert N L, Sedman S A, Schiller J T. Human papillomavirus type 16 E6 increases the degradation rate of p53 in human keratinocytes. J Virol 1992: 66: 6237-6241.

485. Ma L, Wagner J, Rice J J, Hu W, Levine A J, Stolovitzky G A. A plausible model for the digital response of p53 to DNA damage. Proc Natl Acad Sci U S A 2005: 102: 14266-14271.

486. Yin Y, Stephen C W, Luciani M G, Fahraeus R. p53 Stability and activity is regulated by Mdm2-mediated induction of alternative p53 translation products. Nat Cell Biol 2002: 4: 462-467.

487. Michael D, Oren M. The p53-Mdm2 module and the ubiquitin system. Semin Cancer Biol 2003: 13: 49-58.

488. Shangary S, Wang S. Small-molecule inhibitors of the MDM2-p53 protein-protein interaction to reactivate p53 function: a novel approach for cancer therapy. Annu Rev Pharmacol Toxicol 2009: 49: 223-241.

489. Vassilev L T, Vu B T, Graves B, et al. In Vivo Activation of the p53 Pathway by Small-Molecule Antagonists of MDM2. Science 2004: 303: 844-848.

490. Desilet N, Campbell T N, Choy F Y. p53-based anti-cancer therapies: An empty promise? Curr Issues Mol Biol 2010: 12: 143-146.

491. Kumamoto K, Spillare E A, Fujita K, et al. Nutlin-3a activates p53 to both down-regulate inhibitor of growth 2 and up-regulate mir-34a, mir-34b, and mir-34c expression, and induce senescence. Cancer Res 2008: 68: 3193-3203.

492. Tovar C, Rosinski J, Filipovic Z, et al. Small-molecule MDM2 antagonists reveal aberrant p53 signaling in cancer: implications for therapy. Proc Natl Acad Sci U S A 2006: 103: 1888-1893.

493. Langley E, Pearson M, Faretta M, et al. Human SIR2 deacetylates p53 and antagonizes PML/p53-induced cellular senescence. EMBO J 2002: 21: 2383-2396.

494. Fujita Y, Kojima K, Hamada N, et al. Effects of miR-34a on cell growth and chemoresistance in prostate cancer PC3 cells. Biochem Biophys Res Commun 2008: 377: 114-119.

495. Krol J, Loedige I, Filipowicz W. The widespread regulation of microRNA biogenesis, function and decay. Nat Rev Genet: 11: 597-610.

496. Su X, Chakravarti D, Cho M S, et al. TAp63 suppresses metastasis through coordinate regulation of Dicer and miRNAs. Nature 2010: 467: 986-990.

497. Kumar M S, Lu J, Mercer K L, Golub T R, Jacks T. Impaired microRNA processing enhances cellular transformation and tumorigenesis. Nat Genet 2007: 39: 673-677.

498. Martello G, Rosato A, Ferrari F, et al. A MicroRNA targeting dicer for metastasis control. Cell 2010: 141: 1195-1207.

499. Shi M, Liu D, Duan H, Shen B, Guo N. Metastasis-related miRNAs, active players in breast cancer invasion, and metastasis. Cancer Metastasis Rev 2010: 29: 785-799.

500. Herbert K J, Cook A L, Snow E T. SIRT1 inhibition restores apoptotic sensitivity in p53-mutated human keratinocytes. Toxicol Appl Pharmacol 2014: 277: 288-297.

501. Rass K, Reichrath J. UV damage and DNA repair in malignant melanoma and nonmelanoma skin cancer. Adv Exp Med Biol 2008: 624: 162-178.

502. Rodust P M, Stockfleth E, Ulrich C, Leverkus M, Eberle J. UV-induced squamous cell carcinoma--a role for antiapoptotic signalling pathways. Br J Dermatol 2009: 161 Suppl 3: 107-115.

503. Benchimol S. p53-dependent pathways of apoptosis. Cell Death Differ 2001: 8: 1049-1051.

504. Ouyang L, Shi Z, Zhao S, et al. Programmed cell death pathways in cancer: a review of apoptosis, autophagy and programmed necrosis. Cell proliferation 2012: 45: 487-498.

505. Wong R S. Apoptosis in cancer: from pathogenesis to treatment. J Exp Clin Cancer Res 2011: 30: 87.

506. Yamakuchi M. MicroRNA Regulation of SIRT1. Frontiers in physiology 2012: 3: 68.

507. Lu J, Getz G, Miska E A, et al. MicroRNA expression profiles classify human cancers. Nature 2005: 435: 834-838.

508. Lujambio A, Lowe S W. The microcosmos of cancer. Nature 2012: 482: 347-355.

509. Cabelguenne A, Blons H, de Waziers I, et al. p53 alterations predict tumor response to neoadjuvant chemotherapy in head and neck squamous cell carcinoma: a prospective series. J Clin Oncol 2000: 18: 1465-1473.

510. Brown J M, Wouters B G. Apoptosis, p53, and tumor cell sensitivity to anticancer agents. Cancer Res 1999: 59: 1391-1399.

511. Beneke R, Geisen C, Zevnik B, et al. DNA excision repair and DNA damage-induced apoptosis are linked to Poly(ADP-ribosyl)ation but have different requirements for p53. Mol Cell Biol 2000: 20: 6695-6703.

512. Luo X, Kraus W L. On PAR with PARP: cellular stress signaling through poly(ADP-ribose) and PARP-1. Genes Dev 2012: 26: 417-432.

513. Fischer U, Janicke R U, Schulze-Osthoff K. Many cuts to ruin: a comprehensive update of caspase substrates. Cell Death Differ 2003: 10: 76-100.

514. Kaufmann S H, Desnoyers S, Ottaviano Y, Davidson N E, Poirier G G. Specific proteolytic cleavage of poly(ADP-ribose) polymerase: an early marker of chemotherapy-induced apoptosis. Cancer Res 1993: 53: 3976-3985.

515. Raver-Shapira N, Marciano E, Meiri E, et al. Transcriptional activation of miR-34a contributes to p53-mediated apoptosis. Mol Cell 2007: 26: 731-743.

516. Bommer G T, Gerin I, Feng Y, et al. p53-mediated activation of miRNA34 candidate tumor-suppressor genes. Curr Biol 2007: 17: 1298-1307.

517. Shen Z, Zhan G, Ye D, et al. MicroRNA-34a affects the occurrence of laryngeal squamous cell carcinoma by targeting the antiapoptotic gene survivin. Med Oncol 2012: 29: 2473-2480.

518. Cimmino A, Calin G A, Fabbri M, et al. miR-15 and miR-16 induce apoptosis by targeting BCL2. Proc Natl Acad Sci U S A 2005: 102: 13944-13949.

519. Fabbri M, Bottoni A, Shimizu M, et al. Association of a microRNA/TP53 feedback circuitry with pathogenesis and outcome of B-cell chronic lymphocytic leukemia. JAMA 2011: 305: 59-67.

520. Kracikova M, Akiri G, George A, Sachidanandam R, Aaronson S A. A threshold mechanism mediates p53 cell fate decision between growth arrest and apoptosis. Cell Death Differ 2013: 20: 576-588.

521. Olive K P, Tuveson D A, Ruhe Z C, et al. Mutant p53 gain of function in two mouse models of Li-Fraumeni syndrome. Cell 2004: 119: 847-860.

522. Hida Y, Kubo Y, Murao K, Arase S. Strong expression of a longevity-related protein, SIRT1, in Bowen's disease. Arch Dermatol Res 2007: 299: 103-106.

523. Jansson M D, Lund A H. MicroRNA and cancer. Mol Oncol 2012: 6: 590-610.

524. Thomson J M, Newman M, Parker J S, Morin-Kensicki E M, Wright T, Hammond S M. Extensive post-transcriptional regulation of microRNAs and its implications for cancer. Genes Dev 2006: 20: 2202-2207.

525. Sand M, Skrygan M, Sand D, et al. Expression of microRNAs in basal cell carcinoma. Br J Dermatol 2012: 167: 847-855.

526. Sand M, Skrygan M, Sand D, et al. Comparative microarray analysis of microRNA expression profiles in primary cutaneous malignant melanoma, cutaneous malignant melanoma metastases, and benign melanocytic nevi. Cell Tissue Res 2013: 351: 85-98.

527. Sand M, Skrygan M, Georgas D, et al. Microarray analysis of microRNA expression in cutaneous squamous cell carcinoma. J Dermatol Sci 2012: 68: 119-126.

528. Kwon Y W, Kwon K S, Moon H E, et al. Insulin-like growth factor-II regulates the expression of vascular endothelial growth factor by the human keratinocyte cell line HaCaT. J Invest Dermatol 2004: 123: 152-158.

529. Oren M, Rotter V. Mutant p53 gain-of-function in cancer. Cold Spring Harb Perspect Biol 2010: 2: a001107.

530. Wiman K G. Restoration of wild-type p53 function in human tumors: strategies for efficient cancer therapy. Adv Cancer Res 2007: 97: 321-338.

531. Xu J, Reumers J, Couceiro J R, et al. Gain of function of mutant p53 by coaggregation with multiple tumor suppressors. Nat Chem Biol 2011: 7: 285-295.

532. Dickinson M, Johnstone R W, Prince H M. Histone deacetylase inhibitors: potential targets responsible for their anti-cancer effect. Invest New Drugs 2010: 28 Suppl 1: S3-20.

533. Kim M J, Hong K S, Kim H B, et al. Ku70 acetylation and modulation of c-Myc/ATF4/CHOP signaling axis by SIRT1 inhibition lead to sensitization of HepG2 cells to TRAIL through induction of DR5 and down-regulation of c-FLIP. Int J Biochem Cell Biol 2013: 45: 711-723.

534. Concepcion C P, Han Y-C, Mu P, et al. Intact p53-Dependent Responses in miR-34–Deficient Mice. PLoS Genet 2012: 8: e1002797.

535. Ren X, McHale C M, Skibola C F, Smith A H, Smith M T, Zhang L. An Emerging Role for Epigenetic Dysregulation in Arsenic Toxicity and Carcinogenesis. Environ Health Perspect 2010.

536. Kumagai Y, Sumi D. Arsenic: signal transduction, transcription factor, and biotransformation involved in cellular response and toxicity. Annu Rev Pharmacol Toxicol 2007: 47: 243-262.

537. Chervona Y, Hall M N, Arita A, et al. Associations between arsenic exposure and global posttranslational histone modifications among adults in Bangladesh. Cancer Epidemiol Biomarkers Prev 2012: 21: 2252-2260.

538. Clayton A L, Hazzalin C A, Mahadevan L C. Enhanced histone acetylation and transcription: a dynamic perspective. Mol Cell 2006: 23: 289-296.

539. Berger S L. The complex language of chromatin regulation during transcription. Nature 2007: 447: 407-412.

540. Braunstein M, Rose A B, Holmes S G, Allis C D, Broach J R. Transcriptional silencing in yeast is associated with reduced nucleosome acetylation. Genes Dev 1993: 7: 592-604.

541. Chen W Y, Townes T M. Molecular mechanism for silencing virally transduced genes involves histone deacetylation and chromatin condensation. Proc Natl Acad Sci U S A 2000: 97: 377-382.

542. Lengauer C, Kinzler K W, Vogelstein B. Genetic instabilities in human cancers. Nature 1998: 396: 643-649.

543. Shogren-Knaak M, Ishii H, Sun J M, Pazin M J, Davie J R, Peterson C L. Histone H4-K16 acetylation controls chromatin structure and protein interactions. Science 2006: 311: 844-847.

544. Shogren-Knaak M, Peterson C L. Switching on chromatin: mechanistic role of histone H4-K16 acetylation. Cell Cycle 2006: 5: 1361-1365.

545. Barneda-Zahonero B, Parra M. Histone deacetylases and cancer. Mol Oncol 2012.

546. Bae D S, Gennings C, Carter W H, Jr., Yang R S, Campain J A. Toxicological interactions among arsenic, cadmium, chromium, and lead in human keratinocytes. Toxicol Sci 2001: 63: 132-142.

547. Bailey K A, Hester S D, Knapp G W, Owen R D, Thai S F. Gene expression of normal human epidermal keratinocytes modulated by trivalent arsenicals. Mol Carcinog 2010: 49: 981-998.

548. Trouba K J, Geisenhoffer K M, Germolec D R. Sodium arsenite-induced stress-related gene expression in normal human epidermal, HaCaT, and HEL30 keratinocytes. Environ Health Perspect 2002: 110 Suppl 5: 761-766.

549. Schuliga M, Chouchane S, Snow E T. Upregulation of glutathione-related genes and enzyme activities in cultured human cells by sublethal concentrations of inorganic arsenic. Toxicol Sci 2002: 70: 183-192.

550. Liu S X, Athar M, Lippai I, Waldren C, Hei T K. Induction of oxyradicals by arsenic: implication for mechanism of genotoxicity. Proc Natl Acad Sci U S A 2001: 98: 1643-1648.

551. Lemarie A, Bourdonnay E, Morzadec C, Fardel O, Vernhet L. Inorganic arsenic activates reduced NADPH oxidase in human primary macrophages through a Rho kinase/p38 kinase pathway. J Immunol 2008: 180: 6010-6017.

552. Choi S E, Kemper J K. Regulation of SIRT1 by microRNAs. Mol Cells 2013: 36: 385-392.

553. Chen Z, Shentu T P, Wen L, Johnson D A, Shyy J Y. Regulation of SIRT1 by oxidative stress-responsive miRNAs and a systematic approach to identify its role in the endothelium. Antioxid Redox Signal 2013: 19: 1522-1538.

554. Klemperer N S, Pickart C M. Arsenite inhibits two steps in the ubiquitin-dependent proteolytic pathway. J Biol Chem 1989: 264: 19245-19252.

555. Berleth E S, Pickart C M. Mechanism of ubiquitin conjugating enzyme E2-230K: catalysis involving a thiol relay? Biochemistry 1996: 35: 1664-1671.

556. Berleth E S, Kasperek E M, Grill S P, Braunscheidel J A, Graziani L A, Pickart C M. Inhibition of ubiquitin-protein ligase (E3) by mono- and bifunctional phenylarsenoxides. Evidence for essential vicinal thiols and a proximal nucleophile. J Biol Chem 1992: 267: 16403-16411.

557. Kirkpatrick D S, Dale K V, Catania J M, Gandolfi A J. Low-level arsenite causes accumulation of ubiquitinated proteins in rabbit renal cortical slices and HEK293 cells. Toxicol Appl Pharmacol 2003: 186: 101-109.

558. Naqvi A, Hoffman T A, DeRicco J, et al. A single-nucleotide variation in a p53-binding site affects nutrient-sensitive human SIRT1 expression. Hum Mol Genet 2010: 19: 4123-4133.

559. Liu L, Trimarchi J R, Navarro P, Blasco M A, Keefe D L. Oxidative stress contributes to arsenic-induced telomere attrition, chromosome instability, and apoptosis. J Biol Chem 2003: 278: 31998-32004.

560. Larochette N, Decaudin D, Jacotot E, et al. Arsenite induces apoptosis via a direct effect on the mitochondrial permeability transition pore. Exp Cell Res 1999: 249: 413-421.

561. Chen A, Cao E H, Zhang T C, Qin J F. Arsenite-induced reactive oxygen species and the repression of alpha-tocopherol in the MGC-803 cells. Eur J Pharmacol 2002: 448: 11-18.

562. Bau D T, Wang T S, Chung C H, Wang A S, Jan K Y. Oxidative DNA adducts and DNA-protein cross-links are the major DNA lesions induced by arsenite. Environ Health Perspect 2002: 110 Suppl 5: 753-756.

563. Hamadeh H K, Trouba K J, Amin R P, Afshari C A, Germolec D. Coordination of altered DNA repair and damage pathways in arsenite-exposed keratinocytes. Toxicol Sci 2002: 69: 306-316.

564. Partridge M A, Huang S X, Hernandez-Rosa E, Davidson M M, Hei T K. Arsenic induced mitochondrial DNA damage and altered mitochondrial oxidative function: implications for genotoxic mechanisms in mammalian cells. Cancer Res 2007: 67: 5239-5247.

565. Lee C H, Wu S B, Hong C H, Chen G S, Wei Y H, Yu H S. Involvement of mtDNA Damage Elicited by Oxidative Stress in the Arsenical Skin Cancers. J Invest Dermatol 2013: 133: 1890-1900.

566. Salminen A, Kaarniranta K, Kauppinen A. Crosstalk between Oxidative Stress and SIRT1: Impact on the Aging Process. International Journal of Molecular Sciences 2013: 14: 3834-3859.

567. Caito S, Rajendrasozhan S, Cook S, et al. SIRT1 is a redox-sensitive deacetylase that is post-translationally modified by oxidants and carbonyl stress. FASEB J 2010: 24: 3145-3159.

568. Rey N A, Howarth O W, Pereira-Maia E C. Equilibrium characterization of the As(III)-cysteine and the As(III)-glutathione systems in aqueous solution. J Inorg Biochem 2004: 98: 1151-1159.

569. Scott N, Hatlelid K M, MacKenzie N E, Carter D E. Reactions of arsenic(III) and arsenic(V) species with glutathione. Chem Res Toxicol 1993: 6: 102-106.

570. Rodgers J T, Lerin C, Haas W, Gygi S P, Spiegelman B M, Puigserver P. Nutrient control of glucose homeostasis through a complex of PGC-1alpha and SIRT1. Nature 2005: 434: 113-118.

571. Rodgers J T, Lerin C, Gerhart-Hines Z, Puigserver P. Metabolic adaptations through the PGC-1 alpha and SIRT1 pathways. FEBS Lett 2008: 582: 46-53.

572. Price N L, Gomes A P, Ling A J, et al. SIRT1 Is Required for AMPK Activation and the Beneficial Effects of Resveratrol on Mitochondrial Function. Cell Metab 2012: 15: 675-690.

573. Qu X, Du J, Zhang C, et al. Arsenic Trioxide Exerts Antimyeloma Effects by Inhibiting Activity in the Cytoplasmic Substrates of Histone Deacetylase 6. PLoS One 2012: 7: e32215.

574. Ramirez T, Brocher J, Stopper H, Hock R. Sodium arsenite modulates histone acetylation, histone deacetylase activity and HMGN protein dynamics in human cells. Chromosoma 2008: 117: 147-157.

575. Downs J A, Nussenzweig M C, Nussenzweig A. Chromatin dynamics and the preservation of genetic information. Nature 2007: 447: 951-958.

576. Miller K M, Tjeertes J V, Coates J, et al. Human HDAC1 and HDAC2 function in the DNA-damage response to promote DNA nonhomologous end-joining. Nat Struct Mol Biol 2010: 17: 1144-1151.

577. Tamburini B A, Tyler J K. Localized histone acetylation and deacetylation triggered by the homologous recombination pathway of double-strand DNA repair. Mol Cell Biol 2005: 25: 4903-4913.

578. Papamichos-Chronakis M, Peterson C L. Chromatin and the genome integrity network. Nat Rev Genet 2013: 14: 62-75.

579. Janssen A, Medema R H. Genetic instability: tipping the balance. Oncogene 2013: 32: 4459-4470.

580. Sulli G, Di Micco R, di Fagagna F d A. Crosstalk between chromatin state and DNA damage response in cellular senescence and cancer. Nat Rev Cancer 2012: 12: 709-720.

581. Chen F, Lu Y, Zhang Z, et al. Opposite effect of NF-kappa B and c-Jun N-terminal kinase on p53-independent GADD45 induction by arsenite. J Biol Chem 2001: 276: 11414-11419.

582. Ebert F, Weiss A, Bultemeyer M, Hamann I, Hartwig A, Schwerdtle T. Arsenicals affect base excision repair by several mechanisms. Mutat Res 2011: 715: 32-41.

583. Lai Y, Zhao W, Chen C, Wu M, Zhang Z. Role of DNA polymerase beta in the genotoxicity of arsenic. Environ Mol Mutagen 2011.

584. Kligerman A D, Tennant A H. Insights into the carcinogenic mode of action of arsenic. Toxicol Appl Pharmacol 2007: 222: 281-288.

585. Somji S, Garrett S H, Toni C, et al. Differences in the epigenetic regulation of MT-3 gene expression between parental and Cd+2 or As+3 transformed human urothelial cells. Cancer cell international 2011: 11: 2.

586. Leccia M T, Richard M J, Joanny-Crisci F, Beani J C. UV-A1 cytotoxicity and antioxidant defence in keratinocytes and fibroblasts. Eur J Dermatol 1998: 8: 478-482.

587. Bernstam L, Lan C H, Lee J, Nriagu J O. Effects of arsenic on human keratinocytes: morphological, physiological, and precursor incorporation studies. Environ Res 2002: 89: 220-235.

588. Spuches A M, Kruszyna H G, Rich A M, Wilcox D E. Thermodynamics of the As(III)-thiol interaction: arsenite and monomethylarsenite complexes with glutathione, dihydrolipoic acid, and other thiol ligands. Inorg Chem 2005: 44: 2964-2972.

589. Delnomdedieu M, Basti M M, Otvos J D, Thomas D J. Transfer of arsenite from glutathione to dithiols: a model of interaction. Chem Res Toxicol 1993: 6: 598-602.

590. Martinez V D, Becker-Santos D D, Vucic E A, Lam S, Lam W L. Induction of human squamous cell-type carcinomas by arsenic. J Skin Cancer 2011: 2011: 454157.

591. Kitchin K T, Wallace K. Evidence against the nuclear in situ binding of arsenicals--oxidative stress theory of arsenic carcinogenesis. Toxicol Appl Pharmacol 2008: 232: 252-257.

592. Basu A, Mahata J, Gupta S, Giri A K. Genetic toxicology of a paradoxical human carcinogen, arsenic: a review. Mutat Res 2001: 488: 171-194.

593. Nollen M, Ebert F, Moser J, Mullenders L H, Hartwig A, Schwerdtle T. Impact of arsenic on nucleotide excision repair: XPC function, protein level, and gene expression. Mol Nutr Food Res 2009: 53: 572-582.

594. Martinez V D, Vucic E A, Adonis M, Gil L, Lam W L. Arsenic biotransformation as a cancer promoting factor by inducing DNA damage and disruption of repair mechanisms. Mol Biol Int 2011: 2011: 718974.

595. Martinez V D, Vucic E A, Becker-Santos D D, Gil L, Lam W L. Arsenic exposure and the induction of human cancers. J Toxicol 2011: 2011: 431287.

596. Salnikow K, Zhitkovich A. Genetic and epigenetic mechanisms in metal carcinogenesis and cocarcinogenesis: nickel, arsenic, and chromium. Chem Res Toxicol 2008: 21: 28-44.

597. Smith Z D, Meissner A. DNA methylation: roles in mammalian development. Nat Rev Genet 2013: 14: 204-220.

598. Jeltsch A. Molecular enzymology of mammalian DNA methyltransferases. Curr Top Microbiol Immunol 2006: 301: 203-225.

599. Strathdee G, Sim A, Brown R. Control of gene expression by CpG island methylation in normal cells. Biochem Soc Trans 2004: 32: 913-915.

600. Antequera F, Bird A. CpG islands as genomic footprints of promoters that are associated with replication origins. Curr Biol 1999: 9: R661-667.

601. Illingworth R S, Bird A P. CpG islands--'a rough guide'. FEBS Lett 2009: 583: 1713-1720.

602. Varley K E, Gertz J, Bowling K M, et al. Dynamic DNA methylation across diverse human cell lines and tissues. Genome Res 2013: 23: 555-567.

603. Chen R Z, Pettersson U, Beard C, Jackson-Grusby L, Jaenisch R. DNA hypomethylation leads to elevated mutation rates. Nature 1998: 395: 89-93.

604. Kulis M, Esteller M. DNA methylation and cancer. Adv Genet 2010: 70: 27-56.

605. Smeester L, Rager J E, Bailey K A, et al. Epigenetic changes in individuals with arsenicosis. Chem Res Toxicol 2011: 24: 165-167.

606. Clark S J, Melki J. DNA methylation and gene silencing in cancer: which is the guilty party? Oncogene 2002: 21: 5380-5387.

607. Pogribny I P, Beland F A. DNA methylome alterations in chemical carcinogenesis. Cancer Lett 2012.

608. Kim M, Trinh B N, Long T I, Oghamian S, Laird P W. Dnmt1 deficiency leads to enhanced microsatellite instability in mouse embryonic stem cells. Nucleic Acids Res 2004: 32: 5742-5749.

609. O'Hagan H M, Mohammad H P, Baylin S B. Double strand breaks can initiate gene silencing and SIRT1-dependent onset of DNA methylation in an exogenous promoter CpG island. PLoS Genet 2008: 4: e1000155.

610. O'Hagan H M, Wang W, Sen S, et al. Oxidative damage targets complexes containing DNA methyltransferases, SIRT1, and polycomb members to promoter CpG Islands. Cancer Cell 2011: 20: 606-619.

611. Peng L, Yuan Z, Ling H, et al. SIRT1 deacetylates the DNA methyltransferase 1 (DNMT1) protein and alters its activities. Mol Cell Biol 2011: 31: 4720-4734.

612. Chim C S, Wong K Y, Qi Y, et al. Epigenetic inactivation of the miR-34a in hematological malignancies. Carcinogenesis 2010: 31: 745-750.

613. Lodygin D, Tarasov V, Epanchintsev A, et al. Inactivation of miR-34a by aberrant CpG methylation in multiple types of cancer. Cell Cycle 2008: 7: 2591-2600.

614. Wong K Y, Yu L, Chim C S. DNA methylation of tumor suppressor miRNA genes: a lesson from the miR-34 family. Epigenomics 2011: 3: 83-92.

615. Vogt M, Munding J, Gruner M, et al. Frequent concomitant inactivation of miR-34a and miR-34b/c by CpG methylation in colorectal, pancreatic, mammary, ovarian, urothelial, and renal cell carcinomas and soft tissue sarcomas. Virchows Arch 2011: 458: 313-322.

616. Versteeg R, Caron H, Cheng N C, et al. 1p36: every subband a suppressor? Eur J Cancer 1995: 31A: 538-541.

617. Bradbury C A, Khanim F L, Hayden R, et al. Histone deacetylases in acute myeloid leukaemia show a distinctive pattern of expression that changes selectively in response to deacetylase inhibitors. Leukemia 2005: 19: 1751-1759.

618. Chen H C, Jeng Y M, Yuan R H, Hsu H C, Chen Y L. SIRT1 promotes tumorigenesis and resistance to chemotherapy in hepatocellular carcinoma and its expression predicts poor prognosis. Ann Surg Oncol 2012: 19: 2011-2019.

619. Hoffmann M J, Engers R, Florl A R, Otte A P, Muller M, Schulz W A. Expression changes in EZH2, but not in BMI-1, SIRT1, DNMT1 or DNMT3B are

associated with DNA methylation changes in prostate cancer. Cancer Biol Ther 2007: 6: 1403-1412.

620. Blander G, Bhimavarapu A, Mammone T, et al. SIRT1 promotes differentiation of normal human keratinocytes. J Invest Dermatol 2009: 129: 41-49.

621. Cervo P R, Lena A M, Nicoloso M, et al. p63-microRNA feedback in keratinocyte senescence. Proc Natl Acad Sci U S A 2012.

622. Pickard A, Wong P P, McCance D J. Acetylation of Rb by PCAF is required for nuclear localization and keratinocyte differentiation. J Cell Sci 2010: 123: 3718-3726.

623. Simic P, Zainabadi K, Bell E, et al. SIRT1 regulates differentiation of mesenchymal stem cells by deacetylating beta-catenin. EMBO molecular medicine 2013: 5: 430-440.

624. Simic P, Williams E O, Bell E L, Gong J J, Bonkowski M, Guarente L. SIRT1 suppresses the epithelial-to-mesenchymal transition in cancer metastasis and organ fibrosis. Cell Rep 2013: 3: 1175-1186.

625. Rheinwald J G, Green H. Epidermal growth factor and the multiplication of cultured human epidermal keratinocytes. Nature 1977: 265: 421-424.

626. Thompson J D, Higgins D G, Gibson T J. CLUSTAL W: improving the sensitivity of progressive multiple sequence alignment through sequence weighting, position-specific gap penalties and weight matrix choice. Nucleic Acids Res 1994: 22: 4673-4680.

627. McBurney M W, Clark-Knowles K V, Caron A Z, Gray D A. SIRT1 is a Highly Networked Protein That Mediates the Adaptation to Chronic Physiological Stress. Genes Cancer 2013: 4: 125-134.

628. Bailey K, Xia Y, Ward W O, et al. Global gene expression profiling of hyperkeratotic skin lesions from inner Mongolians chronically exposed to arsenic. Toxicol Pathol 2009: 37: 849-859.

629. Wilking M J, Singh C, Nihal M, Zhong W, Ahmad N. SIRT1 deacetylase is overexpressed in human melanoma and its small molecule inhibition imparts anti-proliferative response via p53 activation. Arch Biochem Biophys 2014.

630. Suzuki T, Miyazaki K, Kita K, Ochi T. Trivalent dimethylarsenic compound induces histone H3 phosphorylation and abnormal localization of Aurora B kinase in HepG2 cells. Toxicology and Applied Pharmacology 2009: 241: 275-282.

631. He Z, Ma W Y, Liu G, Zhang Y, Bode A M, Dong Z. Arsenite-induced phosphorylation of histone H3 at serine 10 is mediated by Akt1, extracellular signal-regulated kinase 2, and p90 ribosomal S6 kinase 2 but not mitogen- and stress-activated protein kinase 1. J Biol Chem 2003: 278: 10588-10593.

632. Thomas D J. Unraveling arsenic--glutathione connections. Toxicol Sci 2009: 107: 309-311.

633. Hitchler M J, Domann F E. Redox regulation of the epigenetic landscape in cancer: a role for metabolic reprogramming in remodeling the epigenome. Free Radic Biol Med 2012: 53: 2178-2187.

634. Afanas'ev I. New nucleophilic mechanisms of ros-dependent epigenetic modifications: comparison of aging and cancer. Aging and disease 2014: 5: 52-62.

635. Radak Z, Koltai E, Taylor A W, et al. Redox-regulating sirtuins in aging, caloric restriction, and exercise. Free Radical Biology and Medicine 2013: 58: 87-97.

636. Styblo M, Del Razo L M, Vega L, et al. Comparative toxicity of trivalent and pentavalent inorganic and methylated arsenicals in rat and human cells. Arch Toxicol 2000: 74: 289-299.

637. Benbrahim-Tallaa L, Waterland R A, Styblo M, Achanzar W E, Webber M M, Waalkes M P. Molecular events associated with arsenic-induced malignant transformation of human prostatic epithelial cells: aberrant genomic DNA methylation and K-ras oncogene activation. Toxicol Appl Pharmacol 2005: 206: 288-298.

638. Robertson K D. DNA methylation, methyltransferases, and cancer. Oncogene 2001: 20: 3139-3155.

639. Robertson K D, Keyomarsi K, Gonzales F A, Velicescu M, Jones P A. Differential mRNA expression of the human DNA methyltransferases (DNMTs) 1, 3a and 3b during the G(0)/G(1) to S phase transition in normal and tumor cells. Nucleic Acids Res 2000: 28: 2108-2113.

640. Kim H G, Kim D J, Li S, et al. Polycomb (PcG) proteins, BMI1 and SUZ12, regulate arsenic-induced cell transformation. J Biol Chem 2012: 287: 31920-31928.

641. Christophorou M A, Martin-Zanca D, Soucek L, et al. Temporal dissection of p53 function in vitro and in vivo. Nat Genet 2005: 37: 718-726.

642. Sherr C J, DePinho R A. Cellular senescence: mitotic clock or culture shock? Cell 2000: 102: 407-410.

643. McNeely S C, Xu X, Taylor B F, Zacharias W, McCabe M J, Jr., States J C. Exit from arsenite-induced mitotic arrest is p53 dependent. Environ Health Perspect 2006: 114: 1401-1406.

644. Taylor B F, McNeely S C, Miller H L, Lehmann G M, McCabe M J, Jr., States J C. p53 suppression of arsenite-induced mitotic catastrophe is mediated by p21CIP1/WAF1. J Pharmacol Exp Ther 2006: 318: 142-151.

645. Sun Y, Pi J, Wang X, Tokar E J, Liu J, Waalkes M P. Aberrant cytokeratin expression during arsenic-induced acquired malignant phenotype in human HaCaT keratinocytes consistent with epidermal carcinogenesis. Toxicology 2009: 262: 162-170.

646. Chien C W, Chiang M C, Ho I C, Lee T C. Association of chromosomal alterations with arsenite-induced tumorigenicity of human HaCaT keratinocytes in nude mice. Environ Health Perspect 2004: 112: 1704-1710.

647. Wen G, Calaf G M, Partridge M A, et al. Neoplastic transformation of human small airway epithelial cells induced by arsenic. Mol Med 2008: 14: 2-10.

648. Stueckle T A, Lu Y, Davis M E, et al. Chronic occupational exposure to arsenic induces carcinogenic gene signaling networks and neoplastic transformation in human lung epithelial cells. Toxicology and Applied Pharmacology 2012: 261: 204-216.

649. Wnek S M, Jensen T J, Severson P L, Futscher B W, Gandolfi A J. Monomethylarsonous acid produces irreversible events resulting in malignant transformation of a human bladder cell line following 12 weeks of low-level exposure. Toxicol Sci 2010: 116: 44-57.

650. Treas J N, Tyagi T, Singh K P. Effects of Chronic Exposure to Arsenic and Estrogen on Epigenetic Regulatory Genes Expression and Epigenetic Code in Human Prostate Epithelial Cells. PLoS One 2012: 7: e43880.

651. Achanzar W E, Brambila E M, Diwan B A, Webber M M, Waalkes M P. Inorganic arsenite-induced malignant transformation of human prostate epithelial cells. J Natl Cancer Inst 2002: 94: 1888-1891.

652. Botchkarev V A, Gdula M R, Mardaryev A N, Sharov A A, Fessing M Y. Epigenetic Regulation of Gene Expression in Keratinocytes. J Invest Dermatol 2012.

653. Krishnan V, Chow M Z, Wang Z, et al. Histone H4 lysine 16 hypoacetylation is associated with defective DNA repair and premature senescence in Zmpste24-deficient mice. Proc Natl Acad Sci U S A 2011: 108: 12325-12330.

654. Contrepois K, Thuret J Y, Courbeyrette R, Fenaille F, Mann C. Deacetylation of H4-K16Ac and heterochromatin assembly in senescence. Epigenetics & chromatin 2012: 5: 15.

655. Gentry P R, McDonald T B, Sullivan D E, Shipp A M, Yager J W, Clewell H J, 3rd. Analysis of genomic dose-response information on arsenic to inform key events in a mode of action for carcinogenicity. Environ Mol Mutagen 2010: 51: 1-14.

656. Li Y, Ling M, Xu Y, et al. The repressive effect of NF-kappaB on p53 by mot-2 is involved in human keratinocyte transformation induced by low levels of arsenite. Toxicol Sci 2010: 116: 174-182.

657. Pacholec M, Bleasdale J E, Chrunyk B, et al. SRT1720, SRT2183, SRT1460, and resveratrol are not direct activators of SIRT1. J Biol Chem 2010: 285: 8340-8351.

658. Hsiang Y H, Lihou M G, Liu L F. Arrest of replication forks by drug-stabilized topoisomerase I-DNA cleavable complexes as a mechanism of cell killing by camptothecin. Cancer Res 1989: 49: 5077-5082.

659. Hsiang Y H, Liu L F, Wall M E, et al. DNA topoisomerase I-mediated DNA cleavage and cytotoxicity of camptothecin analogues. Cancer Res 1989: 49: 4385-4389.

660. Mocellin S, Provenzano M. RNA interference: learning gene knock-down from cell physiology. J Transl Med 2004: 2: 39.

661. Fedorov Y, King A, Anderson E, et al. Different delivery methods-different expression profiles. Nat Methods 2005: 2: 241.

662. Sledz C A, Holko M, de Veer M J, Silverman R H, Williams B R. Activation of the interferon system by short-interfering RNAs. Nat Cell Biol 2003: 5: 834-839.

663. Aleman L M, Doench J, Sharp P A. Comparison of siRNA-induced off-target RNA and protein effects. RNA 2007: 13: 385-395.

664. Aagaard L, Rossi J J. RNAi therapeutics: principles, prospects and challenges. Advanced drug delivery reviews 2007: 59: 75-86.

665. Maurisse R, De Semir D, Emamekhoo H, et al. Comparative transfection of DNA into primary and transformed mammalian cells from different lineages. BMC biotechnology 2010: 10: 9.

666. Jiang C K, Connolly D, Blumenberg M. Comparison of methods for transfection of human epidermal keratinocytes. J Invest Dermatol 1991: 97: 969-973.

667. Hawley-Nelson P, Sullivan J E, Kung M, Hennings H, Yuspa S H. Optimized conditions for the growth of human epidermal cells in culture. J Invest Dermatol 1980: 75: 176-182.

668. Distler J H, Jungel A, Kurowska-Stolarska M, et al. Nucleofection: a new, highly efficient transfection method for primary human keratinocytes*. Exp Dermatol 2005: 14: 315-320.

669. Levinger L F, Carter C W, Jr. Superstructural differences between chromatin in nuclei and in solution are revealed by kinetics of micrococcal nuclease digestion. J Biol Chem 1979: 254: 9477-9487.

670. Cousens L S, Gallwitz D, Alberts B M. Different accessibilities in chromatin to histone acetylase. J Biol Chem 1979: 254: 1716-1723.

671. Shechter D, Dormann H L, Allis C D, Hake S B. Extraction, purification and analysis of histones. Nat Protoc 2007: 2: 1445-1457.